REFERENCE

ProQuest LLC.
789 East Eisenhower Parkway
P.O. Box 1346
Ann Arbor, MI 48106 – 1346

THE SYNTHESIS OF NOVEL ORGANOMETALLIC MATERIALS

by

RORY BERRIDGE

A thesis submitted in partial fulfilment of the requirements of Sheffield Hallam University for the degree of Doctor of Philosophy

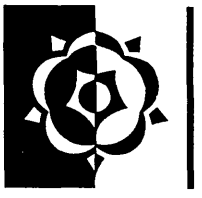

Sheffield Hallam University

October 2001

Revision 5

TABLE OF CONTENTS

1 INTRODUCTION **15**

1.1 SUPERCONDUCTORS AND ORGANIC METALS 15

1.1.1 TTF/TCNQ *17*

1.1.2 MACROCYCLIC COMPLEXES *20*

1.1.3 DITHIOLENE COMPLEXES *21*

1.1.4 DMITS *23*

1.2 MAGNETIC COMPOUNDS 44

1.2.1 FERROMAGNETISM *45*

1.2.2 PARAMAGNETISM *46*

1.2.3 DIAMAGNETISM *47*

1.3 DIHALOGEN ADDUCTS 53

2 EXPERIMENTAL - ANALYTICAL METHODS **63**

2.1 MELTING POINT 63

2.2 MASS SPECTROMETRY 63

2.3 ELEMENTAL ANALYSIS 63

2.4 FOURIER TRANSFORM INFRA-RED SPECTROSCOPY (FTIR) 64

2.5 ULTRAVIOLET/VISIBLE ABSORPTION SPECTROSCOPY (UV/VIS) 64

2.6 NUCLEAR MAGNETIC RESONANCE SPECTROSCOPY (NMR) 65

2.7 X-RAY CRYSTALLOGRAPHY 65

2.8 MAGNETIC SUSCEPTIBILITY MEASUREMENTS 65

2.9 CYCLIC VOLTAMMETRY 66

2.10 RAMAN SPECTROSCOPY 66

3 EXPERIMENTAL - DMIT COMPLEXES **67**

3.1 LIGANDS 67

3.1.1 LIGAND SYNTHESIS *67*

3.1.2 LIGAND ANALYSIS *75*

3.2 METAL COMPLEXES 95

3.2.1 COMPLEX SYNTHESIS *95*

3.2.2 COMPLEX ANALYSIS *106*

3.2.3 MAGNETIC SUSCEPTIBILITY *139*

3.2.4 CYCLIC VOLTAMMETRY *143*

4 CONCLUSIONS & DISCUSSION ON DMIT COMPLEXES 150

5 EXPERIMENTAL - HALOGEN ADDUCTS 159

5.1 THIONE PRECURSORS 159

5.1.1 THIONE SYNTHESIS *159*

5.1.2 THIONE ANALYSIS *168*

5.2 HALOGEN ADDUCTS 175

5.2.1 ADDUCT SYNTHESIS *175*

5.2.2 ADDUCT ANALYSIS *178*

6 CONCLUSION & DISSCUSIONS ON HALOGEN ADDUCTS 204

7 FINAL COMMENTS AND FURTHER WORK 213

7.1 DMIT COMPLEXES 213

7.2 HALOGEN ADDUCTS 215

8 APPENDIX 218

8.1 NMR SHIFT CALCULATIONS 218

8.1.1 "Ethane bridge ligand, compound [35]" *219*

8.1.2 "o-xylene bridge ligand, compound [36]" *220*

8.1.3 "m-xylene bridge ligand, compound [37]" *222*

8.1.4 "p-xylene bridge ligand, compound [38]" *224*

8.1.5 "dimethylpyridine bridge ligand, compound [39]" *226*

8.2 SUPPORTING CRYSTAL DATA 228

8.2.1 Ethane bridge ligand TMA salt, compound [42] *228*

8.2.2 O-Xylene bridge ligand Ni complex, compound [55] *232*

8.2.3 1:1 adduct of [4,5(2'-cyanoethylthio)-1,3-dithione]:[IBr], compound [81] *238*

8.2.4 1:1 adduct of ethane bridge ligand with diiodine, compound [82] *242*

8.2.5 Diiodine adduct of 1,3-dithiole-2-thione-4,5-dicarboxylate, compound [83] *247*

8.2.6 IBr adduct of Dimethyl 1,3-dithiole-2-thione-4,5-dicarboxylate, compound [84] *250*

8.2.7 1,3-dithiole-2-thione-4-ferrocene adduct with diiodine, compound [85] *253*

9 REFERENCE SECTION **257**

LIST OF FIGURES

FIGURE 1, TCNQ [1] 17

FIGURE 2, TTF [2] 17

FIGURE 3, TETRAMETHYLTETRASELENAFULVALENE[3] (TMTSF) 18

FIGURE 4, BEDT-TTF[4], DMET[5], MDT-TTF[6], BEDO-TTF[7] 19

FIGURE 5, PHTHALOCYANINES[8] 20

FIGURE 6, METAL BIS(DITHIOLENE)[9] COMPLEXES 21

FIGURE, 7 MALEONITRILEDITHIOLATE LIGAND[10] 22

FIGURE 8, ISOTRITHIONE[12] 24

FIGURE 9, DMIT[11] 24

FIGURE 10, DMIT[11] SYNTHESIS 25

FIGURE 11, DMIT[11] SYNTHESIS MECHANISM, BECHER ET AL. 26

FIGURE 12, DMIT[11] SYNTHESIS MECHANISM, BRYCE ET AL. 27

FIGURE 13, PROTECTED DMIT[14] & [15] 28

FIGURE 14, THIONE HYDROLYSES 29

FIGURE 15, TRANS-CHALCOGENATION ROUTE TO DITHIOLENE[9] TYPE COMPLEXES 31

FIGURE 16, DMIT'S → TTF'S 32

FIGURE 17, THIONE COUPLING MECHANISM 33

FIGURE 18, UNSYMMETRICALLY SUBSTITUTED DMIT'S 34

FIGURE 19, FURTHER ROUTES TO DMIT'S 35

FIGURE 20, ZINCATE ROUTE TO 4,5-BIS(METHYLTHIO)-1,3-DITHIOLE-2-THIONE[21] 36

FIGURE 21, FURTHER ROUTES TO DMITS EXAMPLE 2 36

FIGURE 22, TTF FROM 4,5-BIS(BENZOYLTHIO)-1,3-DITHIOL-2-THIONE 37

FIGURE 23, MELINE ET AL., PROPOSED MECHANISM 38

FIGURE 24, ELECTROCRYSTALLISATION CELL 41

FIGURE 25, SYNTHESIS OF OTHER DMIT COMPLEXES[23] 42

FIGURE 26, MAGNETIC DIPOLE ARRANGEMENTS 48

FIGURE 27, FE(CP*2) AND TCNE[24] 50

FIGURE 28, OXAMIDOBIS(CARBOXYLATO)CU(II) DIANIONS[25] 51

FIGURE 29, OXAMIDOBIS(N,N'-BENZOATO)CU(II)[25] 51

FIGURE 30, REACTION OF A DONOR ATOM WITH DIHALOGENS 56

FIGURE 31, 1,3-DITHIOLANE-2-THIONE[27], AND 1,3-DITHIOLE-2-THIONE[28] 58

FIGURE 32, 4,5-BIS(METHYLTHIO)-1,3-DITHIOLE-2-THIONE[21] 59

FIGURE 33, REACTION OF 4,5-BIS(METHYLTHIO)-1,3-DITHIOLE-2-THIONE WITH X_2 60

FIGURE 34, CHARGE DELOCALISATION IN THIONES AND TRITHIOCARBONATES. 61

FIGURE 35, GENERAL REACTION SCHEME FOR LIGAND[33] SYNTHESIS. 67

FIGURE 36, ETHANE BRIDGE LIGAND, COMPOUND [35] 68

FIGURE 37, O-XYLENE BRIDGE LIGAND, COMPOUND [36] 69

FIGURE 38, M-XYLENE BRIDGE LIGAND, COMPOUND [37] 70

FIGURE 39, P-XYLENE BRIDGE LIGAND, COMPOUND [38] 72

FIGURE 40, DIMETHYLPYRIDINE BRIDGE LIGAND, COMPOUND [39] 73

FIGURE 41, 4,5-BIS(ETHYLENEDITHIO)-1,3-DITHIOLE-2-THIONE[40] 76

FIGURE 42, PROTON ARRANGEMENT IN ETHANE BRIDGE LIGAND[35] 78

FIGURE 43, CARBON ARRANGEMENT IN ETHANE BRIDGE LIGAND[35] 78

FIGURE 44, 4,5-BIS(A'A'-O-XYLENEDITHIO)-1,3-DITHIOLE-2-THIONE[41] 80

FIGURE 45, PROTON ARRANGEMENT O-XYLENE BRIDGE LIGAND[36] 81

FIGURE 46, CARBON ARRANGEMENT O-XYLENE BRIDGE LIGAND[36] 82

FIGURE 47, PROTON ARRANGEMENT M-XYLENE BRIDGE LIGAND[37] 85

FIGURE 48, CARBON ARRANGEMENT M-XYLENE BRIDGE LIGAND[37] 86

FIGURE 49, PROTON ARRANGEMENT P-XYLENE BRIDGE LIGAND[38] 89

FIGURE 50, CARBON ARRANGEMENT P-XYLENE BRIDGE LIGAND[38] 90

FIGURE 51, PROTON ARRANGEMENT IN DIMETHYLPYRIDINE BRIDGE LIGAND[39] 93

FIGURE 52, CARBON ARRANGEMENT IN DIMETHYLPYRIDINE BRIDGE LIGAND[39] 94

FIGURE 53, ETHANE BRIDGE LIGAND TMA SALT, COMPOUND [42] 95

FIGURE 54, ETHANE BRIDGE LIGAND M^{2+} COMPLEX, [43] TO [51] 96

FIGURE 55, O-XYLENE BRIDGE LIGAND M^{2+} COMPLEX, COMPOUNDS [52] TO [58] 98

FIGURE 56, M-XYLENE BRIDGE LIGAND M^{2+} COMPLEX, COMPOUNDS [59] TO [64] 100

FIGURE 57, P-XYLENE BRIDGE LIGAND M^{2+} COMPLEX, COMPOUNDS **[65]** TO **[70]** 102

FIGURE 58, DIMETHYLPYRIDINE BRIDGE LIGAND M^{2+} COMPLEX, COMPOUNDS **[71]** TO **[76]**..... 104

FIGURE 59, X-RAY CRYSTAL STRUCTURE OF TMA SALT**[42]**..... 106

FIGURE 60, PROTON AND CARBON ARRANGEMENT IN TMA**[42]** SALT 109

FIGURE 61, DIMETHYL TIN COMPLEX OF ETHANE BRIDGE**[35]** LIGAND, COMPOUND **[51]** 112

FIGURE 62, UV/VIS SPECTRA OF COMPOUNDS **[43]** & **[49]** 115

FIGURE 63, PHOSPHORUS ENVIRONMENTS IN COMPOUND **[47]**, $[Ni(DPPE)]^{2+}$ COMPLEX 116

FIGURE 64, UV/VIS SCAN OF COMPOUND **[55]** (O-XYLENE BRIDGE Ni^{2+} COMPLEX) IN DMF..... 121

FIGURE 65, UV/VIS SCAN OF COMPOUND **[55]** (O-XYLENE BRIDGE Ni^{2+} COMPLEX) IN DMSO.... 122

FIGURE 66, X-RAY CRYSTAL STRUCTURE OF COMPOUND **[55]** (O-XYLENE BRIDGE NI COMPLEX), CRYSTALS GROWN FROM PYRIDINE. 124

FIGURE 67, UV/VIS SPECTRA OF COMPOUND **[73]** (DIMETHYLPYRIDINE BRIDGE NI COMPLEX) IN DMF. 137

FIGURE 68, CV TRACE OF COMPOUND **[42]**..... 144

FIGURE 69, CV TRACE OF COMPOUND**[43]** 145

FIGURE 70, CV TRACE OF COMPOUND**[45]** 146

FIGURE 71, CV TRACE OF COMPOUND**[46]** 147

FIGURE 72, CV TRACE OF COMPOUND**[47]** 148

FIGURE 73, CV TRACE OF COMPOUND**[48]** 149

FIGURE 74, S-S BOND FORMATION..... 156

FIGURE 75, REACTION SCHEME FOR THE PREPARATION OF 4,5 BIS(2'-CYANOETHYLTHIO)-1,3-DITHIOLE-2-THIONE, COMPOUND **[15]** 160

FIGURE 76, LIGANDS USED IN THE PREPARATION OF DIHALOGEN ADDUCTS, COMPOUNDS **[35]** TO **[38]**..... 163

FIGURE 77, SYNTHESIS OF DIMETHYL 1,3-DITHIOLE-2-THIONE-4,5-DICARBOXYLATE, COMPOUND **[77]**..... 164

FIGURE 78, SYNTHETIC OUTLINE FOR THE PREPARATION OF 1,3-DITHIOLE-2-THIONE-4-FERROCENE, COMPOUND **[80]**..... 165

FIGURE 79, CHLOROACETYL FERROCENE, COMPOUND **[78]**..... 170

FIGURE 80, ETHYL [(2-OXO-2-FERROCENYLETHYL)SULFANYL]METHANETHIOATE, COMPOUND **[79]** 171

FIGURE 81, 1,3-DITHIOLE-2-THIONE-4-FERROCENE, COMPOUND **[80]** 173

FIGURE 82, 1:1 ADDUCT OF [4,5(2'-CYANOETHYLTHIO)-1,3-DITHIONE-2-THIONE]:[IBR], COMPOUND **[81]** 180

FIGURE 83, X-RAY CRYSTAL PACKING DIAGRAM OF COMPOUND **[81]** 181

FIGURE 84, SOLID STATE STRUCTURE OF COMPOUND **[81]** 181

FIGURE 85, ETHANE BRIDGE LIGAND DIIODINE ADDUCT, COMPOUND **[82]** 183

FIGURE 86, SOLID STATE STRUCTURE OF ETHANE BRIDGE LIGAND DIIODINE ADDUCT, COMPOUND **[82]** 184

FIGURE 87, RAMAN SPECTRA OF ETHANE BRIDGE LIGAND DIIODINE ADDUCT, COMPOUND **[82]** .. 184

FIGURE 88, DIIODINE ADDUCT OF DIMETHYL 1,3-DITHIOLE-2-THIONE-4,5-DICARBOXYLATE, COMPOUND **[83]** 186

FIGURE 89, SOLID STATE STRUCTURE OF COMPOUND **[83]** 187

FIGURE 90, "POLYMERIC" IODINE CHAIN IN COMPOUND **[83]** 187

FIGURE 91, X-RAY CRYSTAL PACKING DIAGRAM OF COMPOUND **[83]** 188

FIGURE 92, DIMETHYL 1,3-DITHIOLE-2-THIONE-4,5-DICARBOXYLATE ADDUCT WITH IBR, COMPOUND **[84]** 189

FIGURE 93, SOLID STATE STRUCTURE OF COMPOUND **[84]** 190

FIGURE 94, PACKING DIAGRAM OF COMPOUND **[84]** 191

FIGURE 95, 1,3-DITHIOLE-2-THIONE-4-FERROCENE ADDUCT WITH DIIODINE, COMPOUND **[85]** 192

FIGURE 96, SOLID STATE STRUCTURE OF 1,3-DITHIOLE-2-THIONE-4-FERROCENE DIIODINE ADDUCT, COMPOUND **[85]** 193

FIGURE 97, COMPOUND **[85]**, MINUS THE FERROCENE UNITS TO SHOW THE SUPRAMOLECULAR POLYIODIDE NETWORK. 194

FIGURE 98, RAMAN SPECTRUM OF COMPOUND **[85]** 195

FIGURE 99, MOSSBAUER SPECTROSCOPY OF COMPOUND **[85]** 196

FIGURE 100, MAGNETISATION AS A FUNCTION OF TEMPERATURE, CARRIED OUT AT 1 TESLA OF EXTERNAL FIELD FOR COMPOUND **[85]** 198

FIGURE 101, A PLOT OF THE TEMPERATURE DEPENDENCE OF THE INVERSE OF THE MAGNETIC SUSCEPTIBILITY FOR COMPOUND **[85]**. 199

FIGURE 102, A PLOT OF χT VS. T FOR COMPOUND **[85]** 200

FIGURE 103, MAGNETISATION VS. EXTERNAL FIELD FOR COMPOUND **[85]** AT 1.8 K..... 201

FIGURE 104, A PLOT OF MAGNETISATION VS. EXTERNAL FIELD FOR COMPOUND **[85]** AT 1.8, 2, 2.5 AND 3K 202

FIGURE 105, A PLOT OF MAGNETISATION VS. EXTERNAL FIELD FOR COMPOUND **[85]** AT RT 203

FIGURE 106, 1:1 ADDUCT OF [4,5(2'-CYANOETHYLTHIO)-1,3-DITHIONE-2-THIONE]:[IBR], COMPOUND **[81]** 204

FIGURE 107, ETHANE BRIDGE LIGAND DIIODINE ADDUCT, COMPOUND **[82]** 205

FIGURE 108, DIIODINE ADDUCT OF DIMETHYL 1,3-DITHIOLE-2-THIONE-4,5-DICARBOXYLATE, COMPOUND **[83]** 207

FIGURE 109, DIMETHYL 1,3-DITHIOLE-2-THIONE-4,5-DICARBOXYLATE ADDUCT WITH IBR, COMPOUND **[84]** 208

FIGURE 110, 1,3-DITHIOLE-2-THIONE-4-FERROCENE ADDUCT WITH DIIODINE, COMPOUND **[85]** .. 211

FIGURE 111, POSSIBLE SOLUTION TO SOLUBILITY PROBLEMS FOR LIGANDS 213

FIGURE 112, "BRIDGED" TTF LIGANDS 214

FIGURE 113, FERROCENYL(PHENYL)PHOSPHINES 216

FIGURE 114, "DITHIONE" AND "DIFERROCENYL" DERIVATIVES OF COMPOUND **[80]** 217

ACKNOWLEDGEMENTS

I would like to thank my academic supervisors Dr P.J.Skabara, Dr N.Bricklebank and Professor D.W.Allen for their much valued guidance and assistance during this research project. I also wish to thank and acknowledge my sponsors, the Materials Research Institute, for their financial support. I also wish to mention the people I have worked with during the last three years. these include the students and staff of the Chemistry Division and Materials Research Institute at Sheffield Hallam University. These include David Crouch, Kevin Osborne, Ken Lewis, Barry Christian, Paul Hatton and Lee Marples whom I most infuriated during the last three years, and finally the 1st year PhD students Tahir Kahn and Cristina Pozo-Gonzalo who provided much entertainment in the darker moments of my final year.

In addition I would like to specifically acknowledge the help of:

- Dr. Chris Sammon and Dr. Chris Constable of the Materials Research Institute (MRI), Sheffield Hallam University (SHU), for obtaining the Raman spectra.
- Dr. Sue Forder of the Division of Physics SHU, for obtaining the Mossbauer spectra (5.2.2.4).
- M.B. Hursthouse, S.J.Coles and M.E. Light of the EPSRC Crystallographic Service at the University of Southampton, for obtaining the crystal structures presented in this Thesis.
- Professor Fernando Palacio of the Inst. de Ciencia de Materiales de Aragon CSIC - Universidad de Zaragoza, for obtaining the magnetic data on compound **[85]**.

DECLARATION

All material published in this thesis is work of Rory Berridge, unless otherwise stated (see acknowledgements on previous page).

Posters on this work were presented at the following conferences:

- Royal Society of Chemistry 1999 Annual Conference, Heriot-Watt University, Edinburgh, UK 6-10 September 1999.
- International Conference on Science and Technology of Synthetic Metals, 15-21 July 2000, Congress Centre Gastien, Austria.

Papers concerning the research presented in this thesis have also been published in scientific journals (copies of which are included at the end of thesis):

- "Novel transition metal complexes based on covalently linked DMIT systems". *R.Berridge, N.Bricklebank, D.W.Allen, P.J.Skabara, K.M.A.Malik, S.J.Coles, M.B.Hursthouse.* Synthetic Metals, 2001, vol 120, iss 1-3, pp 1023-1024
- "Crystal engineering towards highly ordered polymeric structures of 1,3-dithiole-2-thione-dihalogen adducts". *P.J.Skabara N.Bricklebank, R.Berridge, S.Long, M.E.Light, S.J.Coles, M.B.Hursthouse.* Journal of the Chemical. Society-Dalton Transactions., 2000, iss 19, pp 3235-3236

Rory Berridge

Date:

ABSTRACT

Due to their highly interesting electroactive properties, complexes based on the sulphur heterocycle DMIT have been studied extensively for several decades. The literature is abundant with materials exhibiting semiconducting and metallic properties and up to early 2000 there are eight examples of DMIT based superconductors[1].

In the case of the DMIT complexes, previous work has been constrained to the variation of the transition metal and/or the counter-anion. The work herein concerns the synthesis of a novel series of electroactive ligands, similar to the well-known DMIT species. In contrast to the DMIT ligand, our target derivatives incorporate two thioether and two dithiolate environments as the overall chelating entity. The thioether functionality's are linked via suitable spacer groups and this feature should present a major advantage over traditional DMIT complexes, by adding solubility and synthetic versatility to the overall nature of the complex. In addition to the metal complexes based on DMIT ligands, charge transfer (CT) halogen adducts of these DMIT ligands and their synthetic intermediates are described, providing highly interesting and novel solid state structures and atom-to-atom inter- and intra-molecular interactions.

LIST OF ABBREVIATIONS USED IN THIS THESIS

CT	Charge Transfer
CV	Cyclic Voltammetry
DCM	DiChloroMethane
DMAD	DiMethylAcetyleneDicarboxylate
DMF	N,N-DiMethylFormamide
DMIT	DiMercaptoIsoTrithione
DMSO	DiMethylSulphOxide
EI-MS	Electron Ionisation - Mass Spectroscopy
FAB-MS	Fast Atom Bombardment - Mass Spectroscopy
FTIR	Fourier Transform Infra-Red Spectroscopy
IPA	IsoPropylAlcohol
IR	Infra-Red Spectroscopy
mnt	MaleoNitrilediThiolate
MRI	Materials Research Institute
MS	Mass Spectrometry
NLO	Non-Linear Optics
NMR	Nuclear Magnetic Resonance Spectroscopy
OL	Optical Limiting
PMMA	PolyMethylMethAcrylate
RT	Room Temperature
SHU	Sheffield Hallam University
TCNE	TetraCyaNoEthylene
TCNQ	7,7,8,8-tetracyano-p-quinodimethane
THF	Tetrahydrofuran
TLC	Thin Layer Chromatography
TMA	TetraMethylAmmonium
TMTSF	tetramethyltetraselenafulvalene
TTF	tetrathiafulvalene
TTN	TetraThiaNapthalene
UV/VIS	Spectroscopy

"a posse ad esse"

Latin, "from the possible to the actual"

1 INTRODUCTION

1.1 SUPERCONDUCTORS AND ORGANIC METALS

Superconductivity was first demonstrated in mercury metal in 1911 by Kammerlingh-Onnes[2]; below 4.2 K it was established that the electrical resistance of mercury drops to zero[3,4]. Prior to the early 1970's only certain elements and metal alloys were found to demonstrate this property, namely that below a particular temperature (the critical temperature T_c), the electrical resistance of the compound becomes zero. In 1973 the highest T_c reported was 25.5 K for the alloy $[Nb_3Al_{0.8}Ge_{0.2}]$[4]. One of the more publicly[5-8] noteworthy effects of superconductivity was the much demonstrated 'floating magnet'; below T_c the material becomes perfectly diamagnetic [i.e., the magnetic flux lines are expelled from the bulk of the material], this is known as the Meisser effect[2,9].

Other classes of superconductors[4] that have been developed include:

- Superconductors based on copper oxides, such as $[YBa_2Cu_3O_{6+x}]$, possessing a T_c greater than 77 K.
- Chevrel phases from Roger Chevrel 1971[10]. These are ternary molybdenum chalcogenides, with the general formula $M_xMo_6X_8$, where M = Pb, Sn, Cu, Co, Fe, and X = S, Se, or Te. For example $[PbMo_6S_8]$ has a T_c of 15.2 K.
- Molecular superconducting compounds were first obtained in 1980 by Bechgaard et al., derived from a purely organic molecule tetramethyltetraselenafulvalene (TMTSF). The first molecular inorganic

superconductor was synthesised in 1986 from the work of Cassoux et al., $[TTF][Ni(dmit)_2]_2$ (TTF = tetrathiafulvalene, dmit = 1,3-dithiol-2-thione-4,5-dithiolato).

The results obtained with the "Molecular" superconducting compounds, and in particular the chalcogen based compounds, opened an extensive area of interest in this field of research. With much of the momentum in this area due in no small part to the potential range of compounds that could be synthesised. Compounds composed of molecules or molecular ions have also been found to exhibit diverse properties besides those of superconductivity, including electrical, magnetic and optical properties[2-4,10,11], again widening the scope of research in this area. The quest for molecular superconductors also produced remarkable results in the area of organic metals. Many of the organic compounds that were discovered while searching for potential superconductors were found not to superconduct, but did however show conductivity close to that of a metal.

1.1.1 TTF/TCNQ

Perhaps the most well known (and among the most successful) result of attempts towards molecular superconductivity was from the synthesis of 7,7,8,8-tetracyano-p-quinodimethane **[1]** (TCNQ, Figure 1) in 1962[12]. It was found that various salts of TCNQ are electrically conducting[13,14].

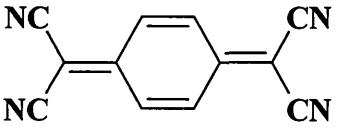

Figure 1, TCNQ **[1]**

A further significant molecule to be discovered was tetrathiafulvalene **[2]** (TTF, Figure 2)[15], this organic molecule could be oxidised to yield conducting salts[16].

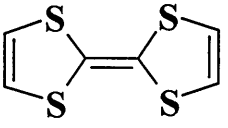

Figure 2, TTF **[2]**

The first 'Organic Metal' was obtained in 1973, when TTF**[2]** and TCNQ**[1]** were combined in a 1:1 donor-acceptor complex[17]. The resulting TTF:TCNQ complex undergoes partial charge transfer between the separately stacked donor (TTF**[2]**) and acceptor (TCNQ**[1]**) molecules. These results led to an extensive

number of studies on TTF:TCNQ and related compounds producing many reports in this area[12,16,18-46].

The interest in this field yielded many benchmark molecules in the following years. In 1980 the TTF derivative tetramethyltetraselenafulvalene**[3]** (TMTSF, Figure 3) was electrochemically oxidised to give the $(TMTSF)_xPF_6$ charge-transfer salt, which became superconducting under pressure. The chlorate analogue showed superconductivity at ambient pressure.

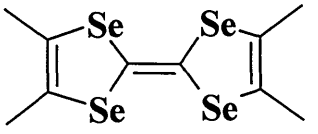

Figure 3, Tetramethyltetraselenafulvalene**[3]** (TMTSF)

Further modifications of TTF**[2]** and subsequent salt formation with inorganic anions such as PF_6^-, ClO_4^-, $[Cu(NCS)_2]^-$ and $[Cu(N(CN)_2)][Cl]$, produced T_cs approaching 13 K at varying pressures. Several of these TTF**[2]** derivatives are shown in Figure 4.

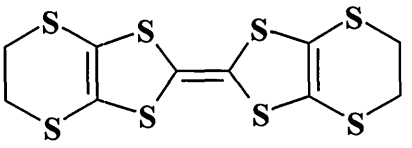

BEDT-TTF[4]

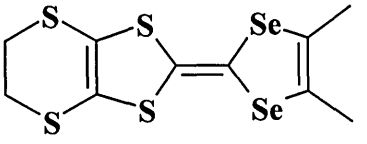

DMET[5]

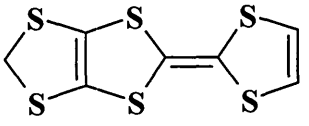

MDT-TTF[6]

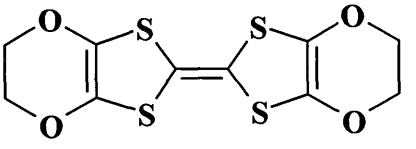

BEDO-TTF[7]

Figure 4, BEDT-TTF**[4]**, DMET**[5]**, MDT-TTF**[6]**, BEDO-TTF**[7]**

Interest in TTF**[2]** type compounds continues at a high pace, and any literature search of the last few years will yield hundreds of reports. The interest in organic based materials has expanded beyond TTF/TCNQ based compounds and many other donor/acceptor molecules are also producing interesting results, several of which are described in subsequent sections.

1.1.2 MACROCYCLIC COMPLEXES

Many macrocyclic metal complexes have been investigated with respect to their potential electronic properties, in particular the potential for acting as electron donor molecules[47]. Many of these compounds proved suitable due to their planarity, which provided in many cases the potential for the formation of an extensive delocalised π electron system[48]. As with TTF/TCNQ, a range of compounds have been prepared[4], including transition metal complexes of glyoximate ligands, tetraazaannulene ligands, porphyrins and, perhaps the most extensively studied, phthalocyanines**[8]**[48-50] shown in Figure 5.

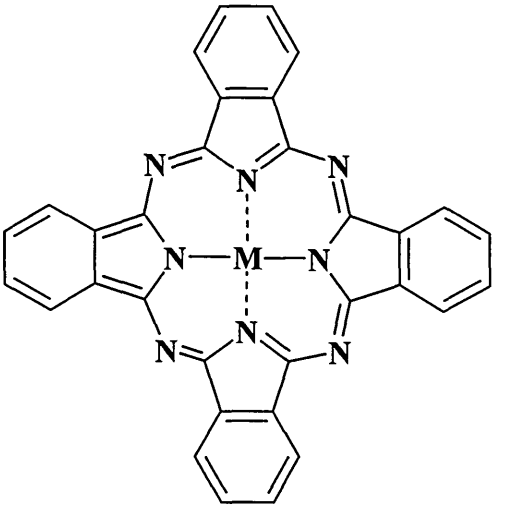

Figure 5, Phthalocyanines**[8]**

The phthalocyanine **[8]** family of aromatic macrocycles are described as "highly stable and versatile compounds, capable of including more than seventy different metallic and non-metallic ions in the ring cavity"[48]. When one considers the

synthetic derivatives possible on the aromatic ring systems, then a huge number of possible structural variations becomes apparent. The vast majority of these compounds are found to form semiconducting donor-acceptor systems, and have found extensive use in the field of non-linear optics.

1.1.3 DITHIOLENE COMPLEXES

Metal complexes based on 1,2-dithiolenes **[9]** are another area of chalcogen chemistry that has produced many interesting results. Charge-transfer salts containing 1,2-dithiolenes **[9]** (Figure 6) have been found to exhibit properties such as metallic conductivity, superconductivity and varying magnetic properties[51-61].

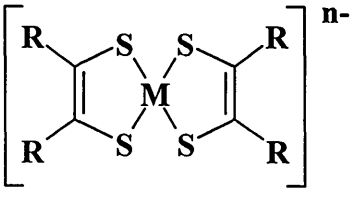

Figure 6, Metal bis(dithiolene)**[9]** complexes

Metal bis(dithiolene)**[9]** complexes are expected to be suitable for use in conducting materials due to their overall planar arrangement (combined with a relative abundance of π and donor electrons), redox properties (generally reversible), and extended π electron systems. These compounds show the promise of having properties similar to TTF**[2]** (namely the π electron system)

and can form charge transfer complexes similar to that of TTF**[2]** (with many dithiolenes studied as charge transfer complexes with ferrocene derivatives)[61], but with the added benefit of the presence of a transition metal (introducing the possibility of metal-metal interactions). Despite these apparent benefits, few metal dithiolenes were found to exhibit high conductivity and metallic behaviour, and in most cases these materials act as semiconductors. The area of materials chemistry in which these complexes have shown promise is in non-linear-optic (NLO) or optical limiting (OL) applications. These properties are generally studied by dispersing the metal bis(dithiolene) in a polymer matrix such as polymethylmethacrylate (PMMA), which is chosen for its relative cheapness, availability in high purity and good processability. Many dithiolene complexes continue to provide significant results in magnetic studies, in particular square planar paramagnetic metal complexes of the maleonitriledithiolate ligand**[10]** (mnt^{2-}), Figure, 7, have been combined in a variety of complexes, including the system $[NH_4][Ni(mnt)_2].H_2O$ which has a ferromagnetic ground state. Derivatives of dithiolenes intended for use in this type of application are still published on a regular basis[51,62-64].

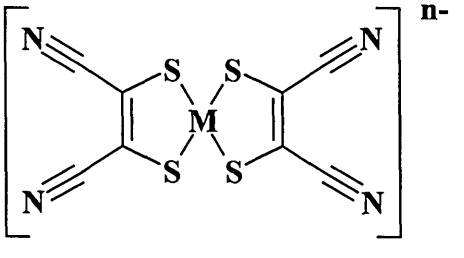

Figure, 7 maleonitriledithiolate ligand**[10]**

While many of the sulphur based metal complexes are studied in respect of their potential uses in materials applications, a further very important area of sulphur metal complex chemistry is in the study of metal sulphur enzymes. This includes the study of the enzymes themselves to the preparation of new sulphur-metal complexes that mimic their active sites, in this respect many of these systems provide an overlapping of structures between bio-inorganic chemistry and materials chemistry[47,65-69].

1.1.4 DMITS

A further popular area of chalcogen chemistry that continues to produce interesting and significant progress in the quest for molecular based compounds for electronic and materials applications is that of DMIT**[11]** and its diverse range of derivatives[1]. The designation DMIT**[11]** is a carryover from the beginnings of heterocyclic sulphur chemistry[70]. In the late 1940s a series of papers was published in which the name "trithione" was suggested for 1,2-dithiole-3-thiones. The system 1,2-dithiole-3-thione was considered a trithionated derivative of propylene, and further derivatives were named by substitution nomenclature. The numbering system being employed in these trithiones varied from that suggested by IUPAC. From this naming system the isomer of 1,2-dithiole-3-thione, namely 1,3-dithiole-2-thione**[12]** then became known as "isotrithione"**[12]**, Figure 8.

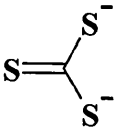

Figure 8, isotrithione[12]

Following on from this naming system the molecule 1,3-dithiole-2-thione-4,5-dithiolate[11] then became *DiMercaptoIsoTrithione*, or DMIT[11], Figure 9. The system of naming these compound does not fit with more modern guidelines on nomenclature, but due to the widespread use of the abbreviation DMIT[11] it would prove very confusing and difficult to the change to a different system. The term DMIT[11] is therefore still used and makes an easier title than the more correct IUPAC name 2-thioxo-1,3-dithiole-4,5-dithiolato[11][1].

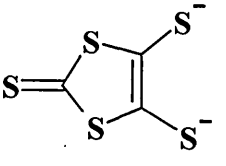

Figure 9, DMIT[11]

A variety of methods for the synthesis of DMIT[11] have been developed over the years. However it is now generally accepted that the best methods for preparing DMIT[11] is the DMF mediated reduction of carbon disulphide by alkali metals[70]. The use of potassium can, however, lead to explosions and the use of sodium was found to be a much more convenient choice. The reduction

method has been developed over recent years to give synthetic strategies that have led to reactions that can yield up to 140 g of the complex $[Zn(DMIT)_2][Et_4N]_2$, commonly referred to as zincate**[13]**. One of the most effective methods developed was that of Becher et al. in 1995[70]. In this method, one mole of sodium is reacted with three moles of carbon disulphide in 200 mL of DMF at 0 ^{O}C under a nitrogen atmosphere, an outline for this route is shown in Figure 10.

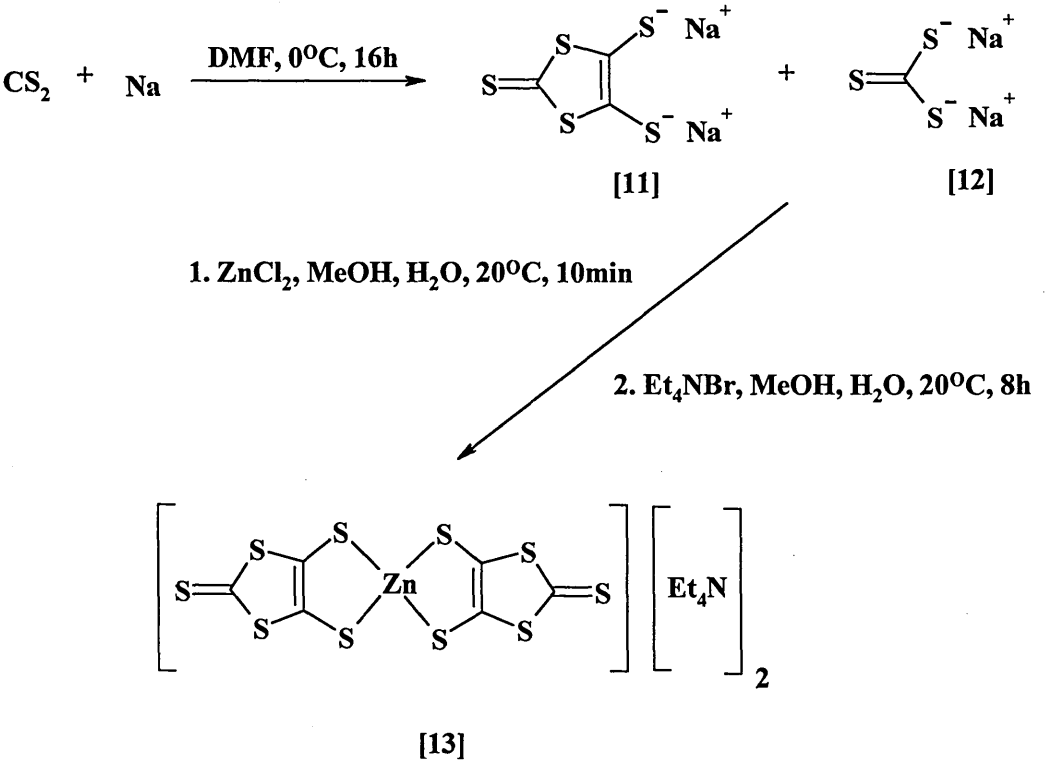

Figure 10, DMIT**[11]** synthesis

The sodium salt of isotrithione **[12]** from this scheme remains in solution whereas the zincate salt **[13]** precipitates as red crystals. The reduction of carbon disulphide can also be carried out electrochemically. The mechanism of the

reaction has been studied extensively by many groups[70], and several possible mechanisms have been proposed. One of these is shown in Figure 11(sodium ions omitted for clarity).

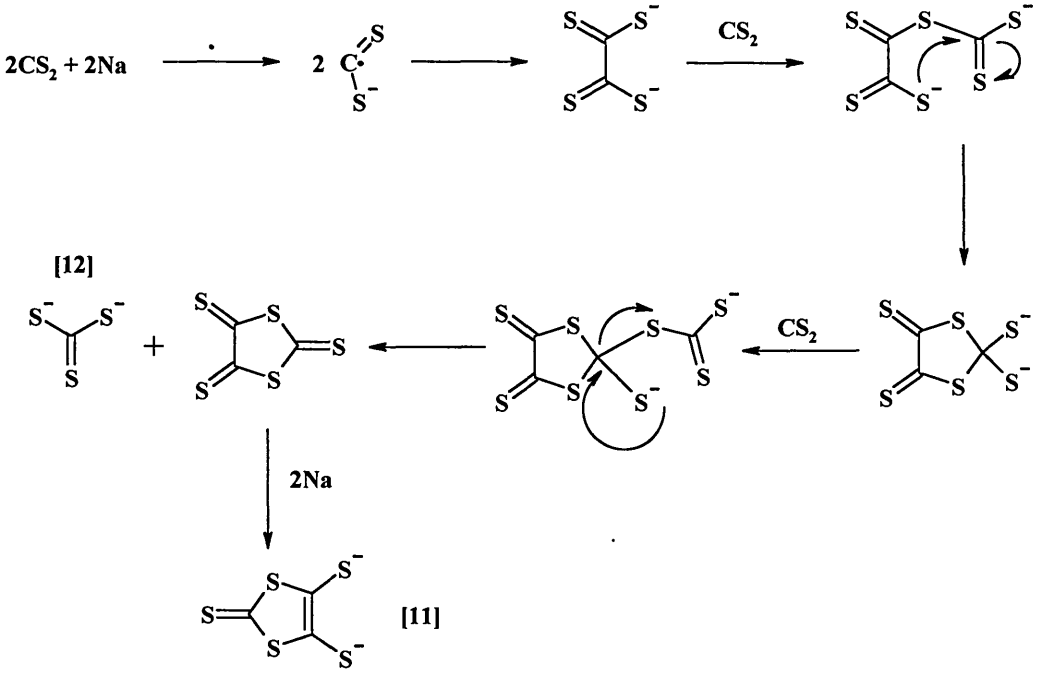

Figure 11, DMIT[**11**] synthesis mechanism, Becher et al.

From this synthetic strategy it became possible to produce the zincate salt **[13]** in batches of up to 77 g. The development of this general method continued and in 1998 Bryce et al.[71], published a slightly revised method for zincate **[13]** synthesis. The route they developed used the same reagents and solvents as the previous technique (carbon disulphide, zinc chloride, sodium metal, DMF and tetraethylammonium bromide), but this revised method uses a significantly reduced amount of sodium metal with an increase in zincate **[13]** yield. In the Bryce method 14.5 g sodium is used to produce 90 g zincate **[13]** compared to

23.0 g yielding 77 g. It was also shown that when this revised technique was scaled to 23.0 g of sodium, the yield of zincate **[13]** increased to 140 g. This development of the previous procedure[70] posed an interesting mechanistic question over the reaction. The mechanism outlined in Figure 11 shows four moles of carbon disulphide reacting with four moles of sodium to give one mole DMIT**[11]** and one mole of the sodium salt of isotrithione**[12]** (Na_2CS_3). The molar amounts utilised in the Bryce method contradict this mechanism, the proposed solution to this discrepancy being that **[12]** is reacting further to give DMIT**[11]** or that a different mechanism is employed. This proposed alternative mechanism is shown in Figure 12 (sodium ions omitted for clarity).

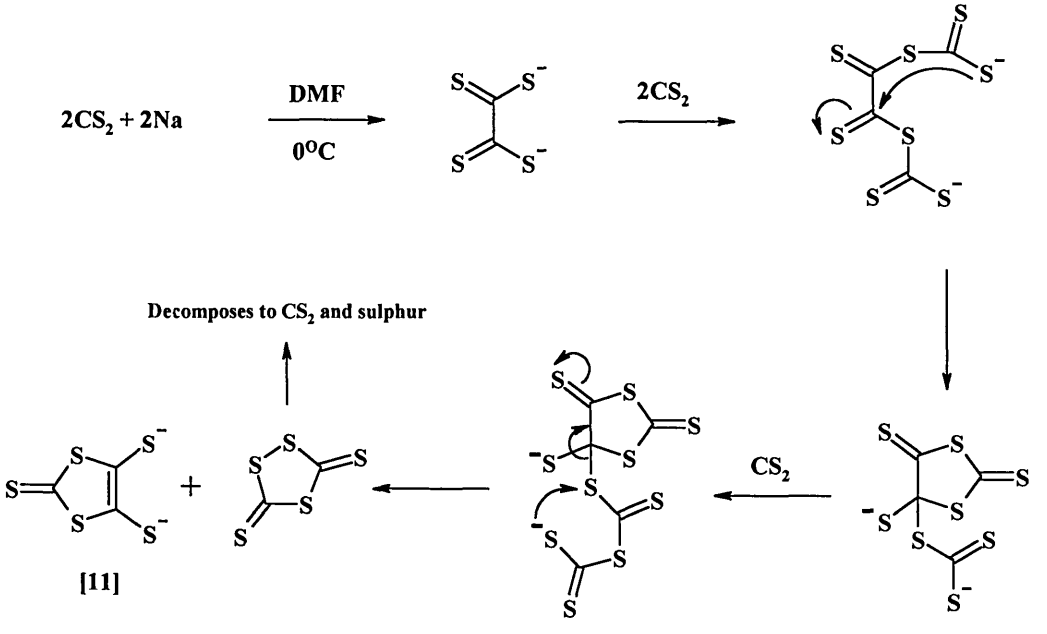

Figure 12, DMIT**[11]** synthesis mechanism, Bryce et al.

From these methods the production of DMIT**[11]** becomes a relatively inexpensive and easy procedure. The zincate salt **[13]** is, however, slightly

hydroscopic and slowly decomposes over several months. For extended storage, and for cleaner subsequent reactions the zincate salt **[13]** is commonly reacted further to give "protected" DMITs, **[14]** & **[15]** shown in Figure 13.

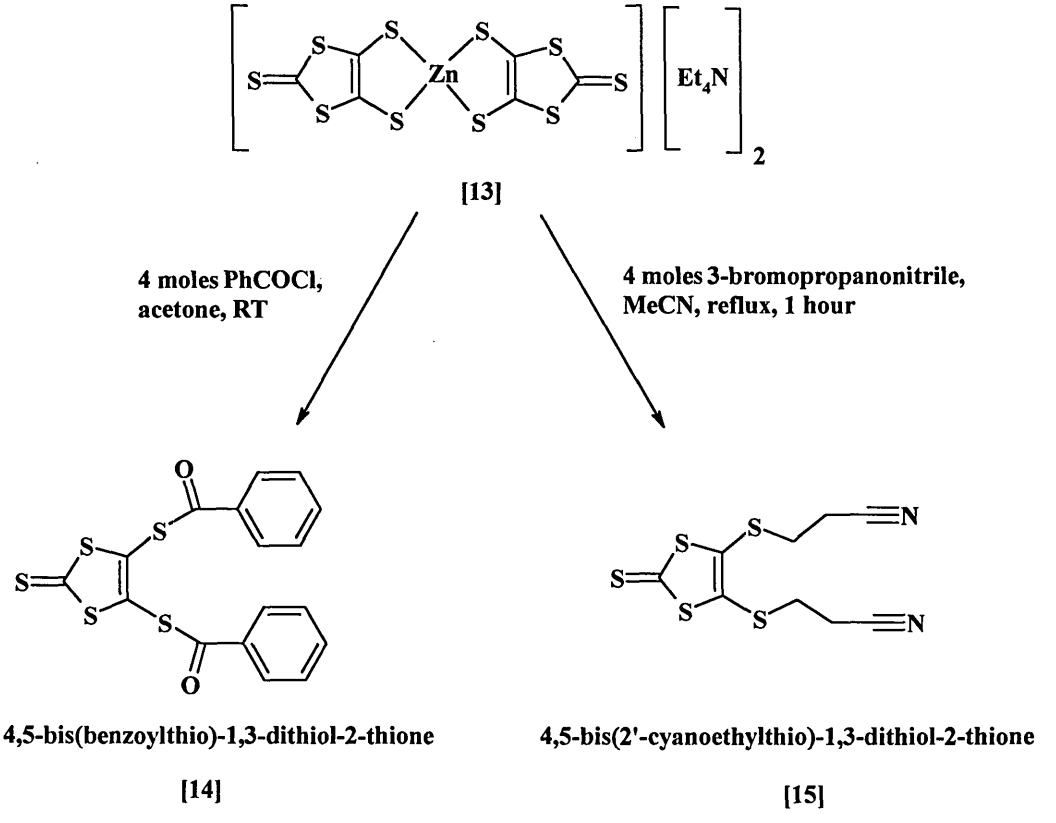

Figure 13, Protected DMIT**[14]** & **[15]**

The resulting protected DMITs, 4,5-bis(benzoylthio)-1,3-dithiol-2-thione**[14]**[1] and 4,5-bis(2'-cyanoethylthio)-1,3-dithiol-2-thione**[15]**[72], when isolated in high purity are stable at room temperature out of direct sunlight for many months, and can be converted easily and quantitatively back to the sodium salt of the DMIT**[11]** ligand by treatment with sodium methoxide or ethoxide. The propanonitrile protected DMIT**[15]** is becoming increasingly popular due to the

"cleaner" deprotection products. The reaction of the thioester**[14]** with methoxide or ethoxide will yield methyl benzoate or ethyl benzoate which will generally require removal before continuing with any reaction scheme. This is most conveniently achieved by precipitating the DMIT**[11]** salt in a large excess of diethyl ether, and filtration under Schlenk conditions. In the case of 4,5-bis(2'-cyanoethylthio)-1,3-dithiol-2-thione**[15]**, the regeneration of the sodium salt of DMIT**[11]** will produce acrylonitrile as a side product.

DMIT**[11]** finds one of its most important uses as a starting point in the synthesis of a variety of conducting and electroactive compounds. DMITs may be used in the synthesis of dithiolene**[9]** type complexes (section 1.1.3). These compounds can be prepared by utilising the electrophilicity of the thione carbon present in DMIT**[11]**. It is known[60,73] that this thione may been hydrolysed by potassium hydroxide to give the corresponding dithiolate**[16]**, Figure 14.

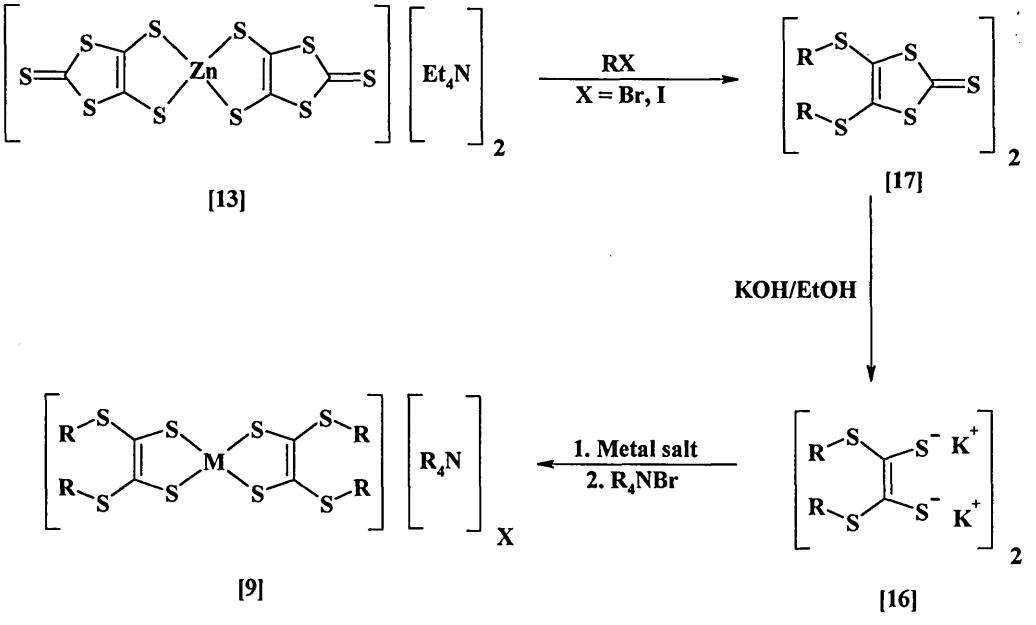

Figure 14, Thione hydrolyses

A more usual route to dithiolenes **[9]** is that of trans-chalcogenation[70]. This route provides an attractive alternative reaction pathway to dithiolenes since it converts the easily obtainable 1,3-dithiole-2-thiones**[17]** to the more reactive 1,3-dithiole-2-ones**[18]**. The subsequent generation of dithiolate moieties**[16]** from 1,3-dithiole-2-ones**[18]** is achieved under relatively mild reaction conditions (sodium methoxide/ethoxide in the appropriate alcohol at room temperature). This procedure is often used in generating dithiolene**[9]** type complexes from DMIT**[11]** derivatives[54,58,74], a general reaction scheme for this type of procedure is shown in Figure 15.

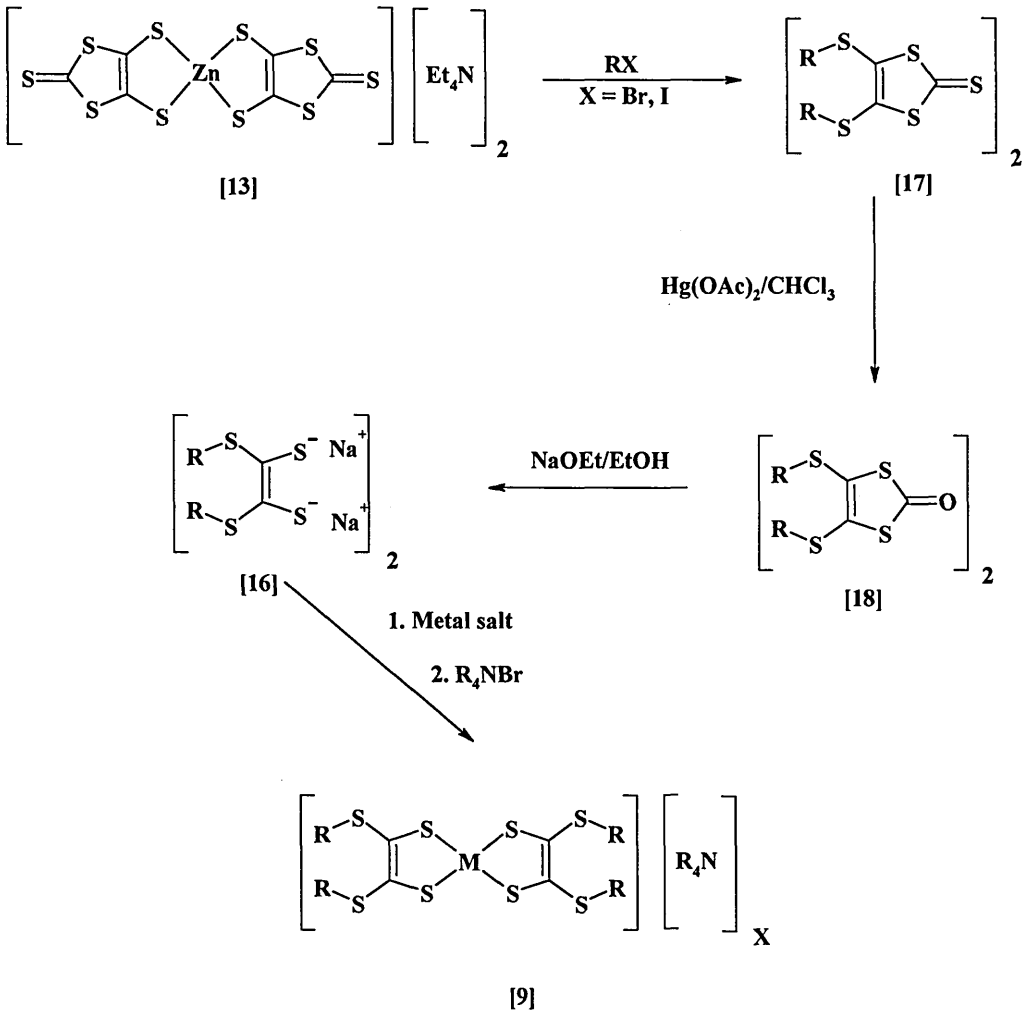

Figure 15, Trans-chalcogenation route to dithiolene**[9]** type complexes

A further very important use of DMIT**[11]** is in the preparation of TTF**[2]** (section 1.1.1) and its derivatives**[19]**. It was shown previously (Figure 13) that the zincate salt **[13]** is relatively reactive with respect to acid chlorides and alkyl halides. From these type of reactions an extensive range of DMIT**[11]** derivatives have been prepared[70,75]. These DMIT**[11]** derivatives may be introduced to the reaction scheme outlined previously to yield dithiolene**[9]** complexes, or again by utilising the properties of the thione or carbonyl, may be used in a coupling reaction to yield TTF derivatives**[19]**. This is commonly achieved by heating the

1,3-dithiole-2-thiones**[17]** and/or 1,3-dithiole-2-ones**[18]** in triethyl phosphite at ~120^{O}C, a general outline to this is shown in Figure 16.

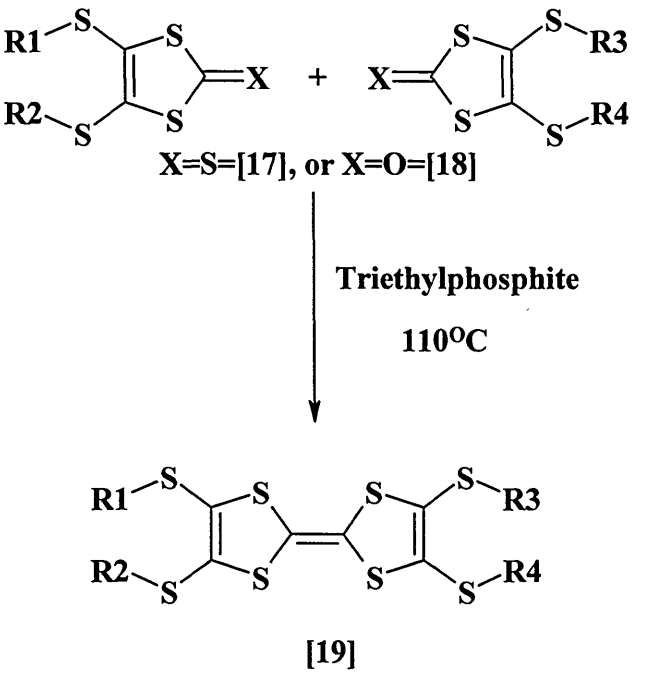

[19]

Figure 16, DMIT's → TTF's

This type of coupling reaction is widely used in TTF synthesis[26,31,39,76-79], and extensive studies have been carried out to elucidate the mechanism of the reaction[41], shown in Figure 17. The scheme applies to 1,3-dithiole-2-ones**[18]** as well as to 1,3-dithiole-2-thiones**[17]**.

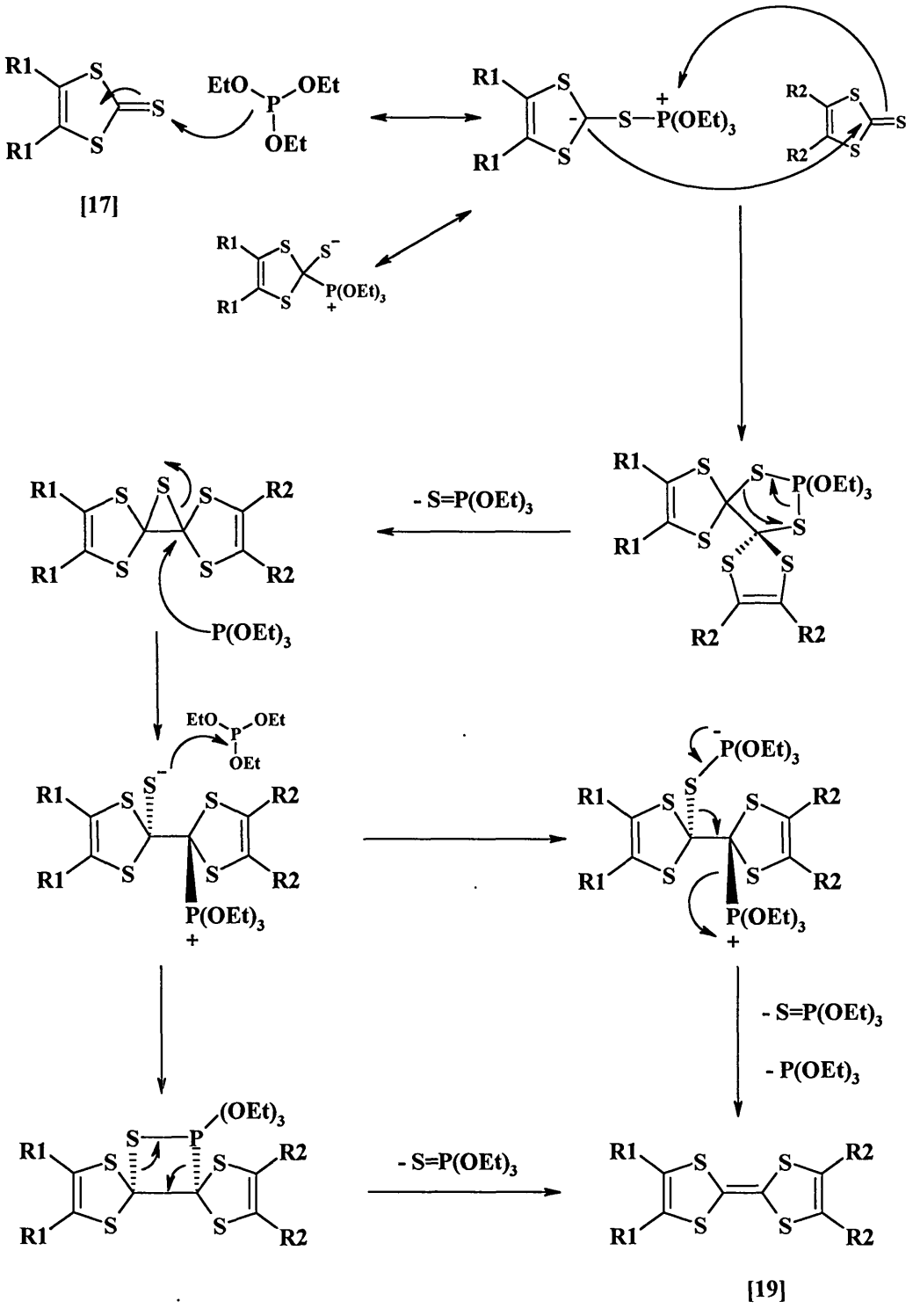

Figure 17, Thione coupling mechanism

From the TTF structure**[19]** shown in Figure 16 it becomes clear that this technique may be used to form a variety of TTF derivatives, particularly

symmetrical and unsymmetrical TTF's (from a mixed coupling reaction). Unsymmetrical 1,3-dithiolethiones**[20]** can be prepared from 4,5-bis(2'-cyanoethylthio)-1,3-dithiol-2-thione**[15]** or 4,5-bis(benzoylthio)-1,3-dithiol-2-thione**[14]** (Figure 13), using the strategy shown in Figure 18.

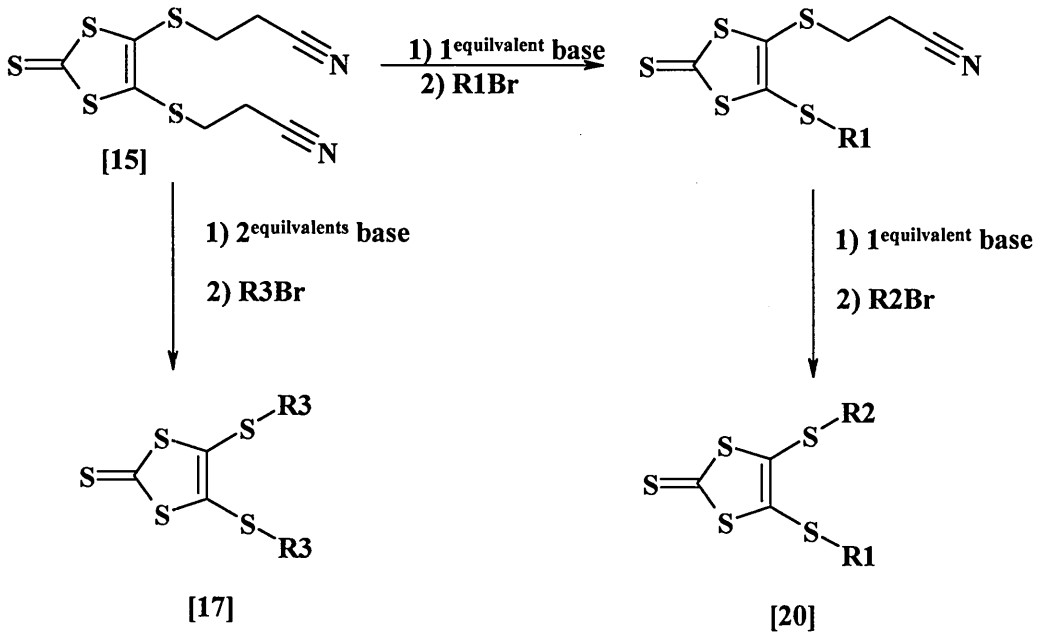

Figure 18, Unsymmetrically substituted DMIT's

This reaction scheme enables a wide range of compounds to be synthesised, and utilising the carbon disulphide reduction method followed by the appropriate use of the protected DMITs, is now the main synthetic scheme to preparing DMIT**[11]** and TTF derivatives**[19]**[1,70,75,80].

Other routes to DMIT[11] containing compounds have been developed over the years, but in comparison to synthetic strategies using zincate[13] as the starting material they generally prove to be long, difficult and relatively low yielding. An example[70] of one of these reaction schemes is shown in Figure 19.

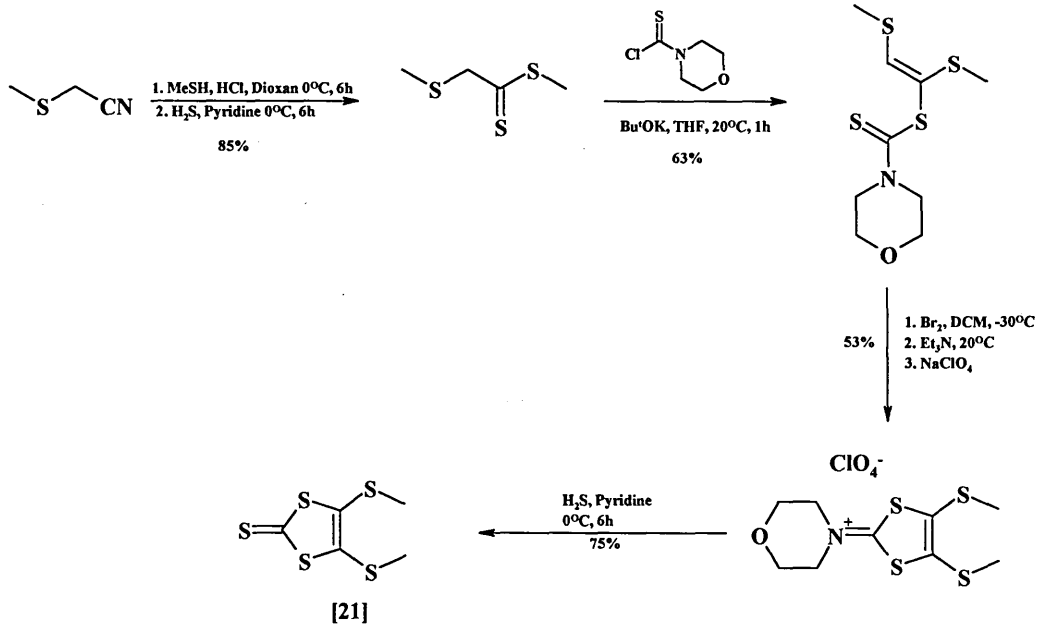

Figure 19, Further routes to DMIT's

If the starting point for the production of this alkyl DMIT, 4,5-bis(methylthio)-1,3-dithiole-2-thione[21], is the zincate[13] salt, then the compound can be synthesised in one step, Figure 20.

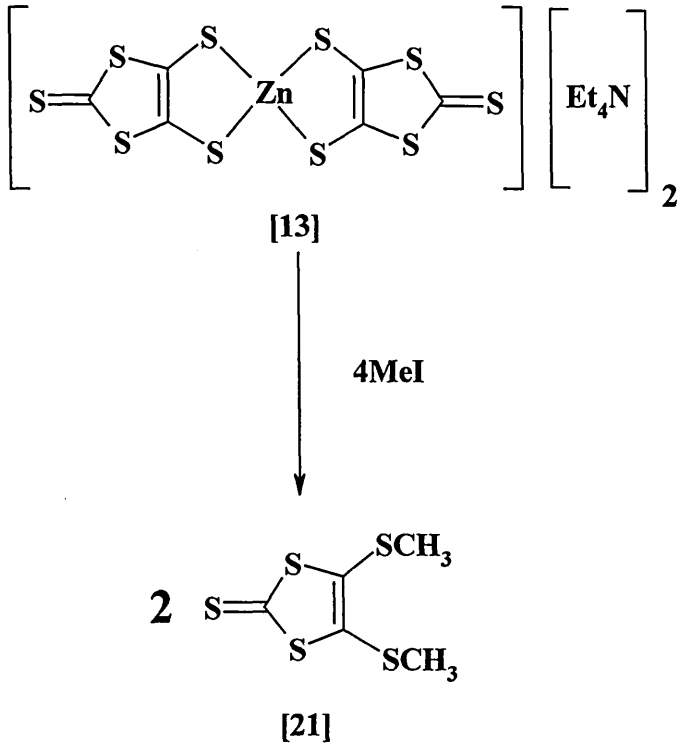

Figure 20, Zincate route to 4,5-bis(methylthio)-1,3-dithiole-2-thione**[21]**

Such attempts at alternative routes to DMITs do however still produce highly interesting and novel synthetic and mechanistic pathways to chalcogen ring systems, a further example of these attempts[70] is shown in Figure 21.

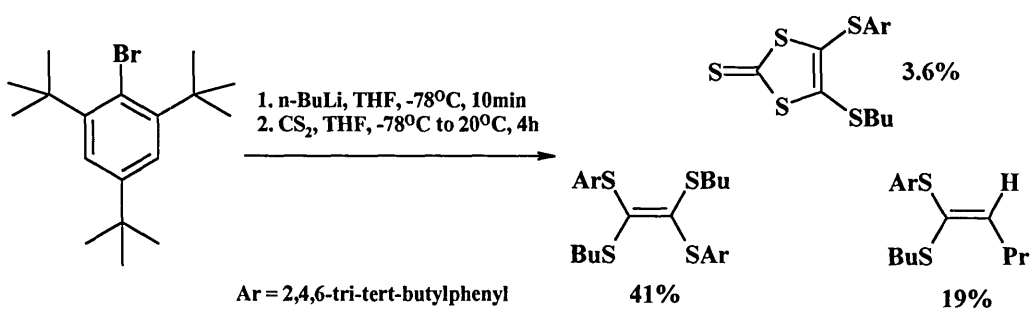

Figure 21, Further routes to DMITs example 2

The mechanism for this reaction is believed to proceed by a tetrathioxalate intermediate, similar to the mechanism for the reduction of carbon disulphide. This scheme provides a highly interesting route to asymmetrically alkylated DMITs, but the yield is very poor.

The extensive study of DMIT**[11]** chemistry has also yielded reaction schemes that enable TTF**[2]** itself to be prepared from a relatively easily obtainable DMIT derivative 4,5-bis(benzoylthio)-1,3-dithiol-2-thione**[14]**[37]. The synthesis of TTF**[2]** remains a popular and important research topic owing to the high cost of commercially available TTF[37,38]. Meline et al. report the synthesis of TTF**[2]** from 4,5-bis(benzoylthio)-1,3-dithiol-2-thione**[14]**[37] by the reaction scheme shown in Figure 22.

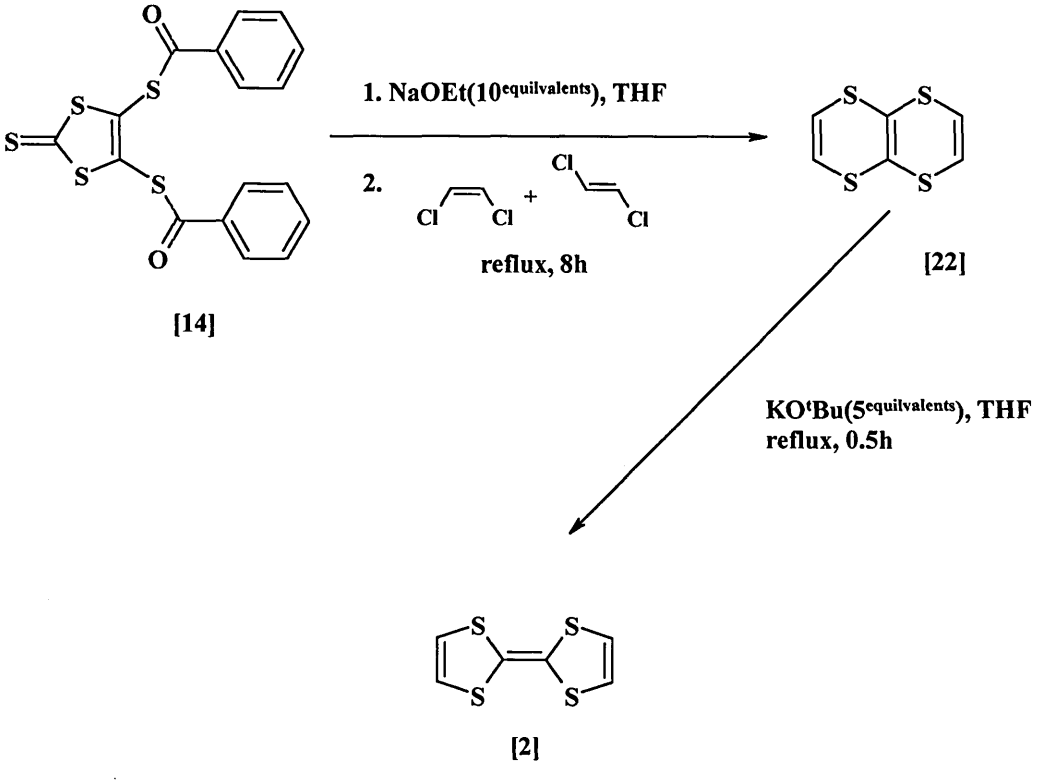

Figure 22, TTF from 4,5-bis(benzoylthio)-1,3-dithiol-2-thione

The reaction is believed to proceed not by the simple nucleophilic displacement of chlorine from cis-1,2-dichloroethylene, but by an elimination-addition mechanism outlined in Figure 23. It is believed[37] that the cis isomer of dichloroethylene not the trans reacts when an excess of sodium ethoxide is used and the presence of the trans isomer becomes unimportant. The use of excess sodium ethoxide under refluxing conditions not only deprotects 4,5-bis(benzoylthio)-1,3-dithiol-2-thione**[14]** to give Na_2DMIT**[11]**, as stated previously, but under these conditions will react with the thione to give the ethylene tetrathiolate intermediate (compare with the reaction shown in Figure 15, in which the carbonyl derivative reacts with ethoxide at room temperature). Subsequent reaction of the TTF isomer TTN**[22]** (tetrathianapthalene), with potassium-*tert*-butoxide causes a rearrangement of TTN**[22]** to yield TTF**[2]**. The mechanism for this reaction still has to be conclusively established, and alternative interpretations of the reaction schemes are still being investigated[81].

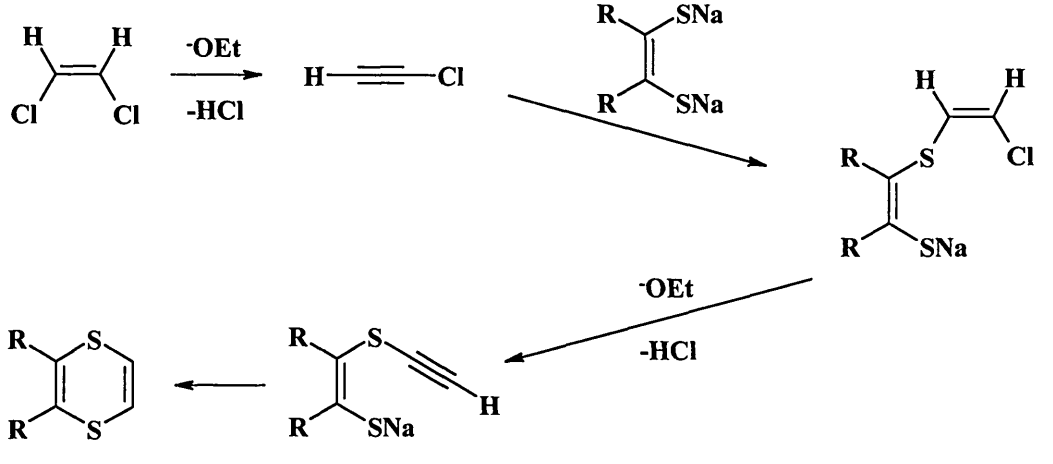

Figure 23, Meline et al., proposed mechanism

The use of DMIT**[11]** in the synthesis of conducting and electroactive compounds is however not just limited to its use as a synthon for TTF**[2]** or dithiolene**[9]** complexes. The DMIT**[11]** molecule itself is known to form superconducting complexes; up to 2000 eight examples of DMIT**[11]** based superconductors had been reported[1]. These complexes being;

- $[TTF][Ni(DMIT)_2]_2$
- α-$[TTF][Pd(DMIT)_2]_2$
- α'-$[TTF][Pd(DMIT)_2]_2$
- α-$[EDT\text{-}TTF][Ni(DMIT)_2]_2$ *EDT-TTF = ethylenedithio-tetrathiafulvane*
- β'-$[Me_2Et_2P]_{0.5}[Pd(DMIT)_2]$
- $[Me_4N]_{0.5}[Ni(DMIT)_2]$
- β-$[Me_4N]_{0.5}[Pd(DMIT)_2]$
- $[Me_2Et_2N]_{0.5}[Pd(DMIT)_2]$

These complexes demonstrate the two types of electron transfer salts that are obtained from $M(DMIT)_2$[1],

(a) Donor-acceptor compounds of the type $[D][M(DMIT)_2]_y$, with D the appropriate donor molecule.

(b) Cation-deficient non-integral oxidation state complexes $[C]_x[M(DMIT)_2]$.

Complexes of these types are typically prepared[1,75,80,82,83] electrochemically or by metathesis, but electrochemical techniques are commonly favoured as they tend to produce cleaner and better quality crystals of the complexes, in particular the use of electrocrystallisation is widespread to overcome the common lack of solubility demonstrated by these type of compounds.

When preparing the $[D][M(DMIT)_2]_y$ donor-acceptor compounds the, $M(DMIT)_2$ complexes can be considered as moderate acceptors and when used with appropriate donor molecules produce donor-acceptor systems in which partial charge transfer occurs. As stated previously these $[D][M(DMIT)_2]_y$ compounds, can be either chemically or electrochemically prepared. For chemical preparation the $[M(DMIT)_2]^0$ neutral complex is required and is often difficult to obtain[1]. Because of this limitation the direct reaction between a neutral donor and acceptor is not generally possible. This has led to the use of a metathesis reaction between D^+ and the $[M(DMIT)_2]^{-1}$ salts by the general reaction scheme:

$$nD^+ + ny[M(DMIT)_2]^{-1} \rightarrow ([D][M(DMIT)_2]_y)_n$$

Electrochemical techniques can also be used to generate D^+, and when used with an appropriate diffusion cell, have yielded numerous electroactive complexes[1,75,80,82-86].

A number of the non-integral oxidation state complexes ($[C]_x[M(DMIT)_2]$) have been produced by electrochemical (and chemical) oxidation, the use of electrocrystallisation being most common for these complexes. Typically a U or H shaped electrolysis cell (an example of which is shown in Figure 24), with the compartments separated by a low porosity glass frit, are used with a solution of the $[C][M(DMIT)_2]$ complex and a solution of the C cation salt are placed in each compartment. The electrodes are then inserted in both compartments, and galvanostatic electrolysis (0.1 to 5 μA) used to produce crystals of the $[C]_x[M(DMIT)_2]$ complex at the anode according to the reaction:

$$n[C][M(DMIT)_2] \rightarrow ([C]_x[M(DMIT)_2])_n + n(1-x)C^+ + n(1-x)e^-$$

Figure 24, Electrocrystallisation cell

Such techniques have been used to prepare a wide range of complexes but most reactions produced compounds that exhibit semi-conducting properties. To date few have been found to show superconducting transitions[1,4,75,80,82].

In preparing metal chelates of DMIT**[11]**, specifically the complexes of the type $[C]_x[M(DMIT)_2]$, generally only the zincate **[13]** is made directly from carbon disulphide (Figure 10 shows the synthesis of zincate). The general method therefore applied to synthesise DMIT chelates is the solvolysis of 4,5-bis(benzoylthio)-1,3-dithiol-2-thione**[14]** by methoxide or ethoxide followed by an in situ reaction of the generated DMIT**[11]** with the corresponding metal salt (Figure 25). Combining the anionic complex with a suitable cation enabled a wide assortment of complexes**[23]** to be isolated as crystalline salts.

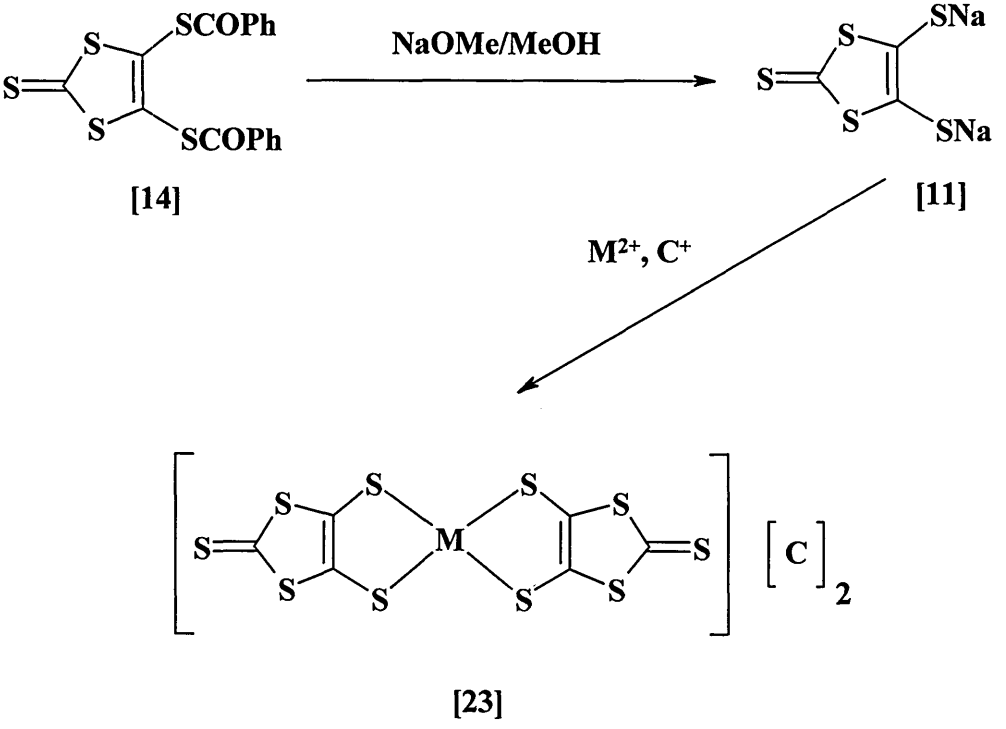

Figure 25, Synthesis of other DMIT complexes**[23]**

Many DMIT complexes**[23]** have been prepared using this general method[1,4,73,75,80,87-95], and many were obtained simply by changing the metal and maintaining the cation as an alkylammonium ion. Numerous chelates have also been prepared (particularly the complexes based on $[Ni(DMIT)_2]^{n-}$) with the alkylammonium ions exchanged for ions based on sulphonium, sulphoxonium, phosphonium, arsonium, sodium, and potassium cations.

All of the organic compounds mentioned so far continue to be the focus of extensive research attention, and sulphur based chalcogen systems remain among the most extensively studied. The synthesis of the other chalcogen analogues, in particular selenium derivatives, of the DMIT**[11]** compounds continues to broaden the knowledge base of organic metals and related areas. It is interesting to note however[4], that except for the area of "doped fullerides" all the molecular organic superconductors and most of the organic conductors are derived from TTF type compounds. Similarly, the molecular inorganic superconductors and conductors are derived from nickel and palladium complexes of DMIT**[23]**.

1.2 MAGNETIC COMPOUNDS

The first molecules exhibiting spontaneous magnetisation below a critical temperature were reported during the mid 1980s[96]. These ground breaking results initiated a large number of research groups from organic, inorganic and organometallic fields to investigate compounds that produced this phenomena and many new molecule-based magnets were discovered and characterised. In most cases, the spin carriers (atoms responsible for the observed magnetic properties) are transition metal ions and in some cases organic based radicals (with the radical centred commonly on S or N atoms)[97-101], the resulting magnetism arising entirely from unpaired p electrons.

Substances were first classified as diamagnetic or paramagnetic by Michael Faraday in 1845[3,10]. It was not until much later however that these phenomena were more fully understood and could be described in terms of electronic structure. The magnetic phenomena is classified under the following titles[2-4,9,102,103].

1.2.1 FERROMAGNETISM

Ferromagnetism is the only type of magnetic interaction that is commonly noticed, the most well known example of this phenomena is observed when an iron nail is picked up by a magnet. Compared with other kinds of magnetic behaviour, this is an extremely powerful interaction and is found to depend on two factors:

- A ferromagnetic substance must contain unpaired electrons, each of which behaves as a tiny magnet and is attracted to an ordinary magnet if properly oriented (north-to-south/south-to-north).
- The phenomenon of cooperativity: one electron that is correctly oriented to be attracted by a magnet assists the other electrons in the substance to achieve the same orientation. So when a piece of iron is placed near a magnet, a very large proportion of its unpaired electrons line up in the direction that causes it to be attracted. From the point of view of classical electromagnetic formalism, the magnetic field lines are drawn into the ferromagnetic substance.

Ferromagnetism is utilised in numerous ways in everyday life, and popular visible uses of this property of matter includes such trivial applications such as refrigerator magnets and magnetised DIY tools. However, the number of substances that exhibit ferromagnetism is quite limited, these include iron, cobalt, nickel, their alloys and a few other elements and compounds[2-4].

1.2.2 PARAMAGNETISM

Paramagnetism is the same general kind of interaction as ferromagnetism, but it is generally unnoticed because it is orders of magnitude weaker. Substances which exhibit this phenomena also have unpaired electrons that can be aligned in a magnetic field and attracted by a magnet. Unlike ferromagnetic substances in which these electrons are close together, in the case of paramagnetic substances they are confined to isolated atoms. As a consequence of this, cooperativity is lacking, i.e. the correct orientation of an unpaired electron in one atom does not influence the orientation of that in another. The reason that all the electrons are not aligned in such a way as to be attracted by a magnet, is that atoms are vibrating from thermal effects, and this vibration tends to disorient the unpaired electrons. With all this movement however, electron spin is quantized, and for the one-electron case the magnetic moment of an electron must at any one time line up with or against an externally applied magnetic field.

1.2.3 DIAMAGNETISM

Diamagnetism is an entirely repulsive interaction with a magnetic field, and is orders of magnitude weaker than paramagnetism, occurring in substances that contain no unpaired electrons. The interaction arises not from the magnetic moment of an electron, which is cancelled out by the electron with which it is paired, but from its charge. In the classical picture, when exposed to a magnetic field, the "orbit" of the electron begins to precess in such a way as to produce a small magnetic moment parallel to the external magnetic field (north-to-north/south-to-south), which tends to force it out of the field. In the classical electromagnetic picture, magnetic field lines avoid the diamagnetic sample. Since all compounds contain some paired electrons, diamagnetism is therefore a universal property of all matter. But as mentioned above the diamagnetic effect is significantly weaker than that of paramagnetism and so substances having only one unpaired electron per molecule will be paramagnetic.

While ferromagnetism, paramagnetism and diamagnetism are the main definitions by which magnetism is quantified, a further aspect of magnetic behaviour is that of *ferri*magnetism and *antiferro*magnetism. When considering ferromagnetism the magnetic dipoles on the neighbouring atoms tend to be aligned parallel to one another i.e. ferromagnetism. It is therefore possible that the tendency for an antiparallel arrangement of the coupled spins is observed i.e. antiferromagnetism. Ferrimagnets, such as magnetite (Fe_3O_4), result from antiferromagnetic coupling that does not lead to complete cancellation and thus have a net magnetic moment. This ordering of magnetic dipoles to a ferro-,

antiferro-, and ferrimagnetic state only occurs below a critical or magnetic ordering temperature, T_c. A diagrammatic representation of this is shown in Figure 26.

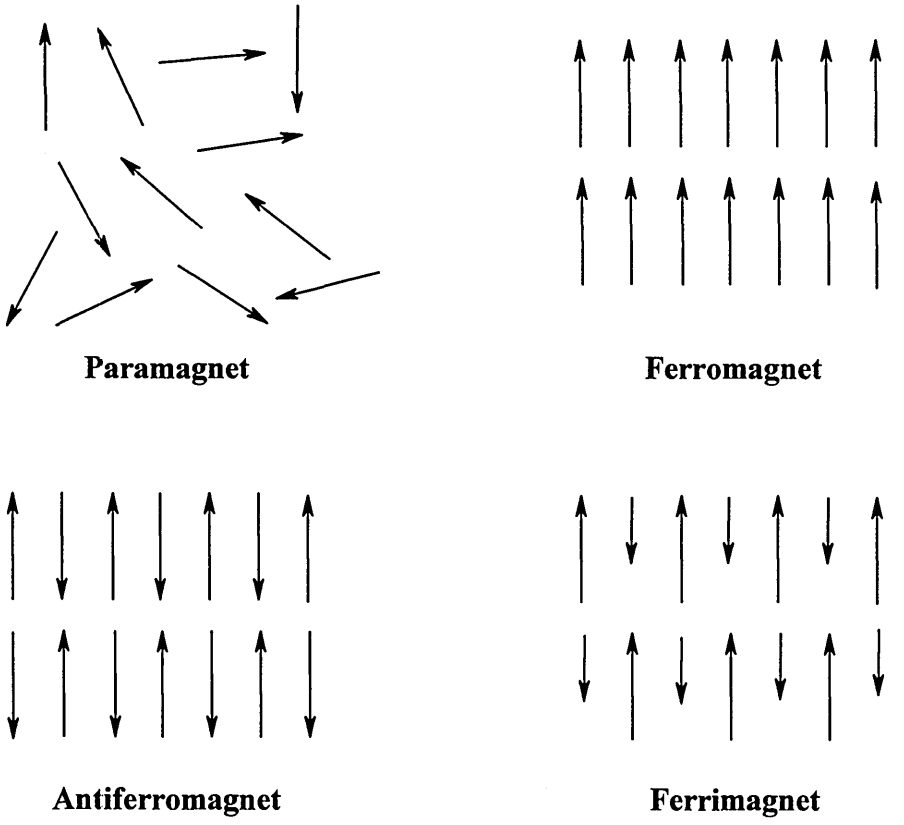

Figure 26, Magnetic dipole arrangements.

One of the main ventures in the field of molecular materials now concerns the design and preparation of molecular based magnetic materials exhibiting spontaneous magnetism below a critical temperature T_c. However in spite of much effort in the field relatively few compounds have so far been prepared[2,4]. Compounds that have been characterised do include such systems as:

Magnetic chain compounds, essentially one dimensional ordering, commonly composed of an array of equally spaced ions with identical spins. An example of which is a ferromagnetically coupled Cu^{2+} chain such as is formed by hexylammonium trichlorocuperate(II), $[CuCl_3(C_6H_{11}NH_3)]$ often referred to as CHAC[4]. Further examples of this type of system have included *ferri*magnetic chains of $[MnCu(dithiooxalato)_2.(H_2O)_3.4.5H_2O]$.

Magnetic long range ordering in molecular compounds, whereas in magnetic chain compounds the magnetic ordering occurs along one axis of the system i.e. along the chain. In other cases two and three dimensional ordering of the magnetism occurs. In such systems the magnetic properties show a marked change at T_c; as the temperature of the system changes the three dimensional ordering changes giving well defined transitions from a paramagnetic state to an ordered magnetic state. Miller et al.[4,104] characterised a ferromagnetic transition in the organometallic donor-acceptor salt decamethylferrocenium tetracyanoethenide. This compound is prepared from a simple electron transfer between an electron donor decamethylferrocenium ($FeCp^*_2$) and an electron acceptor tetracyanoethylene (TCNE), to produce the complex**[24]** shown in Figure 27.

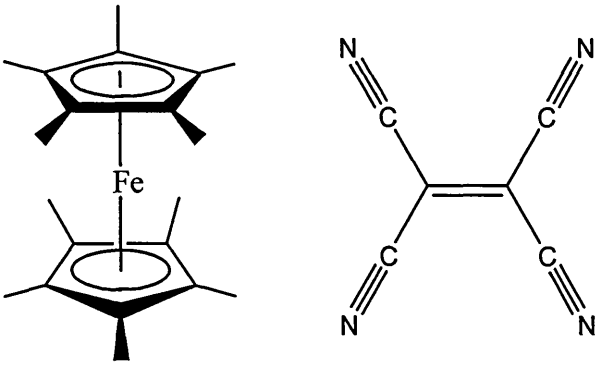

Figure 27, Fe(Cp*2) and TCNE**[24]**

This material was crystallised from acetonitrile, and subsequent crystal analyses showed chains of alternating $[FeCp^*_2]^+$ and $[TCNE]^-$ units with significant inter- and intra-chain interactions with the compound exhibiting bulk ferromagnetic properties with spontaneous magnetism below T_c = 4.8 K. Many important systems found to show ferromagnetism are based on metallocene systems including the manganese complex $[Mn(\eta\text{-}C_5Me_5)_2]^+[TCNQ]^-$; such related donor-acceptor complexes continue to provide new and interesting insights into magnetic molecules[2,4]. A further range of molecules that have been found to produce molecular magnets are those based on oxamidobis(carboxylato)Cu(II) dianions**[25]**[96], Figure 28. On binding Mn(II) through both the oxamido group and one of the carboxylato groups the resulting complexes are found to give magnetic compounds.

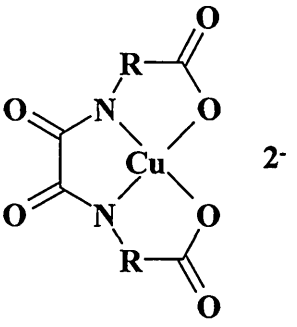

Figure 28, oxamidobis(carboxylato)Cu(II) dianions**[25]**

A good example of these type of complexes is that of $[Cu(obbz)]^{2-}$**[26]**, (obbz = oxamido-bis(N,N'-benzoato), Figure 29) when combined with Mn(II) gave two phases of the formula:

1) $[MnCu(obbz).5H_2O]$ which orders antiferromagnetically at 2.3K.

2) $[MnCu(obbz).H_2O]$ which orders ferromagnetically at 14K.

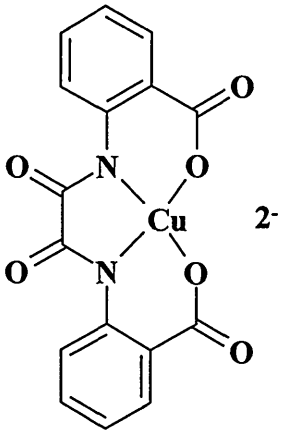

Figure 29, oxamidobis(N,N'-benzoato)Cu(II)**[25]**

Results such as these have maintained the momentum in this important molecular materials area of research. The data obtained continues to give valuable insights in the mechanism of molecular magnetism and the mechanisms involved in the 1D molecular magnets have been convincingly resolved[2,4]. The mechanisms involved in the more complicated systems however still raise questions and new types of compounds continue to widen the knowledge base being used to explain these systems. A popular area of this work at present is the quest to produce soluble ferromagnets, and such a type of processability would provide an interesting further aspect to this area of materials chemistry.

1.3 DIHALOGEN ADDUCTS

In recent years there has been increasing interest in the adducts formed through the interaction of dihalogens (Cl_2, Br_2, I_2), or interhalogens (ICl and IBr) with donor system, D, and in particular the donor systems based on sulphur. The interest in these adducts is in no small part due to their potential in the areas of synthetic reagents, pharmaceuticals and in materials chemistry in the form of electroactive materials[105-108]. The ability of some group 16 compounds to form adducts with dihalogen acceptors has long been known[3,10], a good example of this is demonstrated by diiodine. Diiodine dissolves in numerous organic solvents to give a wide range of colours,

- violet solutions (520-540 nm) in solvents such as aliphatic hydrocarbons and carbon tetrachloride.
- pink-red solutions (490-510 nm) in aromatic hydrocarbons solvents.
- brown solutions (450-480 nm) in alcohols and amines.

The reason for this observation is well understood and is explained by considering the bonding system of diiodine. The electronic structure of diiodine is $1\sigma_g^2$, $1\sigma_u^2$, π_u^4, $2\sigma_g^2$, π_g^4 with an empty $2\sigma_u$ antibonding orbital[3,10]. The normal violet colour of gaseous diiodine is explained by the absorption caused by a $\pi_g \rightarrow 2\sigma_u$ transition. Therefore if the diiodine molecule is dissolved in a solvent that is an electron donor the energy gap between $\pi_g \rightarrow 2\sigma_u$ will change, the more strongly the solvent molecule donates electron density (i.e. the solvent-diiodine

system shows donor-acceptor or charge transfer properties) the greater the energy separation of $\pi_g \rightarrow 2\sigma_u$. In the case of poor donors such as saturated hydrocarbons the interaction is extremely weak (effectively non-existent) and hardly affects the diiodine molecule hence the absorption maximum of the I-I bond in such solutions is similar to that of gaseous diiodine. In the case of aromatic solvents the π electrons are more effective donors, and solvents containing electron-pair donors such as ROH, R_2O, RNH_2, RSH etc., are even more effective at donating electron density to the diiodine and the shift in the absorption maximum is toward shorter wavelengths and hence higher energies. When extremely good donors are used the interaction becomes a "proper" reaction not just a weak electronic interaction, typified by the reaction of diiodine with pyridine:

$$2I_2 + 2py \rightarrow 2pyI_2 \rightarrow [Ipy_2^+][I_3^-]$$

The other dihalogens Cl_2, Br_2 and the interhalogens IBr and ICl are known to undergo similar interactions, and the large range of possible adducts that can be prepared maintains a strong research interest in this area, from solution studies to the very popular isolation and structural determination of crystalline halogen adducts which provide good evidence for the formation of charge-transfer systems.

The majority of the dihalogen and interhalogen adducts that are investigated are described as charge transfer complexes. While this has already been mentioned it is necessary to define the concept of charge

transfer[2,4,10,105,109-119]. In the simplest sense charge transfer is defined as a weak co-ordination involving a transfer of electron density. A better description is that charge transfer occurs from the movement of an electron from an orbital of a donor (mainly a ligand) to an orbital of an acceptor (commonly a metal, and hence ligand to metal charge transfer). These electron transitions often result in very intense absorptions that are easily detectable by electronic spectroscopy and typically gives rise to brightly coloured compounds. A further important characteristic of charge transfer complexes is that of the interesting structures formed by these systems. Many charge transfer complexes prove to be highly crystalline compounds, and early proof for charge transfer was provided from electron density maps in the early 1960s. It became clear that single crystal X-ray diffraction experiments were vital in elucidating the exact nature of charge transfer adducts, by providing vital information on the resulting inter- and intra-molecular distances between all the constituent moieties present in a charge transfer complex.

Although many different donor molecules have been investigated, those containing sulphur or selenium donor atoms remain amongst the most intensively studied, not least because of the wide variety of donors available including thio- and seleno-ethers, thiocarbonyls(thiones), selenocarbonyls(selenones), thio- and seleno-amides, and tertiary phosphine, sulphides and selenides. The precise nature of these adducts has been found to depend on a variety of factors, from the identity of the donor atom (i.e. S or Se) through to the dihalogen or interhalogen used, the stoichiometry of the reactants, the nature of the groups bound to the donor atom(s) and in some cases the solvent present. In many cases even slight

changes in any of these factors was often found to result in a change of the solid state structure of the subsequent complex, and such variation in structure has provided an extensive range of data for researchers interested in the nature of the chemical bond, with many of these halogen adducts showing bonding properties that border on ionic and covalent character.

Treatment of a sulphur or selenium donor with an equivalent of dihalogen can result in the formation of a number of different products (Figure 30) depending on the nature of the donor and acceptor.

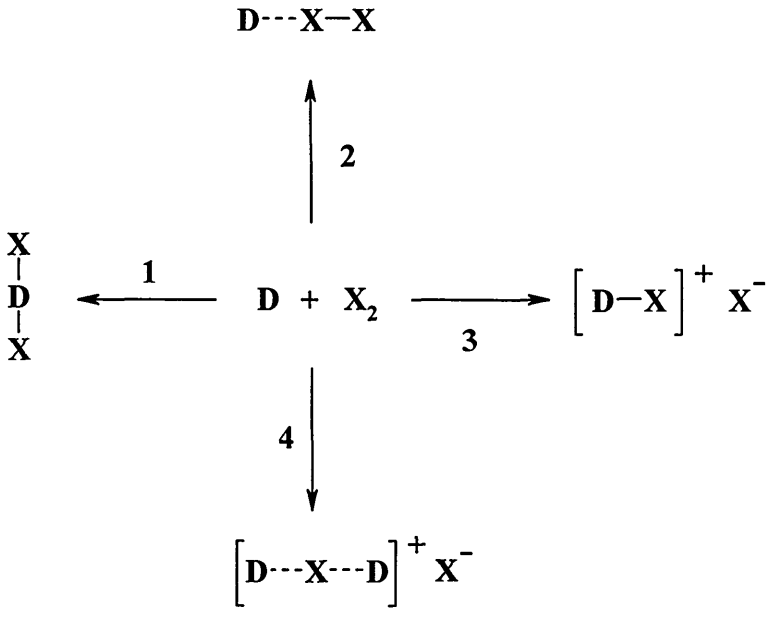

Figure 30, Reaction of a donor atom with dihalogens

For example, insertion/oxidative addition products (Figure 30, reaction 1) formed from the homolytic cleavage of the dihalogen bond. Charge transfer complexes (Figure 30, reaction 2) as described previously, arise from the donation of

electron density from the chalcogen to the vacant antibonding orbital on the dihalogen. The resulting bond lengths of the halogen-halogen interaction produced in these systems have been well characterised, and the apparent strength of the charge transfer in relation to this bond length has been rationalised by Deplano et al.[120]. In cases where the donor-halogen interaction is particularly strong, this can lead to the halogen-halogen bond being broken to yield an ionic species shown by Figure 30, reaction 3. Finally, in some cases more complex compounds such as ionic halogen(I) (Figure 30, reaction 4), and poly(halogen) and poly(halide) systems are produced. While much of the attention on the dihalogen charge transfer adduct systems is in relation to the fascinating structural diversity observed, extensive work on the solution properties and thermodynamic parameters of these systems have been comprehensively studied[108] and provide new insights into the mechanism of formation of such compounds.

As mentioned above a wide range of donors have been investigated in respect to charge transfer complexes of the dihalogens, one of the most popular being those of the thiones (or thiocarbonyls) as a result of their potential in such diverse uses as molecular electronics or the treatment of hyperthyroidism[105]. A significant result that gives insight into the formation of these type of systems was presented by Bigoli et al.[121]. The formation of diiodine adducts in two similar systems was presented which showed the significance of the nature of the groups bonded to the sulphur donor. The diiodine adducts of the related

trithiocarbonate derivatives 1,3-dithiolane-2-thione**[27]**, and 1,3-dithiole-2-thione**[28]** were prepared, Figure 31.

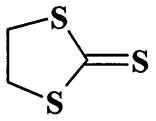

1,3-dithiolane-2-thione[27]

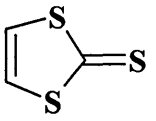

1,3-dithiole-2-thione[28]

Figure 31, 1,3-dithiolane-2-thione**[27]**, and 1,3-dithiole-2-thione**[28]**

The results showed that when a 1:1 complex of I_2 was prepared with these compounds the formation constant for 1,3-dithiole-2-thione**[28]** was almost twice that of 1,3-dithiolane-2-thione**[27]**, and with significantly higher enthalpy of formation. From this data the planar nature of 1,3-dithiole-2-thione**[28]** appears to show that the carbon-carbon double bond is participating in the bonding interactions through delocalisation of the π electrons, which is not possible in the puckered ring system found in the 1,3-dithiolane-2-thione**[27]** moiety thereby making **[28]** a more effective donor system towards dihalogens.

As described in section 1.1.4, the range of trithiocarbonates synthesised is quite extensive, and therefore a wide range of dihalogen adducts of these systems is possible enabling the range of DMIT type compounds to be further expanded. The synthetic utility of DMIT has allowed the effects of various substituents of the thione to be investigated, including the effects of electron donating and withdrawing groups to be elucidated. Recent interesting results which have given insights into the chemistry of thione-dihalogen systems has come from many

research groups[107,108,120,122,123], showing the wide ranging effects of different substituents on the rate and equilibrium constants on thione-I_2 complexes. In a recent publication from the group of Bricklebank and Skabara[105], a practical illustration of the effect of reaction conditions and choice of halogen on the subsequent dihalogen adduct was presented. These workers described the structural nature of the adducts formed from the interaction of diiodine, iodine monobromide and dibromine with the DMIT derivative 4,5-bis(methylthio)-1,3-dithiole-2-thione**[21]**, Figure 32.

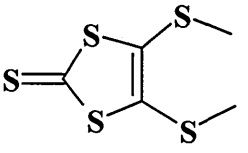

Figure 32, 4,5-bis(methylthio)-1,3-dithiole-2-thione**[21]**

The reactions of 4,5-bis(methylthio)-1,3-dithiole-2-thione**[21]** (diMeDMIT) with I_2, IBr and Br_2 are shown in Figure 33. It was demonstrated that addition of an equimolar quantity of I_2 or IBr to a solution of (diMeDMIT) in refluxing DCM resulted in the development of an orange-red solution from which brown crystals of (diMeDMIT)•I_2**[29]** (85% yield) were deposited. In the reaction with IBr cooling the reaction mixture to -5^{O}C yielded (diMeDMIT)•IBr**[30]**. When this reaction is repeated with Br_2 a brown microcrystalline powder of (diMeDMIT)•Br_2**[31]** in 50% yield is deposited. On evaporation of the remaining DCM a purple oil is produced from which a small amount of purple crystalline material was isolated (10% yield); these crystals proved to be the dithiolylium

salt**[32]** shown in Figure 33, which proved to be hydroscopic and emitted Br_2 on standing. Repeating the reaction at a higher temperature by refluxing in toluene produced only the (diMeDMIT)•Br_2**[31]** complex with no trace of the dithiolylium salt**[32]**.

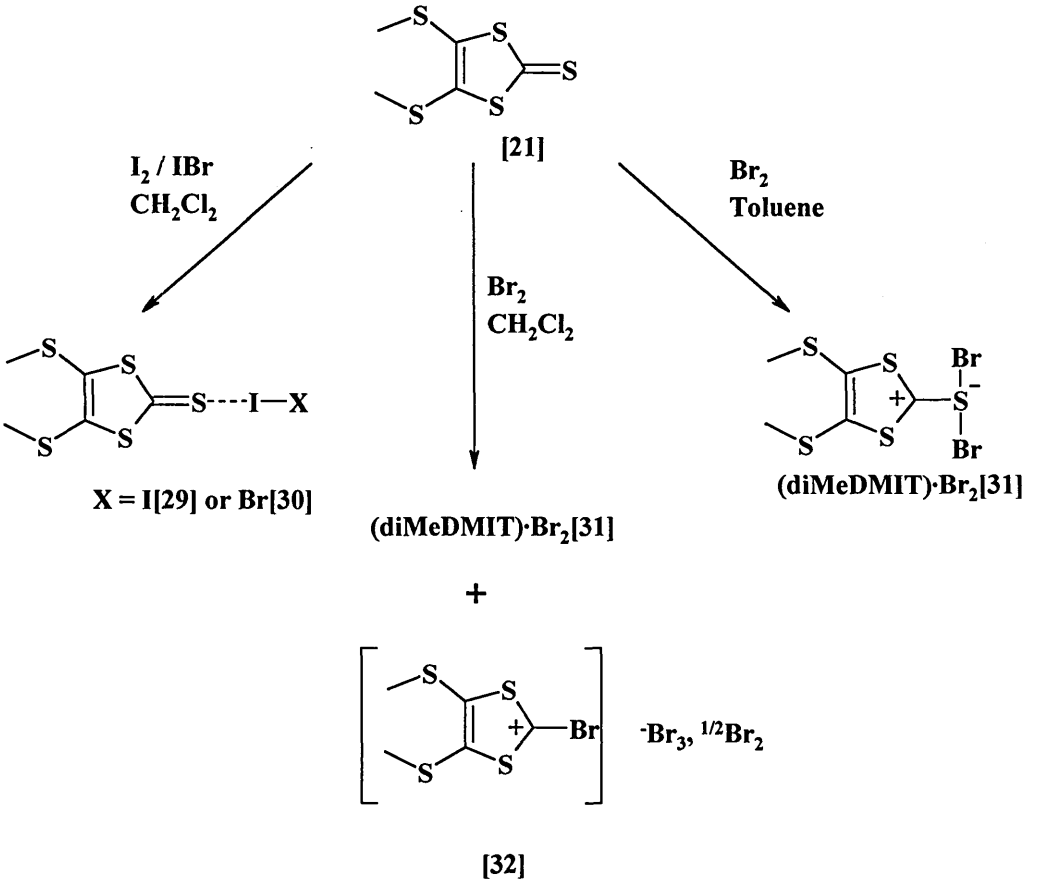

Figure 33, Reaction of 4,5-bis(methylthio)-1,3-dithiole-2-thione with X_2

The molecular structures of charge transfer complexes **[29]** and **[30]** conforms with established theory of the transfer of electron density from the lone pair of a donor atom to the σ* antibonding orbital of the dihalogen leading to the formation of a donor-halogen bond with the concomitant elongation of the halogen-halogen bond. These reactions demonstrate nicely the ability of thiones,

and especially the trithiocarbonates, to delocalise the charge of the resulting complex, the sulphur atom of the thione donor being sp^2 hybridised with a double bond to the adjacent carbon atom rendering these systems good electron donors. The ability of these systems to delocalise the positive charge onto the carbon atom of the C-S bond is an additional factor in the stabilisation of the S-X-X interaction in thiones, and the ability of the additional sulphurs present in the trithiocarbonates provides a further means of stabilisation as the charge may be further delocalised over the S-C-S portion of the compound's ring system forming a 6π pseudo-aromatic system, shown in Figure 34.

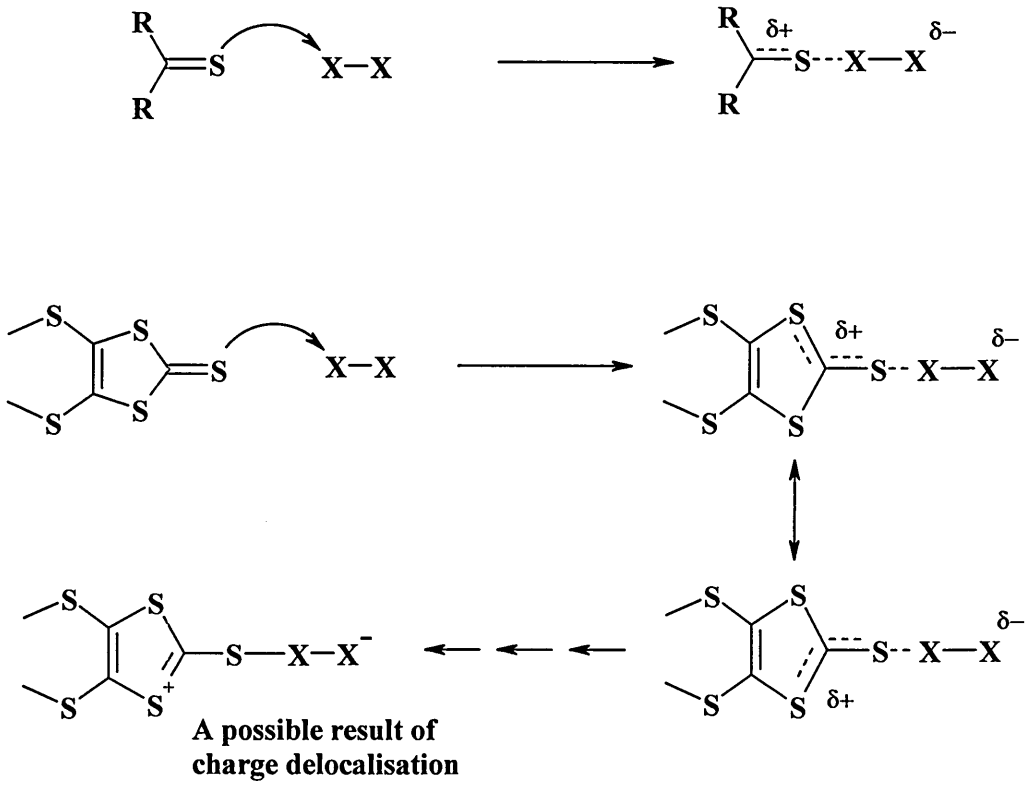

Figure 34, Charge delocalisation in thiones and trithiocarbonates.

From this rationalisation of the interaction of donors with dihalogens it becomes clear that thiones can form stronger S-X bonds than those of other sulphur systems in which the donor atom is sp^3 hybridised, such as thioethers. The range of different structures produced from one thione moiety by simply changing the nature of the halogen and solvent demonstrates that much more data is still required to fully understand and explain the reactions of dihalogens with group 16 donors. The reaction of 4,5-bis(methylthio)-1,3-dithiole-2-thione**[21]** with dihalogens produced the expected charge transfer complexes with I_2, but the unexpected nature of the complexes formed with Br_2 requires further explanation and further experimental data to be collected[105].

2 EXPERIMENTAL - ANALYTICAL METHODS

The following descriptions represent the general methods of analysis applied to the compounds presented in this research, any significant changes in the described analysis technique pertaining to individual compounds is described along with the analytical results for that compound.

2.1 MELTING POINT

Melting points were taken using Electrothermal melting point apparatus and are uncorrected.

2.2 MASS SPECTROMETRY

Mass spectra were recorded on a VG 7070E double focusing analytical mass spectrometer, with data recording and handling carried out on a microcomputer running mass spectrometer services software.

2.3 ELEMENTAL ANALYSIS

Samples intended for elemental analysis were vacuum dried at room temperature or at 50 ^{O}C as sample stability allowed. CHN analysis was carried

out by the analytical and chemical consultancy service company MEDAC Ltd, Brunel Science Centre, Coopers Hill Lane, Englefied Green, Egham, UK.

2.4 FOURIER TRANSFORM INFRA-RED SPECTROSCOPY (FTIR)

Solid samples were dried under vacuum at room temperature and analysed as KBr discs, oils were analysed as thin films between NaCl plates. FTIR spectra were recorded on an ATI Mattson Instruments Genesis Series FTIR spectrometer with data recording and handling carried out on a microcomputer using Winfirst software version 3.57.

2.5 ULTRAVIOLET/VISIBLE ABSORPTION SPECTROSCOPY (UV/VIS)

Samples were dissolved in an appropriate solvent to a concentration of ~$4x10^{-5}$ M and analysed in quartz cuvettes with a 2 cm pathlength. Instrumentation used was a Unicam UV2 UV/VIS spectrometer with data recording and handling carried out on a microcomputer using Unicam Vision software version 3.42.

2.6 NUCLEAR MAGNETIC RESONANCE SPECTROSCOPY (NMR)

Samples were dissolved in an appropriate deuterated solvent to a concentration of 10 to 20 mg mL^{-1} for proton and carbon-13 experiments. Spectra were obtained using a Brucker AC 250 MHz nuclear magnetic resonance spectrometer with data recording and handling carried out using a Brucker mass spec 3000 computer running ADAKOS version 890201.0 software. Chemical shift was expressed as ppm, and *J* values in Hz, samples were individually calibrated using the solvent signal or added TMS (TetraMethylSilane).

2.7 X-RAY CRYSTALLOGRAPHY

Crystalline samples were submitted to the EPSRC National Crystallography Service at the Department of Chemistry, The University of Southampton, Highfield, Southampton, UK.

2.8 MAGNETIC SUSCEPTIBILITY MEASUREMENTS

Vacuum dried finely divided powders or crystals of a sample were analysed using a Sherwood Scientific Magnetic Susceptibility Balance by the techniques outlined in the Sherwood Scientific instruction manual[124].

2.9 CYCLIC VOLTAMMETRY

The measurements were obtained on a BAS CV50W voltammetric analyser with iR compensation, using anhydrous DMF as the solvent, Ag/AgCl as the reference electrode and platinum wire and platinum disc (1.6 mm diameter) as the counter and working electrodes, respectively. All solutions were saturated with N_2 and contained the substrate at 10^{-4} M, together with Bu_4NPF_6 (0.1 M) as the supporting electrolyte. Data collection and handling was performed on a microcomputer using BAS CV-50W version 2.3 software.

2.10 RAMAN SPECTROSCOPY

Low frequency Raman Spectra were obtained on a Renishaw System 1000 spectrometer which comprised an integral Raman microscope (Olympus BH2 system), a stigmatic single spectrograph, and a Peltier-cooled CCD detector (400x600 pixels). The holographic notch filters allowed a lower spectral limit of ~100 cm^{-1}. The excitation wavelength used was 780 nm HeNe laser.

3 EXPERIMENTAL - DMIT COMPLEXES

3.1 LIGANDS

3.1.1 LIGAND SYNTHESIS

The following synthetic methods represent the optimised (with respect to yield and purity) conditions for these compounds. A general reaction scheme for the synthesis of these ligands**[33]** is shown in Figure 35. The synthesis of compound **[15]**(4,5 bis(2'-cyanoethylthio)-1,3-dithiole-2-thione), can be found in section 5.1.1. All chemicals are used as supplied by Aldrich™, unless otherwise stated.

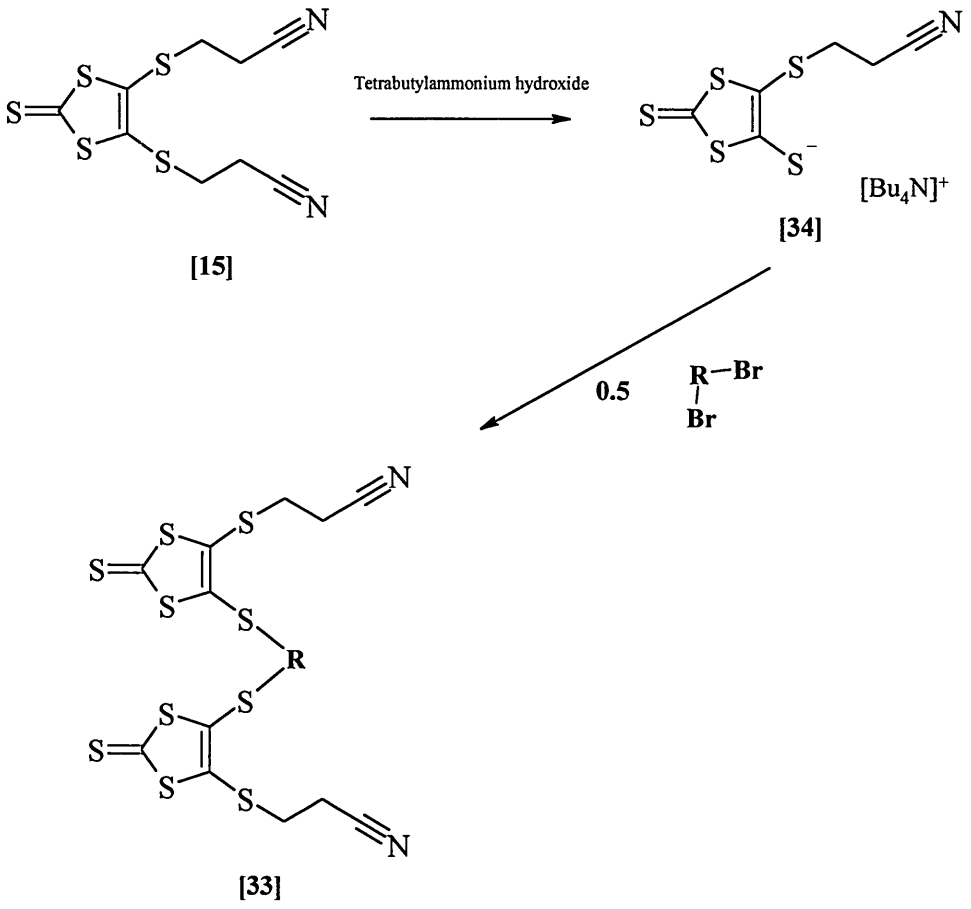

Figure 35, General reaction scheme for ligand**[33]** synthesis.

3.1.1.1 "ETHANE BRIDGE LIGAND, COMPOUND [35]"

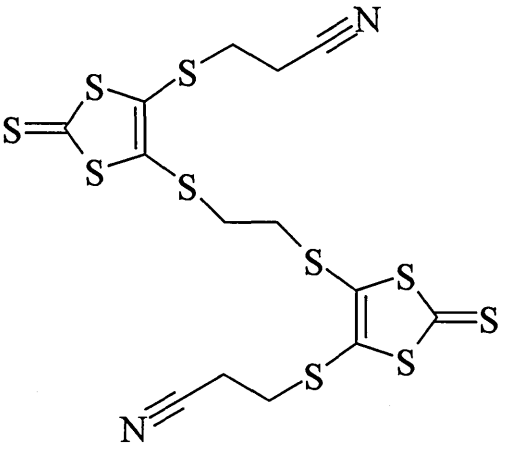

[35]

Figure 36, Ethane Bridge Ligand, compound **[35]**

Under N_2 using Shlenck techniques, compound **[15]** *[4,5 bis(2'-cyanoethylthio)-1,3-dithiole-2-thione]* (2 g, 6.57 mmol) was dissolved in dry distilled THF (40 mL) to give a yellow/orange solution. Maintaining the N_2 atmosphere tetrabutylammonium hydroxide (1.2 equivalents, 7.88 mmol = 7.9 mL of a 1M solution in methanol (Aldrich supplied)) was added dropwise over 20-30 minutes at -5 ^{O}C to give a purple solution of compound **[34]** (colour change yellow→orange→dark red/purple).

Compound **[34]** *is <u>not</u> isolated; it is stable in the dark under N_2 for several days, but appears to decompose in air after a few hours at RT and the solution turns brown with stench after several days in air)*

Maintaining the N_2 atmosphere, to the stirred solution of compound **[34]**, 0.6 equivalents (0.72 g, 3.94 mmol based on compound **[15]**) of 1,2-dibromoethane was added and the reaction stirred over night at RT (~16 hours) to give an orange

solution. The reaction was monitored to completion by TLC; compound **[35]** Rf = 0.3 in DCM. Compound **[35]** was purified on a flash silica column (DCM), to give a yellow solid on evaporation (yield 70%). Crystallisation from a minimum of boiling acetonitrile yielded small yellow crystals, yield 80%.

Compound **[35]** *is air stable for several months in the dark, but slowly decomposes to an orange powder with stench under air in light.*

3.1.1.2 "o-XYLENE BRIDGE LIGAND, COMPOUND [36]"

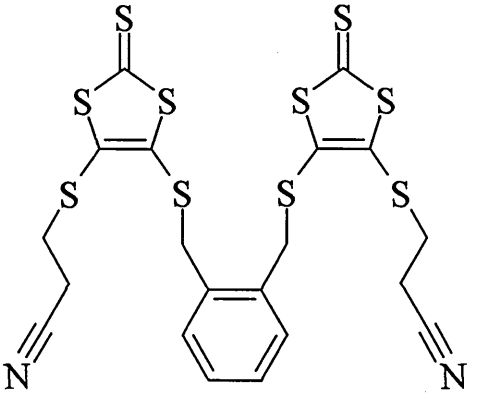

[36]

Figure 37, o-Xylene Bridge Ligand, compound **[36]**

Under N_2 using Shlenck techniques, compound **[15]** *[4,5 bis(2'-cyanoethylthio)-1,3-dithiole-2-thione]* (2 g, 6.57 mmol) was dissolved in dry distilled THF (40 mL) to give a yellow/orange solution. Maintaining the N_2 atmosphere tetrabutylammonium hydroxide (1.2 equivalents, 7.88 mmol = 7.9 mL of a 1M solution in methanol (Aldrich supplied)) was added dropwise over 20-30 minutes

at -5 ^{O}C to give a purple solution of compound **[34]** (colour change yellow→orange→dark red/purple).

Compound **[34]** *is not isolated; it is stable in the dark under N_2 for several days, but appears to decompose in air after a few hours at RT and the solution turns brown with stench after several days in air)*

Maintaining the N_2 atmosphere , to the stirred solution of compound **[34]**, 0.6 equivalents (1.04 g, 3.94 mmol based on compound **[15]**) of α'α-dibromo-o-xylene was added and the reaction stirred overnight at RT (~16 hours) to give a yellow solution. The reaction was monitored to completion by TLC; compound **[36]** Rf = 0.38 in DCM. The product was purified on a flash silica column (DCM), to give an orange oil on evaporation (yield 75%).

Compound **[36]** *is air stable for several months in the dark, but slowly decomposes to a dark orange oil with stench under air in light.*

3.1.1.3 "m-XYLENE BRIDGE LIGAND, COMPOUND [37]"

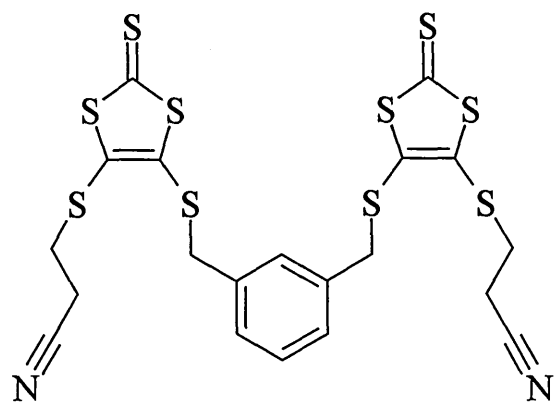

[37]

Figure 38, m-Xylene Bridge Ligand, compound **[37]**

Under N_2 using Shlenck techniques, compound **[15]** *[4,5 bis(2'-cyanoethylthio)-1,3-dithiole-2-thione]* (2 g, 6.57 mmol) was dissolved in dry distilled THF (40 mL) to give a yellow/orange solution. Maintaining the N_2 atmosphere tetrabutylammonium hydroxide (1.2 equivalents, 7.88 mmol = 7.9 mL of a 1M solution in methanol (Aldrich supplied)) was added dropwise over 20-30 minutes at -5 ^{O}C to give a purple solution of compound **[34]** (colour change yellow→orange→dark red/purple).

Compound **[34]** *is <u>not</u> isolated; it is stable in the dark under N_2 for several days, but appears to decompose in air after a few hours at RT and the solution turns brown with stench after several days in air)*

Maintaining the N_2 atmosphere, to the stirred solution of compound **[34]**, 0.6 equivalents (1.04 g, 3.94 mmol based on compound **[15]**) of α'α-dibromo-m-xylene was added and the reaction stirred overnight at RT (~16 hours) to give a yellow solution. The reaction was monitored to completion by TLC, compound **[37]** Rf = 0.33 in DCM. The product was purified on a flash silica column (DCM), to give an orange oil on evaporation (yield 65%).

Compound **[37]** *is air stable for several months in the dark, but slowly decomposes to a dark orange oil with stench under air in light.*

3.1.1.4 "p-XYLENE BRIDGE LIGAND, COMPOUND [38]"

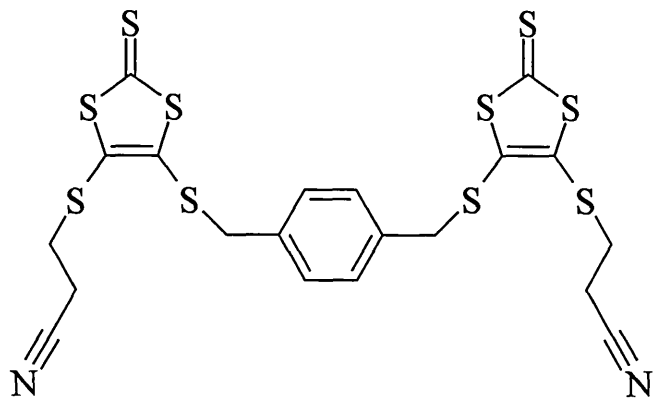

[38]

Figure 39, p-Xylene Bridge Ligand, compound **[38]**

Under N_2 using Shlenck techniques, compound **[15]** *[4,5 bis(2'-cyanoethylthio)-1,3-dithiole-2-thione]* (2 g, 6.57 mmol) was dissolved in dry distilled THF (40 mL) to give a yellow/orange solution. Maintaining the N_2 atmosphere tetrabutylammonium hydroxide (1.2 equivalents, 7.88 mmol = 7.9 mL of a 1M solution in methanol (Aldrich supplied)) was added dropwise over 20-30 minutes at -5 ^{O}C to give a purple solution of compound **[34]** (colour change yellow→orange→dark red/purple).

Compound **[34]** *is <u>not</u> isolated; it is stable in the dark under N_2 for several days, but appears to decompose in air after a few hours at RT and the solution turns brown with stench after several days in air)*

Maintaining the N_2 atmosphere, to the stirred solution of compound **[34]**, 0.6 equivalents (1.04 g, 3.94 mmol based on compound **[15]**) of α'α-dibromo-p-xylene was added and the reaction stirred overnight at RT (~16 hours) to give a yellow solution/solid. The reaction was monitored to completion by TLC;

compound **[38]** Rf = 0.38 in DCM. The product was purified on a flash silica column (DCM), to give a yellow solid on evaporation, yield 60%. Crystallised from a minimum of boiling acetonitrile to give a yellow powder, yield 70%.

Compound **[38]** *is air stable for several months in the dark, but slowly decomposes to a dark orange powder with stench under air in light.*

3.1.1.5 "DIMETHYLPYRIDINE BRIDGE LIGAND, COMPOUND [39]"

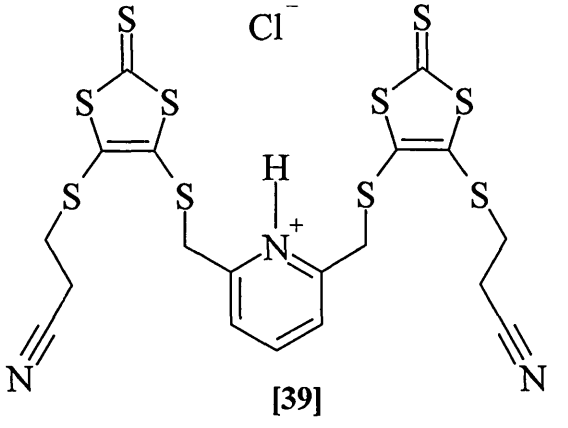

[39]

Figure 40, Dimethylpyridine Bridge Ligand, compound **[39]**

Under N_2 using Shlenck techniques, compound **[15]** *[4,5 bis(2'-cyanoethylthio)-1,3-dithiole-2-thione]* (2 g, 6.57 mmol) was dissolved in dry distilled THF (40 mL) to give a yellow/orange solution. Maintaining the N_2 atmosphere tetrabutylammonium hydroxide (1.2 equivalents, 7.88 mmol = 7.9 mL of a 1M solution in methanol (Aldrich supplied)) was added dropwise over 20-30 minutes at -5 ^{o}C to give a purple solution of compound **[34]** (colour change yellow→orange→dark red/purple).

Compound **[34]** *is* <u>*not*</u> *isolated; it is stable in the dark under* N_2 *for several days, but appears to decompose in air after a few hours at RT and the solution turns brown with stench after several days in air)*

Maintaining the N_2 atmosphere, to the stirred solution of compound **[34]**, 0.6 equivalents (1.04 g, 3.94 mmol based on compound **[15]**) 2,6-bis(bromomethyl)pyridine was added and the reaction stirred overnight at RT (~16 hours) to give an orange solution. The reaction was monitored to completion by TLC; compound **[39]** (as the free base) Rf = 0.31 in DCM and 0.54 in 1:1 EtOAc:DCM. The product was purified on a flash silica column (DCM), to give an orange oil on evaporation (yield 50%).

Compound **[39]** as the hydrochloride salt, was obtained by dissolving the free base in ethyl acetate then adding an excess of HCl dissolved in ethyl acetate (made from the addition of an equivalent of acetyl chloride to an equivalent of ethanol at $0^{O}C$) to give a yellow solid, yield 80% (from amount of free base).

Compound **[39]** *is air stable for several months in the dark, but slowly decomposes to a dark orange powder with stench under air in light.*

3.1.2 LIGAND ANALYSIS

3.1.2.1 "ETHANE BRIDGE LIGAND, COMPOUND [35]"

Compound **[35]** was assigned a more structurally accurate name by the use of the "Autnom" feature of the Belstein™ online database; 3-[(5-[2-(5-[(2-cyanoethyl)sulfanyl]-2-thioxo-1,3-dithiol-4-ylsulfanyl)ethyl]sulfanyl-2-thioxo-1,3-dithiol-4-yl)sulfanyl]propanenitrile.

The structure of compound **[35]** is shown in Figure 36, compound **[35]** was isolated as a fine yellow powder (melting point 125 °C). Attempted isolation of compound **[35]** as crystals yielded yellow plates but these proved unsuitable for X-ray analysis.

MASS SPECTROMETRY

Formula: $C_{14}H_{12}N_2S_{10}$, Formula weight: 528.92

EI, M/z = 527.5, 528, 529, fragments corresponding to CS, CS_2, C_2S_2, CS_3.

FAB, M/z = 528.8, fragments corresponding to CS, CS_2, C_2S_2, CS_3.

Both EI and FAB show a peak corresponding to the fragmentation product cation 4,5-bis(ethylenedithio)-1,3-dithiole-2-thione**[40]**, shown in Figure 41.

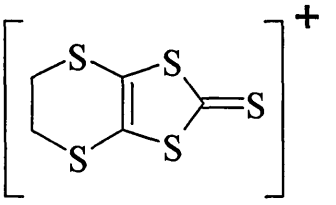

Figure 41, 4,5-bis(ethylenedithio)-1,3-dithiole-2-thione**[40]**

Mass Spectrometry yielded molecular ions consistent with the molecular formula for compound **[35]**, and the fragment peaks conform to the structure given in Figure 36.

ELEMENTAL ANALYSIS

Compound **[35]** = $C_{14}H_{12}N_2S_{10}$

Element	C	H	N
Theory	31.80 %	2.29 %	5.29 %
Found	31.86 %	2.23 %	5.39 %

FTIR

Peak assignments were determined by reference to standard tables[125-132], the major features of the spectra are shown in the table below.

Wavenumber cm^{-1}	Peak description	Assignment
2919	weak peak/s, appears to be several peaks not just a broad peak	C-H stretching, sp^3 Aliphatic also suggests presence of sp^2 Alkene
2245	sharp well defined weak intensity peak	Nitrile stretching
1461 & 1419	two sharp medium intensity peaks	C-H bending sp^3 Aliphatic
1217 & 1129	weak intensity peaks	possibly C-S bonds
1050	very strong intensity peak	C=S bond
893	medium intensity sharp peak	possibly Aliphatic C-H features
733	medium intensity sharp peak	possibly Aliphatic C-H features
519 & 465	medium intensity sharp peaks	possibly Alkene/Aromatic Carbon

UV/VIS

λ_{max} in acetone was determined to be 380 nm.

NMR

The 'expected' chemical shift values described here are calculated from standard tables of data[125-130,133]. The shift calculations can be found in chapter 8.1.

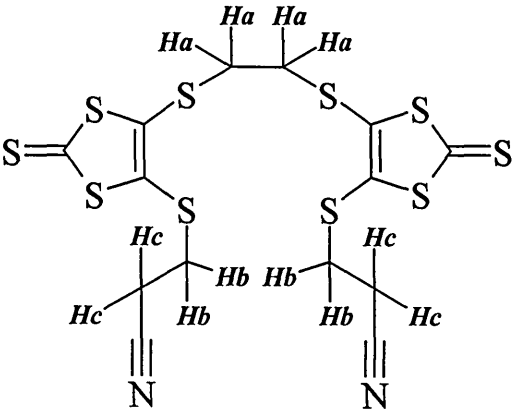

Figure 42, Proton arrangement in ethane bridge ligand[35]

Proton	Expected			Observed			
	Shift, δ ppm	Integral	Comment	Shift, δ ppm	Integral	Comment	*J* Hz
Ha	2.86	4	singlet	3.31	with Hb	singlet	N/A
Hb	2.93	4	triplet	3.26	8	triplet	6.5
Hc	2.71	4	triplet	2.95	4	triplet	6.5

Solvent used D6 Dimethylsulfoxide.

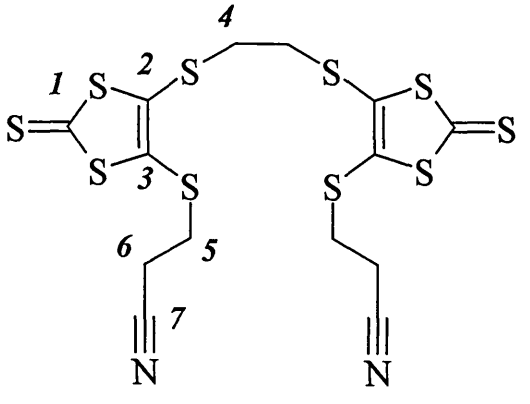

Figure 43, Carbon arrangement in ethane bridge ligand[35]

Carbon	Expected	Observed
	Shift, δ, ppm	
1	208	210.8
2	125	137.6 or 135.5
3	125	137.6 or 135.5
4	30.5	35.7
5	23.6	31.5
6	20.4	18.2
7	117.7	118.8

Solvent used D6 Dimethylsulfoxide.

3.1.2.2 "o-XYLENE BRIDGE LIGAND, COMPOUND [36]"

Compound **[36]** was assigned a more structurally accurate name by the use of the "Autnom" feature of the Belstein™ online database; 3-[5-(2-[(5-[(2-cyanoethyl)sulfanyl]-2-thioxo-1,3-dithiol-4-ylsulfanyl)methyl]benzylsulfanyl)-2-thioxo-1,3-dithiol-4-yl]sulfanylpropanenitrile.

The structure of compound **[36]** is shown in Figure 37, compound **[36]** was isolated as an orange/red oil. Attempts to isolate the compound as a crystalline solid suitable for X-ray analysis proved unsuccessful, compound **[36]** is an oil at RT.

MASS SPECTROMETRY

Formula = $C_{20}H_{16}N_2S_{10}$, Formula weight: 604.96

EI, M/z = 604.0, fragments corresponding to CS, CS_2, C_2S_2, CS_3.

FAB, M/z = 605.0, fragments corresponding to CS, CS_2, C_2S_2, CS_3.

EI spectra showed a peak corresponding to the fragmentation product cation of 4,5-bis(α'α'-o-xylenedithio)-1,3-dithiole-2-thione**[41]**, shown in Figure 44.

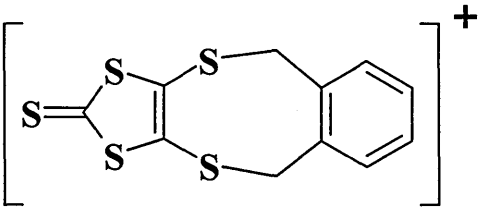

Figure 44, 4,5-bis(α'α'-o-xylenedithio)-1,3-dithiole-2-thione**[41]**

Mass Spectrometry yielded molecular ions conforming to the formula of **[36]**, and the fragment peaks conform to the structure given in Figure 37.

ELEMENTAL ANALYSIS

$C_{20}H_{16}N_2S_{10}$

Element	C	H	N
Theory	39.71 %	2.67 %	4.63 %
Found	39.85 %	2.63 %	4.60 %

FTIR

The spectra obtained were of poor quality; several techniques were attempted with the best results obtained when compound **[36]** was dispersed as a thin film on NaCl plates. The features observed conform to the structure given in Figure 37.

NMR

The 'expected' chemical shift values described here are calculated from standard tables of data[125-130,133]. The shift calculations can be found in chapter 8.1.

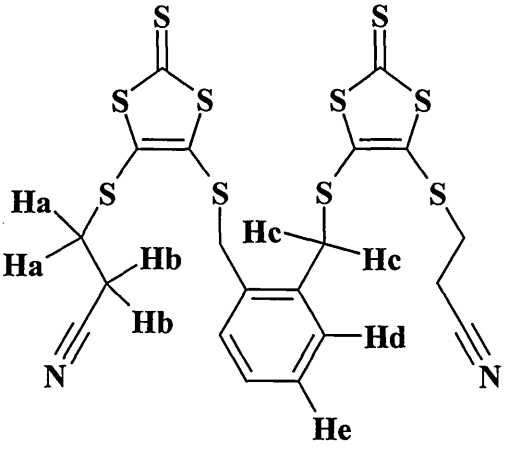

Figure 45, Proton arrangement o-xylene bridge ligand**[36]**

Proton	Expected			Observed			
	Shift, δ ppm	Integral	Comment	Shift, δ ppm	Integral	Comment	*J* Hz
Ha	2.93	4	triplet	2.95	4	triplet	6.95
Hb	2.71	4	triplet	2.57	4	triplet	6.95
Hc	3.82	4	singlet	4.29	4	singlet	N/A
Hd	6.94	2	doublet	with Hd	with Hd	with Hd	N/A
He	6.95	2	triplet	7.29	4	complex	4.8&7.8

Solvent used $CDCl_3$.

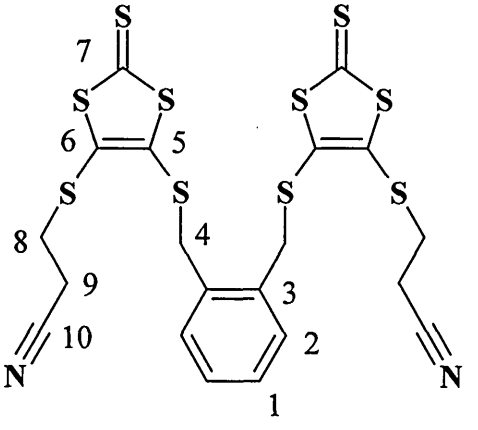

Figure 46, Carbon arrangement o-xylene bridge ligand**[36]**

Carbon	Expected	Observed
	Shift, δ, ppm	
1	126.9	129.4
2	127.9	131.6
3	140.4	134.5
4	27.0	39.1
5	115.0	136.2
6	126.0	139.0
7	208.0	210.5
8	23.6	32.4
9	20.4	19.1
10	117.7	117.8

Solvent used $CDCl_3$.

3.1.2.3 "m-XYLENE BRIDGE LIGAND, COMPOUND [37]"

Compound **[37]** was assigned a more structurally accurate name by the use of the "Autnom" feature of the Belstein™ online database; 3-[5-(3-[(5-[(2-cyanoethyl)sulfanyl]-2-thioxo-1,3-dithiol-4-ylsulfanyl)methyl]benzylsulfanyl)-2-thioxo-1,3-dithiol-4-yl]sulfanylpropanenitrile.

The structure of compound **[37]** is shown in Figure 38. Compound **[37]** was isolated as an orange/red oil. Attempts to isolate the compound as a crystalline solid suitable for X-ray analysis proved unsuccessful, compound **[37]** is an oil at RT.

MASS SPECTROMETRY

Formula: $C_{20}H_{16}N_2S_{10}$, Formula weight: 604.96

EI, Shows no molecular ion, fragments corresponding to CS, CS_2, C_2S_2, CS_3.

FAB, M/z = 605.0, fragments corresponding to CS, CS_2, C_2S_2, CS_3.

FAB-MS provided molecular ions consistent with the formula for compound **[37]**, and the fragment peaks conform to the structure given in Figure 38.

FTIR

The spectra obtained were of poor quality. Several techniques were attempted with the best results obtained when compound **[37]** was dispersed as a thin film on NaCl plates. The features observed conform to the structure given in Figure 38.

NMR

The 'expected' chemical shift values described here are calculated from standard tables of data[125-130,133]. The shift calculations can be found in chapter 8.1.

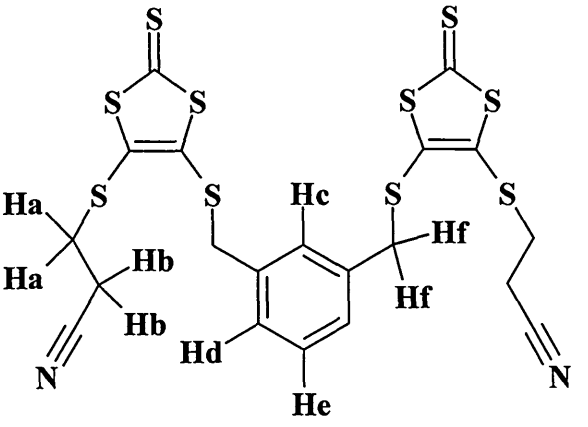

Figure 47, Proton arrangement m-xylene bridge ligand[37]

Proton	Expected			Observed			
	Shift, δ ppm	Integral	Comment	Shift, δ ppm	Integral	Comment	*J* Hz
Ha	2.93	4	triplet	2.99	with Hb	triplet	7.01
Hb	2.71	4	triplet	2.61	8	triplet	6.89
Hc	6.86	1	singlet	7.36	with Hd	singlet	N/A
Hd	6.87	2	doublet	7.30	4	broad singlet	N/A
He	7.02	1	triplet	with Hd	with Hd	with Hd	N/A
Hf	3.82	4	singlet	4.10	4	singlet	N/A

Solvent used $CDCl_3$.

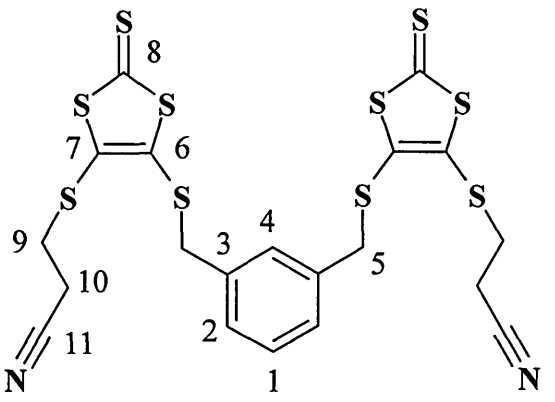

Figure 48, Carbon arrangement m-xylene bridge ligand[37]

Carbon	Expected	Observed
	Shift, δ, ppm	
1	128.5	140.1
2	126.3	with C3
3	141.0	129.3
4	127.3	134.1
5	34.2	41.1
6	115.0	130.0
7	126.0	137.0
8	208.0	210.6
9	23.6	32.4
10	20.4	19.1
11	117.7	117.7

Solvent used $CDCl_3$.

3.1.2.4 "p-XYLENE BRIDGE LIGAND, COMPOUND [38]"

Compound **[38]** was assigned a more structurally accurate name by the use of the "Autnom" feature of the Belstein™ online database; 3-[5-(4-[2-(5-[(2-cyanoethyl)sulfanyl]-2-thioxo-1,3-dithiol-4-ylsulfanyl)ethyl]benzylsulfanyl)-2-thioxo-1,3-dithiol-4-yl]sulfanylpropanenitrile.

The structure of compound **[38]** is shown in Figure 39. Compound **[38]** was isolated as a fine yellow powder (melting point 120 °C). Attempts to isolate compound **[38]** as crystals yielded yellow plates but these proved unsuitable for X-ray analysis.

MASS SPECTROMETRY

Formula: $C_{20}H_{16}N_2S_{10}$, Formula weight: 604.96

EI, Shows no molecular ion, fragments corresponding to CS, CS_2, C_2S_2, CS_3.

FAB, Shows no molecular ion, fragments corresponding to CS, CS_2, C_2S_2, CS_3.

Mass spectrometry yielded no trace of molecular ions, the data obtained suggests a DMIT type compound synthesised.

Peak assignments were determined by reference to standard tables[125-132], the major features of the spectra are shown in the table below.

Wavenumber cm^{-1}	Peak description	Assignment
2250	sharp well defined weak intensity peak	Nitrile stretching
1509 & 1461	sharp well defined weak intensity peak	C=C aromatic stretching
1422	medium intensity	C-H bending sp^3 Aliphatic
1322	weak intensity peak	sp^3 C-H bending
1239	weak intensity peak	possibly C-S bond
1065	very strong intensity peak	C=S bond
886	medium intensity sharp peak	possibly C-H features
761 & 666	medium intensity sharp peaks	possibly Aromatic C-H features
517	medium intensity sharp peak	possibly Alkene/Aromatic Carbon

The 'expected' chemical shift values described here are calculated from standard tables of data[125-130,133]. The shift calculations can be found in chapter 8.1.

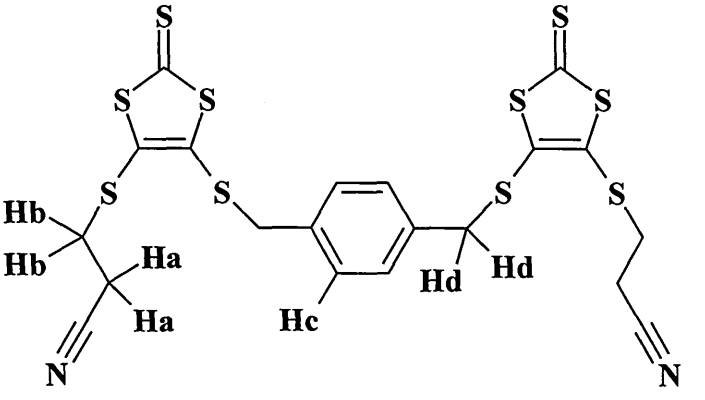

Figure 49, Proton arrangement p-xylene bridge ligand**[38]**

Proton	Expected			Observed			
	Shift, δ ppm	Integral	Comment	Shift, δ ppm	Integral	Comment	*J* Hz
Ha	2.71	4	triplet	2.83	4	triplet	6.7
Hb	2.93	4	triplet	3.15	4	triplet	6.7
Hc	6.94	4	singlet	7.35	4	singlet	N/A
Hd	3.82	4	singlet	4.26	4	singlet	N/A

Solvent used D6 Dimethylsulfoxide.

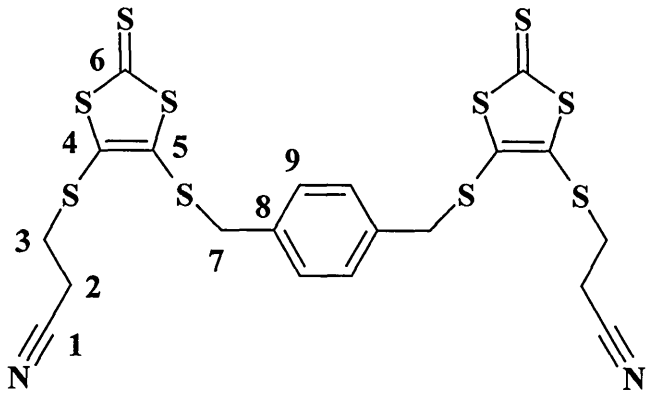

Figure 50, Carbon arrangement p-xylene bridge ligand[38]

Carbon	Expected	Observed
	Shift, δ, ppm	
1	117.7	118.8
2	20.4	18.1
3	23.6	31.5
4	126.0	138.8
5	115.0	135.2
6	208.0	210.9
7	33.9	(with DMSO) 40
8	139.4	136.1
9	127.9	129.4

Solvent used D6 Dimethylsulfoxide.

ELEMENTAL ANALYSIS

$C_{20}H_{16}N_2S_{10}$

Element	C	H	N
Theory	39.71 %	2.67 %	4.63 %
Found	39.93 %	2.81 %	4.86 %

3.1.2.5 "DIMETHYLPYRIDINE BRIDGE LIGAND, COMPOUND [39]"

Compound **[39]** was assigned a more structurally accurate name by the use of the "Autnom" feature of the Belstein™ online database;

As the free base:

3-(5-[(6-[2-(5-[(2-cyanoethyl)sulfanyl]-2-thioxo-1,3-dithiol-4-ylsulfanyl)ethyl]-2-pyridylmethyl)sulfanyl]-2-thioxo-1,3-dithiol-4-ylsulfanyl)propanenitrile

As the HCl salt:

3-(5-[(6-[2-(5-[(2-cyanoethyl)sulfanyl]-2-thioxo-1,3-dithiol-4-ylsulfanyl)ethyl]-2-pyridiniumylmethyl)sulfanyl]-2-thioxo-1,3-dithiol-4-ylsulfanyl)propanenitrile chloride

The structure of compound **[39]** is shown in Figure 40. Compound **[39]** was isolated as a fine yellow powder (melting point (as the HCl salt) 154 °C). Attempted isolation as crystals yielded orange plates but these proved unsuitable for X-ray analysis.

MASS SPECTROMETRY

Formula: $C_{19}H_{16}ClN_3S_{10}$, Formula weight: 642.46

EI, Shows no molecular ion, fragments corresponding to CS, CS_2, C_2S_2, CS_3.

FAB, Shows no molecular ion, fragments corresponding to CS, CS_2, C_2S_2, CS_3.

Mass spectrometry did not yield molecular ions, the fragments observed suggest a DMIT type compound was synthesised.

ELEMENTAL ANALYSIS

$C_{19}H_{16}ClN_3S_{10}$

Element	C	H	N
Theory	35.52 %	2.51 %	6.54 %
Found	35.91 %	2.49 %	6.52 %

FTIR

Peak assignments were determined by reference to standard tables[125-132], the major features of the spectra are shown in the table below.

Wavenumber cm^{-1}	Peak description	Assignment
3397	weak ill defined peak	possibly N^+-H, possibly O-H but compound was extensively dried
2917	weak peak/s, appears to be several peaks not just a broad peak	C-H stretching, sp^3 Aliphatic also suggests presence of sp^2 Alkene
2246	sharp well defined weak intensity peak	Nitrile stretching
1630	sharp medium intensity peak	pyridine ring stretching
1453 & 1414	two sharp medium intensity peaks	C-H bending sp^3 Aliphatic
1281 & 1166	weak intensity peaks	possibly C-S bonds
1060	very strong intensity peak	C=S bond
892	medium intensity sharp peak	possibly Aliphatic C-H features
751	medium intensity sharp peak	possibly Aliphatic C-H features
514	medium intensity sharp peaks	possibly Alkene/Aromatic Carbon

The 'expected' chemical shift values described here are calculated from standard tables of data[125-130,133]. The shift calculations can be found in chapter 8.1.

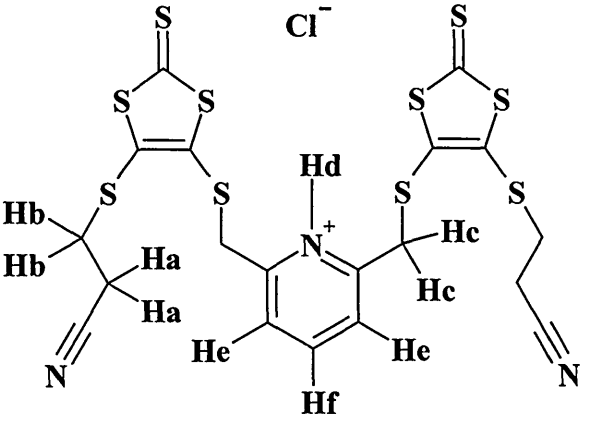

Figure 51, Proton arrangement in Dimethylpyridine bridge ligand**[39]**

Proton	Expected			Observed			
	Shift, δ ppm	Integral	Comment	Shift, δ ppm	Integral	Comment	*J* Hz
Ha	2.71	4	triplet	2.86	with Hb	triplet	6.80
Hb	2.93	4	triplet	3.17	8	triplet	6.80
Hc	3.82	4	singlet	4.34	4	singlet	N/A
Hd	?	?	?	6.89	N/A	v.broad peak	N/A
He	8.23	2	doublet	7.46	2	doublet	7.72
Hf	9.02	1	triplet	7.90	1	triplet	7.74

Solvent used D6 Dimethylsulfoxide.

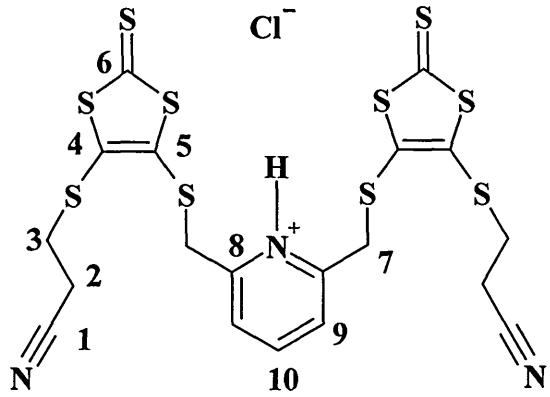

Figure 52, Carbon arrangement in Dimethylpyridine bridge ligand[**39**]

Carbon	Expected	Observed
	Shift, δ, ppm	
1	117.7	118.7
2	20.4	18.2
3	23.6	31.5
4	126	138
5	124	136
6	208.0	219
7	34.2	under DMSO peak
8	142.5	139.2
9	129.0	122.9
10	148.4	155.6

Solvent used D6 Dimethylsulfoxide.

3.2 METAL COMPLEXES

3.2.1 COMPLEX SYNTHESIS

3.2.1.1 ETHANE BRIDGE LIGAND[35] DERIVATIVES, COMPOUNDS [42] to [51]

Two types of compound were synthesised from the Ethane bridged ligand (compound **[35]**), shown in Figure 53 and Figure 54.

TMA SALT, COMPOUND [42]

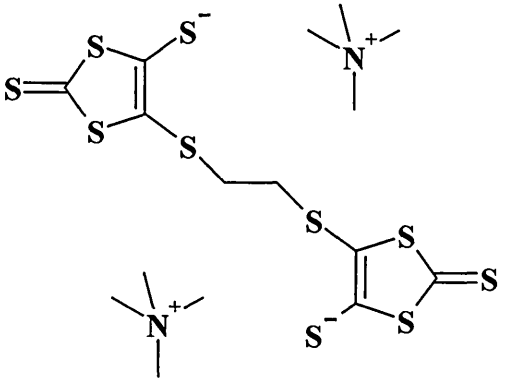

Figure 53, Ethane Bridge Ligand TMA salt, compound **[42]**

Under N_2, to a stirred solution of compound **[35]** (0.50 g, 0.945 mmol) in dry distilled THF (20 mL), tetramethylammonium hydroxide (0.724 g of 25% w/w solution in methanol = 0.181 g base = 1.98 mmol = 2.1 equivalents) was added dropwise over 10 minutes at RT to give a red solution. After 30 minutes an orange precipitate of compound **[42]** was observed and was isolated by filtration

and washed with an excess of dry distilled THF then dry distilled diethyl ether to give an orange powder, yield 0.52 g = 96%.

METAL COMPLEXES, COMPOUNDS [43] to [51]

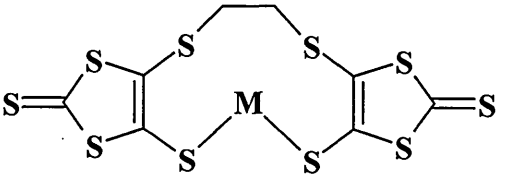

M = Metal^{2+}

Figure 54, Ethane Bridge ligand M^{2+} complex, **[43]** to **[51]**

The general method for the synthesis of these complexes is shown below. The following M complexes were prepared:

Metal M	Compound Number	Metal salt used
$[Ti(Cp)_2]^{2+}$	**[43]**	$[Ti(Cp)_2]Cl_2$
Fe^{2+}	**[44]**	$FeCl_2$
Co^{2+}	**[45]**	$CoBr_2$
Ni^{2+}	**[46]**	$NiBr_2$
$[Ni(dppe)]^{2+}$	**[47]**	$[Ni(dppe)]Cl_2$
Cu^{2+}	**[48]**	$CuBr_2$
Zn^{2+}	**[49]**	$ZnCl_2$
Hg^{2+}	**[50]**	$HgCl_2$
$[Sn(Me)_2]^{2+}$	**[51]**	$[Sn(Me)_2]Cl_2$

Under N_2, to a stirred solution of compound **[35]** in dry distilled THF (0.50g in 10mL THF = 0.945 mmol in 10 mL) at room temperature, NaOEt (2.2 equivalents, 2.1 mmol, 0.143 g) in dry ethanol (5 mL, just enough to dissolve the base) was added to give a dark orange/red solution. To this solution at room temperature, 1 equivalent of a metal salt MX_2, see table, dissolved in a minimum of dry ethanol is added and the resulting mixture stirred for 1 hour at RT to give a dark solution and precipitate. The metal complex was removed by filtration, washed with ethanol (to remove unreacted thiolate and transition metal halides), deionised water (to remove metal halides), IPA (to remove water), then diethyl ether to give the metal complex as a powder. Yields varied from 50% for the Co^{2+} complex**[45]** to 80% for $[Sn(Me)_2]^{2+}$**[51]**.

3.2.1.2 o-XYLENE BRIDGE LIGAND[36] DERIVATIVES, COMPOUNDS [52] to [58]

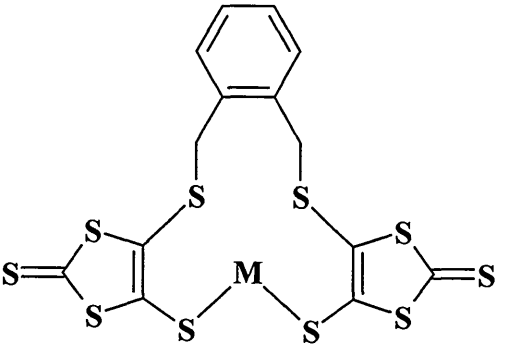

M = Metal^{2+}

Figure 55, o-xylene bridge ligand M^{2+} complex, compounds **[52]** to **[58]**

The general method for the synthesis of these complexes is shown below, the following M complexes were prepared:

Metal M	Compound Number	Metal salt used
$[Ti(Cp)_2]^{2+}$	**[52]**	$[Ti(Cp)_2]Cl_2$
Fe^{2+}	**[53]**	$FeCl_2$
Co^{2+}	**[54]**	$CoBr_2$
Ni^{2+}	**[55]**	$NiBr_2$
Cu^{2+}	**[56]**	$CuBr_2$
Zn^{2+}	**[57]**	$ZnCl_2$
$[Sn(Me)_2]^{2+}$	**[58]**	$[Sn(Me)_2]Cl_2$

Under N_2, to a stirred solution of compound **[36]** in dry distilled THF (0.50g in 10mL THF = 0.827 mmol in 10 mL) at room temperature, NaOEt (2.2 equivalents, 1.8 mmol, 0.124 g) in dry ethanol (5 mL, just enough to dissolve the base) is added to give a dark orange/red solution. To this solution at room temperature, 1 equivalent of a metal salt MX_2, see table, dissolved in a minimum of dry ethanol is added and the resulting mixture stirred for 1 hour at RT to give a dark solution and precipitate. The metal complex was removed by filtration, washed with ethanol (to remove unreacted thiolate and transition metal halides), deionised water (to remove metal halides), IPA (to remove water), then diethyl ether to give the metal complex as a powder. Yields varied from 40% for the Co^{2+}**[54]** complex to 85% for $[Sn(Me)_2]^{2+}$**[58]**.

3.2.1.3 m-XYLENE BRIDGE LIGAND[37] DERIVATIVES, COMPOUNDS [59] to [64]

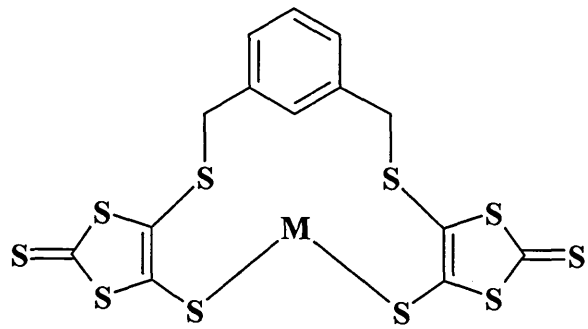

M = Metal^{2+}

Figure 56, m-xylene bridge ligand M^{2+} complex, compounds **[59]** to **[64]**

The general method for the synthesis of these complexes is shown below, the following M complexes were prepared:

Metal M	Compound Number	Metal salt used
Fe^{2+}	**[59]**	$FeCl_2$
Co^{2+}	**[60]**	$CoBr_2$
Ni^{2+}	**[61]**	$NiBr_2$
Cu^{2+}	**[62]**	$CuBr_2$
Zn^{2+}	**[63]**	$ZnCl_2$
$[Sn(Me)_2]^{2+}$	**[64]**	$[Sn(Me)_2]Cl_2$

Under N_2, to a stirred solution of compound **[37]** in dry distilled THF (0.50g in 10mL THF = 0.827 mmol in 10 mL) at room temperature, NaOEt (2.2 equivalents, 1.8 mmol, 0.124 g) in dry ethanol (5 mL, just enough to dissolve the base) is added to give a dark orange/red solution. To this solution at room

temperature, 1 equivalent of a metal salt MX_2, see table, dissolved in a minimum of dry ethanol is added and the resulting mixture stirred for 1 hour at RT to give a dark solution and precipitate. The metal complex was removed by filtration, washed with ethanol (to remove unreacted thiolate and transition metal halides), deionised water (to remove metal halides), IPA (to remove water), then diethyl ether to give the metal complex as a powder. Yields varied from 40% for the Co^{2+}**[60]** complex to 80% for $[Sn(Me)_2]^{2+}$**[64]**.

3.2.1.4 p-XYLENE BRIDGE LIGAND[38] DERIVATIVES, COMPOUNDS [65] to [70]

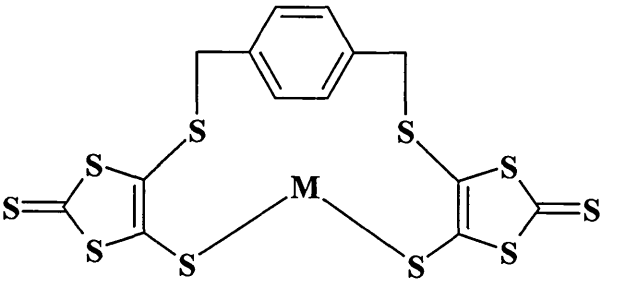

M = Metal^{2+}

Figure 57, p-xylene bridge ligand M^{2+} complex, compounds **[65]** to **[70]**

The general method for the synthesis of these complexes is shown below, the following M complexes were prepared:

Metal M	Compound Number	Metal salt used
Fe^{2+}	**[65]**	$FeCl_2$
Co^{2+}	**[66]**	$CoBr_2$
Ni^{2+}	**[67]**	$NiBr_2$
Cu^{2+}	**[68]**	$CuBr_2$
Zn^{2+}	**[69]**	$ZnCl_2$
$[Sn(Me)_2]^{2+}$	**[70]**	$[Sn(Me)_2]Cl_2$

Under N_2, to a stirred solution of compound **[38]** in dry distilled THF (0.50g in 10mL THF = 0.827 mmol in 10 mL) at room temperature, NaOEt (2.2 equivalents, 1.8 mmol, 0.124 g) in dry ethanol (5 mL, just enough to dissolve the base) is added to give a dark orange/red solution. To this solution at room

temperature, 1 equivalent of a metal salt MX_2, see table, dissolved in a minimum of dry ethanol is added and the resulting mixture stirred for 1 hour at RT to give a dark solution and precipitate. The metal complex was removed by filtration, washed with ethanol (to remove unreacted thiolate and transition metal halides), deionised water (to remove metal halides), IPA (to remove water), then diethyl ether to give the metal complex as a powder. Yields varied from 50% for the Co^{2+}**[66]** complex to 80% for $[Sn(Me)_2]^{2+}$**[70]**.

3.2.1.5 DIMETHYLPYRIDINE BRIDGE LIGAND[39] DERIVATIVES

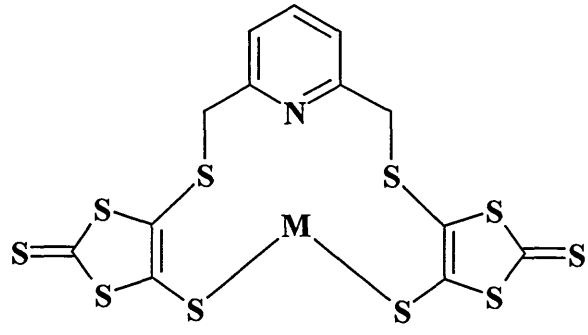

M = Metal^{2+}

Figure 58, dimethylpyridine bridge ligand M^{2+} complex, compounds **[71]** to **[76]**

The general method for the synthesis of these complexes is shown below, the following M complexes were prepared:

Metal M	Compound Number	Metal salt used
Fe^{2+}	**[71]**	$FeCl_2$
Co^{2+}	**[72]**	$CoBr_2$
Ni^{2+}	**[73]**	$NiBr_2$
Cu^{2+}	**[74]**	$CuBr_2$
Zn^{2+}	**[75]**	$ZnCl_2$
$[Sn(Me)_2]^{2+}$	**[76]**	$[Sn(Me)_2]Cl_2$

Under N_2, to a stirred solution of compound **[39]** in anhydrous DMF (0.50g in 10mL DMF = 0.778 mmol in 10 mL) at room temperature, NaOEt (3.3 equivalents, 2.6 mmol, 0.175 g) in dry ethanol (5 mL , just enough to dissolve the base) is added to give a dark orange/red solution. To this solution at room temperature, 1 equivalent of a metal salt MX_2, see table, dissolved in a minimum

of dry ethanol is added and the resulting mixture stirred for 1 hour at RT to give a dark solution and precipitate. The metal complex was removed by filtration, washed with ethanol (to remove unreacted thiolate and transition metal halides), deionised water (to remove metal halides), IPA (to remove water), then diethyl ether to give the metal complex as a powder. Yields varied from 40% for the Co^{2+}**[72]** complex to 70% for $[Sn(Me_2)]^{2+}$**[76]**.

3.2.2 COMPLEX ANALYSIS

3.2.2.1 "ETHANE BRIDGE LIGAND[35] DERIVATIVES, COMPOUNDS [42] to [51]"

TMA SALT, COMPOUND [42]

The structure of compound **[42]** is shown in Figure 53. Compound **[42]** is isolated as a fine orange powder. The compound gave no melting point, but was found to decompose at 165 °C. Recrystallisation from methanol yielded orange plates, these proved suitable for X-ray analysis. Compound **[42]** proved unsuitable for CHN analysis due to the compound decomposing on drying, even under a vacuum at room temperature.

X-RAY CRYSTAL STRUCTURE

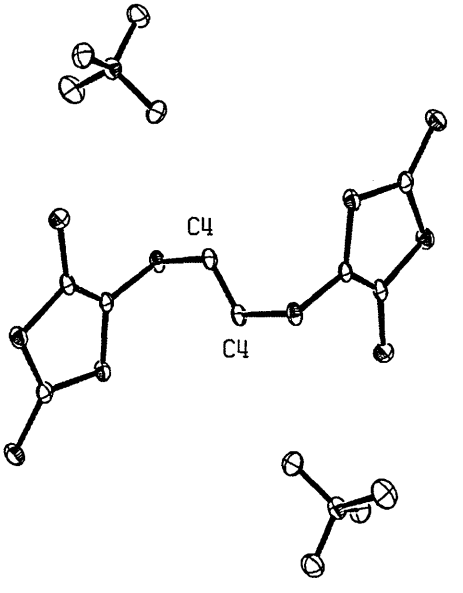

Figure 59, X-ray crystal structure of TMA salt**[42]**

X-ray crystallography conforms to the structure shown in Figure 53, supporting tables of data can be found in section 8.2.1.

MASS SPECTROMETRY

Formula: $C_{16}H_{28}N_2S_{10}$, Formula weight: 569.07

EI, Shows no molecular ion, fragments corresponding to CS, CS_2, C_2S_2, CS_3.

FAB, Shows no molecular ion, fragments corresponding to CS, CS_2, C_2S_2, CS_3.

Both EI and FAB show a peak for $^{+}N(CH_3)_4$

Mass spectrometry did not yield molecular ions but the fragmentation seen suggests a DMIT type compound synthesised.

FTIR

Peak assignments were determined by reference to standard tables[125-132], the major features of the spectra are shown in the table below.

Wavenumber cm^{-1}	Peak description	Assignment
3433	broad ill defined peak	possibly N^{+}-H, compound unstable in air, compound was well dried not O-H
3002	sharp well defined peak	possibly N^{+}-S^{-} interaction
2915	weak peak/s, appears to be several peaks not just a broad peak	C-H stretching, sp^3 Aliphatic also suggests presence of sp^2 Alkene
1484 & 1403	two sharp strong intensity peaks	C-H bending sp^3 Aliphatic
1195 & 1123	weak intensity peaks sharp peaks	possibly C-S bonds
1058 & 1034	very strong intensity peak, appears to be two peaks	C=S bond and N-C bond
948 & 988	two sharp medium intensity peaks	possibly C-N bonds
859	medium intensity sharp peak	possibly Aliphatic C-H features
737	medium intensity sharp peak	possibly Aliphatic C-H features
527	medium intensity sharp peaks	possibly Alkene/Aromatic Carbon

UV/VIS

Solvent	λmax / nm
DMF	488
Acetone	484
MeCN	476
MeOH	436
H_2O	430

UV/VIS spectroscopy appears to show that the TMA**[42]** salt is solvatochromic, i.e. the change in the charge separation between the thiolate and ammonium ions as the polarity of the solvent is changed[134].

NMR

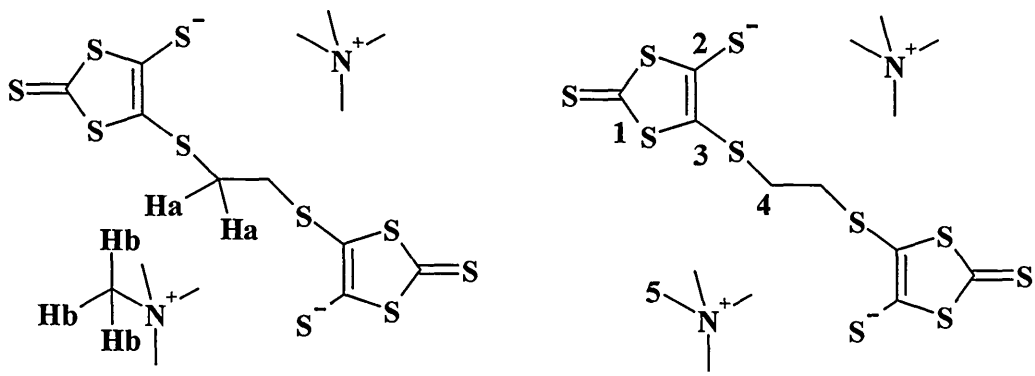

Figure 60, Proton and Carbon arrangement in TMA**[42]** salt

Proton	Shift, δ ppm	Integral	Comment
Ha	3.01	4	singlet
Hb	3.12	24	singlet

Solvent used D6 Dimethylsulfoxide.

Carbon	Shift, δ ppm
1	210.9
2	171.7
3	110.4
4	34.2
5	54.5

Solvent used D6 Dimethylsulfoxide.

METAL COMPLEXES, COMPOUNDS [43] to [51]

Metal M	Compound Number	Metal salt used
$[Ti(Cp)_2]^{2+}$	**[43]**	$[Ti(Cp)_2]Cl_2$
Fe^{2+}	**[44]**	$FeCl_2$
Co^{2+}	**[45]**	$CoBr_2$
Ni^{2+}	**[46]**	$NiBr_2$
$[Ni(dppe)]^{2+}$	**[47]**	$[Ni(dppe)]Cl_2$
Cu^{2+}	**[48]**	$CuBr_2$
Zn^{2+}	**[49]**	$ZnCl_2$
Hg^{2+}	**[50]**	$HgCl_2$
$[Sn(Me)_2]^{2+}$	**[51]**	$[Sn(Me)_2]Cl_2$

A general structure for these complexes is shown in Figure 54.

MELTING POINTS

Complex (compound N°)	Initial colour	Initial colour Change	Melting point	Decomposition
*$[Ti(Cp)_2]^{2+}$ (43)	green/black	Not possible to see	None	~170 °C
Fe^{2+} (44)	dark green	darkens 85 °C	None	~110 °C
*Co^{2+} (45)	black	Not possible to see	None	~150 °C
Ni^{2+} (46)	dark brown/black	darkens 104 °C	None	~150 °C
$[Ni(dppe)]^{2+}$ (47)	brown	darkens 100 °C	None	~160 °C
Cu^{2+} (48)	red/brown	darkens 115 °C	None	~180 °C
Zn^{2+} (49)	orange/yellow	darkens 100 °C	None	~190 °C
Hg^{2+} (50)	yellow	darkens 80 °C	None	~190 °C
$[Sn(Me)_2]^{2+}$ (51)	yellow	change to orange as melts	124 °C to 130 °C	~170 °C

*compounds **[43]** and **[45]** difficult to judge due to darkness of the complex

MASS SPECTROMETRY

Both EI and FAB showed no trace of molecular ions for any of the metal complexes, EI and FAB show fragments corresponding to CS, CS_2, C_2S_2, CS_3.

Both EI and FAB show a peak corresponding to the fragment product cation 4,5-bis(ethylenedithio)-1,3-dithiole-2-thione, shown in Figure 41.

Mass spectrometry only provides evidence that DMIT type compounds have been synthesised.

CHN analysis of the transition metal complexes proved to be unhelpful due to the difficulty in removing all traces of solvent from the complexes. It appears that the solvents used in the synthesis of these compounds also co-ordinated to the metals (contrast NMR data below). After prolonged drying attempts the compounds were found to have started to decompose (darkened in colour and produced stench). In contrast to this however the dimethyl tin complex**[51]** of this ligand was prepared and found to be comparatively stable, and easier to dry.

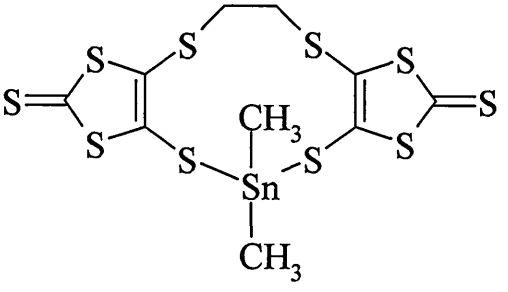

Figure 61, Dimethyl tin complex of ethane bridge**[35]** ligand, compound **[51]**

$C_{10}H_{10}S_{10}Sn$

Element	C	H	N
Theory	21.09 %	1.77 %	0 %
Found	21.17 %	1.79 %	0 %

FTIR

Peak assignment was determined with reference to standard tables[125-132]. The IR spectra of the metal complexes proved to be very similar to the IR trace for the

ligand, the main differences being the absence of the nitrile peak at 2245 cm^{-1} and a reduction in the intensity of the peaks due to the aliphatic features of the compounds. The carbon-sulphur features of the IR spectra of the complexes were observed at a slightly greater wavenumber. The main sulphur feature in the ligand was observed at 1050 cm^{-1}, whereas in the transition metal complexes it was observed at ~1056 cm^{-1}. A shift of similar magnitude was observed in the other sulphur features of the spectra, however the shift in wavenumber is relatively small (~6 cm^{-1}) and could be argued to be due to spectrometer resolution and/or experimental error. The carbon-sulphur bonds in the $[Sn(Me)_2]^{2+}$ complex **[51]** yielded a greater shift in value (~12 cm^{-1}) to 1062 cm^{-1} with a similar shift seen for the other sulphur features of the spectra. In general the IR spectra demonstrated features consistent with the structure shown in Figure 54.

X-RAY CRYSTALLOGRAPHY

Isolation of the complexes as crystals proved fruitless, all the complexes were obtained as powders.

UV/VIS

Complex (compound N°)	Solvent	λmax, nm
$[Ti(Cp)_2]^{2+}$ (43)	DMF (300-900 nm)	328, 376, 488
Fe^{2+} (44)	DMF (300-900 nm)	328, 380, 484
Co^{2+} (45)	DMF (300-900 nm)	336, 436
Ni^{2+} (46)	DMF (300-900 nm)	324, 436
	Acetone (350-900 nm)	430
	Pyridine (310-900 nm)	322, 424, 482
$[Ni(dppe)]^{2+}$ (47)	DMF (300-900 nm)	316, 420
	DCM (230-900 nm)	276, 320, 422
Cu^{2+} (48)	DMF (300-900 nm)	338, 426
Zn^{2+} (49)	DMF (300-900 nm)	308, 408
Hg^{2+} (50)	DMF (300-900 nm)	320, 404
$[Sn(Me)_2]^{2+}$ (51)	DMF (300-900 nm)	328, 392, 484

All spectra that were scanned below 350 nm show peaks in the UV region at ~330 nm, this is most likely due to the C=S feature of the ligand itself. The second peak that was observed in some of the spectra at ~380 nm was only seen as a 'shoulder' to the peak at ~330 nm, and was most likely present in all the spectra. The final peak seen at 484 nm in the Fe^{2+} complex **[44]**, is seen to shift towards shorter wave length as the period is crossed, i.e. shifting towards higher energy from $[Ti(Cp)_2]^{2+} \rightarrow Zn^{2+}$ (**[43]** → **[49]**), sample spectra of which are shown in Figure 62.

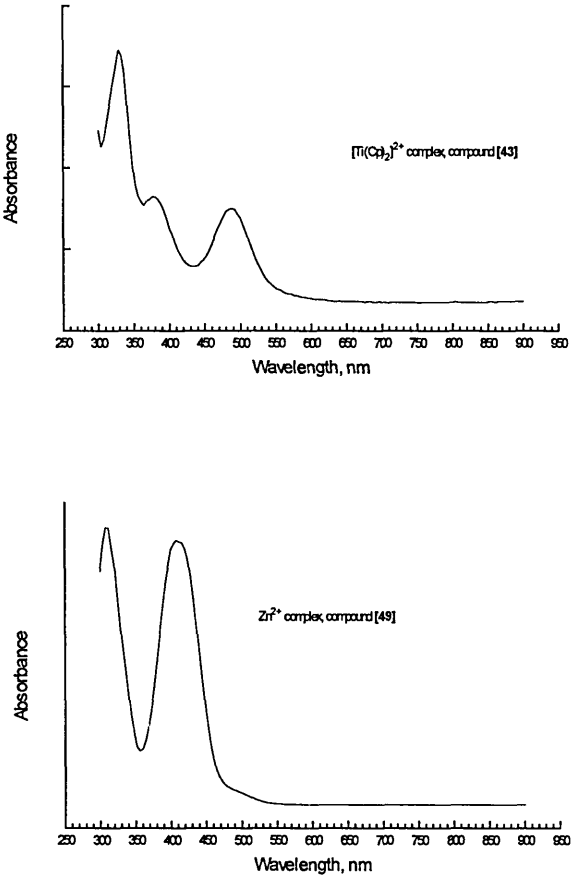

Figure 62, UV/VIS spectra of compounds **[43]** & **[49]**

NMR

NMR analysis of these complexes proved to be difficult, the complexes are only sparingly soluble in most solvents, this in turn led to no useful carbon NMR being obtained due to the very low concentrations of complex dissolved in the solvent. Proton NMR however did yield the following data:

- Compound **[43]**, $[Ti(Cp)_2]^{2+}$, the Cp peak was observed at 6.69 δ, SCH_2 at 2.99 δ in D6 DMSO

- Compound **[45]**, Co^{2+}, produced one very broad peak at 3.2 δ with a peak width from ~0 to 6 δ, suggesting the complex is paramagnetic.
- Compound **[46]**, Ni^{2+}, the peak for SCH_2 seen at 3.07 δ in D6 DMSO, the DMSO peak appears slightly shifted in position to 2.48 δ. Some spectra show a split DMSO peak possibly explained by the metal complexing with the solvent causing a change in the proton environment of the solvent, DMSO and similar solvents are known to complex metals[10,135].
- Compound **[47]**, $[Ni(dppe)]^{2+}$, the peak for SCH_2 seen at 2.17 δ and PCH_2 at 1.60 δ, two peaks are also observed in the aromatic region for the phenyl groups at 7.51 & 8.00 δ in $CDCl_3$. All the observed peaks are noticeably broader than those seen in the spectra of the unreacted ligand, ^{31}P NMR gave data consistent with three types of phosphorus environments shown in Figure 63. The initial ^{31}P NMR shows a peak due to P1 at 57.01 δ, with small peaks due to P2 & P3 at 32.46 δ & 60.13 δ. After being in solution for several hours the peaks for P2 & P3 became the predominant feature of the spectra suggesting the complex is unstable in solution.

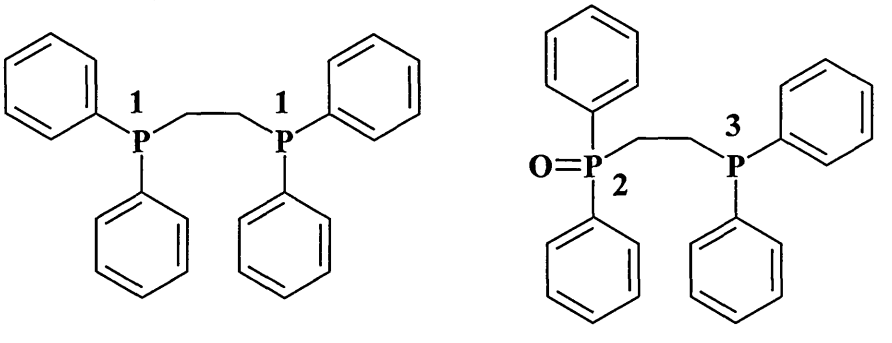

Figure 63, Phosphorus environments in Compound **[47]**, $[Ni(dppe)]^{2+}$ complex

- Compound **[48]**, Cu^{2+}, SCH_2 observed at 3.44 δ in D6 acetone.
- Compound **[49]**, Zn^{2+}, SCH_2 observed at 3.18 δ in D6 DMSO.
- Compound **[50]**, Hg^{2+}, SCH_2 observed at 3.19 δ in D6 DMSO, the complex was also found to be unstable in solution, Hg metal was seen to form as the solution was left to stand.

3.2.2.2 "o-XYLENE BRIDGE[36] LIGAND DERIVATIVES, COMPOUNDS [52] to [58]"

Metal M	Compound Number	Metal salt used
$[Ti(Cp)_2]^{2+}$	**[52]**	$[Ti(Cp)_2]Cl_2$
Fe^{2+}	**[53]**	$FeCl_2$
Co^{2+}	**[54]**	$CoBr_2$
Ni^{2+}	**[55]**	$NiBr_2$
Cu^{2+}	**[56]**	$CuBr_2$
Zn^{2+}	**[57]**	$ZnCl_2$
$[Sn(Me)_2]^{2+}$	**[58]**	$[Sn(Me)_2]Cl_2$

A general structure for these complexes is shown in Figure 55.

MELTING POINTS

Complex (compound N°)	Initial colour	Initial colour Change	Melting point	Decomposition
*$[Ti(Cp)_2]^{2+}$ (52)	green/black	Not possible to see	None	~110 °C
Fe^{2+} (53)	dark green	darkens 88 °C	None	~130 °C
*Co^{2+} (54)	black	Not possible to see	None	~168 °C
Ni^{2+} (55)	dark brown/black	darkens 140 °C	None	~170 °C
Cu^{2+} (56)	red/brown	darkens 135 °C	None	~174 °C
Zn^{2+} (57)	orange/yellow	darkens 126 °C	None	~180 °C
$[Sn(Me)_2]^{2+}$ (58)	yellow	change to orange as melts	104 °C to 108 °C	~150 °C

*compounds **[52]** & **[54]** difficult to judge due to darkness of the initial colour

MASS SPECTROMETRY

Both EI and FAB showed no trace of molecular ions for any of the metal complexes. EI and FAB show fragments corresponding to CS, CS_2, C_2S_2, CS_3. Both EI and FAB show a peak corresponding to the fragment product cation of 4,5-bis(αα'-o-xylenedithio)-1,3-dithiole-2-thione, shown in Figure 44.
Mass spectrometry data suggests that DMIT type compounds have been synthesised.

ELEMENTAL ANALYSIS

As with the ethane bridge complexes CHN analysis proved unhelpful due to difficulty in drying the complexes. It again suggested that that the solvents used

in the synthesis of these compounds also co-ordinated with the metals (contrast NMR data below). After prolonged drying and repeated sample submission the compounds began to decompose (darkened in colour and produced stench). CHN analysis did not prove helpful in determining the structure of the complexes.

FTIR

Peak assignment was determined with reference to standard tables[125-132]. As with the ethane bridge complexes the IR spectra of the metal complexes proved to be very similar to the IR trace for the unreacted ligand, the main differences being the absence of the nitrile peak at 2245 cm^{-1} and a reduction in the intensity of the peaks due to the aliphatic features of the compounds. The carbon-sulphur features of the IR spectra of the complexes were observed at much the same position. The main sulphur feature in the ligand was observed at ~1060 cm^{-1}, whereas in the transition metal complexes it was observed at ~1062 cm^{-1}. A further effect to the spectra was a broadening of the aromatic features of the spectra leading to less well defined peaks. In general the IR spectra demonstrated features consistent with the structure shown in Figure 55.

Complex (compound N°)	Solvent	λmax, nm
$[Ti(Cp)_2]^{2+}$ (52)	DMF (300-900 nm)	332, 368, 484
Fe^{2+} (53)	DMF (300-900 nm)	332, 380, 480
Co^{2+} (54)	DMF (300-900 nm)	332, 368, 472
Ni^{2+} (55)	DMF (300-900 nm)	320, 396, 444, 588, 620
	DMSO (270-900 nm) initial scan (orange/brown solution)	330, 482
	DMSO (270-900 nm) after standing (green solution)	320, 384, 420, 618
	Pyridine (310-900 nm)	328, 432, 478
Cu^{2+} (56)	insoluble	
Zn^{2+} (57)	DMF (300-900 nm)	324, 484
$[Sn(Me)_2]^{2+}$ (58)	DMF (300-900 nm)	324, 380, 484

All spectra that were scanned below 350 nm show peaks in the UV region at ~330 nm; this is likely due to the C=S feature of the ligand itself. The second peak that was observed in some of the spectra at ~380 nm was only seen as a 'shoulder' to the peak at ~330 nm, and was most likely present in all the spectra. Of all the complexes scanned the most interesting appears to be the solutions of the nickel complex**[55]**. The solution in DMF gave the peaks seen in the other spectra plus a split relatively weak intensity peak at ~600 nm, shown in Figure 64.

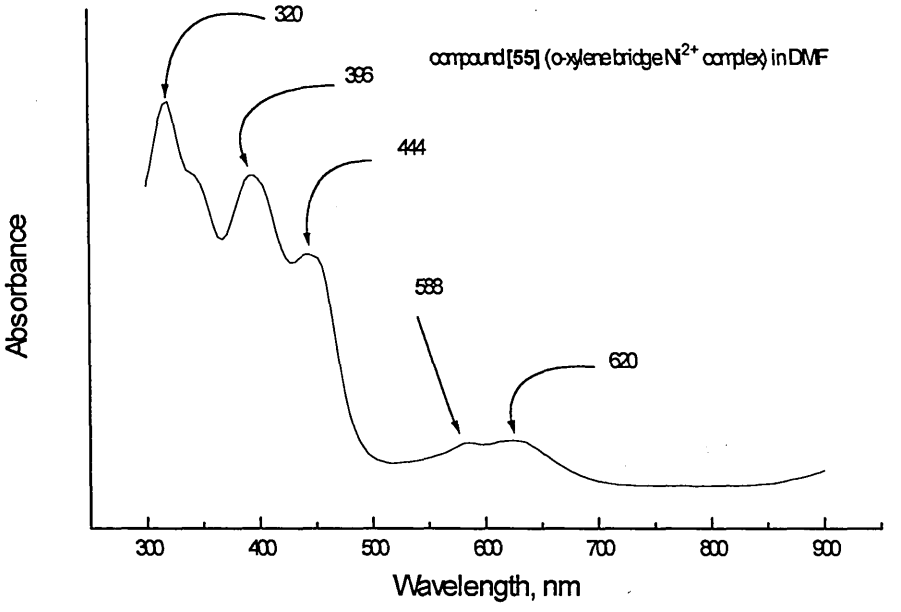

Figure 64, UV/VIS scan of compound **[55]** (o-xylene bridge Ni^{2+} complex) in DMF.

The next significant result was from the solution in DMSO, on dissolving compound **[55]** in DMSO it was observed as on orange/brown solution, on standing for about an hour the colour of the solution changed to dark green, an example of this is shown in Figure 65.

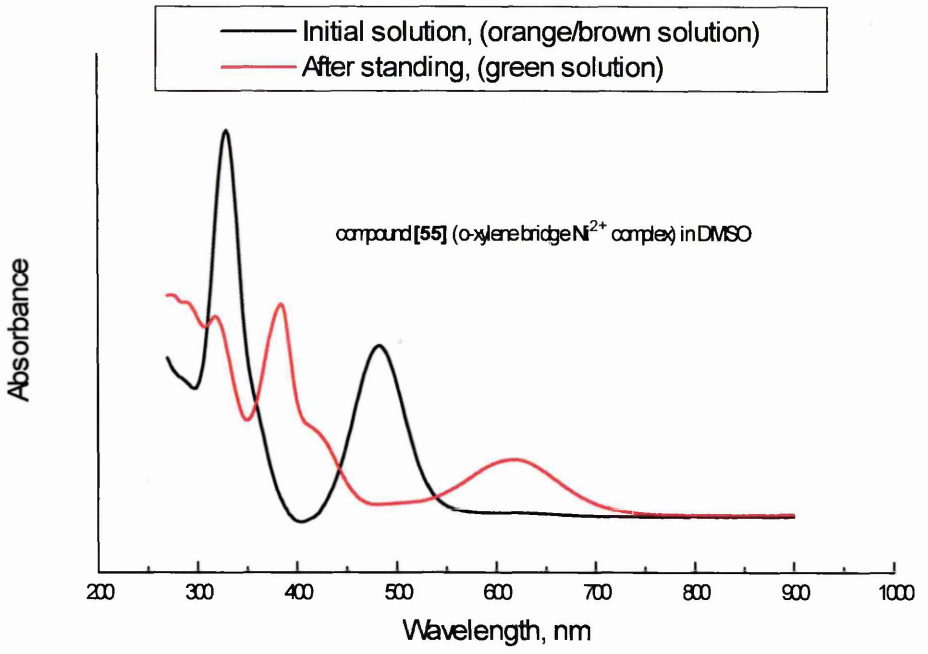

Figure 65, UV/VIS scan of compound **[55]** (o-xylene bridge Ni^{2+} complex) in DMSO.

This change from an initial orange/brown solution to a dark green could well be due to a conformational change of the complex from tetrahedral to octahedral as the Ni interacts with the DMSO. This phenomena was also observed in the DMF solutions, but the change was not as easily detected due to the colour change being much faster (under 30 seconds).

NMR of the complexes proved to be difficult, the complexes are sparingly soluble in most solvents, this in turn led to no useful carbon NMR being obtained due to the low concentration of the resulting solutions. Proton NMR yielded the following results:

- Compound **[52]**, $[Ti(Cp)_2]^{2+}$, the Cp peak was observed at 6.6 δ, SCH_2Ar at 4.2 δ and the peaks due to o-xylene as two multiplets at 7.5 & 7.7 δ in $CDCl_3$.
- Compound **[54]**, Co^{2+}, produced one band across the proton shift range with no defined peaks, suggesting the complex is paramagnetic.
- Compound **[55]**, Ni^{2+}, the peak for SCH_2Ar seen at 4.3 δ and a single peak for the o-xylene protons at 7.02 δ in D6 DMSO with both peaks noticeably broader suggesting some paramagnetic character to the solution, the DMSO peak appears significantly shifted in position to 2.88 δ from a more usual value of 2.50 δ [133]. This is possibly explained by the Ni complexing with the solvent causing a change in the proton environment of the solvent, this data complements the UV/VIS shown previously, DMSO and similar solvents are known to complex metals[10].
- Compound **[57]**, Zn^{2+}, the peak for SCH_2Ar seen at 4.6 δ and a single doublet peak for the o-xylene protons at 7.34 δ, (J = 20 Hz) in D6 acetone.

The NMR data proved consistent with the structure shown in Figure 55.

Attempts to isolate the complexes as crystals proved generally ineffectual, all the complexes were obtained as powders from the reaction mixtures. Attempts at growing crystals produced results for only one of the o-xylene complexes namely the Ni complex**[55]**. Slow evaporation from pyridine yielded small black crystals suitable for X-ray analysis. The solid state structure for this complex is shown in Figure 66.

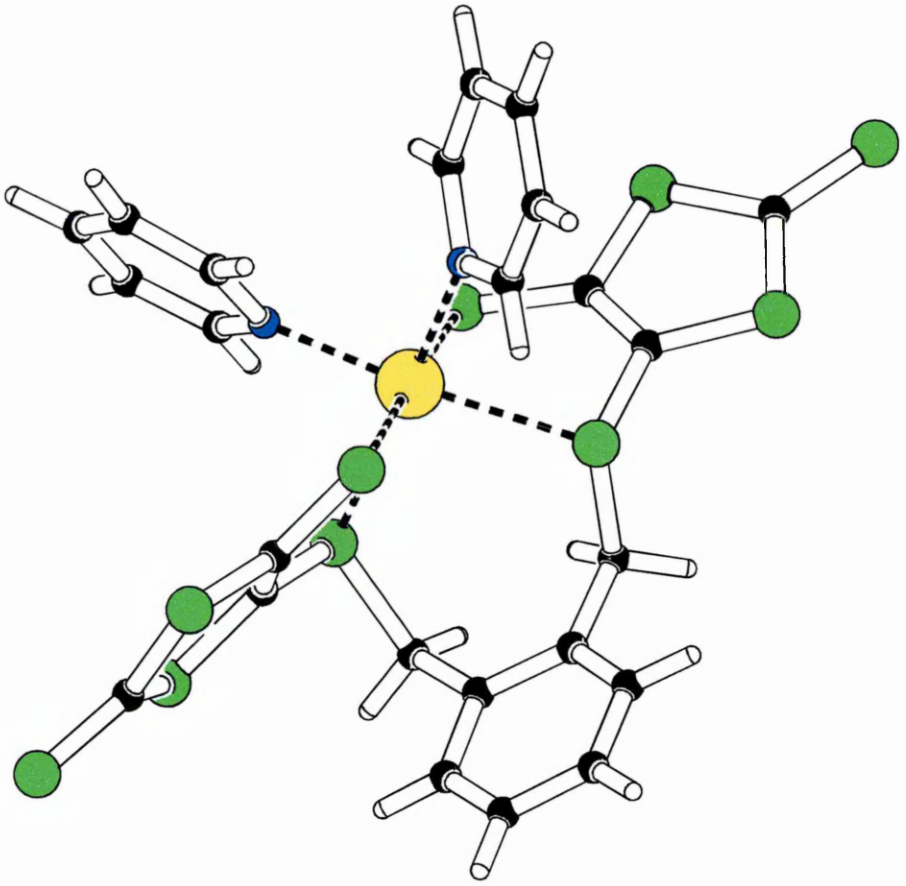

Figure 66, X-ray crystal structure of compound **[55]** (o-xylene bridge Ni complex), crystals grown from pyridine.

Tables of supporting data are shown in section 8.2.2. From the crystal structure it is clearly seen that the pyridine solvent is forming an octahedral complex with the Nickel, this complex/solvent interaction supports the data from UV/VIS and NMR spectra which suggested an interaction with the solvents used. This data also helps explain the solubility problems found with these complexes; it now seems apparent that the powders produced in the reactions were not dissolving in the solvents used (DMSO, acetone, pyridine), but forming octahedral complexes comparable to the structure for the Nickel-o-xylene compound**[55]** shown in Figure 66. Data obtained to this point is therefore unable to confirm if the complexes as synthesised are tetrahedral or square planar in configuration. Crystals of other o-xylene complexes were obtained but were found to be unsuitable for X-ray analysis.

3.2.2.3 "m-XYLENE BRIDGE LIGAND[37] DERIVATIVES, COMPOUNDS [59] to [64]"

Metal M	Compound Number	Metal salt used
Fe^{2+}	**[59]**	$FeCl_2$
Co^{2+}	**[60]**	$CoBr_2$
Ni^{2+}	**[61]**	$NiBr_2$
Cu^{2+}	**[62]**	$CuBr_2$
Zn^{2+}	**[63]**	$ZnCl_2$
$[Sn(Me)_2]^{2+}$	**[64]**	$[Sn(Me)_2]Cl_2$

A general structure for these complexes is shown in Figure 56.

MELTING POINTS

Complex (compound N°)	Initial colour	Initial colour Change	Melting point	Decomposition
Fe^{2+} (59)	dark green	darkens 84 °C	None	~134 °C
*Co^{2+} (60)	black	Not possible to see	None	~185 °C
Ni^{2+} (61)	dark brown/black	darkens 120 °C	None	~175 °C
Cu^{2+} (62)	red/brown	darkens 140 °C	None	~174 °C
Zn^{2+} (63)	orange/yellow	darkens 130 °C	None	~166 °C
$[Sn(Me)_2]^{2+}$ (64)	yellow	change to orange as melts	100 °C to 110 °C	~130 °C

*compound **[60]** difficult to judge due to darkness of the initial colour

MASS SPECTROMETRY

Both EI and FAB showed no trace of molecular ions for any of the metal complexes, EI and FAB show fragments corresponding to CS, CS_2, C_2S_2, CS_3. Mass spectrometry suggests that DMIT type compounds have been synthesised.

ELEMENTAL ANALYSIS

As with the o-xylene bridge complexes CHN analysis proved unhelpful due to difficulty in drying the complexes of all traces of solvent. After prolonged drying and repeated sample submission the compounds were found to have begun to decompose (darkened in colour and produced stench). CHN analysis did not prove helpful in determining the structure of the complexes.

FTIR

Peak assignment was determined with reference to standard tables[125-132]. The IR spectra of the metal complexes proved to be very similar to the IR trace for the unreacted ligand, the main differences being the absence of the nitrile peak at 2245 cm^{-1} and a reduction in the intensity of the peaks due to the aliphatic features of the compounds. The carbon-sulphur features of the IR spectra of the complexes were observed at much the same position, the main sulphur feature in the ligand was observed at ~1060 cm^{-1}, whereas in the transition metal complexes it was observed at ~1057 cm^{-1}. A further effect to the spectra was a broadening of the aromatic features of the spectra leading to less well defined

peaks. In general the IR spectra demonstrated features consistent with the structure shown in Figure 56.

UV/VIS

Complex (compound N°)	Solvent	λmax, nm
Fe^{2+} (59)	DMF (300-900 nm)	328, 384, 480
*Co^{2+} (60)	DMF (300-900 nm)	332, 380, 484
Ni^{2+} (61)	DMF (300-900 nm)	332, 480
	Pyridine (310-900 nm)	330, 480
Cu^{2+} (62)	insoluble	
Zn^{2+} (63)	DMF (300-900 nm)	332, 392, 484
$[Sn(Me)_2]^{2+}$ (64)	DMF (300-900 nm)	324, 380, 484

As with the previous complex all spectra that were scanned below 350 nm show peaks in the UV region at ~330 nm, this is likely due to C=S feature of the ligand itself. The second peak that was observed in some of the spectra at ~380 nm was only seen as a 'shoulder' to the peak at ~330 nm, and was most likely present in all the spectra.

In comparison to the UV/VIS data for the o-xylene complexes the spectra for the m-xylene complexes appeared significantly less complicated. The Nickel complex**[61]** in this case showed no indication of producing the peak at higher wavelengths (>600 nm).

NMR of the complexes again proved to be difficult, the m-xylene complexes proved to be sparingly soluble in most solvents, this in turn led to no useful carbon NMR due to the low concentration of the resulting solutions, except in the case of the Ni complex**[61]**. NMR yielded the following results:

- Compound **[60]**, Co^{2+}, produced one band across the proton shift range with no defined peaks, suggesting the complex is paramagnetic.
- Compound **[61]**, Ni^{2+}, the peak for SCH_2Ar seen at 4.03 δ and a single peak for the o-xylene protons at 7.16 δ in D6 DMSO with both peaks noticeably broader suggesting some paramagnetic character to the solution, in contrast to the o-xylene complex the DMSO peak appears at its more usual position at 2.51 δ[133]. The Carbon-13 NMR gave peaks for the sp^2 carbon features as two clusters of broadened peaks centred at 128.9, 136.5 δ, the feature for SCH_2Ar was hidden under the very broad peak for DMSO at 39.8 δ, and C=S observed at 210.9 δ.
- Compound **[63]**, Zn^{2+}, the peak for SCH_2Ar seen at 4.3 δ and a single peak for the m-xylene protons at 7.24 δ in D6 acetone.

3.2.2.4 "p-XYLENE BRIDGE LIGAND[38] DERIVATIVES, COMPOUNDS [65] to [70]"

Metal M	Compound Number	Metal salt used
Fe^{2+}	**[65]**	$FeCl_2$
Co^{2+}	**[66]**	$CoBr_2$
Ni^{2+}	**[67]**	$NiBr_2$
Cu^{2+}	**[68]**	$CuBr_2$
Zn^{2+}	**[69]**	$ZnCl_2$
$[Sn(Me)_2]^{2+}$	**[70]**	$[Sn(Me)_2]Cl_2$

A general structure for these complexes is shown in Figure 57.

MELTING POINTS

Complex (compound No)	Initial colour	Initial colour Change	Melting point	Decomposition
Fe^{2+} (65)	dark green	darkens 96 °C	None	~130 °C
*Co^{2+} (66)	black	Not possible to see	None	~166 °C
Ni^{2+} (67)	dark brown/black	darkens 120 °C	None	~160 °C
Cu^{2+} (68)	red/brown	darkens 162 °C	None	~180 °C
Zn^{2+} (69)	orange/yellow	darkens 135 °C	None	~170 °C
$[Sn(Me)_2]^{2+}$ (70)	yellow	change to orange as melts	155 °C to 160 °C	~180 °C

*compound **[66]** difficult to judge due to darkness of the initial colour

MASS SPECTROMETRY

Both EI and FAB showed no trace of molecular ions for any of the metal complexes, EI and FAB show fragments corresponding to CS, CS_2, C_2S_2, CS_3. Mass spectrometry suggests that DMIT type compounds have been synthesised.

ELEMENTAL ANALYSIS

As with the o-xylene bridge complexes CHN analysis proved unhelpful due to difficulty in drying the complexes of all traces of solvent. After prolonged drying and repeated sample submission the compounds were found to have begun to decompose (darkened in colour and produced stench). CHN analysis did not prove helpful in determining the structure of the complexes.

FTIR

Peak assignment was determined with reference to standard tables[125-132]. The IR spectra of the metal complexes proved to be very similar to the IR trace for the unreacted ligand, the main differences being the absence of the nitrile peak at 2245 cm^{-1} and a reduction in the intensity of the peaks due to the aliphatic features of the compounds. The carbon-sulphur features of the IR spectra of the complexes were observed at much the same position, the main sulphur feature in the ligand was observed at ~1065 cm^{-1}, whereas in the transition metal complexes it was observed at ~1060 cm^{-1}. A further effect to the spectra was a broadening of the aromatic features of the spectra leading to less well defined

peaks. In general the IR spectra demonstrated features consistent with the structure shown in Figure 57.

UV/VIS

Complex (compound N°)	Solvent	λmax, nm
Fe^{2+} (65)	DMF (300-900 nm)	328, 380, 480
Co^{2+} (66)	DMF (300-900 nm)	332, 380, 480
Ni^{2+} (67)	DMF (300-900 nm)	328, 368, 484
	Pyridine (310-900 nm)	330, 364, 482
Cu^{2+} (68)	insoluble	
Zn^{2+} (69)	DMF (300-900 nm)	328, 408, 484
$[Sn(Me)_2]^{2+}$ (70)	DMF (300-900 nm)	324, 372, 484

The UV/VIS spectra of the p-xylene complexes proved to be similar to those of the m-xylene complex, all spectra that were scanned below 350 nm show peaks in the UV region at ~330 nm, this is likely due to C=S feature of the ligand itself. The second peak that was observed in some of the spectra at ~380 nm was only seen as a 'shoulder' to the peak at ~330 nm, and was most likely present in all the spectra. In comparison to the UV/VIS data for the o-xylene complexes the spectra for the p-xylene complexes appeared significantly less complicated. The Nickel complex**[67]** in this case showed no indication of producing the peak at higher wavelengths (>600 nm).

NMR of the complexes again proved to be difficult, the p-xylene complexes proved to be sparingly soluble in most solvents, this in turn led to no useful carbon NMR of the resulting solutions. NMR yielded the following results:

- Compound **[66]**, Co^{2+}, produced one band across the proton shift range with no defined peaks, suggesting the complex is paramagnetic.
- Compound **[67]**, Ni^{2+}, the peak for SCH_2Ar seen at 3.8 δ and a single peak for the p-xylene protons at 7.0 δ in D6 DMSO with both peaks noticeably broader suggesting some paramagnetic character to the solution, in contrast to the o-xylene complex the DMSO peak appears at its more usual position at 2.48 δ[133].
- Compound **[69]**, Zn^{2+}, the peak for SCH_2Ar seen at 4.2 δ and a single peak for the p-xylene protons at 7.3 δ in D6 acetone.
- Compound **[70]**, $[Sn(Me)_2]^{2+}$, the peak for SCH_2Ar seen at 4.1 δ and a single peak for the p-xylene protons at 7.2 δ, and the peak for $Sn(CH_3)$ at 0.9 δ with the splitting due to Sn at 0.7 and 1.1 δ in D6 DMSO, $J = 140$ Hz.

3.2.2.5 "DIMETHYLPYRIDINE BRIDGE[39] LIGAND DERIVATIVES, COMPOUNDS [71] to [76]"

Metal M	Compound Number	Metal salt used
Fe^{2+}	**[71]**	$FeCl_2$
Co^{2+}	**[72]**	$CoBr_2$
Ni^{2+}	**[73]**	$NiBr_2$
Cu^{2+}	**[74]**	$CuBr_2$
Zn^{2+}	**[75]**	$ZnCl_2$
$[Sn(Me)_2]^{2+}$	**[76]**	$[Sn(Me)_2]Cl_2$

A general structure for these complexes is shown in Figure 58.

MELTING POINTS

Complex (compound N°)	Initial colour	Initial colour Change	Melting point	Decomposition
Fe^{2+} (71)	dark green	darkens 100 °C	None	~140 °C
Co^{2+} (72)	black	Not possible to see	None	~140 °C
Ni^{2+} (73)	dark brown/black	darkens 130 °C	None	~200 °C
Cu^{2+} (74)	red/brown	darkens 140 °C	None	~176 °C
Zn^{2+} (75)	orange/yellow	darkens 120 °C	None	~140 °C
$[Sn(Me)_2]^{2+}$ (76)	yellow	change to orange as melts	64 °C to 70 °C	~120 °C

*Compound **[72]** difficult to judge due to darkness of the initial colour*

MASS SPECTROMETRY

Both EI and FAB showed no trace of molecular ions for any of the metal complexes, EI and FAB show fragments corresponding to CS, CS_2, C_2S_2, CS_3. Mass spectrometry suggests that DMIT type compounds have been synthesised.

ELEMENTAL ANALYSIS

As with the o-xylene bridge complexes CHN analysis proved unhelpful due to difficulty in drying the complexes of all traces of solvent. After prolonged drying and repeated sample submission the compounds were found to have begun to decompose (darkened in colour and produced stench). CHN analysis did not prove helpful in determining the structure of the complexes.

FTIR

Peak assignment was determined with reference to standard tables[125-132]. The IR spectra of the metal complexes proved to be very similar to the IR trace for the unreacted ligand, the main differences being the absence of the nitrile peak at 2245 cm^{-1} and a reduction in the intensity of the peaks due to the aliphatic features of the compounds. The carbon-sulphur features of the IR spectra of the complexes were observed at much the same position, the main sulphur feature in the ligand was observed at ~1060 cm^{-1}, whereas in the transition metal complexes it was observed at ~1058 cm^{-1}. A further effect to the spectra was a broadening of the aromatic features of the spectra leading to less well defined

peaks. In general the IR spectra demonstrated features consistent with the structure shown in Figure 58.

UV/VIS

Complex (compound N°)	Solvent	λmax, nm
Fe^{2+} (71)	DMF (300-900 nm)	320, 384, 476
Co^{2+} (72)	DMF (300-900 nm)	324, 384, 480
Ni^{2+} (73)	DMF (300-900 nm)	324, 384, 476
Cu^{2+} (74)	insoluble	
Zn^{2+} (75)	DMF (300-900 nm)	324, 404, 480
$[Sn(Me)_2]^{2+}$ (76)	DMF (300-900 nm)	332, 384, 484

The UV/VIS spectra of the complexes proved to be similar to those of the xylene complexes, all spectra that were scanned below 350 nm show peaks in the UV region at ~330 nm, this is likely due to the C=S feature of the ligand itself. The second peak that was observed in some of the spectra at ~380 nm was only seen as a 'shoulder' to the peak at ~330 nm, and was most likely present in all the spectra, an example of which is shown in Figure 67.

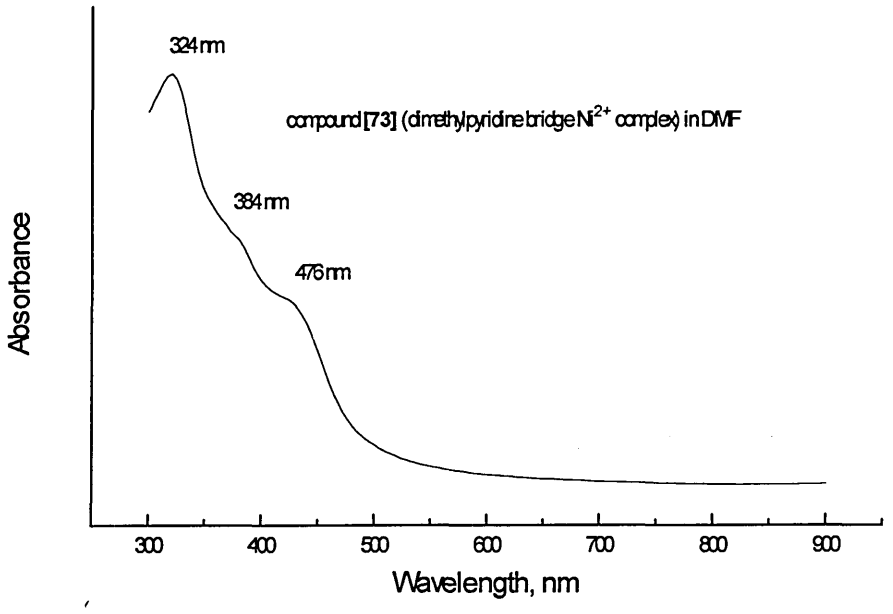

Figure 67, UV/VIS spectra of compound **[73]** (dimethylpyridine bridge Ni complex) in DMF.

In comparison to the UV/VIS data for the o-xylene complexes the spectra for the p-xylene complexes appeared significantly less complicated. The Nickel complex in this case showed no indication of producing the peak at higher wavelengths (>600 nm).

NMR

NMR of the complexes again proved to be difficult, these complexes proved to be sparingly soluble in most solvents, this in turn led to no useful carbon NMR of the resulting solutions. NMR yielded the following results:

- Compound **[72]**, Co^{2+}, produced one band across the proton shift range with no defined peaks, suggesting the complex is paramagnetic.
- Compound **[73]**, Ni^{2+}, the NMR spectra produced very broad ill defined peaks. The peak for SCH_2Ar seen at 4.2 δ with a width of ~0.5 δ and a single peak for the pyridine protons at 7.6 δ with a width of ~1.0 δ in D6 DMSO. The peaks were noticeably broader than those of the xylene Ni complexes suggesting some paramagnetic character to the solution. In contrast to the o-xylene complex the DMSO peak appears at its more usual position at 2.48 δ[133].
- Compound **[75]**, Zn^{2+}, the peak for SCH_2Ar seen at 4.2 δ integral 4, and two peaks observed for the aromatic protons at 7.26 δ (complex multiplet, appears to be a doublet J = 7.7 Hz, integral 2) and 7.71 δ (complex multiplet, appears to be a triplet J = 7.6 Hz, integral 1) in D6 DMSO.
- Compound **[76]**, $[Sn(Me)_2]^{2+}$, the peak for SCH_2Ar seen at 4.2 δ and two peaks observed for the aromatic protons at 7.26 δ (a very complex multiplet) and 7.75 δ (a very complex multiplet), the peak due to the $SnMe_2$ protons at 0.9 δ with the splitting due to Sn at 0.7 and 1.1 δ in D6 DMSO, J = 140 Hz.

3.2.3 MAGNETIC SUSCEPTIBILITY

The data obtained from the magnetic susceptibility balance was recorded as stated in section 2, this experimental data required further handling to produce the magnetic data in its more commonly stated value of magnetic moment. The data obtained produced the following information:

l = Length of sample in tube (cm)

m = Mass of sample (g)

R = Instrument reading for sample and tube (cm^2)

R_0 = Instrument reading for empty tube (cm^2)

C = Calibration constant for the magnetic susceptibility balance used

The magnetic susceptibility per gram χ_g ($cm^3\ g^{-1}$) is given by the equation:

$$\chi_g = [(C*l)\div(10^9 m)]*[R-R_0]$$

The magnetic susceptibility per mole χ_m ($cm^3\ mol^{-1}$) is given by the equation:

$$\chi_m = \chi_g M$$

M = molecular weight of complex

In a metal complex all the components of the compound have a magnetic effect on the recorded values. These generally possess a fixed diamagnetic susceptibility which is generally much smaller than the paramagnetic susceptibility. The correction factor is calculated from standard tables [124, 3].

Therefore the corrected magnetic susceptibility per mole χ'_m ($cm^3\ mol^{-1}$) is given by the equation:

$\chi'_m = \chi_m$ + Diamagnetic correction

The units for χ'_m need to be converted from $cm^3\ mol^{-1}$ to $m^3\ mol^{-1}$:

χ'_m(in $cm^3\ mol^{-1}$) * $[4\pi 10^{-6}] = \chi'_m$(in $m^3\ mol^{-1}$)

The magnetic moment μ, in Bohr magnetons (BM) is then obtained by the equation:

$\mu = 797.5*[\sqrt{(\chi'_m * T)}]$

T= Temperature, in Kelvin

The results for the complexes are shown below

The equation

$\chi_g = [(C*l)\div(10^9 m)]*[R-R_0]$

was applied to the generated data to produce χ_g:

value for C given as C = 0.999

Complex (compound Number)	l cm	R cm^2	R_0 cm^2	m g	χ_g $cm^3\ g^{-1}$
Eth $[Ti(Cp)_2]^{2+}$ **(43)**	2.05	-37	-35	0.0396	-1.03432E-07
Eth Fe^{2+} **(44)**	2.65	565	-34	0.0591	2.68319E-05
Eth Ni^{2+} **(46)**	1.90	144	-35	0.0576	5.89861E-06
Eth $[Ni(dppe)]^{2+}$ **(47)**	1.80	-5	-35	0.0529	1.01977E-06
Eth Cu^{2+} **(48)**	3.00	-37	-36	0.1041	-2.87896E-08
Eth Zn^{2+} **(49)**	1.85	-52	-35	0.0827	-3.7991E-07
o-xyl $[Ti(Cp)_2]^{2+}$ **(52)**	2.40	-42	-33	0.0537	-4.01832E-07
o-xyl Fe^{2+} **(53)**	2.10	119	-33	0.0400	7.97202E-06
o-xyl Co^{2+} **(54)**	2.20	260	-34	0.0496	1.30273E-05
o-xyl Ni^{2+} **(55)**	1.90	343	-34	0.0896	7.98643E-06
o-xyl Cu^{2+} **(56)**	2.50	-30	-34	0.0606	1.64851E-07
o-xyl Zn^{2+} **(57)**	2.00	-48	-35	0.0484	-5.36653E-07
o-xyl $[Sn(Me)_2]^{2+}$ **(58)**	2.40	-52	-36	0.0655	-5.85673E-07
m-xyl Fe^{2+} **(59)**	2.30	110	-34	0.0442	7.48572E-06
m-xyl Co^{2+} **(60)**	2.25	401	-34	0.0623	1.56946E-05
m-xyl Ni^{2+} **(61)**	2.40	67	-34	0.0570	4.24838E-06
m-xyl Cu^{2+} **(62)**	2.70	-36	-35	0.0582	-4.63454E-08
m-xyl Zn^{2+} **(63)**	2.55	-42	-34	0.0510	-3.996E-07
p-xyl Fe^{2+} **(65)**	2.30	76	-35	0.0390	6.53961E-06
p-xyl Co^{2+} **(66)**	2.20	202	-35	0.0505	1.03144E-05
p-xyl Ni^{2+} **(67)**	2.50	40	-36	0.0451	4.20865E-06
p-xyl Cu^{2+} **(68)**	2.00	-40	-34	0.0323	-3.71146E-07
p-xyl Zn^{2+} **(69)**	2.40	-47	-36	0.0541	-4.87497E-07
meth-py Fe^{2+} **(71)**	2.45	109	-35	0.0480	7.34265E-06
meth-py Ni^{2+} **(73)**	1.75	66	-35	0.0418	4.22424E-06
meth-py Cu^{2+} **(74)**	2.40	-35	-34	0.0747	-3.20964E-08

The equations $\chi_m = \chi_g M$, and $\chi'_m = \chi_m$ + Diamagnetic correction, and χ'_m(in $cm^3\ mol^{-1}$) * [$4\pi 10^{-6}$] = χ'_m(in $m^3\ mol^{-1}$), and $\mu = 797.5*[\sqrt{(\chi'_m * T)}]$, with the data below were used to determine the magnetic moment.

Complex (compound Number)	Molecular weight M	Temperature T K	Diamagnetic correction $cm^3\ mol^{-1}$	Magnetic moment, μ BM
Eth $[Ti(Cp)_2]^{2+}$ **(43)**	598.83	299	0.00033348	0.81
Eth Fe^{2+} **(44)**	476.62	299	0.00017998	5.57
Eth Ni^{2+} **(46)**	479.47	299	0.00018038	2.68
Eth $[Ni(dppe)]^{2+}$ **(47)**	877.89	299	0.00031350	1.70
Eth Cu^{2+} **(48)**	484.32	299	0.00018038	0.63
Eth Zn^{2+} **(49)**	486.17	299	0.00018268	χ'_m negative
o-xyl $[Ti(Cp)_2]^{2+}$ **(52)**	674.93	299	0.00034416	0.42
o-xyl Fe^{2+} **(53)**	552.72	299	0.00019066	3.31
o-xyl Co^{2+} **(54)**	555.81	299	0.00019106	4.21
o-xyl Ni^{2+} **(55)**	555.57	299	0.00019106	3.33
o-xyl Cu^{2+} **(56)**	560.42	299	0.00019106	0.82
o-xyl Zn^{2+} **(57)**	562.26	299	0.00019336	χ'_m negative
o-xyl $[Sn(Me)_2]^{2+}$ **(58)**	645.65	299	0.00020848	χ'_m negative
m-xyl Fe^{2+} **(59)**	552.72	299	0.00019066	3.22
m-xyl Co^{2+} **(60)**	555.81	299	0.00019106	4.62
m-xyl Ni^{2+} **(61)**	555.57	299	0.00019106	2.47
m-xyl Cu^{2+} **(62)**	560.42	299	0.00019106	0.63
m-xyl Zn^{2+} **(63)**	562.26	295	0.00019336	χ'_m negative
p-xyl Fe^{2+} **(65)**	552.72	295	0.00019066	3.00
p-xyl Co^{2+} **(66)**	555.81	295	0.00019106	3.74
p-xyl Ni^{2+} **(67)**	555.57	295	0.00019106	2.44
p-xyl Cu^{2+} **(68)**	560.42	295	0.00019106	χ'_m negative
p-xyl Zn^{2+} **(69)**	562.26	297	0.00019336	χ'_m negative
meth-py Fe^{2+} **(71)**	553.71	298	0.00019264	3.19
meth-py Ni^{2+} **(73)**	556.55	298	0.00019304	2.46
meth-py Cu^{2+} **(74)**	561.41	298	0.00019304	0.65

From this table of data it becomes clear that several complexes were not investigated using the magnetic susceptibility balance. This was due to their powder form, i.e. to obtain a reliable reading from the balance the sample must be well packed in the tube so as to produce an even distribution of the compound to ensure as much air is removed from the sample tube as possible. The best complexes for this technique were therefore the samples that were found to be relatively dry from solvent with a fine powder structure. Of the compounds analysed by this technique the compounds that produced the most notable results are discussed in section 4.

3.2.4 CYCLIC VOLTAMMETRY

The data obtained by cyclic voltammetry was determined by the method outlined in section 2[136,137]. While the majority of the metal complexes were analysed by this technique only the data obtained on the ethane bridged**[35]** complexes are shown here (compounds **[42]**, **[43]**, **[45]**, **[46]**, **[47]** and **[48]**). This was due to the observation that under the conditions of analysis used in these CV experiments, many compounds appeared to rapidly undergo a multitude of degradation and/or chemical (with respect to the starting complex) reactions, producing unreadable traces:

Compound **[42]**, ethane bridged **[35]** ligand TMA salt, the CV is shown in Figure 68. The notable features of this CV trace being the irreversible oxidation features at 365 and 1250 mV. The reduction peak at -900 mV is due to the DMF solvent used[136,138].

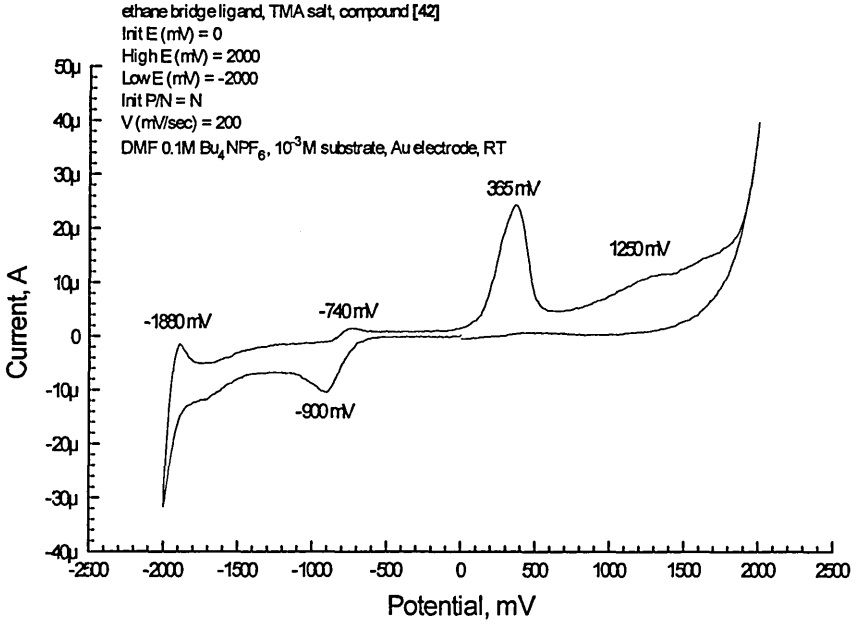

Figure 68, CV trace of compound **[42]**

Compound **[43]**, ethane bridged **[35]** Ligand $[Ti(Cp)_2]^{2+}$ complex, the CV is shown in Figure 69. The notable features of this CV trace being the irreversible oxidation features at 380 and 1440 mV and the irreversible reduction peak at -560 mV, again the reduction peak at -940 mV is due to the DMF solvent used[136,138].

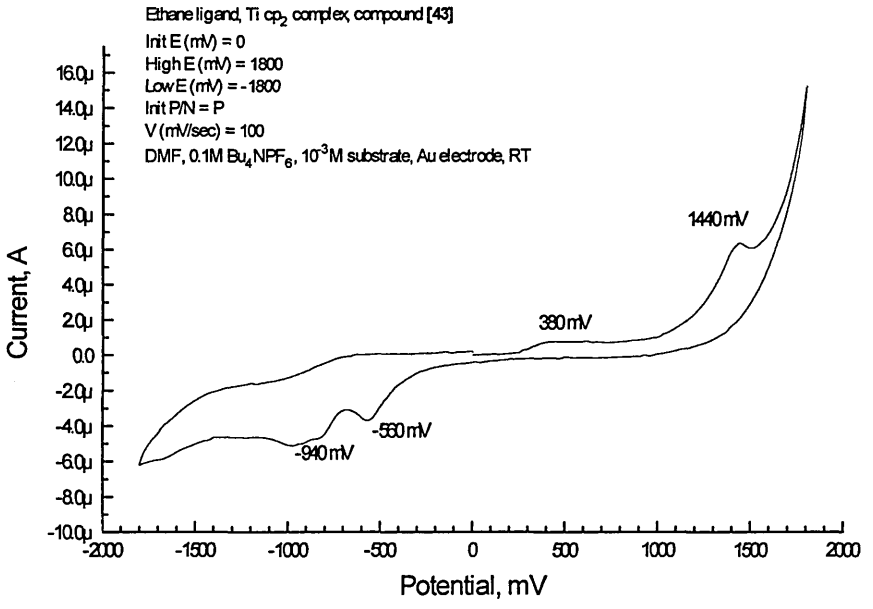

Figure 69, CV trace of compound**[43]**

Compound **[45]**, ethane bridged **[35]** Ligand Co^{2+} complex, the CV is shown in Figure 70. The notable features of this CV trace being the irreversible oxidation features at 950 and 1600 mV and the irreversible reduction peak at -540 mV. The reduction peak at -1030 mV is due to the DMF solvent used[136,138].

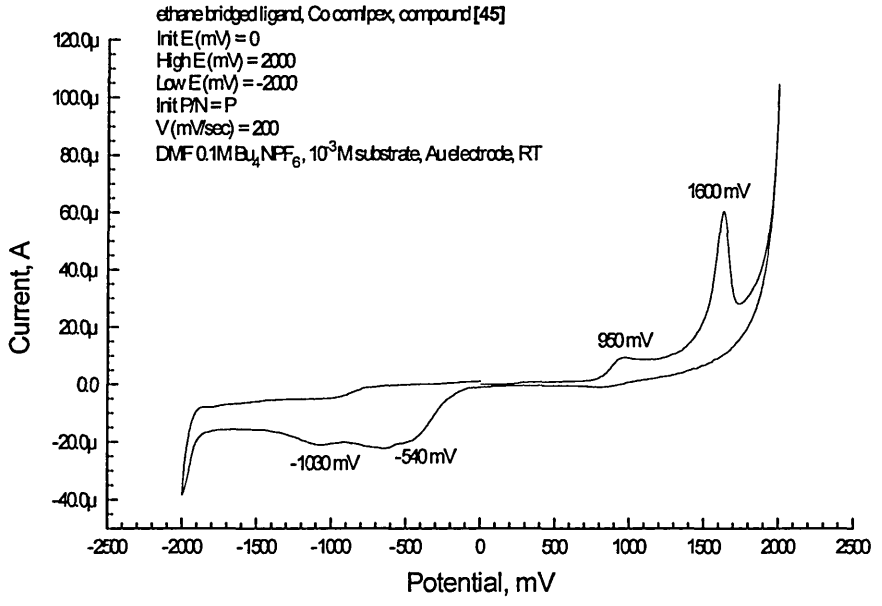

Figure 70, CV trace of compound**[45]**

Compound **[46]**, ethane bridged **[35]** Ligand Ni^{2+} complex, the CV is shown in Figure 71. The notable features of this CV trace being the irreversible oxidation features at 570, 1040 and 1640 mV. The reduction peak at -1050 mV is due to the DMF solvent used[136,138].

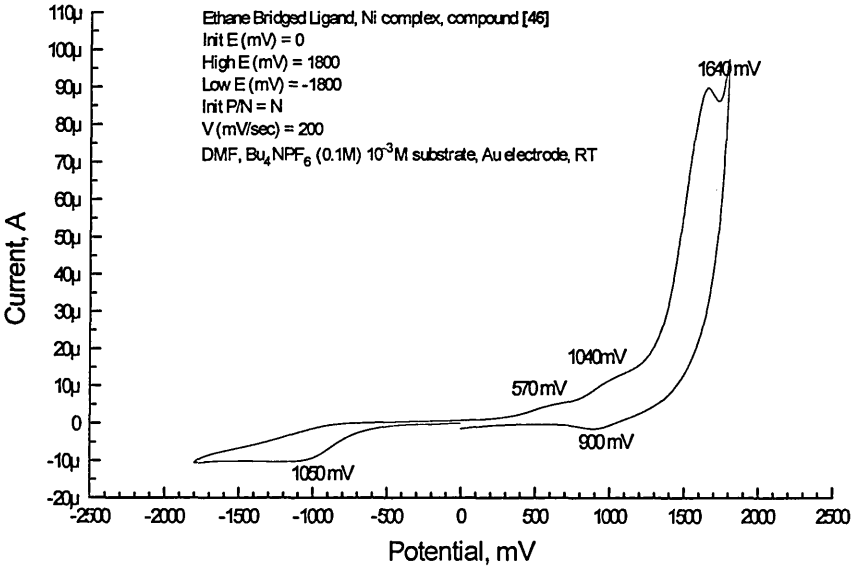

Figure 71, CV trace of compound**[46]**

Compound **[47]**, ethane bridged **[35]** Ligand $Ni(dppe)^{2+}$ complex, the CV is shown in Figure 72. The notable features of this CV trace being the irreversible oxidation features at 870 and 1400 mV, the reduction peak at -1200 mV is due to the DMF solvent used[136,138] but the peak is relatively to high in potential and may well be due to the complex.

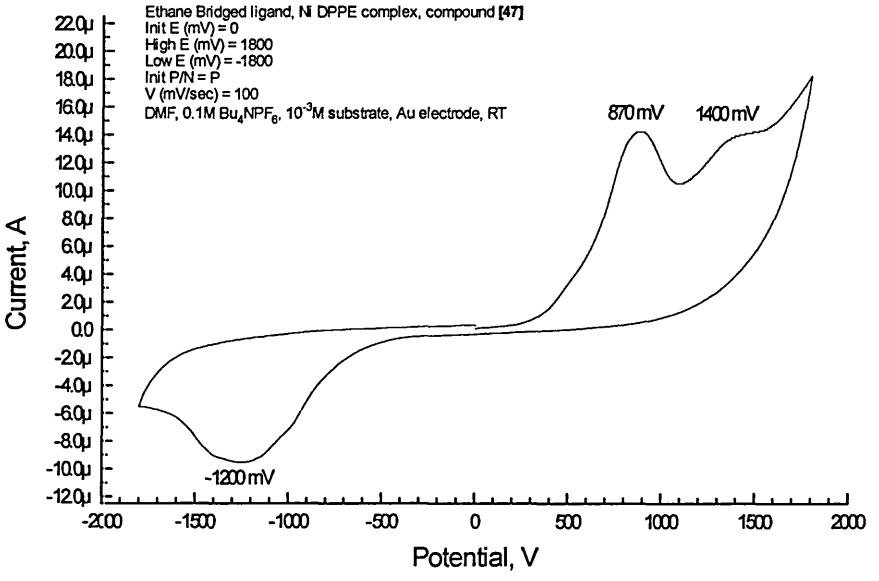

Figure 72, CV trace of compound**[47]**

Compound **[48]**, ethane bridged **[35]** Ligand Cu^{2+} complex, the CV is shown in Figure 73. The notable features of this CV trace being the irreversible oxidation features at 600 and 1480 mV, and the irreversible reduction peaks at 900 and -600 mV. The reduction peak at -1050 mV is due to the DMF solvent used[136,138].

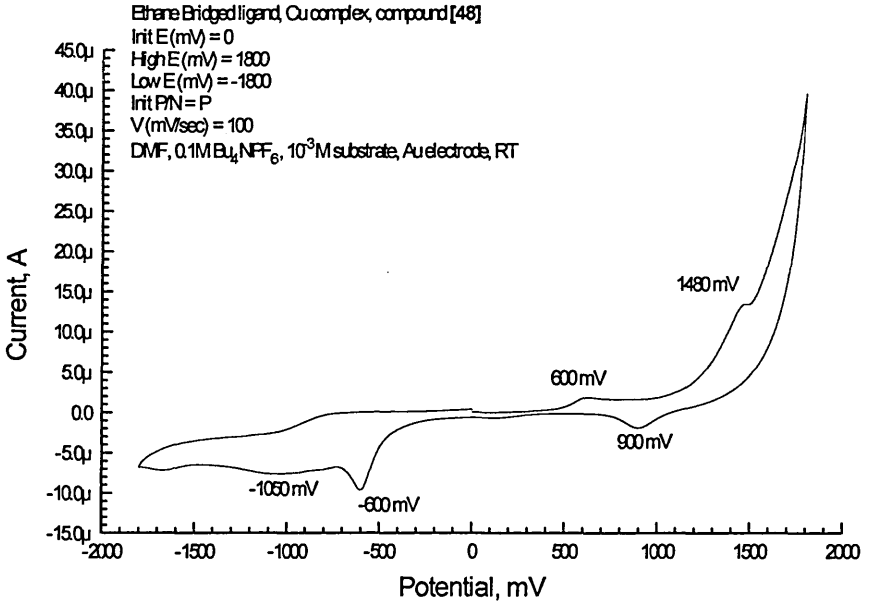

Figure 73, CV trace of compound**[48]**

4 CONCLUSIONS & DISCUSSION ON DMIT COMPLEXES

The data presented in section 3.1.2 provides good evidence that the ligands prepared have the structures shown in section 3.1. Whereas the more usual NMR, MS and FTIR analysis provided conclusive data on the nature of the ligands, the lack of any X-ray crystal data on these ligands did prove unfortunate. After many attempts it proved to be impossible to obtain these compounds in a form suitable for single crystal X-ray analysis.

Crystallographic evidence that these ligands did contain a covalent linkage between the component DMIT moieties was however provided by compound **[42].** Tetramethylammonium hydroxide was initially intended as a convenient base for the preparation of the dithiolate**[42]** prior to the insertion of a metal salt. This intermediate soon demonstrated its limitation as a synthon for the preparation of subsequent metal complexes (Figure 54), this was due to the observation that transition metal halides were unable to displace the tetramethylammonium moiety from the salt (or only partially displace the tetramethylammonium ion to give a mixture of complexes). This was supported by the fact that only crystals of **[42]** were isolated. Subsequent reactions proved that the ideal base of choice for the preparation of the metal complex precursors was sodium ethoxide or methoxide. This observation does however contrast with previous work on thiolate-metal complexes in which the tetramethylammonium salt of a thiolate does provide a convenient route to thiolate complexes[139,140]

The metal complexes did however provide a more difficult prospect for determining structures due to a lack of X-ray crystal data. While in each case the NMR, FTIR and MS provided data consistent with the expected metal complexes this data alone is not enough to conclusively elucidate their structures. In all cases the complexes were initially obtained as fine powders from the reaction mixtures, and the only complex obtained as crystals suitable for X-ray analysis was compound **[55]**, with the crystal structure for this compound showing the complex as an octahedral Nickel system. Repeating the experiment that led to the crystals of compound **[55]** with the other metal complexes also provided crystals but in every case they proved to be unsuitable for single crystal X-ray analysis. This result also helps to explain the lack of solubility encountered in these complexes. The compounds only dissolve in solvents that could co-ordinate with the metal centres (pyridine, acetone, DMSO, DMF), therefore it became important to analyse the complexes in their isolated powder form.

The data obtained from the magnetic susceptibility balance provided some useful and interesting insights into the structures of the complexes prepared. This data proved to be of most help due to the fact that limited crystallographic data was obtained on these systems. From the use of standard tables and equations[3,10,102,124,126,141], it became possible to define the structural nature of these systems more convincingly:

$$\mu_{effective} = \sqrt{[n(n+2)]}$$

where n = the number of unpaired electrons

$\therefore$ the values of $\mu_{effective}$ as a function of n are:

n	$\mu_{effective}$ (BM)
1	1.73
2	2.83
3	3.87
4	4.90
5	5.92
6	6.93

Of the compounds analysed by the magnetic susceptibility balance the most notable features seen are therefore:

1. **Titanium complexes**, compounds **[43]** and **[52]**, the ethane and o-xylene bridge systems respectively. The metal salt used in the preparation of these complexes was the Ti^{IV} salt $Ti(Cp)_2Cl_2$, Ti^{IV} is a d^0 system with no unpaired electrons and should therefore give a magnetic moment of 0. Ti^{III} a d^1 system is known to produce complexes with a magnetic moment, but provide values in the region of 1.7 to 1.8 BM (n=1)[3,10,102,124,126].The small magnetic moment found for these systems (0.81 and 0.42 BM respectively), falls well below this value and the most likely explanation being that these complexes are Ti^{IV} of tetrahedral or octahedral geometry, with the magnetic moment

readings due to experimental error, contamination with a paramagnetic impurity, or errors in the diamagnetic corrections used (the standard tables do not include correction values for Ti^{IV} and C=S).

2. **Zinc and Tin complexes**, compounds **[49]**, **[57]**, **[58]**, **[63]** and **[69]**. Both Zn^{II} and Sn^{IV} are d^{10} systems with no unpaired electrons (n=0, therefore 0 BM), χ'_m for these compounds proved to be a negative value and the complexes can therefore be considered diamagnetic.
3. **Copper complexes**, compounds **[48]**(ethane bridge complex), **[56]**(o-xylene bridge complex), **[62]**(m-xylene bridge complex), **[68]**(p-xylene bridge complex) and **[74]**(dimethyl pyridine bridge complex). The Cu^{II} complexes produced interesting if somewhat confusing data from the magnetic susceptibility balance. Cu^{II} being a d^9 system (with 1 unpaired electron) should produce a magnetic moment of about 1.7 BM. The magnetic moment of the complexes gave results of 0.6 to 0.8 BM except for complex **[68]** which proved to be diamagnetic. Diamagnetic copper complexes are invariably based on Cu^{I} (a d^{10} system with no unpaired electrons). Possible explanations for this discrepancy could be due to the isolated compound being a mixture of both Cu^{I} and Cu^{II} systems or entirely based on Cu^{I} with the measured paramagnetic character due to experimental error. In either case the data obtained here suggests the complex or complexes produced are not the structures shown in Figure 54, Figure 55, Figure 56, Figure 57 and Figure 58, in terms of the metal centre being M^{2+}.
4. **Iron complexes**, compounds **[44]**(ethane bridge complex), **[53]**(o-xylene bridge complex), **[59]**(m-xylene bridge complex), **[65]**(p-xylene bridge complex) and **[71]**(dimethyl pyridine bridge complex). The magnetic moment

for compound **[44]**, 5.57 BM, falls into the established range for high spin d^6 Fe^{II} with 4 unpaired electrons (5.0 to 5.6 BM[3,10,102,124,126]), but interestingly the value also falls close to the range quoted for high spin d^5 Fe^{III} with 5 unpaired electrons (5.6 to 6.0 BM[3,10,102,124,126]). The other complexes prepared **[53]**(o-xylene bridge complex), **[59]**(m-xylene bridge complex), **[65]**(p-xylene bridge complex) and **[71]**(dimethyl pyridine bridge complex) all give a magnetic moment of 3.0 to 3.3 BM, which gives a similar problem to that encountered with copper; the value taken alone suggests a complex containing 2 unpaired electrons. In this case, low spin or high spin Fe^{II} or Fe^{III} cannot easily explain this observation. Again an explanation for this could be that the isolated compound contains a mixture of Fe atoms in several electron configurations, and the observed paramagnetic character is an average of these systems (e.g. a mix of high and low spin Fe^{II}), however the large magnetic moment measured (>3.0 BM) is certainly too high a value to be explained by experimental error and the compounds must be considered to have paramagnetic character.

5. **Cobalt complexes**, compounds **[54]**(o-xylene bridge complex), **[60]**(m-xylene bridge complex) and **[66]**(p-xylene bridge complex). The magnetic moments determined for these complexes (4.2, 4.6 and 3.7 BM) closely match the values quoted for high spin d^7 Co^{II}(4.3 to 5.2 BM[3,10,102,124,126]).
6. **Nickel complexes**, compounds **[46]**(ethane bridge complex), **[55]**(o-xylene bridge complex), **[61]**(m-xylene bridge complex), **[67]**(p-xylene bridge complex), **[73]**(dimethyl pyridine bridge complex) and **[47]**(ethane bridge complex, Nickel dppe). The first and most obvious conclusion from the

magnetic balance data was that all the Nickel complexes are paramagnetic, and therefore are not planar complexes (planar low spin d^8 Ni^{II} complexes have no unpaired electrons and are invariably diamagnetic). Tetrahedral high spin d^8 Ni^{II} has two unpaired electrons with a $\mu_{effective}$ of 2.83 BM which the complexes **[46]**, **[55]**, **[61]**, **[67]** and **[73]** closely match. The notable exception to this being complex **[47]**, with the magnetic moment data suggesting(1.70 BM) that the complex contains 1 unpaired electron, possibly explained by Nickel being in the +3 oxidation state(low spin d^7), Ni^{III} complexes are however very rare[3,10,102,126] and such an explanation is entirely speculative.

The magnetic data does provide further information on the structural nature of these complexes. Compound **[55]** analysed in its fine powder state on the magnetic susceptibility balance, clearly indicates the complex is tetrahedral and undergoes a conformational change in solution to an octahedral complex as demonstrated in the crystal structure. This feature is also seen in the UV/VIS measurements (Figure 64 and Figure 65). The initial scan in DMSO for **[55]** shows a λ_{max} of 482 nm, and after several minutes changes to a λ_{max} of 618 nm, a shift of 134 nm. Further evidence of the complexes interacting with the solvents was provided by the NMR data for the nickel complex **[55]** which showed a measurable shift in the position of the DMSO peak (2.50 δ to 2.88 δ). The magnetic data, as is mentioned on the previous page, does provided important data on the Nickel complexes. However, the magnetic susceptibility data for some of the other complexes are not readily explained.

A further set of data that gave indications about the complexes properties was provided by the melting point data. All complexes except the dimethyl tin derivatives (**[51]**, **[58]**, **[64]**, **[70]** and **[76]**) decomposed on heating, and compound **[50]**, as was mentioned in the NMR section of chapter 3.2.2.1, decomposed in solution to produce Hg metal. A possible explanation is provided by the CV data and the known reactions of thiolates[142-144], typified by the reaction outlined in Figure 74.

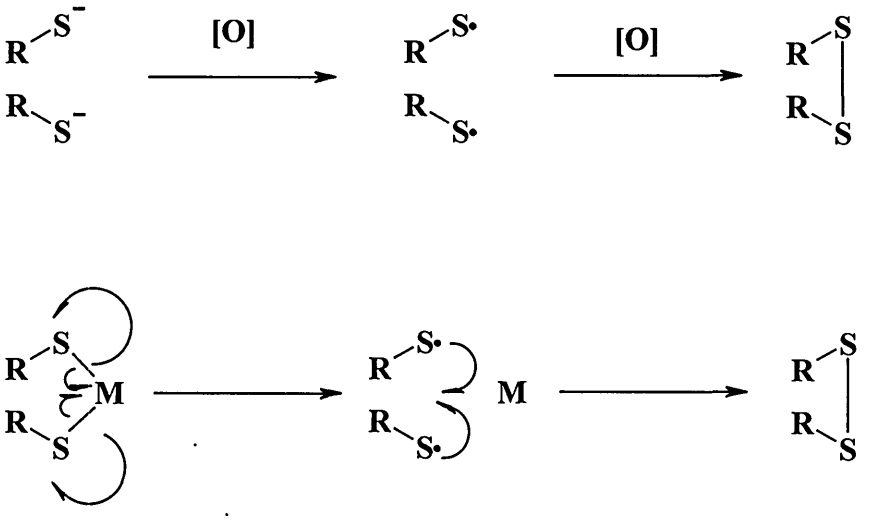

Figure 74, S-S bond formation

A reaction scheme of this type would explain the decomposition under relatively mild heating and the production of Hg metal from solutions of **[50]**. Attempts were made to determine the nature of the "organic" residue left after compound **[50]** had decomposed to give Hg metal, repeated analysis in each case provided evidence (from MS) that the decomposition products contained DMIT

type structures, but in each case the data was not reproducible, possibly explained by crosslinked or polymer type structures being obtained. Further support for this type of oxidation is provided by the CV trace for compound **[42]**(Figure 68, the TMA salt of **[35]**) which shows a strong oxidation peak at 385 mV, and a further less intense but broadened peak at 1250 mV. The peak at the lower potential is likely to be due to a reaction of the type outlined in Figure 74 and is visible in the majority of the CV traces of the complexes. The peak at the higher potential is however harder to explain. This feature may well be due to the production of polymeric type structures or a build up of oxidised species. The trace for compound **[43]** (the $[Ti(Cp)_2]^{2+}$ complex of **[35]**) showed a similar set of peaks except for the presence of a reduction peak at -550 mV, which was found in all but the Nickel complexes of compound **[35]**. In comparison to these CV traces, the ligands themselves (**[35]**, **[36]**, **[37]**, **[38]** and **[39]**) showed no trace of electroactivity, demonstrating that the observed features are based on the thiolate moieties. Initial conclusions that the higher oxidation peak (seen at ~1400 mV) was due to the metal centres themselves, for example oxidising Co^{II} to Co^{III} or higher, can be discounted by the fact that this peak is seen in the Titanium complex **[43]**. The metal centre in this titanium complex is already at +4 and the oxidation features observed in the CV must therefore be due to the dithiolate ligand itself.

The conclusions from the data presented here, suggests that the complexes prepared conform to the general structures outlined in Figure 54, Figure 55, Figure 56, Figure 57 and Figure 58. However the data presented demonstrated that the complexes as prepared were tetrahedral with respect to the metal centres, and in the case of the nickel, iron, cobalt and copper complexes become octahedral in solution with solvents such as pyridine and DMSO.

5 EXPERIMENTAL - HALOGEN ADDUCTS

5.1 THIONE PRECURSORS

5.1.1 THIONE SYNTHESIS

These synthetic methods represent, with respect to yield and purity, an optimised route to these compounds. As was stated in section 3.1.1 the synthesis of compound **[15]** (4,5 bis(2'-cyanoethylthio)-1,3-dithiole-2-thione), from which all of the metal complexes, and several of the dihalogen adducts (section 5.2) were ultimately prepared from, is described in this section. While many thiones were utilised in the preparation of the thione-dihalogen adducts, only those thiones which subsequently produced quantifiable adducts are described here.

5.1.1.1 SYNTHESIS OF 4,5 BIS(2'-CYANOETHYLTHIO)-1,3-DITHIOLE-2-THIONE, COMPOUND [15]

Literature methods for the synthesis of 4,5 bis(2'-cyanoethylthio)-1,3-dithiole-2-thione**[15]** are known[31,72]. The method used in this study is a development of these published techniques. 4,5 bis(2'-cyanoethylthio)-1,3-dithiole-2-thione**[15]** is prepared from the zincate**[13]** salt in one step; an outline of this reaction was shown previously in Figure 13. The zincate**[13]** salt used in this synthesis was prepared using a method slightly modified from that of the published technique by Bryce et al.[71]. The synthesis of compound **[15]** then becomes a two step process outlined in Figure 75.

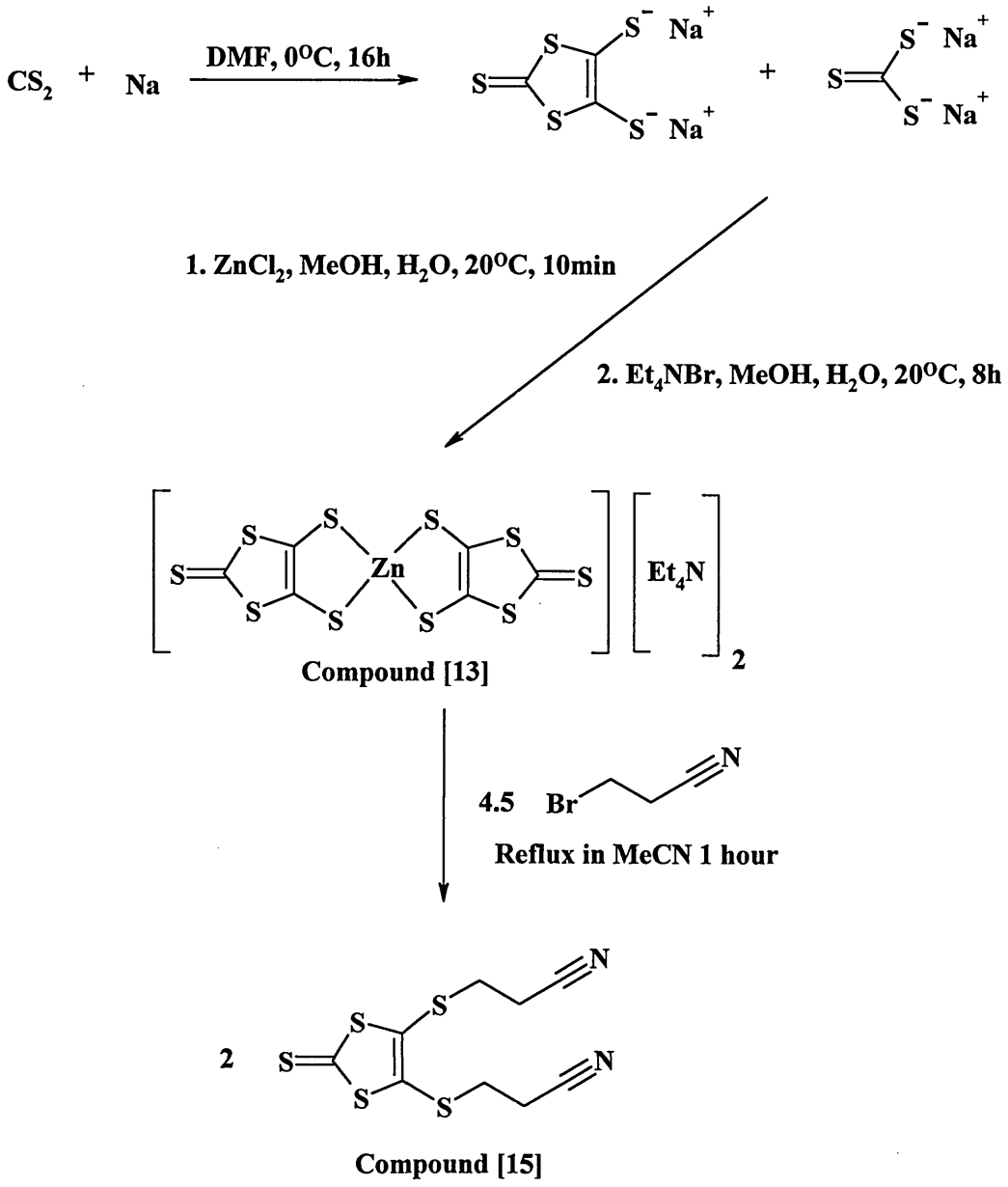

Figure 75, Reaction scheme for the preparation of 4,5 bis(2'-cyanoethylthio)-1,3-dithiole-2-thione, compound **[15]**

*synthesis of zincate salt, compound **[13]**:*

Dry distilled DMF (240 mL) was sparged with dry nitrogen for 30 minutes at -5^{O}C. Maintaining the nitrogen atmosphere and the temperature at -5^{O}C, carbon disulphide (120 mL, 2 moles) was added and the resulting mixture stirred vigorously for 30 minutes, to this mixture, ensuring the temperature did not rise above 0^{O}C and under a constant nitrogen atmosphere, finely cut sodium metal pieces (7.2 g, 0.31 moles) was added and the resulting mixture stirred at -5^{O}C for 6 hours to give a dark red solution. Unreacted sodium metal (if any) was removed by the careful addition of a minimum of MeOH. 10 mL aliquots of two different solutions (solution 1 = 10.65 g $ZnCl_2$ (0.078 moles) in 50 mL H_2O + 175 mL NH_4OH, solution 2 = 33 g tetraethylammonium Bromide (0.157 moles) in 250 mL H_2O) were added alternately to produce zincate salt **[13]** as a red microcrystalline powder. This solution was stirred at 0^{O}C for 16 hours and the zincate**[13]** salt removed by filtration, and washed with propan-2-ol then diethyl ether to give 42 g of zincate**[13]** salt (yield 88%).

synthesis of 4,5 bis(2'-cyanoethylthio)-1,3-dithiole-2-thione, compound [15]:

Zincate**[13]** (20 g, 27.8 mmol) was dissolved in acetonitrile (300 mL) to give a red solution. To this mixture 3-bromopropanonitrile (5 equivalents, 139.2 mmol = 12.46 g) was added and the reaction mixture refluxed for 2 hours to give a yellow/brown solid/solution. The acetonitrile was removed under vacuum to give a brown oil. This was dissolved in DCM (300 mL) and stirred with decolourising charcoal for 30 minutes and filtered through a small (~100 mL) flash silica plug to give a yellow solution. Evaporation of the DCM yielded a yellow powder which was recrystallised by dissolving in a minimum of ethylacetate and precipitation with excess petroleum ether to give 14.5 g 4,5 bis(2'-cyanoethylthio)-1,3-dithiole-2-thione**[15]** (86% yield).

5.1.1.2 LIGAND PREPARATION, COMPOUNDS [35] TO [38]

The unreacted or protected ligands prepared previously (section 3.1.1) were also investigated as to their potential as donor systems in the preparation of thione-dihalogen adducts. The synthesis of these compounds is described in section 3.1.1 and is therefore not repeated in this section. The ligands used in the preparation of dihalogen adducts are shown in Figure 76.

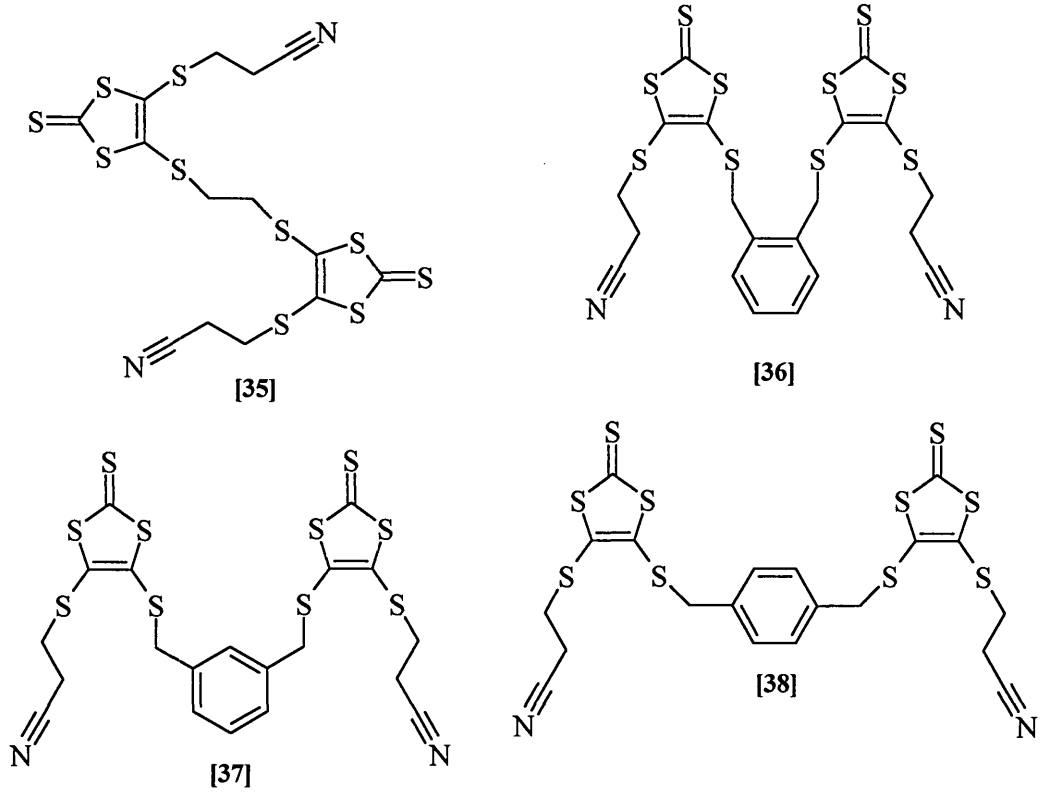

Figure 76, Ligands used in the preparation of dihalogen adducts, compounds **[35]** to **[38]**

5.1.1.3 SYNTHESIS OF DIMETHYL 1,3-DITHIOLE-2-THIONE-4,5-DICARBOXYLATE, COMPOUND [77]

Dimethyl 1,3-dithiole-2-thione-4,5-dicarboxylate**[77]** has been known in the area of 1,3-dithiole-2-thione chemistry for over 30 years[39,145]. While several synthetic methods have been developed one of the most popular routes is that outlined in Figure 77.

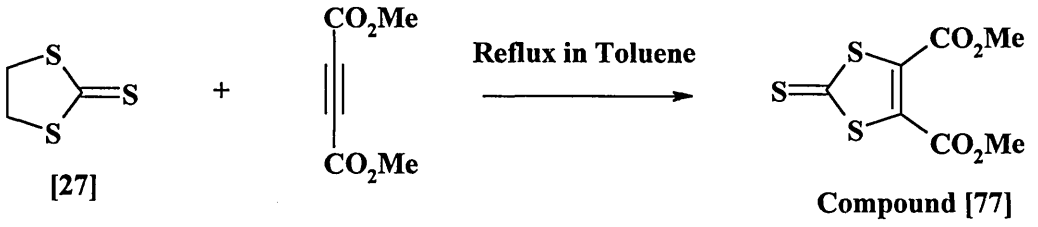

Figure 77, Synthesis of dimethyl 1,3-dithiole-2-thione-4,5-dicarboxylate, compound **[77]**

Equivalent molar quantities of 1,3-dithiolane-2-thione**[27]** (ethylene trithiocarbonate) and dimethylacetylenedicarboxylate (DMAD) were heated under reflux for 12 hours in Toluene. The solvent was removed under vacuum to yield a dark yellow solid**[77]** and purified on a flash silica column using 9:1 toluene:40/60 petroleum ether.

5.1.1.4 SYNTHESIS OF 1,3-DITHIOLE-2-THIONE-4-FERROCENE, COMPOUND [80]

Compound **[80]** is prepared in three steps from Ferrocene, the scheme used is outlined in Figure 78.

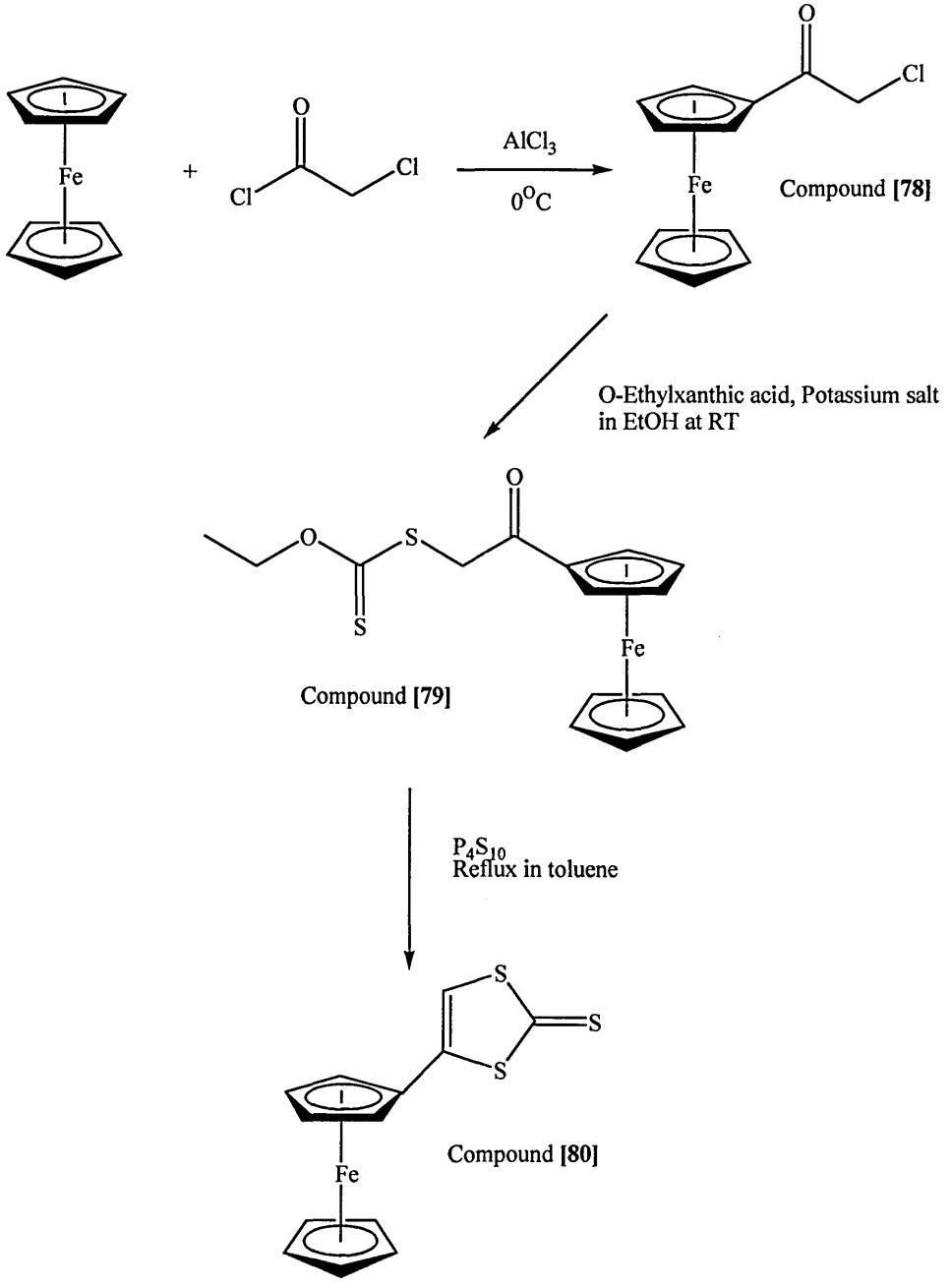

Figure 78, Synthetic outline for the preparation of 1,3-dithiole-2-thione-4-ferrocene, compound **[80]**

Step 1, preparation of Chloroacetyl Ferrocene, compound [78]

Under an atmosphere of N_2 using Shlenck techniques, freshly sublimed ferrocene (10 g, 53.8 mmol) was dissolved in anhydrous DCM (80 mL) and cooled to $0^{O}C$ to give an orange solution. Under an atmosphere of N_2 was added dropwise to this solution over approximately 30 minutes and ensuring the temperature remained at 0 ^{O}C, a second solution comprising of $AlCl_3$ (7.2 g) and chloroacetyl chloride (4.4 mL) in anhydrous DCM (20 mL). During this addition the ferrocene solution was observed to change in colour from orange to a dark purple/blue. The reaction mixture was allowed to warm to room temperature, upon which a small volume of water (10 mL) was added to destroy excess $AlCl_3$ and chloroacetyl chloride. The resulting DCM solution was washed with 100 mL volumes of water until the water washes were observed to be colourless. The resulting dark brown/orange DCM solution was dried over magnesium sulphate and the required product separated from the reaction mixture on a flash silica column using DCM as eluent, compound **[78]** Rf = 0.39 in DCM, to give 3.26 g of a red/orange oil, yield 23 %.

Step 2, preparation of ethyl [(2-oxo-2-ferrocenylethyl)sulfanyl]methanethioate, compound [79]

Chloroacetyl ferrocene, compound **[78]** (2.96 g, 11.3 mmol), was dissolved in dry ethanol (100 mL) to give an orange solution. To this solution potassium o-ethylxanthate (3.62 g, 22.6 mmol, 2 equivalents) was added and the resulting mixture stirred at room temperature for 16 hours. The required compound was purified on a flash silica column using DCM as eluent, compound **[79]** Rf = 0.47 in DCM, to give 2.58 g (8.8 mmol) of an orange solid (yield = 78 %).

Step 3, preparation of 1,3-dithiole-2-thione-4-ferrocene, compound [80]

Compound **[79]** (2.58 g, 8.8 mmol) was dissolved in dry toluene (200 mL) to give an orange solution, this solution was refluxed under N_2 for 6 hours with P_4S_{10} (3.52 g, 7.92 mmol, 0.9 equivalents), the resulting brown solution was cooled to room temperature and stirred over night. Compound **[80]**, was purified on a flash silica column using toluene as eluent (Rf = 0.78 in toluene). The fraction containing compound **[80]** was stirred for 30 minutes with decolourising charcoal, filtered and evaporated to give a brown solid. The compound was recrystallised by dissolving in a minimum of DCM and precipitated with hexane to give 0.64 g (2 mmol) of a light brown/orange solid (yield = 23 %).

5.1.2 THIONE ANALYSIS

5.1.2.1 4,5-BIS(2'-CYANOETHYLTHIO)-1,3-DITHIOLE-2-THIONE, COMPOUND [15]

Compound **[15]**, Figure 75, is isolated as a fine yellow microcrystalline powder (melting point 80 °C), literature value 82 °C[72].

Formula $C_9H_8N_2S_5$, Formula weight = 304.51

EI mass spectrometry yielded molecular ion M/z = 303.9, (literature value[72] M/z = 304), and fragments corresponding to CS, CS_2, C_2S_2, CS_3.

FTIR spectra showed features consistent with the structure shown in Figure 75, notable peaks being the nitrile feature seen at 2245 cm^{-1} (literature value[72] 2249 cm^{-1}), 2924 cm^{-1} (aliphatic C-H stretching), 1456 / 1408 cm^{-1} (Aliphatic C-H bending), 1065 cm^{-1} (C=S bond).

Proton NMR (solvent $CDCl_3$) showed peaks at δ = 2.82 (triplet, integration 4 H, J = 6.7 Hz) and δ = 3.17 (triplet, integration 4 H, J = 6.9 Hz) corresponding to SCH_2CH_2CN. Carbon 13 NMR (solvent $CDCl_3$) showed peaks at δ = 19.4 and 32.1 (CH_2CH_2), δ = 117.4 (CN), δ = 136.2 (C=C), δ = 209.5 (C=S).

5.1.2.2 DIMETHYL-1,3-DITHIOLE-2-THIONE-4,5-DICARBOXYLATE, COMPOUND [77]

Compound **[77]**, Figure 77, is isolated as a yellow-orange powder, melting point 73 °C, literature value 72 °C[145].

Formula $C_7H_6O_4S_3$, Formula weight = 250.30

EI mass spectrometry yielded molecular ion M/z = 249.9, and fragments corresponding to CS, CS_2, C_2S_2, CS_3, and fragmentation of the ester groups.

FTIR spectra showed features consistent with the structure shown in Figure 77, notable peaks being the methyl ester features seen at 1850 cm^{-1} (C=O), and vinylene trithiocarbonate features including C=S bond at 1060 cm^{-1}.

Proton NMR spectra provided additional data for compound **[77]**, (solvent $CDCl_3$) showed a single peak at $\delta = 3.92$ for the methyl ester protons. Carbon 13 spectra (solvent $CDCl_3$) showed peaks at $\delta = 208$ (C=S), $\delta = 169$ (C=O), $\delta = 123$ (C=C), $\delta = 52$ (CH_3).

5.1.2.3 1,3-DITHIOLE-2-THIONE-4-FERROCENE, COMPOUND [80]

As was shown in section 5.1.1.4 and Figure 78, 1,3-Dithiole-2-thione-4-ferrocene, compound **[80]**, is prepared in 3 steps from ferrocene.

Step 1, Chloroacetyl ferrocene, compound [78]

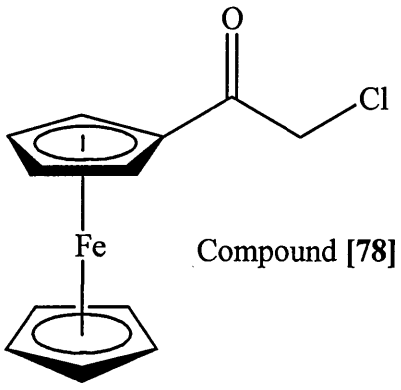

Compound **[78]**

Figure 79, Chloroacetyl ferrocene, compound **[78]**

The structure of compound **[78]** is shown in Figure 79. Compound **[78]** was isolated as a red/orange oil.

Formula $C_{12}H_{11}OFeCl$, Formula weight = 262.518

EI mass spectrometry yielded molecular ion M/z = 261.9, and fragments corresponding to loss of $^{\cdot}CH_2Cl$, $^{\cdot}COCH_2Cl$, and fragmentation consistent of the ferrocene moiety.

Proton NMR spectra provided additional data for compound **[78]**, (solvent $CDCl_3$) showed a single peak at δ = 4.24 (integration 5 hydrogens) for the

unsubstituted cyclopentadiene (Cp) ring, the chloroacetyl CH_2 protons observed as a single peak at $\delta = 4.42$ (integration 2 hydrogens), and the four protons of the substituted ring seen as two singlets at $\delta = 4.59$ and $\delta = 4.83$ (integration 2 hydrogens for each peak) whereas one might have expected them to be observed as two multiplets. Carbon-13 spectra (solvent $CDCl_3$) showed peaks at $\delta = 195.6$ (C=O), $\delta = 70.5$ (unsubstituted Cp ring), peaks at $\delta = 73.4$, 69.9 and 68.3 (for the substituted Cp ring), and a peak at $\delta = 46.4$ (CH_2Cl).

*Step 2, ethyl [(2-oxo-2-ferrocenylethyl)sulfanyl]methanethioate, compound **[79]***

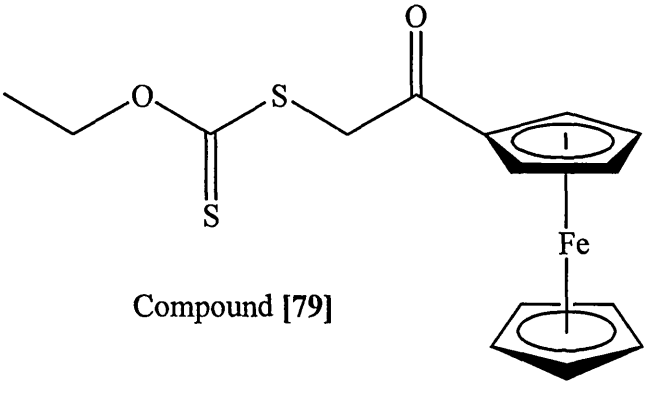

Compound **[79]**

Figure 80, ethyl [(2-oxo-2-ferrocenylethyl)sulfanyl]methanethioate, compound **[79]**

The structure of compound **[79]** is shown in Figure 80, compound **[79]** is isolated as an orange "tar" like solid with no definitive melting point.

Formula $C_{15}H_{16}O_2S_2Fe$, Formula weight = 348.23

EI mass spectrometry yielded molecular ion M/z = 347.9, and fragments corresponding to loss of $^{\cdot}(C{=}S)OCH_2CH_3$, $^{\cdot}CH_2S(C{=}S)OCH_2CH_3$ and fragmentation consistent of the ferrocene moiety.

Proton NMR spectra provided additional data for compound **[79]**, (solvent $CDCl_3$) showed a single peak at δ = 4.27 (integration 5 hydrogens) for the unsubstituted cyclopentadiene (Cp) ring, the $(C{=}O)CH_2S$ protons observed as a single peak at δ = 4.47 (integration 2 hydrogens), and the four protons of the substituted ring seen as two multiplets at δ = 4.59 (complex multiplet appears to be a triplet J = 1.9 Hz, integration 2 hydrogens) and δ = 4.89 (complex multiplet appears to be a doublet J = 1.7 Hz, integration 2 hydrogens). The peaks due to the OCH_2CH_3 were observed as a quartet at δ = 4.68 (integration 2 hydrogens J = 7.0 Hz) and a triplet at δ = 1.44 (integration 3 hydrogens J = 7.1 Hz)

Carbon 13 spectra (solvent $CDCl_3$) showed peaks at δ = 214.2 (C=S) δ = 196.7 (C=O), δ = 70.5 (unsubstituted Cp ring) a broad peak with several peaks in close proximity with resolved peaks at δ = 71.0 and δ = 70.0 and a further resolved peak at δ = 73.2 (all accounting for the substituted Cp ring, and most probably the OCH_2), and a peak at δ = 46.4 (CH_2S) and δ = 14.1 (CH_3).

*Step 3, 1,3-dithiole-2-thione-4-ferrocene, compound **[80]***

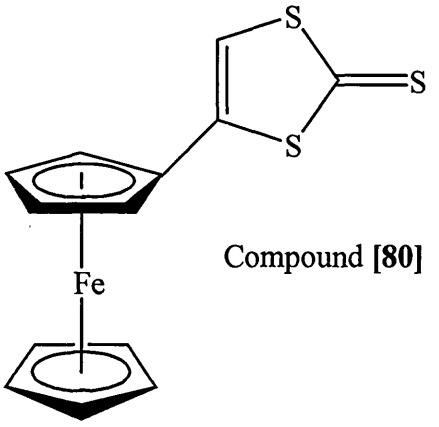

Compound **[80]**

Figure 81, 1,3-dithiole-2-thione-4-ferrocene, compound **[80]**

Compound **[80]**, Figure 81, is isolated as an orange/brown solid, melting point 134-138 °C, literature value 142 °C[146].

Formula $C_{13}H_{10}S_3Fe$, Formula weight = 318.24

EI mass spectrometry yielded molecular ion M/z = 318.0, and fragments corresponding to CS, CS_2, C_2S_2, CS_3.

Proton NMR spectra provided additional data for compound **[80]**, (solvent $CDCl_3$) showed a single peak at δ = 4.21 (integration 5 hydrogens) for the unsubstituted cyclopentadiene (Cp) ring, the four protons of the substituted ring seen as two multiplets at δ = 4.38 (complex multiplet appears to be a triplet J = 1.7 Hz, integration 2 hydrogens) and δ = 4.47 (complex multiplet appears to be a split doublet J = 1.8 Hz, integration 2 hydrogens). The peak due to the vinyl Cp-C=CH is observed at δ = 6.76 (integration 1 hydrogen).

Carbon-13 spectra (solvent $CDCl_3$) showed peaks at $\delta = 210.2$ (C=S) $\delta = 118.5$ (C=C), $\delta = 70.5$ (unsubstituted Cp ring) a broad peak with several peaks in close proximity with resolved peaks at $\delta = 70.2$ and $\delta = 67.6$ (substituted Cp ring).

5.2 HALOGEN ADDUCTS

5.2.1 ADDUCT SYNTHESIS

5.2.1.1 REACTION OF 4,5 BIS(2'-CYANOETHYLTHIO)-1,3-DITHIOLE-2-THIONE, COMPOUND [15], WITH DIHALOGENS

To a refluxing solution of 4,5 bis(2'-cyanoethylthio)-1,3-dithiole-2-thione, compound **[15]**, in DCM (100 mg in 5 mL), a refluxing solution of the required dihalogen in DCM (1 or 1.5 molar equivalents, in an equivalent volume of solvent) is added to give a dark brown (with I_2) or orange (with IBr) solution. The resulting solution is refluxed for a further ten minutes and then placed in a freezer at -10 ^{o}C for three days. The crystals formed were isolated by filtration and dried at room temperature under a slight flow of N_2 for thirty minutes. In cases where no crystals were observed after three days in a freezer, the DCM solution was stored in the dark at room temperature for one to two days for the solvent to evaporate yielding crystals or a powder.

5.2.1.2 REACTION OF LIGANDS (COMPOUNDS [35] TO [38]) WITH DIHALOGENS

To a refluxing solution of the ligand (compounds **[35]** to **[38]**) in DCM (100 mg in 5 mL), a refluxing solution of the required dihalogen in DCM (2 equivalents, in an equivalent volume of solvent) was added to give a black solution with I_2 or an orange solution with IBr. The resulting mixture was

refluxed for a further ten minutes and placed in a freezer at -10 ^{O}C for three days. The crystals formed were removed by filtration and dried at room temperature under a slight flow of N_2 for thirty minutes. In the case of compounds **[36]** and **[37]** the resulting adducts were obtained as oils.

5.2.1.3 REACTION OF DIMETHYL-1,3-DITHIOLE-2-THIONE-4,5-DICARBOXYLATE, COMPOUND [77], WITH DIHALOGENS

To a refluxing solution of dimethyl 1,3-dithiole-2-thione-4,5-dicarboxylate, compound **[77]**, in acetonitrile (100 mg in 5 mL), a refluxing solution of the required dihalogen in acetonitrile (1 or 1.5 molar equivalents, in an equivalent volume of solvent) was added to give a dark brown (with I_2) or dark orange (with IBr) solution. The resulting solution was refluxed for a further ten minutes and then placed in a freezer at -10 ^{O}C for three days. The crystals formed were removed by filtration and dried at room temperature under a slight flow of N_2 for thirty minutes. In the cases where no crystals were observed after three days in a freezer, the acetonitrile solution was stored in the dark at room temperature for one to two days for the solvent to evaporate yielding crystals or a powder.

5.2.1.4 REACTION OF 1,3-DITHIOLE-2-THIONE-4-FERROCENE, COMPOUND [80], WITH DIHALOGENS

To a refluxing solution of 1,3-dithiole-2-thione-4-ferrocene, compound **[80]**, in DCM (100 mg in 5 mL), a refluxing solution of the required dihalogen in DCM (1 equivalent, in an equivalent volume of solvent) was added to give a black/blue (with I_2) or dark orange/brown (with IBr) solution. The resulting solution was refluxed for a further ten minutes to produce a dark solution over a blue/black crystalline solid. The reaction mixture was placed in a freezer at -10 ^{O}C overnight and the crystalline powder removed by filtration, washed with ice cold DCM and dried at room temperature under a slight flow of N_2 for thirty minutes to yield a dark crystalline solid.

5.2.2 ADDUCT ANALYSIS

5.2.2.1 4,5-BIS(2'-CYANOETHYLTHIO)-1,3-DITHIOLE-2-THIONE, COMPOUND [15], PRODUCTS OBTAINED FROM THE REACTION WITH DIHALOGENS

Following the general synthetic procedure outlined in section 5.2, a range of dihalogen adducts based on 4,5(2'-cyanoethylthio)-1,3-dithione-2-thione**[15]** were prepared. The results obtained highlighted the diverse range of compounds that can be obtained from these systems.

REACTION WITH DIIODINE

The reaction of compound **[15]** with diiodine was attempted in a variety of solvents. The resulting solutions of the thione-dihalogen adduct, when left standing in the dark at -5 ^{O}C for up to ten days, produced fine black glassy needles. Attempted isolation of these "crystals" by filtration initially produced a solid on the filter paper but within seconds the compound was seen to change to an oil that emitted pungent fumes of diiodine. The decomposition of these "glassy" needles to an oil was also observed in solution, when the reaction mixture containing these glassy black needles is warmed from the crystallisation temperature of -5 ^{O}C to room temperature, the needles rapidly become a black oil. Attempts at obtaining the compound by slow evaporation yielded a black oil. Extended evaporation of the solvent (over a period of two weeks or more) yielded brown crystals, but X-ray crystal analysis showed this to be the starting

material compound **[15]**. Repeated attempts to isolate and quantify this black oil proved fruitless. Repeated analysis of the oils produced gave a wide range of inconsistent analytical results as the isolated oil was observed to emit fumes of diiodine. NMR and MS gave evidence of the presence of the starting material 4,5(2'-cyanoethylthio)-1,3-dithione-2-thione**[15]**. The Raman spectrum of the oil indicated the presence of Iodine to Iodine bonds but the spectra were of such a poor quality that the data was of extremely limited use in elucidating the nature of the compound (i.e. the observed peaks in the halogen region were barely recognisable above the background noise, and could easily be argued to be due to noise or instrument spikes).

REACTION WITH IBr

4,5(2'-cyanoethylthio)-1,3-dithione-2-thione IBr adduct, compound [81]

The reaction of 4,5(2'-cyanoethylthio)-1,3-dithione-2-thione**[15]** with IBr under similar conditions yielded the 1:1 adduct shown in Figure 82.

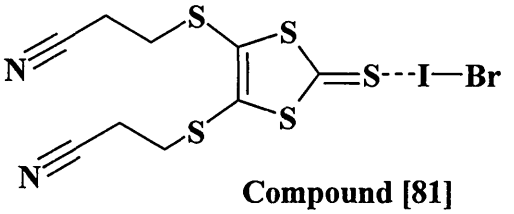

Compound [81]

Figure 82, 1:1 adduct of [4,5(2'-cyanoethylthio)-1,3-dithione-2-thione]:[IBr], compound **[81]**

In contrast to the reaction with diiodine, the reaction with IBr yielded yellow/golden crystalline needles suitable for X-ray analysis, shown in Figure 83 and Figure 84, which conform to the presence of a 1:1 adduct as shown in Figure 82 (tables of supporting data are shown in section 8.2.3). NMR and MS confirmed the presence of the donor 4,5(2'-cyanoethylthio)-1,3-dithione-2-thione**[15]**. Attempts at elemental analysis proved to be unhelpful due to the fact that the adduct**[81]** was observed to slowly lose IBr. The crystals were also seen to have no definite melting point, as heating **[81]** above 40 ^{O}C caused the adduct to rapidly lose IBr thereby decomposing the complex.

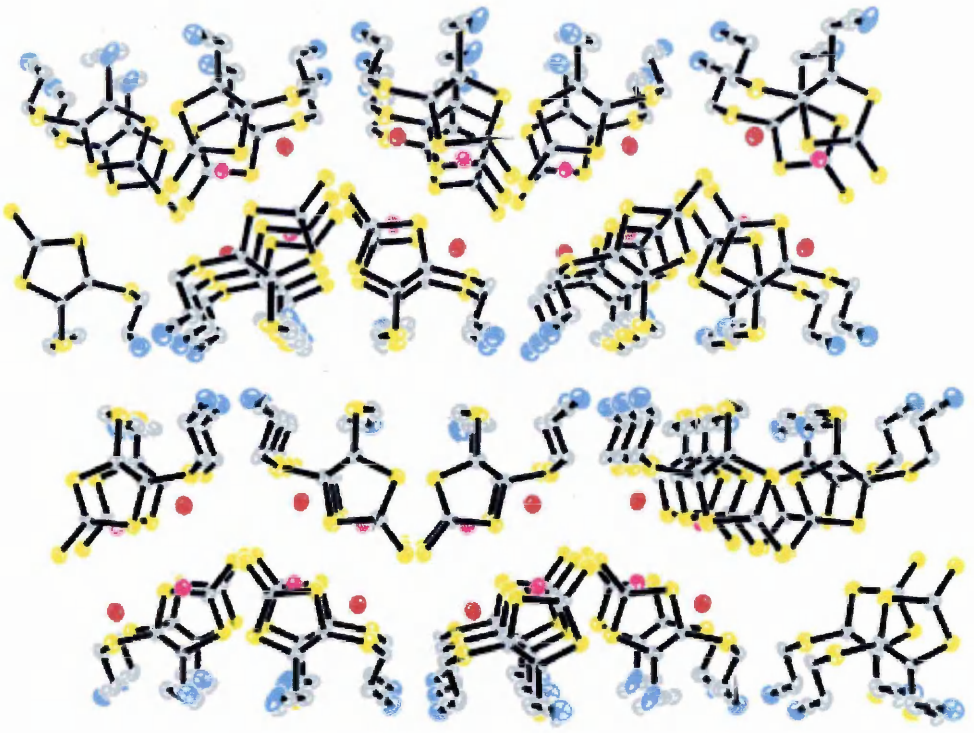

Figure 83, X-ray crystal packing diagram of compound **[81]**

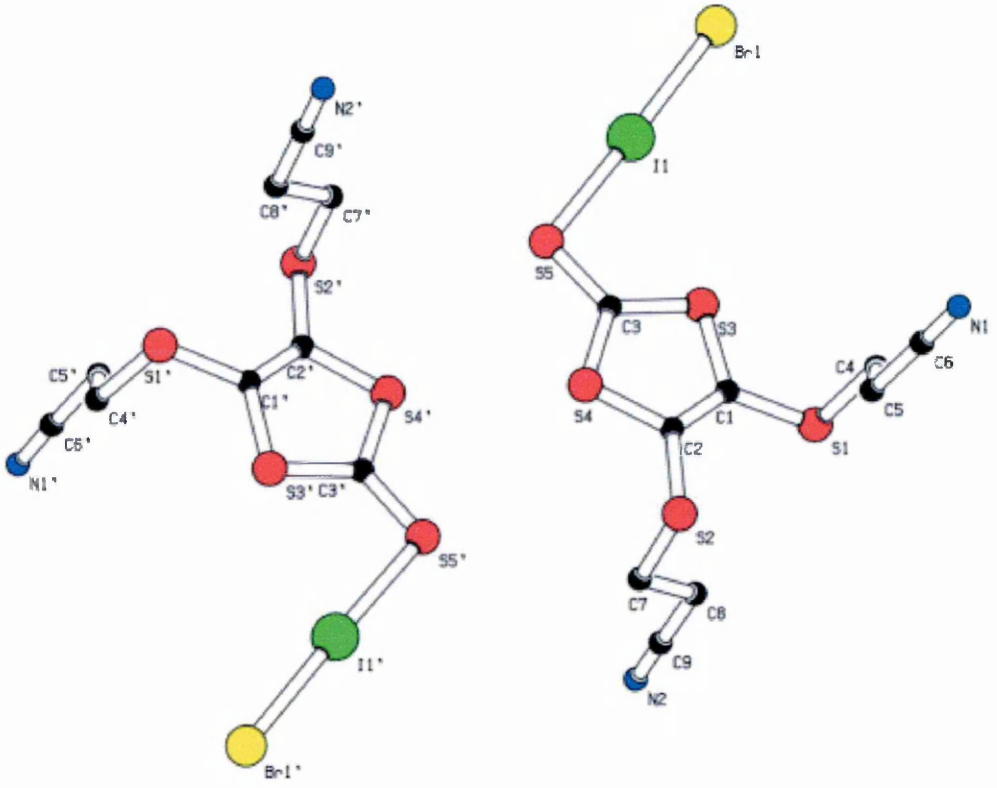

Figure 84, Solid state structure of compound **[81]**

5.2.2.2 LIGANDS, COMPOUNDS [35] TO [38], PRODUCTS OBTAINED FROM THE REACTION WITH DIHALOGENS

o-m-p-XYLENE LIGANDS REACTION WITH DIHALOGENS

Compounds **[36]** and **[37]**, the *o*-xylene and *m*-xylene ligands, produced results similar to those obtained with 4,5(2'-cyanoethylthio)-1,3-dithione-2-thione**[15]**, in that when reacted with diiodine the resulting adducts were found to be oils. Analysis of these oils by NMR, MS and FTIR could only confirm the presence of the ligand structure. Elemental analysis again proved unhelpful due to the oils visibly emitting diiodine fumes over several hours. Raman analysis of these oils again produced very poor spectra that could only suggest the presence of Iodine-Iodine bonds in the compounds and were not of sufficient quality for elucidating the nature of the adducts. Attempts to prepare the IBr analogues for these two ligands produced similar results. The reaction of the *p*-xylene ligand, compound **[38]**, with diiodine again produced an oil, but reaction with IBr produced a fine orange powder. This orange powder however proved to be highly insoluble, and defied analysis by NMR due to its lack of solubility in the common deuterated solvents. MS and FTIR only allowed the conclusion that the compound contained a DMIT type moiety.

ETHANE BRIDGED LIGAND DIIODINE ADDUCT, COMPOUND [82]

The reaction of the ethane bridged ligand, compound **[35]**, with diiodine provided more quantifiable results, producing the 1:2 adduct**[82]**, shown in Figure 85.

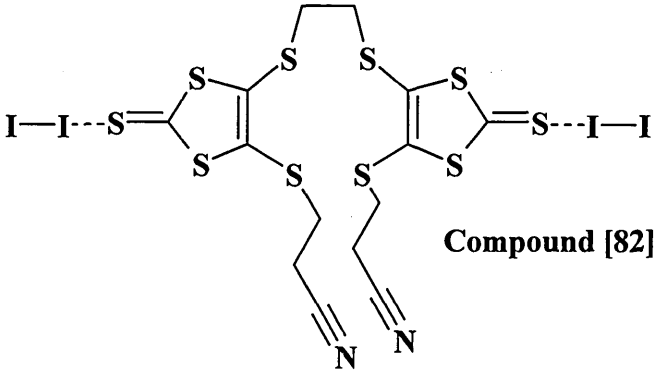

Compound [82]

Figure 85, Ethane bridge ligand diiodine adduct, compound **[82]**

The reaction with diiodine produced red/black plates suitable for X-ray analysis (structure is shown in Figure 86, and the supporting tables of crystal data are shown in section 8.2.4). Compound **[82]** did not melt cleanly and was found to decompose and produce fumes of diiodine at temperatures above 50 ^{O}C. NMR, MS and FTIR confirm the presence of the ethane bridge ligand in the complex but elemental analysis proved unhelpful as the adduct slowly produced fumes of diiodine over several days. The Raman spectrum did however show the presence of the diiodine bonds showing a clear peak at 142 cm^{-1} for complexed diiodine and a small peak at 179 cm^{-1} for "free" diiodine, Figure 87.

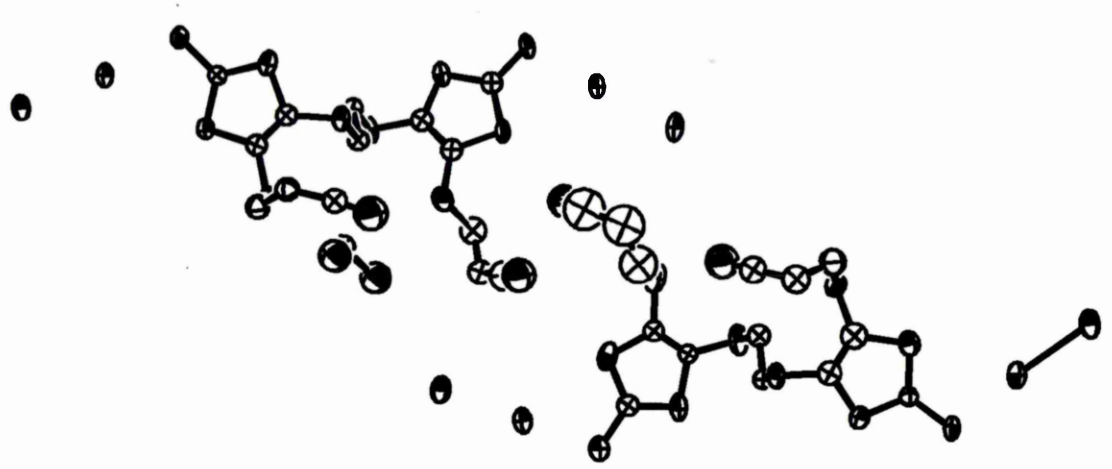

Figure 86, solid state structure of Ethane bridge ligand diiodine adduct, compound **[82]**

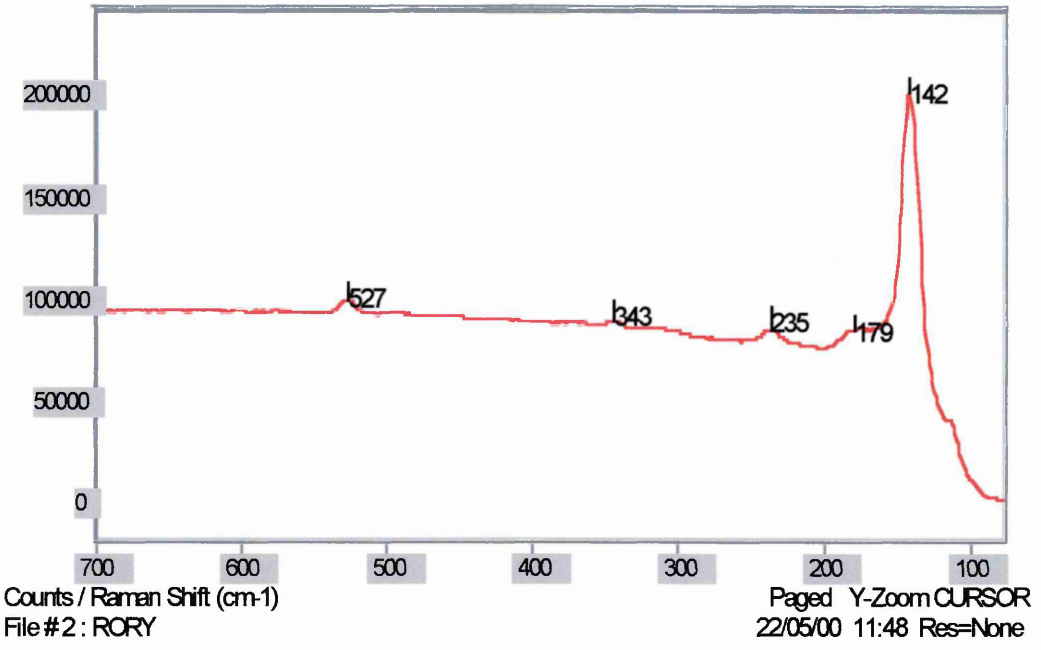

Figure 87, Raman spectra of Ethane bridge ligand diiodine adduct, compound **[82]**

Repeating the reaction with IBr however provided a compound similar to that obtained with the reaction between the *p*-xylene ligand**[38]** and IBr, namely that the resulting fine orange powder proved to be very insoluble and only provided evidence through MS of the presence of a DMIT type moiety in the compound. Further attempts at analysis provided unreproducible and conflicting data on the exact nature of this compound.

5.2.2.3 DIMETHYL-1,3-DITHIOLE-2-THIONE-4,5-DICARBOXYLATE, COMPOUND [77], PRODUCTS OBTAINED FROM THE REACTION WITH DIHALOGENS

In contrast to the compounds presented so far compound **[77]** provided identifiable compounds for the reactions with both diiodine and IBr.

DIMETHYL-1,3-DITHIOLE-2-THIONE-4,5-DICARBOXYLATE ADDUCT WITH DIIODINE, COMPOUND [83]

Dimethyl 1,3-dithiole-2-thione-4,5-dicarboxylate**[77]**, was found to produce a 1:1 adduct with diiodine **[83]** as shown in Figure 88. The compound was isolated as red/black plates suitable for X-ray analysis. The crystal structure of which is shown in Figure 89, and the crystal packing diagram in Figure 90 and Figure 91, tables of supporting data can be found in section 8.2.5.

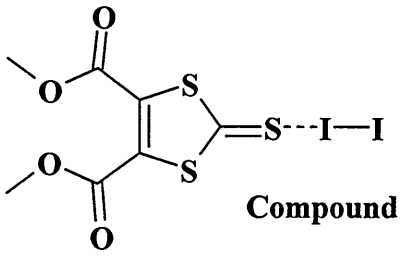

Compound [83]

Figure 88, Diiodine adduct of Dimethyl 1,3-dithiole-2-thione-4,5-dicarboxylate, compound **[83]**

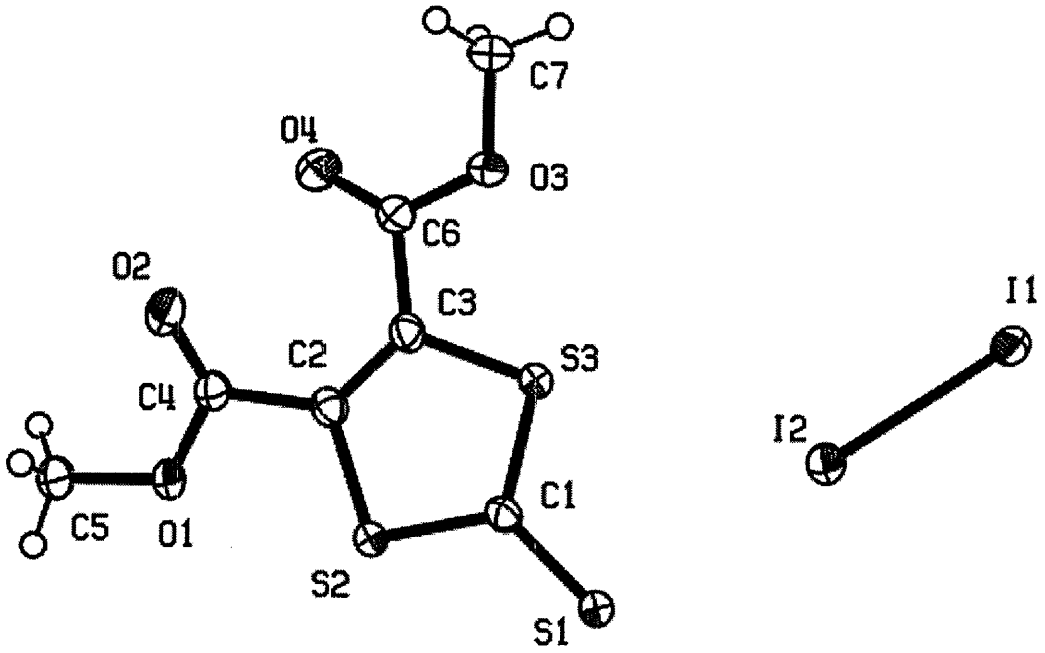

Figure 89, Solid state structure of compound **[83]**

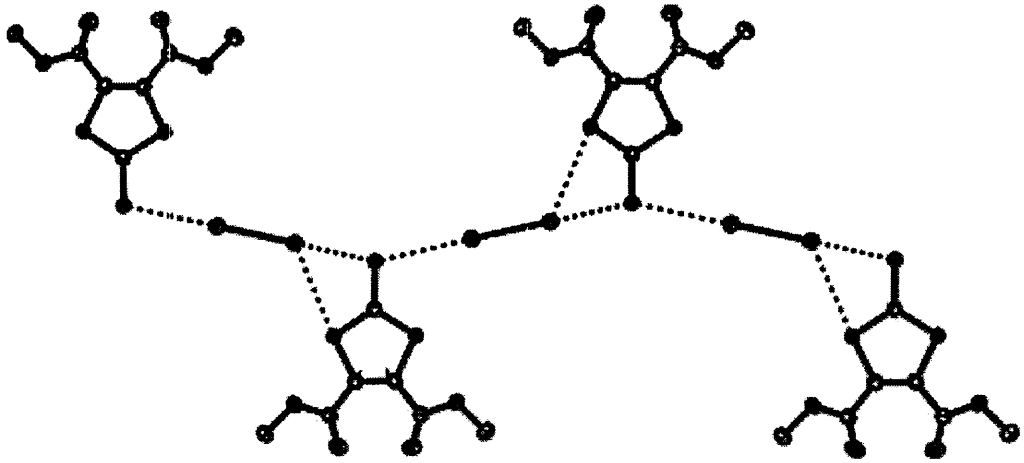

Figure 90, "polymeric" iodine chain in compound **[83]**

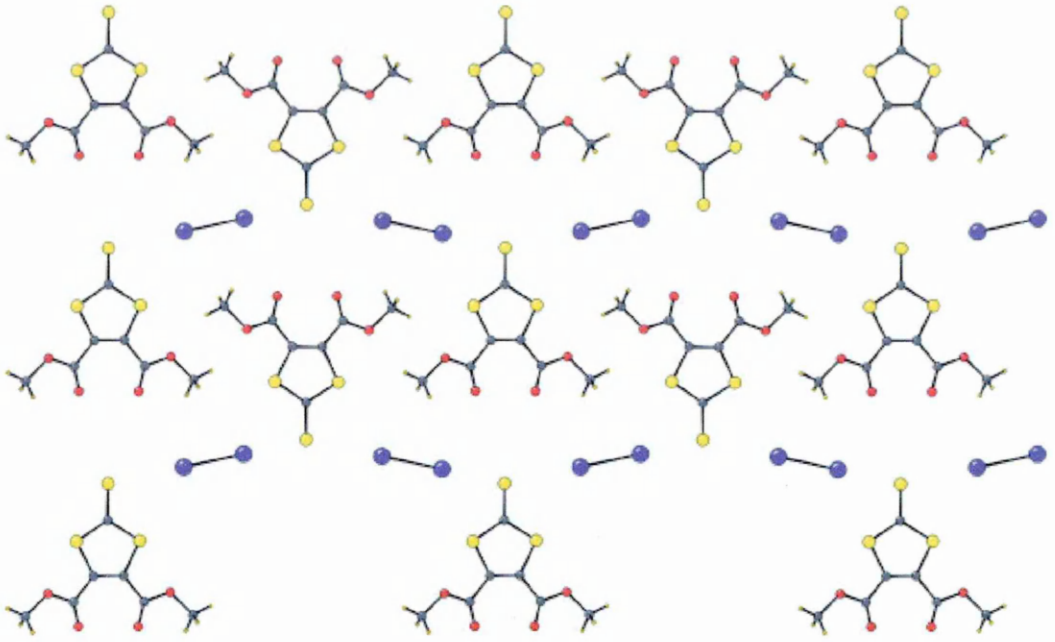

Figure 91, X-ray crystal packing diagram of compound **[83]**

NMR, MS and FTIR all provided data consistent with the donor unit of the adduct (dimethyl 1,3-dithiole-2-thione-4,5-dicarboxylate**[77]**), and as was observed in many of the previously described compounds, the adduct slowly lost diiodine making elemental analysis difficult. Melting point determination demonstrated that **[83]** rapidly decomposed above 50 ^{O}C emitting diiodine fumes. Raman analysis of the crystals produced very poor spectra consisting of a large fluorescence signal across the range 100 to 900 cm^{-1} and could only imply the presence of iodine-iodine bonds and were not of sufficient quality for elucidating the nature of the adduct.

DIMETHYL 1,3-DITHIOLE-2-THIONE-4,5-DICARBOXYLATE ADDUCT WITH IBr, COMPOUND [84]

Dimethyl 1,3-dithiole-2-thione-4,5-dicarboxylate**[77]**, was found to produce a 2:3 (1:1.5) adduct with IBr **[84]** as shown in Figure 92. Compound **[84]** was isolated as orange crystals suitable for X-ray analysis. The crystal structure is shown in Figure 93, and the crystal packing diagram in Figure 94, tables of supporting data can be found in section 8.2.6.

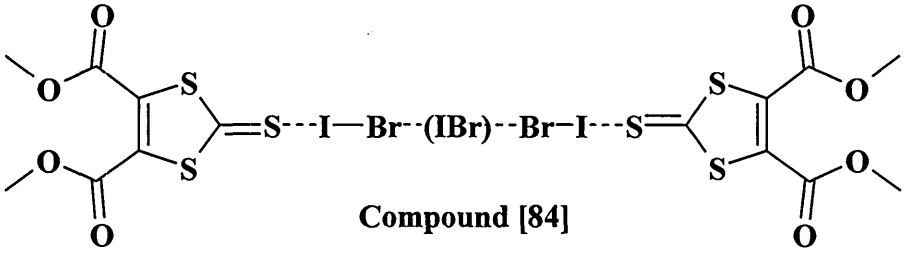

Compound [84]

Figure 92, Dimethyl 1,3-dithiole-2-thione-4,5-dicarboxylate adduct with IBr, compound **[84]**

NMR and MS provided data consistent with the donor component of the adduct (Dimethyl 1,3-dithiole-2-thione-4,5-dicarboxylate**[77]**), and, as was observed in the diiodine adduct**[83]**, the complex**[84]** was observed to slowly lose the dihalogen making elemental analysis impracticable. Melting point determination demonstrated that **[84]** rapidly decomposed above 45 ^{O}C emitting IBr fumes. Raman analysis of the crystals provided evidence of several peaks, a very strong band at 188 cm^{-1}, and two weaker bands at 177 cm^{-1} and 150 cm^{-1}.

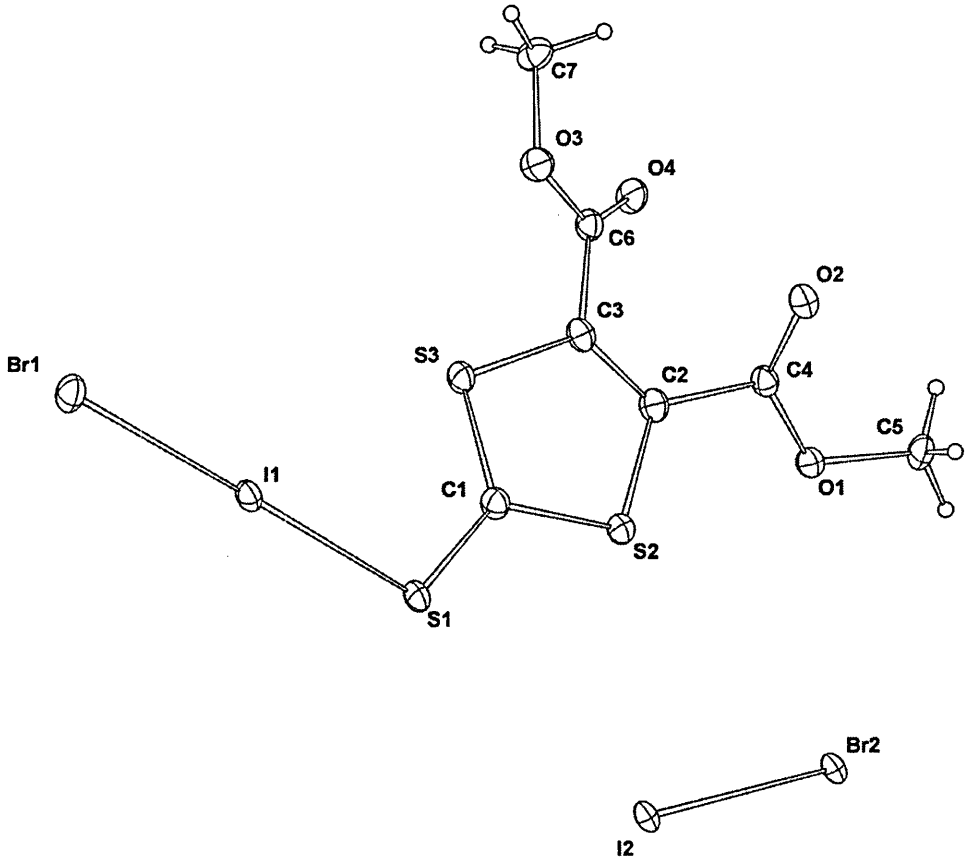

Figure 93, Solid state structure of compound **[84]**

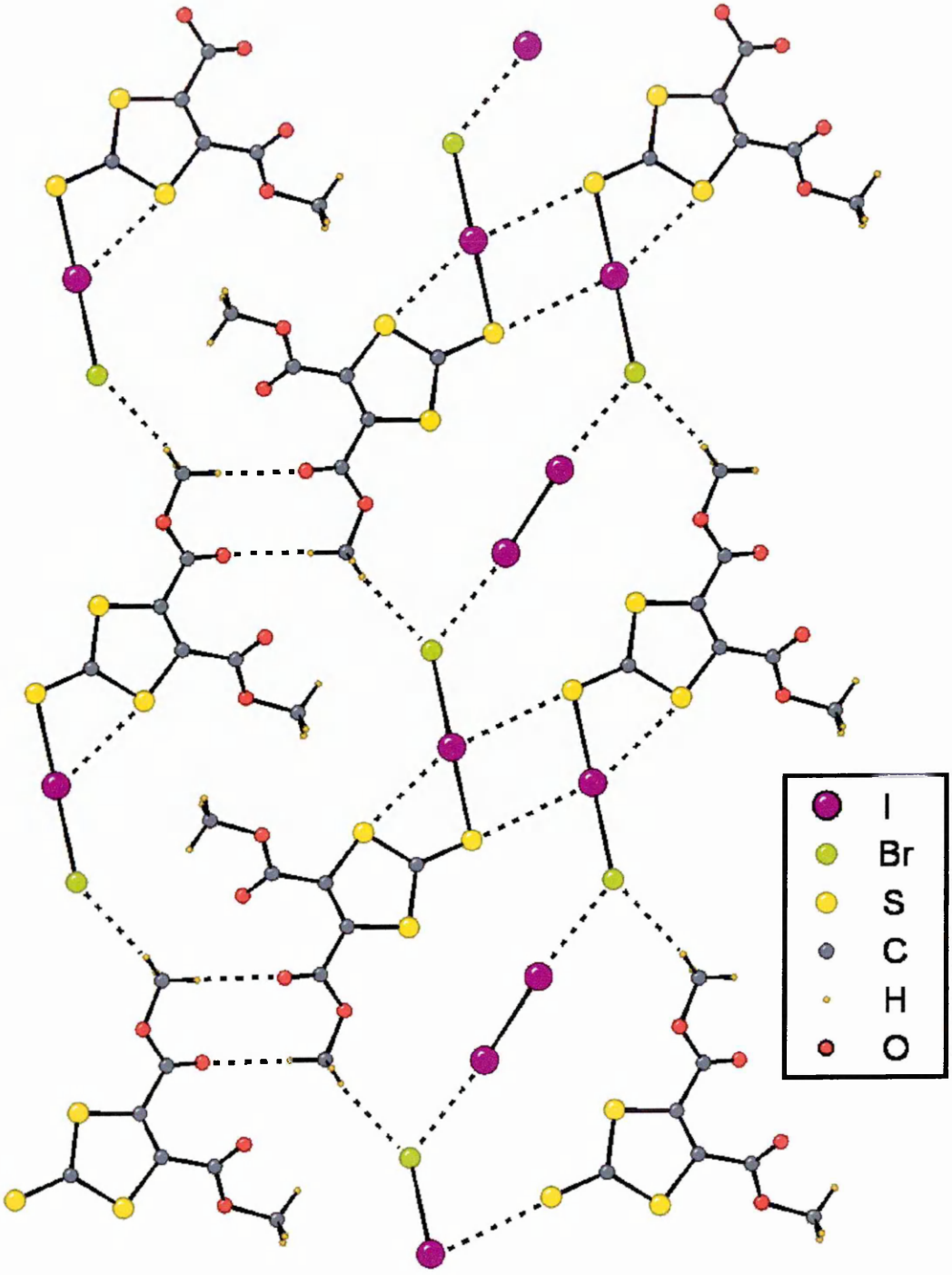

Figure 94, Packing diagram of compound **[84]**

5.2.2.4 1,3-DITHIOLE-2-THIONE-4-FERROCENE, COMPOUND [80], PRODUCTS OBTAINED FROM THE REACTION WITH DIHALOGENS

1,3-DITHIOLE-2-THIONE-4-FERROCENE ADDUCT WITH DIIODINE, COMPOUND [85]

Several reactions between 1,3-dithiole-2-thione-4-ferrocene and diiodine were attempted. In each reaction the molar ratio of donor to diiodine was varied and in each case the isolated crystals proved to be the adduct**[85]** shown in Figure 95 (1 donor to $3.5I_2$).

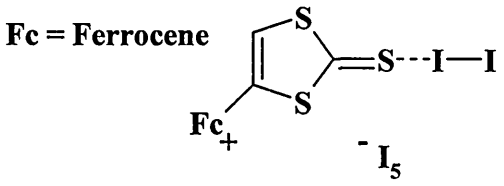

Compound [85]

Figure 95, 1,3-dithiole-2-thione-4-ferrocene adduct with diiodine, compound **[85]**

The diiodine adduct**[85]** of 1,3-dithiole-2-thione-4-ferrocene**[80]**, was isolated as small blue/black crystals suitable for X-ray analysis. The crystal structure is shown in Figure 96, and a representation of the polyiodide network is shown in Figure 97. Tables of supporting data can be found in section 8.2.7.

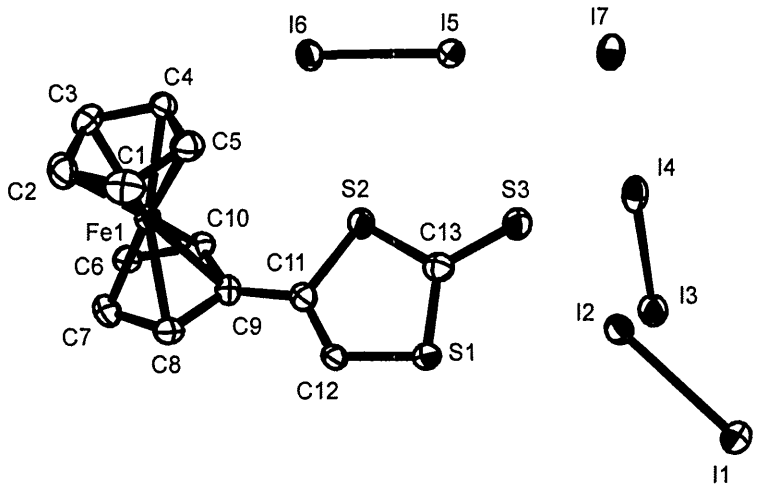

Figure 96, Solid state structure of 1,3-dithiole-2-thione-4-ferrocene diiodine adduct, compound **[85]**

As with the previous dihalogen adducts NMR, MS and FTIR analysis provided data consistent with the presence of the donor molecule**[80]**. In comparison to the other adducts described, the FTIR spectra did show a very definite shift in the wavenumber for the thione feature of the compound. In the uncomplexed donor **[80]** it is seen at 1055 cm^{-1} (literature value 1060 cm^{-1}[146]) and in the diiodine adduct at 1021 cm^{-1}. Moreover, this compound was found to be stable with respect to the loss of diiodine at room temperature **[85]** and gave no indication of emitting fumes of diiodine. Attempts to determine a melting point for **[85]** showed that the compound decomposed at 122 ^{O}C, emitting diiodine fumes above this temperature. Due to the more stable nature of this adduct, elemental analysis was able to provide further conformation of this complex:

Compound **[85]**, $C_{13}H_{10}S_3FeI_7$, theoretically contains 12.94 % C and 0.84 % H, experimental data provided 13.16 % C and 0.78 % H.

The Raman spectrum (Figure 98) of this compound showed two clear peaks at 146 cm^{-1} and 160 cm^{-1}, due to the I_2 and I_5^- species respectively.

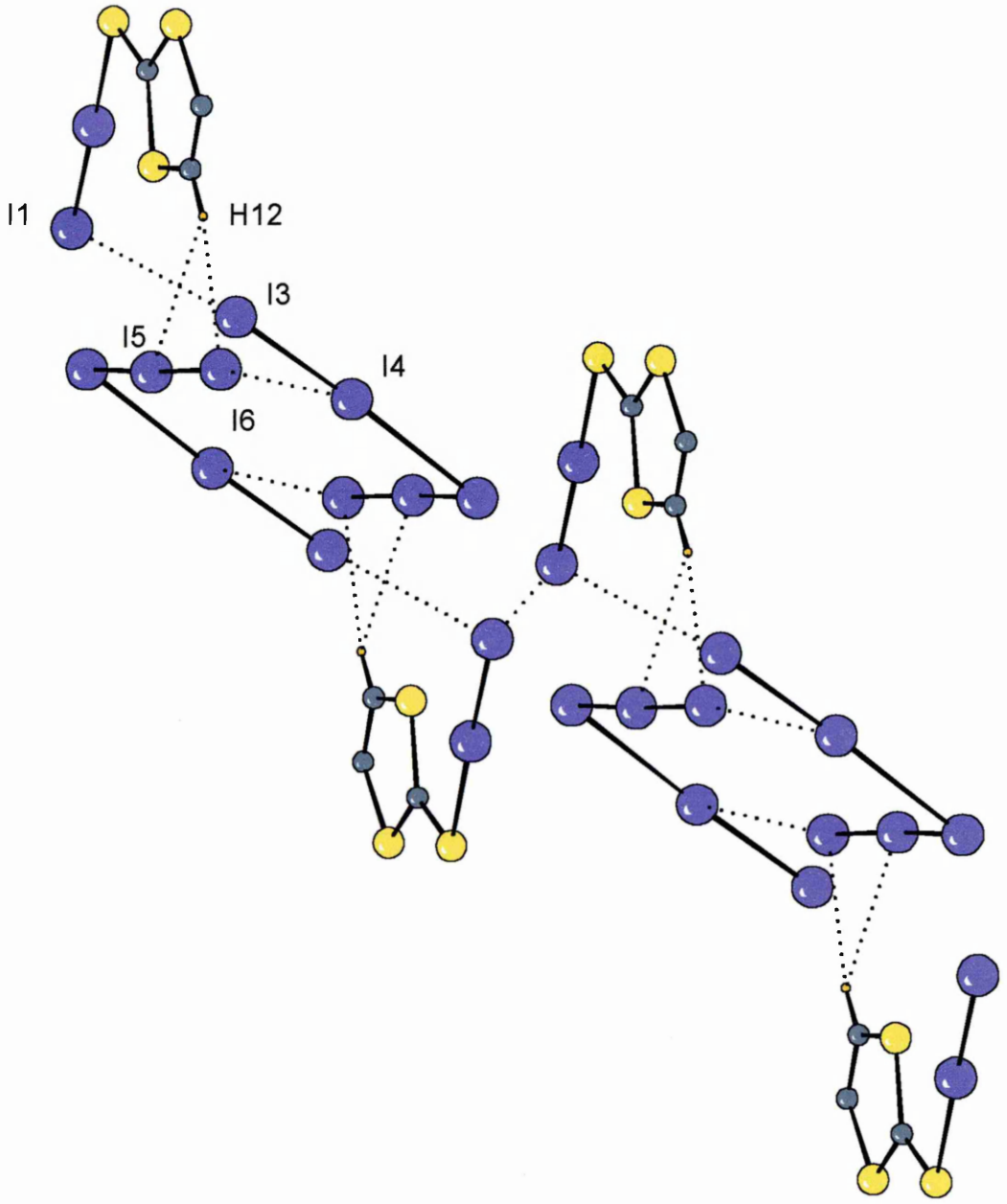

Figure 97, Compound **[85]**, minus the ferrocene units to show the supramolecular polyiodide network.

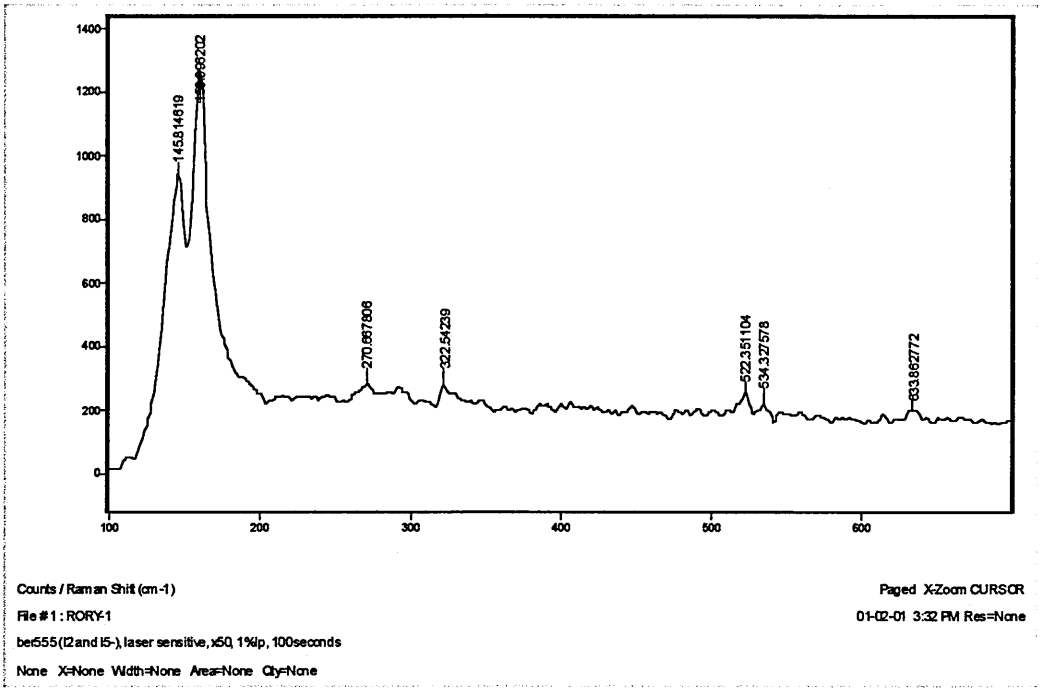

Figure 98, Raman spectrum of compound **[85]**

While the structure shown in Figure 96 and Figure 97 clearly shows the presence of a I_5^- ion, the crystal structure alone can not confirm if the corresponding counter positive charge is located on the iron atom or on one of the sulphur atoms of the trithiocarbonate. Theoretically the charge could be present on either centre. The initial observation of the adduct, in that the colour of the complex is blue/black, provides an indication that the charge is located on the ferrocene; ferrocenium compounds are known to be blue[10,52,147] but this is by no means a conclusive or concrete piece of evidence.

Using the magnetic balance and the appropriate equations (section 3.2.3) the magnetic moment of **[85]** was determined and found to be 2.53 BM, corresponding to low spin d^5 Fe^{3+} and not Fe^{2+}[10,124]. Further evidence that the

charge is located on the ferrocene is provided by Mossbauer spectroscopy (Figure 99). The Mossbauer data gave an isomer shift value, Δ, of 0.187 mm/s. Typically the range for Fe^{2+} being >0.5 mm/s and for Fe^{3+} 0 to 0.5 mm/s[148,149].

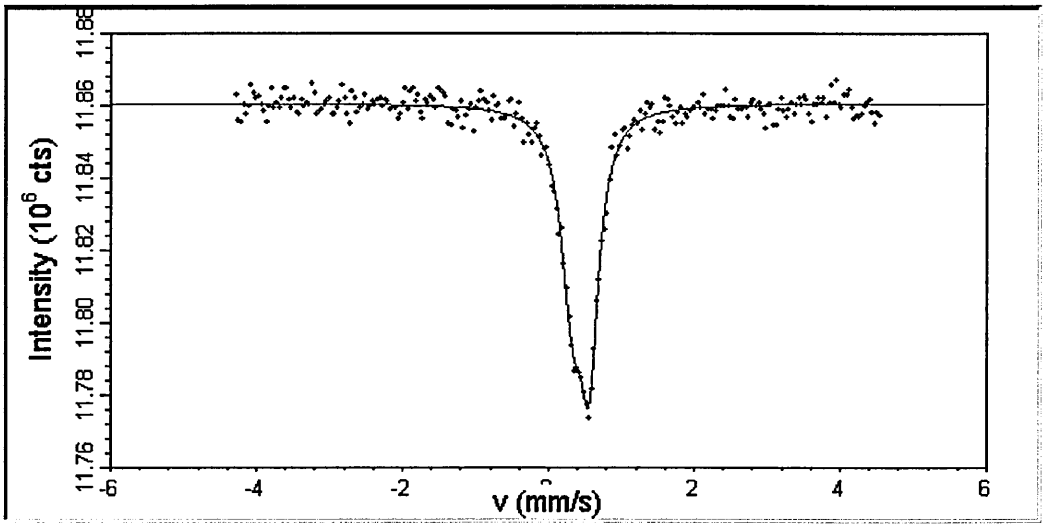

Figure 99, Mossbauer spectroscopy of compound **[85]**

REACTION WITH IBr, COMPOUND [86]

Repeating the reactions with IBr in the place of diiodine produced a black powder that unlike the diiodine adduct of 1,3-dithiole-2-thione-4-ferrocene, proved very difficult to characterise. Analysis by NMR and MS suggested that the donor molecule was present but the spectra were of very poor quality. Similarly the Raman spectrum which because of excessive fluorescence could not provide data on the presence of any dihalogens. However, as with the diiodine adduct the compound showed no indication of emitting fumes of dihalogen at room temperature. Heating to near 80 ^{o}C, did however cause the compound to decompose and emit brown fumes, most probably IBr. Elemental analysis does

provide an indication that **[86]** is comparable to compound **[85]** (1 donor to $3.5I_2$), analysis gave C = 15.16 %, H = 0.76 %, S = 9.20 %. In theory 1 donor to 3.5IBr would be C = 14.98 %, H = 0.97 %, S = 9.23 %, but this data alone is not enough to positively elucidate the structure of **[86]**.

MAGNETIC MEASUREMENTS ON COMPOUND [85]

Crystalline samples of **[85]** were sent to Professor Fernando Palacio of the Inst. de Ciencia de Materiales de Aragon, CSIC - Universidad de Zaragoza, Zaragoza (Spain), who kindly provided the following magnetic data for compound **[85]**.

1. TEMPERATURE DEPENDENCE OF THE MAGNETISATION

Magnetisation measurements as a function of temperature carried out at 1 tesla of external field indicate paramagnetic behaviour all the way down to about 2K (Figure 100) where the magnetisation data shows a maximum (see inset in Figure 100). This might be indicative of antiferromagnetic ordering at a temperature not far below the maximum.

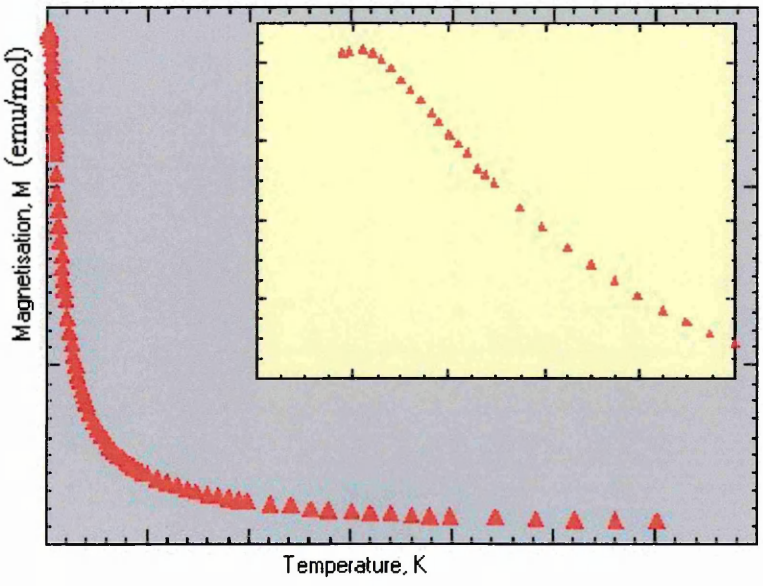

Figure 100, Magnetisation as a function of temperature, carried out at 1 tesla of external field for compound **[85]**

The paramagnetic behaviour, however, does not follow a typical Curie Weiss (C-W) law as shown in Figure 101, where the temperature dependence of the inverse of the susceptibility is represented. We should expect a linear dependence of $1/\chi$ vs. temperature for a typical Curie Weiss compound.

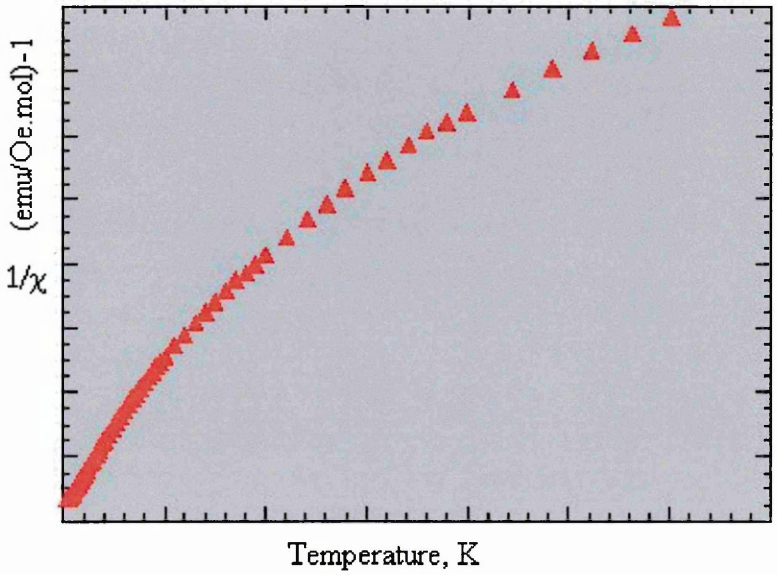

Figure 101, A plot of the temperature dependence of the inverse of the magnetic susceptibility for compound **[85]**.

To understand the origin of the deviation from the C-W law it is useful to represent the effective moment, the effective spin or χT (all are related, T = temperature) as a function of the temperature. Figure 102 χT vs. T is represented, and clearly indicates a decrease of the value of the effective moment. This may be due to a progressive depopulation of upper levels in the Fe ion as the temperature decreases. Below about 15K a more rapid decrease of the effective moment is observed from the presence of antiferromagnetic interactions.

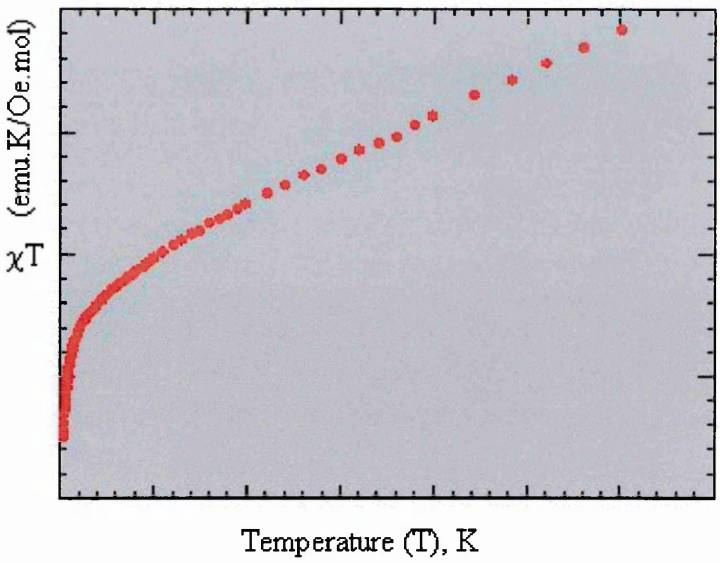

Figure 102, A plot of χT vs. T for compound **[85]**

2. FIELD DEPENDENCE OF THE MAGNETISATION

Magnetisation isotherm measurements were carried out at 1.8, 2, 2.5 and 3K. Their behaviour as a function of the external field is rather intriguing. This is particularly so for the isotherms measured at 1.8 and 2K which exhibit a marked "S" shape as shown in Figure 103 for T = 1.8K.

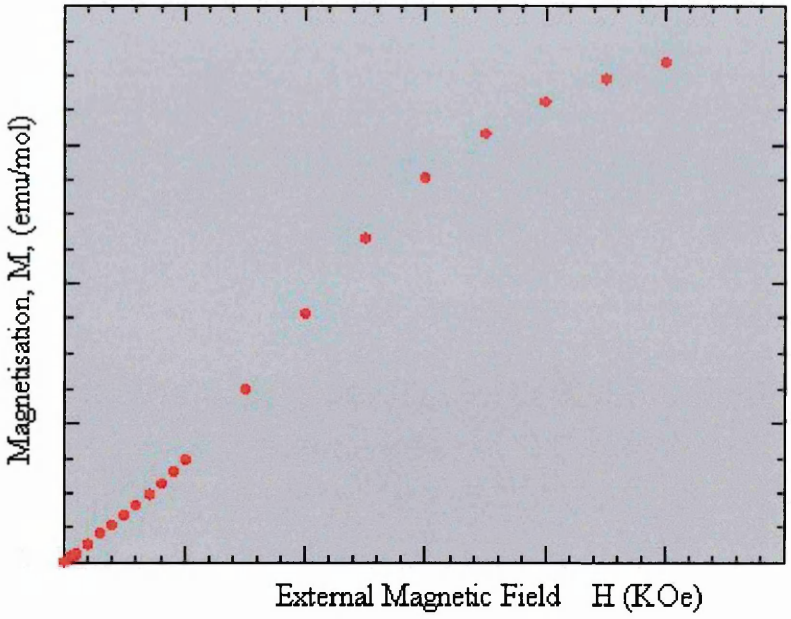

Figure 103, Magnetisation vs. External field for compound **[85]** at 1.8 K

This behaviour could be associated with a metamagnetic transition from an antiferromagnetic state into a field-induced ferromagnetic state. However, 1.8K (not to say 2K) must be very close (if not above) the temperature at which one would expect the antiferromagnetic ordering transition. In addition, the phase diagram of a metamagnet presents a tricritical point above which no such field-induced transition arises[150]. Things are even more confusing when one observes that even above 2K this "S"-shape of the magnetisation curves is not completely lost, as shown in Figure 104. In the paramagnetic regime a Brillouin dependence of the magnetisation as a function of the external field should be expected.

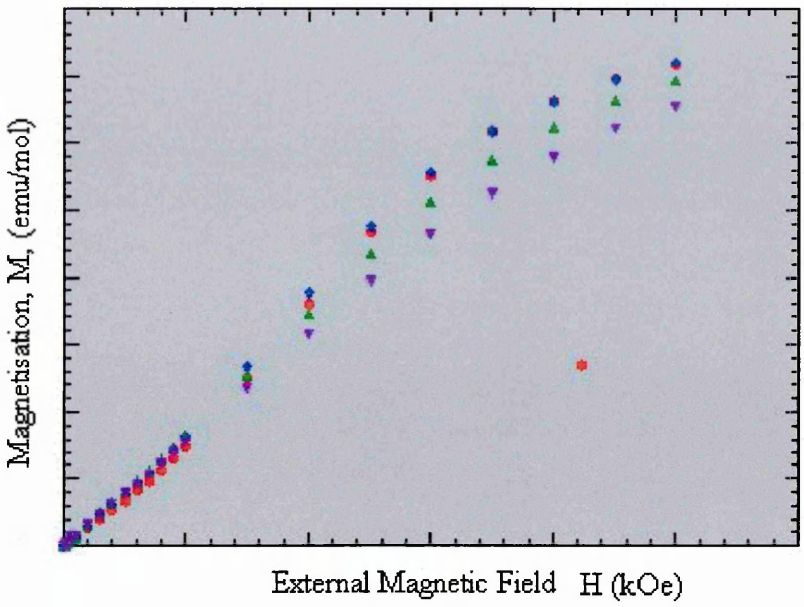

Figure 104, A plot of Magnetisation vs. External field for compound **[85]** at 1.8, 2, 2.5 and 3K

Finally, a minor ferromagnetic impurity in the sample can be detected from the room temperature isotherm of M(H). In Figure 105 the rapid increase of the magnetisation at low fields is most likely due to a small impurity.

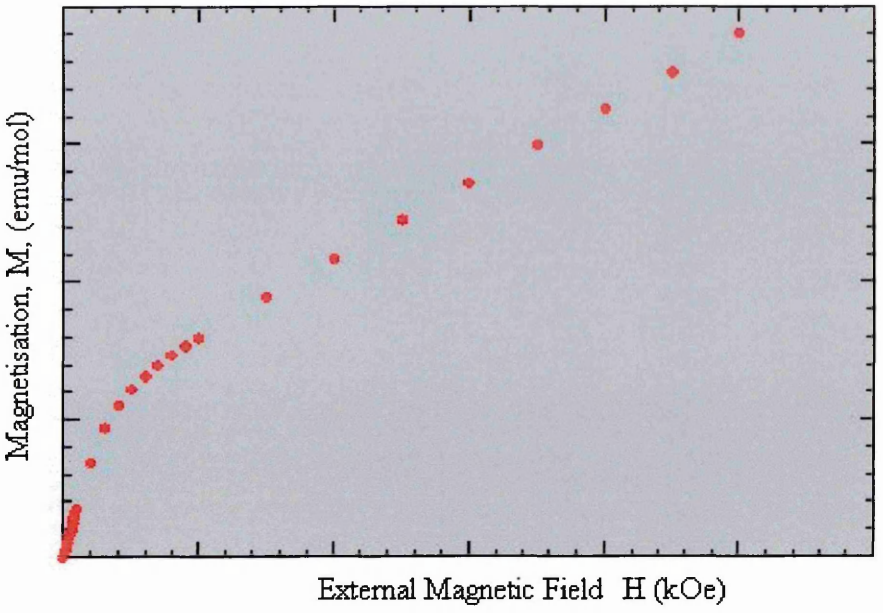

Figure 105, A plot of Magnetisation vs. External field for compound **[85]** at RT

6 CONCLUSION & DISSCUSIONS ON HALOGEN ADDUCTS

Compound [81], Figure 106, provided an interesting comparison on the differences that can be found in structure by changing the dihalogen used in preparing these type of charge transfer systems.

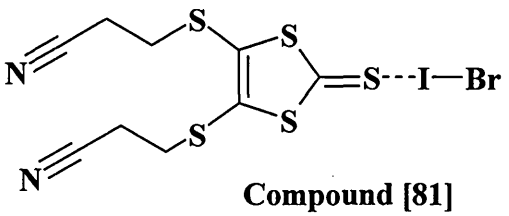

Compound [81]

Figure 106, 1:1 adduct of [4,5(2'-cyanoethylthio)-1,3-dithione-2-thione]:[IBr], compound **[81]**

As was described previously, attempts to obtain I_2 adducts of 4,5(2'-cyanoethylthio)-1,3-dithione-2-thione**[15]** provided only oils, whereas the IBr adduct gave striking golden yellow needles. Figure 83, page 181, shows the crystal packing diagram for **[81]** showing the 1,3-dithiole-2-thione moieties forming stacks in the solid state. Figure 84, page 181, shows that between each row of these stacks the 4,5(2'-cyanoethylthio)-1,3-dithione-2-thione donors are producing a "head to tail" type arrangement with respect to the thione. This also shows the close contact (see section 8.2.3) between the thione sulphur atom (S5) and the I of IBr (I1) arising from the charge transfer process, producing the weak bond of 2.611 Å, which is shorter than the sum of the van der Waals radii of the

corresponding atoms (3.75 Å)[3]. The charge transfer process is further demonstrated by a lengthened I1-Br1 bond of 2.7044 Å (uncoordinated IBr bond length 2.521 Å)[151] caused by the donation of electrons into the σ* antibonding orbital of the IBr molecule. The bond angle of S5-I1-Br1 is shown to be 177.56 °, giving a near linear conformation. In conclusion compound **[81]** gives a typical, or expected interaction between a sulphur donor and dihalogen acceptor[105,107,123,152-154].

Compound [82], Figure 107, and the adducts attempted from the other ligands (compounds **[35]** to **[38]**) again demonstrated the wide range of reactions that can occur between structurally similar compounds and dihalogens.

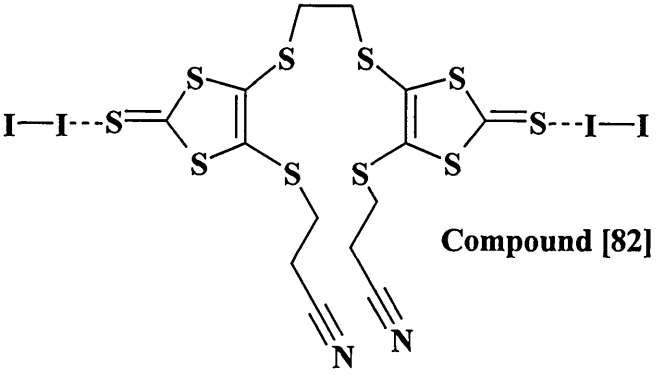

Compound [82]

Figure 107, Ethane bridge ligand diiodine adduct, compound **[82]**

The majority of the "xylene" bridged ligands (**[36]** to **[38]**) produced unidentifiable oils, except for the reaction of IBr with the p-xylene ligand (**[38]**) which gave an orange powder and only produced fumes of dihalogen after heating to well over 100 °C. A likely explanation for this being that the IBr had

undergone a chemical reaction with **[38]** not a "simple" donor-acceptor interaction. However the lack of any conclusive analytical data proved a hindrance in determining the exact nature of the compound.

In contrast to the previous compound **[81]**, the ethane bridged ligand **[35]** provided crystals only for the I_2 adduct **[82]**, Figure 86, page 184. This also shows the close contact (see section 8.2.4) between the thione sulphur atom and one of the iodine's in I_2 arising from the charge transfer process, producing the weak bond of 2.685 Å, which is shorter than the sum of the van der Waals radii of the corresponding atoms (3.75 Å)[3]. The charge transfer process is further demonstrated by a lengthened I-I bond of 2.845 Å (uncoordinated I-I bond length in the solid state 2.715 Å)[120]. The bond angle of the (thione) S-I-I is found to be 173.90 °, giving a near linear conformation. The Raman data (Figure 87) also conforms nicely with established charge transfer complexes between I_2 and thiones, compound **[82]** gives a strong peak at 142 cm^{-1} which falls into the established range for D-I_2[120]. In conclusion compound **[82]** gives a typical, or expected interaction between a sulphur donor and dihalogen acceptor[105,107,123,152,153].

Compound [83], Figure 108, Dimethyl 1,3-dithiole-2-thione-4,5-dicarboxylate **[77]** proved unique among the thione donors studied in that it provided quantifiable adducts for both I_2 and IBr.

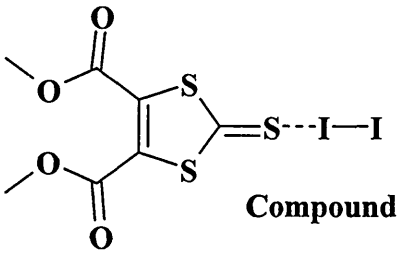

Compound [83]

Figure 108, Diiodine adduct of dimethyl 1,3-dithiole-2-thione-4,5-dicarboxylate, compound **[83]**

While the 1:1 adduct (I_2) of dimethyl 1,3-dithiole-2-thione-4,5-dicarboxylate gave black/red plates suitable for single crystal X-ray analysis unfortunately the Raman data proved to be very poor quality. Such information would have proved useful in a comparison with compound **[82]** and literature examples[120]. Initial examination of the solid state structure of **[83]**, Figure 89 page 187, shows an adduct that conforms to established adducts[105,107,123,152,153]. The close contacts are also again evident in Figure 89 (see section 8.2.5) between the thione sulphur atom (S1) and one of the iodines in I_2 (I2) arising from the charge transfer process, producing the weak bond of 3.505 Å, which is shorter than the sum of the van der Waals radii of the corresponding atoms (3.75 Å)[3]. The charge transfer process is further demonstrated by a lengthened I2-I1 bond of 2.7899 Å (uncoordinated I-I bond length in the solid state 2.715 Å)[120]. The bond angle of the (thione) S1-I2-I1 is

found to be 172.12 °, giving a near linear conformation. In addition to the structure shown in Figure 89, the polymer chain linking each donor and acceptor molecule to its neighbours is also clearly seen through the I-S interactions highlighted in Figure 90, page 187. Expanding the view (Figure 91, page 188) to include several rows of donor/acceptor stacks the interactions between each donor and acceptor molecule to its neighbours becomes even clearer. As was seen in compound **[81]** the 1,3-dithiole-2-thione moiety adopts a "head to tail" arrangement, but additionally in compound **[83]** there is significant hydrogen bonding between the ester units of adjacent donor molecules producing a highly ordered structure with alternating layers of donor and acceptor stacks.

Compound [84], Figure 109, the adduct with IBr shows a very different solid state structure to that of **[83]**.

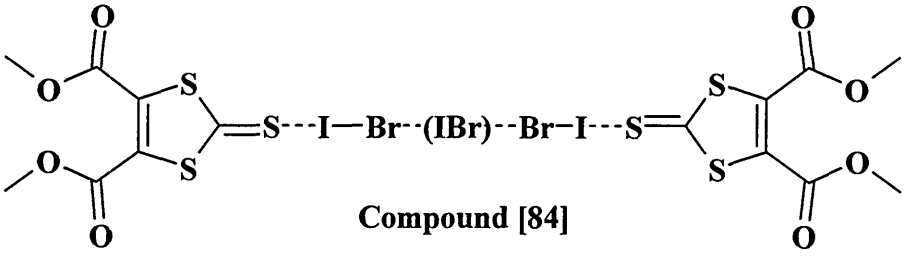

Compound [84]

Figure 109, Dimethyl 1,3-dithiole-2-thione-4,5-dicarboxylate adduct with IBr, compound **[84]**

The X-ray crystal structure of **[84]** is shown in Figure 93. The close contact between atoms S(1) and I(1) arises from the charge-transfer process from the thiocarbonyl-sulphur to the interhalogen (see section 8.2.6). Thus, electron

density from a lone pair of the sulphur is donated to the σ^* antibonding orbital of the I-Br bond. This situation results in the formation of a weak bond (2.605 Å) which is significantly shorter than the sum of the van der Waals radii of the corresponding atoms (3.75 Å)[3], and a lengthened I(1)-Br(1) bond of 2.7107 Å (bond length of uncoordinated IBr is 2.521 Å)[151]. The bond angle S(1)···I(1)-Br(1) between the two components is 178.01 ° giving a linear conformation. A further significant intramolecular interaction is seen between the heterocyclic sulphur S(3) and I(1) (3.361(3) Å); thus, the donor effectively chelates the iodine monobromide, resulting in a four-membered ring involving the S(1)···I(1)···S(3)-C(1) atoms.

A further half molecule of IBr is included in the asymmetric unit, with a 50% probability of iodine or bromine (Figure 93 shows the complete I(2)-Br(2) molecule). This molecule is independent of any interactions from the heterocycle and effectively acts as a bridge between two adjacent **[84]** units; the I-Br bond in the bridging iodine monobromide molecule is elongated (2.7173 Å). The distances between the terminal bromine atoms of the **[77]**·IBr moieties of **[84]** and the bridging IBr molecule, Br(1)···I(2)/Br(2), are 3.3614 Å. The bond angles between I(2)-Br(2)···Br(1) and I(1)-Br(1)···Br(2) are 175.21 Å and 130.14 Å, respectively.

The supramolecular structure of **[84]** is illustrated in Figure 94, page 191 . The structure contains perfectly eclipsed stacks of the donor and interhalogen acceptor and the interatomic distance between identical atoms in each layer is

5.816 Å. The S(1)-I(1) unit of the complex forms dimers through weak intermolecular bonds (3.669 Å) between S(1)-I(1)' and S(1)'-I(1), forming a four-membered ring between the adducts. In conjunction with the interactions between the dihalogen molecules, this feature gives rise to polymer chains within each sheet of the structure, which can be seen in Figure 94.

The role of the diester functionality in the solid is also identified in Figure 94, which includes further interactions through hydrogen bonding. A second set of dimers is formed between the methyl protons of one ester group and the carbonyl oxygen in the equivalent functional group of an adjacent molecule (H(5a)···O(2) = 2.427 Å). Through a similar interaction, the second ester functionality serves to link adjacent molecules within the same stack, giving rise to a second polymer chain rather than forming dimers (H(7b)···O(4) = 2.430 Å, not shown in Figure 94). Finally, a third hydrogen bond between H(5b) and Br(1) (2.8183 Å) provides an additional intrastack interaction. Overall, the hydrogen bonding network serves as a cross-linker to the linear polymer chain, resulting in a very rigid three-dimensional self-assembled superstructure.

The low frequency Raman spectrum of **[84]** contains two bands, a strong, broad, band at 186 cm^{-1}, together with a slightly weaker one at 147 cm^{-1}. These two bands can be attributed to the antisymmetric and symmetric stretching vibrations of the S-I-Br components of **[84]** respectively. Given the similarity in the bond lengths between the chelated and the bridging IBr molecules in **[84]**, it seems likely that the band at 186 cm^{-1} also has a contribution from the bridging IBr molecules.

Compound [85], Figure 110, in comparison to the other thione donors presented, **[85]** provided yet another novel dihalogen adduct. As was shown in section 5.2.2.4 the ferrocene provided an additional centre from which to derive electron density.

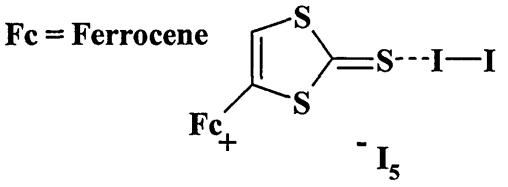

Compound [85]

Figure 110, 1,3-dithiole-2-thione-4-ferrocene adduct with diiodine, compound **[85]**

The solid state structure of **[85]**, Figure 96, page 193 (see also section 8.2.7) shows the bound I_2 molecule interacts in the expected manner[105,107,123,152,153]. Thus, the sulphur atom of the thiocarbonyl unit forms a strong intermolecular bond the diiodine molecule. The distance between S(3) and I(2) (2.705 Å) is significantly shorter than the sum of the van der Waals radii for sulphur and iodine (3.75 Å)[3]. The I(1)-I(2) bond length is 2.8566 Å, which is greater than that of uncoordinated diiodine in the solid state (2.715 Å)[120], again demonstrating the effect of electron donation into the σ^* orbital of the dihalogen. A second weaker interaction exists between S(1) and I(2) (3.539 Å), forming a four-membered ring between the heterocycle and I(2).

The pentaiodide (the I_5^- from Figure 110) counterion adopts the well established V-shaped geometry[155] with an angle of 96.88 ° (I(5)-I(7)-I(4)). The unit comprises two diiodine molecules coordinating to I^-; the bond lengths of the dihalogens are 2.818 Å [I(6)I(5)] and 2.799 [I(4)I(3)], whilst the coordination distances are 3.054 Å [I(5)I(7)] and 3.160 Å [I(4)I(7)]. On closer examination of the crystal structure of **[85]**, one can identify a series of halogen-halogen contacts. Close intermolecular distances are observed between I(1)-I(1) (3.6775 Å), I(1)-I(3) (3.7037 Å) and I(4)-I(6) (3.8948 Å), which are all shorter than the sum of the van der Waals radii for two iodine atoms (3.96 Å)[3]. Molecules I(3)-I(4) and I(5)-(6) experience different intermolecular close contacts. In the absence of secondary interactions, the pentaiodide species normally adopts C_{2v} symmetry[155]; therefore, it is this difference in the supramolecular chemistry of the I_5^- unit that is responsible for the asymmetric arrangement. The entire network of contacts results in a polymeric structure, consisting of eight-membered iodine macrocycles, linked by four iodine atoms, to form a 'chain of beads' type arrangement (Figure 97, page 194). The polyiodide chain is also interacting with the heterocycle via hydrogen bonding [C(12)-H(12)•••I(6) = 3.041 Å; C(12)-H(12)•••I(5) = 3.1765 Å; sum of the van der Waals radii for iodine and hydrogen - 3.18 Å], which holds the dithiole ring almost perpendicular to the polymer chain.

7 FINAL COMMENTS AND FURTHER WORK

7.1 DMIT COMPLEXES

As has been mentioned previously the main disadvantage encountered in these DMIT type metal complexes was their inherent lack of solubility. A possible solution to this problem could be provided by the introduction of solublising groups onto the bridging units, an example of which is shown in Figure 111, were R = long chain alkyls, esters or ethers.

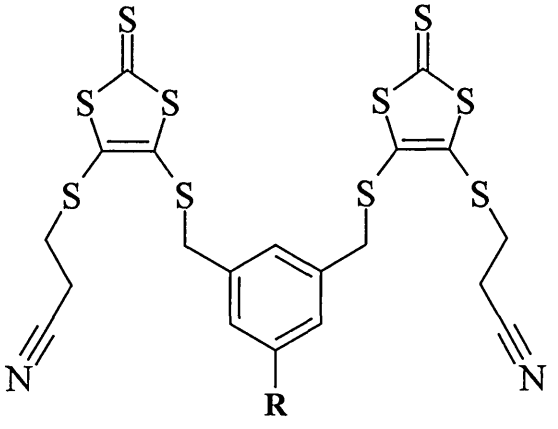

Figure 111, Possible solution to solubility problems for ligands

However a possible consequence to such a solution could be the impact such long chain alkyl groups would have on the solid state structures of the subsequent metal complexes, in particular steric effects.

Perhaps a more worthwhile investigation would be to carry on this work by making the "bridged" TTF derivatives of these ligands, an example of such a system is shown in Figure 112.

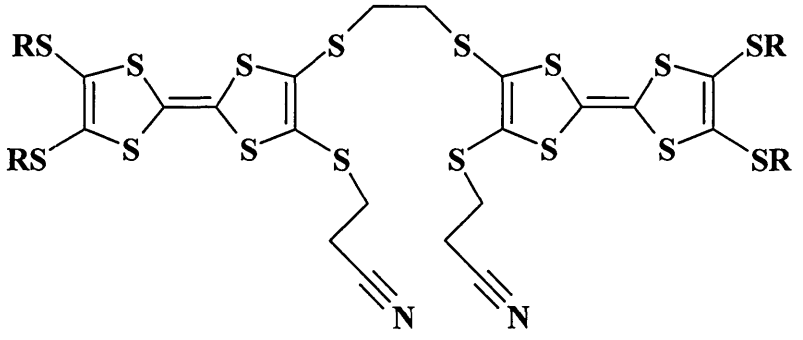

Figure 112, "Bridged" TTF ligands

This type of ligand should not only introduce solubility to the metal complexes but could also introduce the range of electroactive properties established for TTF based systems(see section 1.1.1). "Unbridged" ligands of this general type (i.e. compounds not containing the CH_2-CH_2 linkage as is shown in Figure 112, and thereby providing a tetrathiolate co-ordination centre) have been investigated and would provide a good point of reference for comparing to these "Bridged" TTF ligands[139,140,156-158].

7.2 HALOGEN ADDUCTS

The compounds presented in thesis demonstrate that a very interesting and varied range of new compounds can be prepared through relatively simple synthetic pathways. The range of structures obtained clearly demonstrates some of the points made in section 1.3, that small variations in donor structure or that changing the dihalogen used can cause such a marked difference in the isolated compound. This was nicely demonstrated in the results for compounds **[83]** and **[84]**.

The IBr adduct **[84]** provides two key insights into dihalogen-sulphur adducts

(i) the precedence for occluding a free molecule of IBr, which could interact with suitable strong donors analogous to **[77]**, thereby providing open shell species *via* a formal charge-transfer process;

(ii) a highly ordered array of supramolecular interactions which is desirable for magnetic and/or conducting properties in the bulk solid. In the pursuit of electroactive thiocarbonyl-dihalogen adducts for molecular electronics applications, the major challenge now is to design stronger thiocarbonyl electron donors than **[84]**, whilst retaining a highly ordered structure through suitable supramolecular functionalities.

An interesting point to note about the dihalogen adducts presented in this thesis is their tendency (or not) to crystallise. In the cases where crystals are obtained it actually became difficult to prevent the adducts forming as crystals. This is most clearly seen in the adduct **[85]**, a range of different solvent/temperature/diiodine

concentrations were investigated and in every case good quality crystals of **[85]** were obtained. However in changing the dihalogen to IBr, only fine powders could be obtained. The use of ferrocene in compound **[85]** introduced a new aspect to these adducts, i.e. magnetic properties, and while the magnetic data on **[85]** presented here is the initial report, we hope to publish more complete magnetic data on the compound in the coming months. An interesting comparison to **[85]** was recently published[159], concerning the iodine adducts of the structurally related ferrocenyl(phenyl)phosphines (an example of these systems is shown in Figure 113).

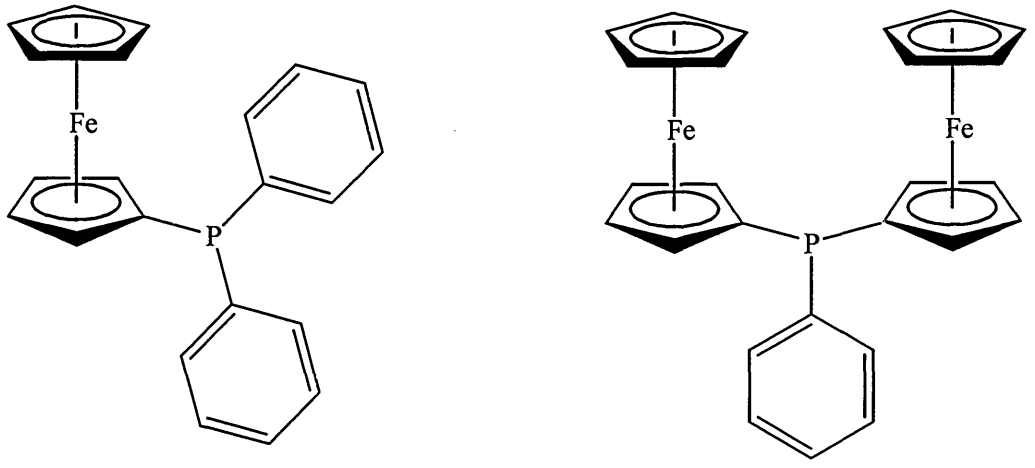

Ferrocenyl(phenyl)phosphines

Figure 113, Ferrocenyl(phenyl)phosphines

When systems of this type were reacted with diiodine they yielded iodo(ferrocenyl)(phenyl)phosphonium salts and not ferricenium salts, i.e. the counter positive charge was found on the phosphorus atoms, and the iron remained as Fe(II).

In terms of further work on these halogen systems it seems clear that the unusual adduct (or "double charge transfer") found in **[85]** would be worth further investigation, possibly in terms of other derivatives of the ferrocene moiety. Such examples could include "diferrocenyls" or "dithione" derivatives, such as those in Figure 114.

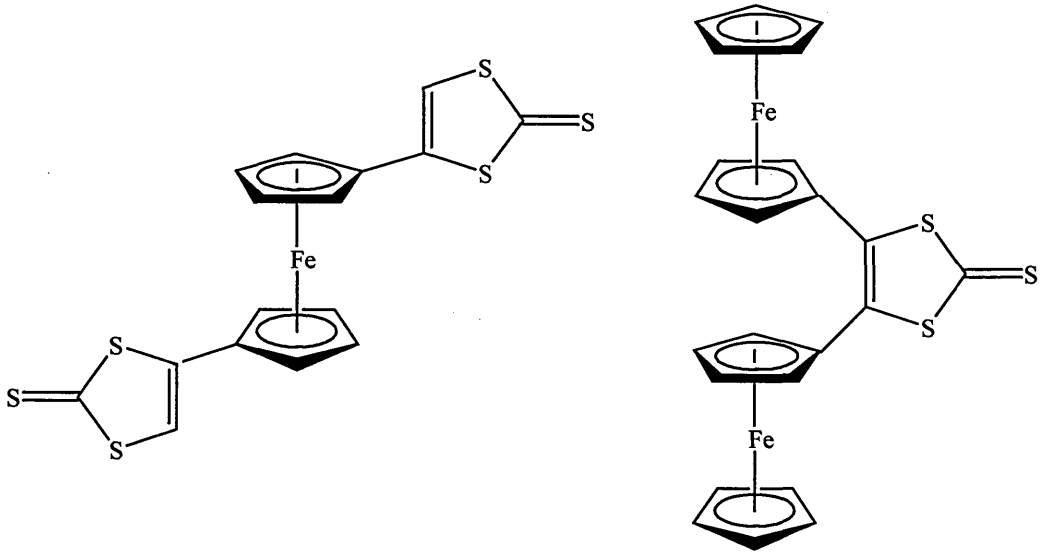

Figure 114, "dithione" and "diferrocenyl" derivatives of compound **[80]**

Another area that would be worth investigating could be the use of the other metallocenes, namely those based on Vanadium, Chromium, Manganese, Cobalt and Nickel. Which could introduce a further range of oxidation reactions with the dihalogen used and hence introduce a further range of charge transfer or "transfer of charge" interactions, which should significantly affect nature of the solid state structures obtained. While the variations in the metal centre could provide a further range magnetic properties.

8 APPENDIX

8.1 NMR SHIFT CALCULATIONS

Calculations carried out by the software package:

CS ChemDraw(R) version 4.5

For Microsoft Windows 3.1, Windows 95 and Windows NT

(c) 1997, CambridgeSoft Corporation

8.1.1 "Ethane bridge ligand, compound [35]"

Proton Node	Estimate	Base	Incr.	Comment
Hb	2.93	1.37		methylene
			1.23	1 alpha -S
			0.33	1 beta -C+N
Ha	2.86	1.37		methylene
			1.23	1 alpha -S
			0.26	1 beta -S
Hc	2.71	1.37		methylene
			1.08	1 alpha -C+N
			0.26	1 beta -S

Carbon Node	Estimate	Base	Incr.	Comment
C1	208	232		1-thiocarbonyl
			-24	2 -S
C2/3	125	123.3		1-ethylene
			-17.5	1 -S-C
			?	1 unknown substituent(s)
			19	1 -S-C
			?	1 unknown substituent(s)
			->	2 increment(s) not found
C7	117.7	117.7		1-nitrile
			0	1 -C-C
C4	30.5	-2.3		aliphatic
			9.1	1 alpha -C
			11.9	1 alpha -S
			6.9	1 beta -C=C
			11.4	1 beta -S
			-2.1	1 gamma -C=C
			-3.6	1 gamma -S-C=S
			0	1 delta -S-C=S
			-0.8	2 delta -S
C5	23.6	-2.3		aliphatic
			9.1	1 alpha -C
			11.9	1 alpha -S
			6.9	1 beta -C=C
			2.4	1 beta -C+N
			-3.6	1 gamma -S-C=S
			-0.8	2 delta -S
C6	20.4	-2.3		aliphatic
			4.3	1 alpha -C+N
			9.1	1 alpha -C
			11.4	1 beta -S
			-2.1	1 gamma -C=C
			0	1 delta -S-C=S

8.1.2 "o-xylene bridge ligand, compound [36]"

Proton

Node	Estimate	Base	Incr.	Comment	
He	6.95	7.26		1-benzene	
			-0.19	1 -C	
			-0.12	1 -C	
Hd	6.94	7.26		1-benzene	
			-0.12	1 -C	
			-0.2	1 -C	
Hc	3.82	1.37		methylene	
			1.22	1 alpha	-1:C*C*C*C*C*C*1
			1.23	1 alpha	#NAME?
Ha	2.93	1.37		methylene	
			1.23	1 alpha	#NAME?
			0.33	1 beta	-C+N
Hb	2.71	1.37		methylene	
			1.08	1 alpha	-C+N
			0.26	1 beta	#NAME?

Carbon

Node	Estimate	Base	Incr.	Comment
C7	208	232		1-thiocarbonyl
			-24	2 -S
C3	140.4	128.5		1-benzene
			-0.6	1 -C-S
			12.5	1 -C-S
C2	127.9	128.5		1-benzene
			0	1 -C-S
			-0.6	1 -C-S
C1	126.9	128.5		1-benzene
			-1.6	1 -C-S
			0	1 -C-S
C6	126	123.3		1-ethylene
			-16.4	1 -S-C-1:C*C*C*C*C*C*1
			?	1 unknown substituent(s)
			19	1 -S-C
			?	1 unknown substituent(s)
			->	2 increment(s) not found
C10	117.7	117.7		1-nitrile
			0	1 -C-C
C5	115	123.3		1-ethylene
			9.5	1 -S-C-1:C*C*C*C*C*C*1
			?	1 unknown substituent(s)
			-17.5	1 -S-C
			?	1 unknown substituent(s)
			->	2 increment(s) not found
C4	27	-2.3		aliphatic
			24.3	1 alpha -1:C*C*C*C*C*C*1
			11.9	1 alpha -S
			6.9	1 beta -C=C
			-2.5	1 gamma -C
			-3.6	1 gamma -S-C=S

			-1.2	3 delta -S
			-2.5	steric corrections
			-4	gamma corrections
C8	23.6	-2.3		aliphatic
			9.1	1 alpha -C
			11.9	1 alpha -S
			6.9	1 beta -C=C
			2.4	1 beta -C+N
			-3.6	1 gamma -S-C=S
			-0.8	2 delta -S
C9	20.4	-2.3		aliphatic
			4.3	1 alpha -C+N
			9.1	1 alpha -C
			11.4	1 beta -S
			-2.1	1 gamma -C=C
			0	1 delta -S-C=S

8.1.3 "m-xylene bridge ligand, compound [37]"

Proton

Node	Estimate	Base	Incr.	Comment	
He	7.02	7.26		1-benzene	
			-0.12	1 -C	
			-0.12	1 -C	
Hd	6.87	7.26		1-benzene	
			-0.19	1 -C	
			-0.2	1 -C	
Hc	6.86	7.26		1-benzene	
			-0.2	1 -C	
			-0.2	1 -C	
Hf	3.82	1.37		methylene	
			1.22	1 alpha	-1:C*C*C*C*C*C*1
			1.23	1 alpha	#NAME?
Ha	2.93	1.37		methylene	
			1.23	1 alpha	#NAME?
			0.33	1 beta	-C+N
Hb	2.71	1.37		methylene	
			1.08	1 alpha	-C+N
			0.26	1 beta	#NAME?

Carbon

Node	Estimate	Base	Incr.	Comment
C8	208	232		1-thiocarbonyl
			-24	2 -S
C3	141	128.5		1-benzene
			0	1 -C-S
			12.5	1 -C-S
C1	128.5	128.5		1-benzene
			0	1 -C-S
			0	1 -C-S
C4	127.3	128.5		1-benzene
			-0.6	1 -C-S
			-0.6	1 -C-S
C2	126.3	128.5		1-benzene
			-1.6	1 -C-S
			-0.6	1 -C-S
C7	126	123.3		1-ethylene
			-16.4	1 -S-C-1:C*C*C*C*C*C*1
			?	1 unknown substituent(s)
			19	1 -S-C
			?	1 unknown substituent(s)
			->	2 increment(s) not found
C11	117.7	117.7		1-nitrile
			0	1 -C-C
C6	115	123.3		1-ethylene
			9.5	1 -S-C-1:C*C*C*C*C*C*1
			?	1 unknown substituent(s)
			-17.5	1 -S-C
			?	1 unknown substituent(s)
			->	2 increment(s) not found

C5	34.2	-2.3		aliphatic
			24.3	1 alpha -1:C*C*C*C*C*C*1
			11.9	1 alpha -S
			6.9	1 beta -C=C
			-3.6	1 gamma -S-C=S
			0.3	1 delta -C
			-0.8	2 delta -S
			-2.5	steric corrections
C9	23.6	-2.3		aliphatic
			9.1	1 alpha -C
			11.9	1 alpha -S
			6.9	1 beta -C=C
			2.4	1 beta -C+N
			-3.6	1 gamma -S-C=S
			-0.8	2 delta -S
C10	20.4	-2.3		aliphatic
			4.3	1 alpha -C+N
			9.1	1 alpha -C
			11.4	1 beta -S
			-2.1	1 gamma -C=C
			0	1 delta -S-C=S

8.1.4 "p-xylene bridge ligand, compound [38]"

Proton

Node	Estimate	Base	Incr.	Comment	
Hc	6.94	7.26		1-benzene	
			-0.12	1 -C	
			-0.2	1 -C	
Hd	3.82	1.37		methylene	
			1.22	1 alpha	-1:C*C*C*C*C*C*1
			1.23	1 alpha	#NAME?
Hb	2.93	1.37		methylene	
			1.23	1 alpha	#NAME?
			0.33	1 beta	-C+N
Ha	2.71	1.37		methylene	
			1.08	1 alpha	-C+N
			0.26	1 beta	#NAME?

Carbon

Node	Estimate	Base	Incr.	Comment
C6	208	232		1-thiocarbonyl
			-24	2 -S
C8	139.4	128.5		1-benzene
			-1.6	1 -C-S
			12.5	1 -C-S
C9	127.9	128.5		1-benzene
			0	1 -C-S
			-0.6	1 -C-S
C4	126	123.3		1-ethylene
			-16.4	1 -S-C-1:C*C*C*C*C*C*1
			?	1 unknown substituent(s)
			19	1 -S-C
			?	1 unknown substituent(s)
			->	2 increment(s) not found
C1	117.7	117.7		1-nitrile
			0	1 -C-C
C5	115	123.3		1-ethylene
			9.5	1 -S-C-1:C*C*C*C*C*C*1
			?	1 unknown substituent(s)
			-17.5	1 -S-C
			?	1 unknown substituent(s)
			->	2 increment(s) not found
C7	33.9	-2.3		aliphatic
			24.3	1 alpha -1:C*C*C*C*C*C*1
			11.9	1 alpha -S
			6.9	1 beta -C=C
			-3.6	1 gamma -S-C=S
			-0.8	2 delta -S
			-2.5	steric corrections
C3	23.6	-2.3		aliphatic
			9.1	1 alpha -C
			11.9	1 alpha -S
			6.9	1 beta -C=C
			2.4	1 beta -C+N

			-3.6	1 gamma -S-C=S
			-0.8	2 delta -S
C2	20.4	-2.3		aliphatic
			4.3	1 alpha -C+N
			9.1	1 alpha -C
			11.4	1 beta -S
			-2.1	1 gamma -C=C
			0	1 delta -S-C=S

8.1.5 "dimethylpyridine bridge ligand, compound [39]"

Proton Node	Estimate	Base	Incr.	Comment
Hf	9.02	9.04		pyridinium
			-0.01	1 -C from 2-pyridine, in DMSO
			-0.01	1 -C from 2-pyridine, in DMSO
He	8.23	8.5		pyridinium
			-0.11	1 -C from 2-pyridine, in DMSO
			-0.16	1 -C from 2-pyridine, in DMSO
Hc	3.82	1.37		methylene
			1.22	1 alpha -C*R
			1.23	1 alpha -S
Hb	2.93	1.37		methylene
			1.23	1 alpha -S
			0.33	1 beta -C+N
Ha	2.71	1.37		methylene
			1.08	1 alpha -C+N
			0.26	1 beta -S
Hd	?	?		pyridinium

Carbon Node	Estimate	Base	Incr.	Comment
C6	208	232		1-thiocarbonyl
			-24	2 -S
C10	148.4	148.4		pyridinium
C8	142.5	142.5		pyridinium
C9	129	129		pyridinium
C4	126	123.3		1-ethylene
			-16.4	1 -S-C-C*R
			?	1 unknown substituent(s)
			19	1 -S-C
			?	1 unknown substituent(s)
			->	2 increment(s) not found
C5	124	123.3		1-ethylene
			18.5	1 -S-C-C*R
			?	1 unknown substituent(s)
			-17.5	1 -S-C
			?	1 unknown substituent(s)
			->	2 increment(s) not found
C1	117.7	117.7		1-nitrile
			0	1 -C-C
C7	34.2	-2.3		aliphatic
			24.3	1 alpha -1:C*R*R*R*R*R*1
			11.9	1 alpha -S
			6.9	1 beta -C=C
			-3.6	1 gamma -S-C=S
			0.3	1 delta -C
			-0.8	2 delta -S
			-2.5	steric corrections
C3	23.6	-2.3		aliphatic
			9.1	1 alpha -C
			11.9	1 alpha -S
			6.9	1 beta -C=C

			2.4	1 beta -C+N
			-3.6	1 gamma -S-C=S
			-0.8	2 delta -S
C2	20.4	-2.3		aliphatic
			4.3	1 alpha -C+N
			9.1	1 alpha -C
			11.4	1 beta -S
			-2.1	1 gamma -C=C
			0	1 delta -S-C=S

8.2 Supporting crystal data

8.2.1 Ethane bridge ligand TMA salt, compound [42]

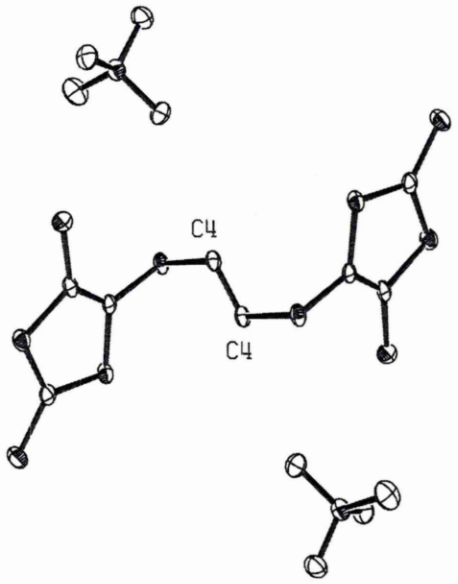

Table 1. Crystal data and structure refinement for salt.

Identification code	s92	
Empirical formula	C8 H14 N S5	
Formula weight	284.50	
Temperature	293(2) K	
Wavelength	0.71069 Å	
Crystal system	Monoclinic	
Space group	P2(1)/n	
Unit cell dimensions	a = 12.213(2) Å	a= 90°.
	b = 8.716(2) Å	b= 01.861(14)°.
	c = 12.548(3) Å	c = 90°.
Volume	1307.2(5) $Å^3$	
Z	4	
Density (calculated)	1.446 Mg/m^3	
Absorption coefficient	0.851 mm^{-1}	
F(000)	596	
Crystal size	0.28 x 0.20 x 0.10 mm^3	
Theta range for data collection	2.12 to 25.04°.	
Index ranges	-12<=h<=13, -7<=k<=9, -14<=l<=13	
Reflections collected	5416	
Independent reflections	2012 [R(int) = 0.1064]	
Refinement method	Full-matrix least-squares on F^2	
Data / restraints / parameters	2012 / 0 / 183	
Goodness-of-fit on F^2	1.051	
Final R indices [I>2sigma(I)]	R1 = 0.0466, wR2 = 0.1136	
R indices (all data)	R1 = 0.0537, wR2 = 0.1150	
Largest diff. peak and hole	0.587 and -0.492 $e.Å^{-3}$	

Table 2. Atomic coordinates (x 10^4) and equivalent isotropic displacement parameters ($Å^2$x 10^3) for salt. U(eq) is defined as one third of the trace of the orthogonalized U^{ij} tensor.

	x	y	z	U(eq)
S(1)	-236(1)	2408(1)	-610(1)	19(1)
S(2)	2591(1)	3057(1)	-705(1)	26(1)
S(3)	2701(1)	4323(1)	1490(1)	23(1)
S(4)	460(1)	3683(1)	1637(1)	21(1)
S(5)	1990(1)	5203(1)	3526(1)	27(1)
C(1)	816(3)	3193(3)	406(3)	16(1)
C(2)	1902(3)	3468(3)	323(3)	18(1)
C(3)	1717(3)	4432(3)	2297(3)	20(1)
C(4)	119(3)	367(3)	-508(3)	18(1)
N(1)	-1289(3)	7508(3)	3906(3)	22(1)
C(5)	-826(4)	8541(5)	3164(4)	33(1)
C(6)	-2523(4)	7707(5)	3740(4)	29(1)
C(7)	-764(4)	7901(5)	5059(4)	31(1)
C(8)	-1032(4)	5876(5)	3673(4)	38(1)

Table 3. Bond lengths [Å] and angles [°] for salt

Table 4. Bond lengths [A] and angles [deg] for 98src138.

S(1)-C(1)	1.753(3)
S(1)-C(4)	1.829(3)
S(2)-C(2)	1.717(4)
S(3)-C(3)	1.727(4)
S(3)-C(2)	1.750(3)
S(4)-C(3)	1.717(4)
S(4)-C(1)	1.741(3)
S(5)-C(3)	1.652(4)
C(1)-C(2)	1.373(5)
C(4)-C(4)#1	1.508(7)
N(1)-C(5)	1.488(5)
N(1)-C(6)	1.488(5)
N(1)-C(7)	1.497(5)
N(1)-C(8)	1.499(5)
C(4)-H(4A)	0.97(4)
C(4)-H(4B)	0.92(4)
C(5)-H(5A)	0.90(5)
C(5)-H(5B)	1.05(5)
C(5)-H(5C)	0.93(4)
C(6)-H(6A)	0.96(5)
C(6)-H(6B)	0.84(5)
C(6)-H(6C)	1.01(4)
C(7)-H(7A)	1.01(4)
C(7)-H(7B)	0.92(5)
C(7)-H(7C)	0.90(5)
C(8)-H(8A)	1.07(5)
C(8)-H(8B)	1.04(4)
C(8)-H(8C)	0.90(5)
C(1)-S(1)-C(4)	101.6(2)
C(3)-S(3)-C(2)	100.3(2)
C(3)-S(4)-C(1)	99.2(2)
C(2)-C(1)-S(4)	116.5(3)
C(2)-C(1)-S(1)	126.0(3)
S(4)-C(1)-S(1)	117.5(2)
C(1)-C(2)-S(2)	130.6(3)
C(1)-C(2)-S(3)	113.1(3)
S(2)-C(2)-S(3)	116.3(2)
S(5)-C(3)-S(4)	126.5(2)
S(5)-C(3)-S(3)	122.6(2)
S(4)-C(3)-S(3)	110.9(2)
C(4)#1-C(4)-S(1)	112.8(3)
C(4)#1-C(4)-H(4A)	111(2)
S(1)-C(4)-H(4A)	106(2)
C(4)#1-C(4)-H(4B)	113(2)
S(1)-C(4)-H(4B)	107(2)
H(4A)-C(4)-H(4B)	108(3)
C(5)-N(1)-C(6)	110.3(3)
C(5)-N(1)-C(7)	108.9(3)
C(6)-N(1)-C(7)	109.2(3)
C(5)-N(1)-C(8)	109.3(3)
C(6)-N(1)-C(8)	109.3(3)
C(7)-N(1)-C(8)	109.9(3)
N(1)-C(5)-H(5A)	107(3)
N(1)-C(5)-H(5B)	109(2)
H(5A)-C(5)-H(5B)	111(4)
N(1)-C(5)-H(5C)	110(3)
H(5A)-C(5)-H(5C)	101(4)
H(5B)-C(5)-H(5C)	119(4)
N(1)-C(6)-H(6A)	116(3)

N(1)-C(6)-H(6B)	105(3)
H(6A)-C(6)-H(6B)	110(4)
N(1)-C(6)-H(6C)	113(2)
H(6A)-C(6)-H(6C)	106(3)
H(6B)-C(6)-H(6C)	106(4)
N(1)-C(7)-H(7A)	111(2)
N(1)-C(7)-H(7B)	112(3)
H(7A)-C(7)-H(7B)	111(3)
N(1)-C(7)-H(7C)	105(3)
H(7A)-C(7)-H(7C)	105(3)
H(7B)-C(7)-H(7C)	112(4)
N(1)-C(8)-H(8A)	107(2)
N(1)-C(8)-H(8B)	109(2)
H(8A)-C(8)-H(8B)	97(3)
N(1)-C(8)-H(8C)	108(3)
H(8A)-C(8)-H(8C)	111(4)
H(8B)-C(8)-H(8C)	123(4)

Symmetry transformations used to generate equivalent atoms:
#1 -x,-y,-z

Table 4. Anisotropic displacement parameters ($Å^2 x\ 10^3$)for salt. The anisotropic displacement factor exponent takes the form: $-2p^2[\ h^2a^{*2}U^{11} + ... + 2\ h\ k\ a^*\ b^*\ U^{12}\ ]$

	U^{11}	U^{22}	U^{33}	U^{23}	U^{13}	U^{12}
S(1)	19(1)	12(1)	24(1)	1(1)	-3(1)	0(1)
S(2)	25(1)	28(1)	25(1)	-2(1)	9(1)	-4(1)
S(3)	17(1)	24(1)	26(1)	-4(1)	3(1)	-5(1)
S(4)	18(1)	19(1)	27(1)	-5(1)	6(1)	-4(1)
S(5)	28(1)	28(1)	25(1)	-9(1)	3(1)	-4(1)
C(1)	19(2)	8(2)	21(2)	1(1)	2(2)	0(1)
C(2)	20(2)	9(2)	24(2)	-2(1)	0(2)	0(1)
C(3)	24(2)	11(2)	23(2)	2(1)	1(2)	0(1)
C(4)	19(2)	10(2)	25(2)	-3(1)	5(2)	1(1)
N(1)	20(2)	21(2)	27(2)	-4(1)	5(1)	0(1)
C(5)	25(3)	43(3)	35(3)	-4(2)	14(2)	-15(2)
C(6)	19(2)	31(2)	35(3)	-1(2)	6(2)	-1(2)
C(7)	28(3)	36(3)	27(2)	-5(2)	1(2)	-5(2)
C(8)	41(3)	25(2)	46(3)	-8(2)	8(2)	10(2)

Table 5. Hydrogen coordinates ($x\ 10^4$) and isotropic displacement parameters ($Å^2 x\ 10^3$) for salt.

	x	y	z	U(eq)
H(4A)	-320(30)	-99(35)	-1157(31)	13(8)
H(4B)	864(34)	296(33)	-553(28)	15(9)
H(5A)	-78(44)	8381(44)	3304(37)	40(13)
H(5B)	-1187(37)	8252(43)	2355(38)	40(11)
H(5C)	-854(36)	9554(47)	3393(34)	33(12)
H(6A)	-2889(40)	7074(47)	4186(41)	45(13)
H(6B)	-2768(39)	7518(39)	3080(41)	29(12)
H(6C)	-2752(34)	8800(47)	3854(33)	37(11)
H(7A)	-904(34)	9012(47)	5227(31)	32(10)
H(7B)	-1004(41)	7257(44)	5543(40)	45(13)
H(7C)	-21(43)	7830(41)	5098(36)	36(13)
H(8A)	-141(45)	5789(46)	3794(37)	52(13)
H(8B)	-1201(35)	5704(41)	2837(38)	36(11)
H(8C)	-1300(40)	5265(46)	4139(41)	40(13)

8.2.2 O-Xylene bridge ligand Ni complex, compound [55]

Sulphur shown in green, Nitrogen in blue, and Nickel in yellow

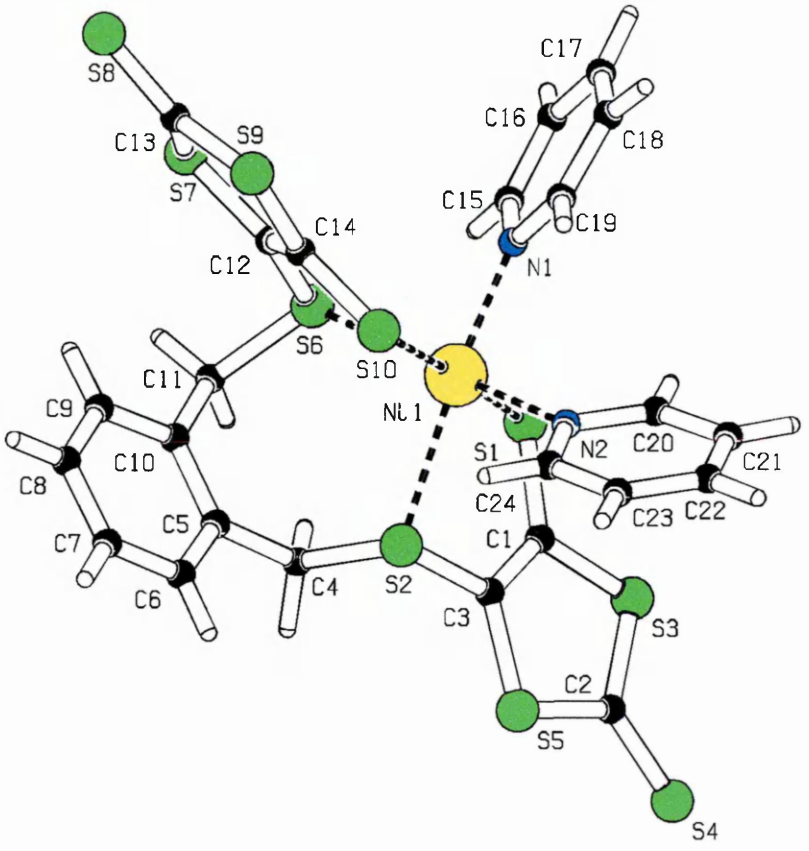

Table 1. Crystal data and structure refinement for C24H18N2NiS10.

Identification code	98src291
Empirical formula	C24 H18 N2 Ni S10
Formula weight	713.71
Temperature	298(2) K
Wavelength	0.71073 A
Crystal system	Triclinic
Space group	P-1
Unit cell dimensions	a = 9.5662(6) A b = 12.5254(8) A c = 14.0131(8) A alpha = 76.558(3) deg. beta = 86.314(3) deg. gamma = 67.969(3) deg.

Volume	1513.32(16) A^3
Z	2
Density (calculated)	1.566 Mg/m^3
Absorption coefficient	1.350 mm^-1
F(000)	728
Crystal size	0.20 x 0.20 x 0.10 mm
Theta range for data collection	2.95 to 23.25 deg.
Index ranges	-10<=h<=10, -13<=k<=13, -15<=l<=15
Reflections collected	18864
Independent reflections	4319 [R(int) = 0.1189]
Max. and min. transmission	0.879 and 0.765
Refinement method	Full-matrix least-squares on F^2
Data / restraints / parameters	4319 / 0 / 334
Goodness-of-fit on F^2	1.017
Final R indices [I>2sigma(I)]	R1 = 0.0517, wR2 = 0.1149
R indices (all data)	R1 = 0.1009, wR2 = 0.1364
Largest diff. peak and hole	0.502 and -0.463 e.A^-3

Table 2. Atomic coordinates (x 10^4) and equivalent isotropic displacement parameters (A^2 x 10^3) for C24H18N2NiS10. U(eq) is defined as one third of the trace of the orthogonalized Uij tensor.

	x	y	z	U(eq)
Ni(1)	6598(1)	1878(1)	2154(1)	42(1)
S(1)	6219(2)	2082(2)	427(1)	56(1)
S(2)	3961(2)	3493(1)	2017(1)	43(1)
S(10)	6961(2)	1792(2)	3842(1)	53(1)
S(6)	8151(2)	3220(2)	1818(1)	47(1)
S(5)	1397(2)	3643(2)	760(1)	53(1)
S(3)	3383(2)	2254(2)	-483(1)	59(1)
S(9)	9494(2)	1892(2)	4861(1)	66(1)
S(7)	10501(2)	3201(2)	3184(1)	66(1)
S(4)	90(2)	3099(2)	-858(2)	85(1)
S(8)	12023(2)	2638(2)	5132(2)	97(1)
C(3)	3319(6)	3191(6)	1007(4)	45(2)
N(1)	8694(5)	550(4)	2042(3)	46(1)
C(2)	1526(7)	2999(6)	-211(4)	52(2)
C(1)	4283(6)	2583(5)	401(4)	43(2)
C(14)	8457(6)	2242(5)	3770(4)	46(2)
C(12)	8956(6)	2834(6)	2990(4)	47(2)
C(13)	10724(7)	2609(7)	4420(5)	61(2)
C(4)	4083(7)	4948(5)	1501(5)	57(2)
C(10)	6111(7)	5249(5)	2373(4)	49(2)
C(5)	4622(7)	5301(5)	2325(5)	48(2)
C(15)	9623(7)	660(6)	1301(5)	54(2)
C(11)	7240(7)	4832(6)	1630(5)	57(2)
C(19)	9117(7)	-498(6)	2682(4)	55(2)
N(2)	5409(5)	738(4)	2617(3)	44(1)
C(16)	10937(7)	-222(7)	1169(5)	63(2)
C(24)	4527(6)	837(6)	3397(4)	47(2)
C(9)	6519(9)	5599(6)	3154(5)	66(2)
C(6)	3646(8)	5672(6)	3038(5)	63(2)
C(20)	5560(8)	-158(7)	2201(5)	67(2)
C(8)	5503(11)	5969(7)	3862(6)	80(2)
C(18)	10410(8)	-1434(6)	2575(5)	65(2)
C(17)	11353(8)	-1280(7)	1821(5)	72(2)
C(7)	4074(9)	5994(6)	3816(6)	73(2)
C(23)	3806(7)	72(6)	3786(5)	58(2)
C(22)	3986(9)	-826(7)	3341(6)	79(2)
C(21)	4877(10)	-959(7)	2552(6)	93(3)

Table 3. Bond lengths [A] and angles [deg] for C24H18N2NiS10.

Ni(1)-N(1)	2.095(5)	Ni(1)-N(2)	2.109(5)
Ni(1)-S(10)	2.3842(17)	Ni(1)-S(1)	2.4105(17)
Ni(1)-S(2)	2.5585(17)	Ni(1)-S(6)	2.5827(18)
S(1)-C(1)	1.717(6)	S(2)-C(3)	1.749(5)
S(2)-C(4)	1.841(6)	S(10)-C(14)	1.714(6)
S(6)-C(12)	1.743(6)	S(6)-C(11)	1.835(7)
S(5)-C(2)	1.712(6)	S(5)-C(3)	1.741(5)
S(3)-C(2)	1.734(6)	S(3)-C(1)	1.757(5)
S(9)-C(13)	1.737(7)	S(9)-C(14)	1.752(5)
S(7)-C(13)	1.711(7)	S(7)-C(12)	1.757(6)
S(4)-C(2)	1.644(6)	S(8)-C(13)	1.659(6)
C(3)-C(1)	1.351(8)	N(1)-C(19)	1.338(7)
N(1)-C(15)	1.340(7)	C(14)-C(12)	1.340(8)
C(4)-C(5)	1.509(8)	C(10)-C(9)	1.395(8)
C(10)-C(5)	1.407(8)	C(10)-C(11)	1.487(9)
C(5)-C(6)	1.362(9)	C(15)-C(16)	1.363(8)
C(19)-C(18)	1.377(8)	N(2)-C(20)	1.337(8)
N(2)-C(24)	1.337(7)	C(16)-C(17)	1.355(10)
C(24)-C(23)	1.377(8)	C(9)-C(8)	1.377(10)
C(6)-C(7)	1.381(9)	C(20)-C(21)	1.377(10)
C(8)-C(7)	1.361(10)	C(18)-C(17)	1.371(9)
C(23)-C(22)	1.360(9)	C(22)-C(21)	1.354(10)

N(1)-Ni(1)-N(2)	96.17(19)	N(1)-Ni(1)-S(10)	94.61(13)
N(2)-Ni(1)-S(10)	87.79(13)	N(1)-Ni(1)-S(1)	87.01(13)
N(2)-Ni(1)-S(1)	94.88(13)	S(10)-Ni(1)-S(1)	176.71(7)
N(1)-Ni(1)-S(2)	171.09(13)	N(2)-Ni(1)-S(2)	83.39(14)
S(10)-Ni(1)-S(2)	94.26(6)	S(1)-Ni(1)-S(2)	84.16(5)
N(1)-Ni(1)-S(6)	83.23(15)	N(2)-Ni(1)-S(6)	172.75(13)
S(10)-Ni(1)-S(6)	85.05(6)	S(1)-Ni(1)-S(6)	92.31(6)
S(2)-Ni(1)-S(6)	98.32(6)	C(1)-S(1)-Ni(1)	98.20(19)
C(3)-S(2)-C(4)	102.4(3)	C(3)-S(2)-Ni(1)	96.9(2)
C(4)-S(2)-Ni(1)	109.7(2)	C(14)-S(10)-Ni(1)	100.5(2)
C(12)-S(6)-C(11)	101.6(3)	C(12)-S(6)-Ni(1)	97.7(2)
C(11)-S(6)-Ni(1)	121.5(2)	C(2)-S(5)-C(3)	98.0(3)
C(2)-S(3)-C(1)	98.7(3)	C(13)-S(9)-C(14)	98.1(3)
C(13)-S(7)-C(12)	97.2(3)	C(1)-C(3)-S(5)	117.4(4)
C(1)-C(3)-S(2)	121.7(4)	S(5)-C(3)-S(2)	120.8(4)
C(19)-N(1)-C(15)	116.5(5)	C(19)-N(1)-Ni(1)	120.6(4)
C(15)-N(1)-Ni(1)	122.7(4)	S(4)-C(2)-S(5)	125.3(4)
S(4)-C(2)-S(3)	122.5(4)	S(5)-C(2)-S(3)	112.1(3)
C(3)-C(1)-S(1)	128.0(4)	C(3)-C(1)-S(3)	113.6(4)
S(1)-C(1)-S(3)	118.4(3)	C(12)-C(14)-S(10)	129.0(4)
C(12)-C(14)-S(9)	114.5(4)	S(10)-C(14)-S(9)	116.5(4)
C(14)-C(12)-S(6)	122.5(4)	C(14)-C(12)-S(7)	117.2(4)
S(6)-C(12)-S(7)	120.2(4)	S(8)-C(13)-S(7)	124.7(4)
S(8)-C(13)-S(9)	122.4(4)	S(7)-C(13)-S(9)	112.8(3)
C(5)-C(4)-S(2)	106.8(4)	C(9)-C(10)-C(5)	117.9(6)
C(9)-C(10)-C(11)	119.9(6)	C(5)-C(10)-C(11)	122.2(6)
C(6)-C(5)-C(10)	119.4(6)	C(6)-C(5)-C(4)	119.2(6)
C(10)-C(5)-C(4)	121.4(6)	N(1)-C(15)-C(16)	123.9(6)
C(10)-C(11)-S(6)	114.9(4)	N(1)-C(19)-C(18)	122.4(6)
C(20)-N(2)-C(24)	116.4(6)	C(20)-N(2)-Ni(1)	122.9(5)
C(24)-N(2)-Ni(1)	120.5(4)	C(17)-C(16)-C(15)	119.1(7)
N(2)-C(24)-C(23)	123.8(6)	C(8)-C(9)-C(10)	121.2(7)
C(5)-C(6)-C(7)	122.0(7)	N(2)-C(20)-C(21)	123.0(7)

C(7)-C(8)-C(9)	120.3(7)	C(17)-C(18)-C(19)	119.5(7)
C(16)-C(17)-C(18)	118.6(7)	C(8)-C(7)-C(6)	119.1(8)
C(22)-C(23)-C(24)	117.9(6)	C(21)-C(22)-C(23)	120.0(7)
C(22)-C(21)-C(20)	118.9(7)		

Symmetry transformations used to generate equivalent atoms:

Table 4. Anisotropic displacement parameters (A^2 x 10^3) for C24H18N2NiS10.
The anisotropic displacement factor exponent takes the form:
-2 pi^2 [h^2 a*^2 U11 + ... + 2 h k a* b* U12]

	U11	U22	U33	U23	U13	U12
Ni(1)	37(1)	48(1)	39(1)	-6(1)	4(1)	-16(1)
S(1)	39(1)	75(1)	43(1)	-12(1)	5(1)	-10(1)
S(2)	37(1)	51(1)	42(1)	-13(1)	1(1)	-17(1)
S(10)	52(1)	75(1)	40(1)	-8(1)	6(1)	-35(1)
S(6)	40(1)	60(1)	44(1)	-6(1)	0(1)	-24(1)
S(5)	39(1)	76(1)	51(1)	-19(1)	2(1)	-26(1)
S(3)	68(1)	61(1)	51(1)	-18(1)	-5(1)	-24(1)
S(9)	61(1)	97(2)	43(1)	-10(1)	-7(1)	-34(1)
S(7)	49(1)	97(2)	61(1)	-12(1)	-4(1)	-41(1)
S(4)	81(1)	115(2)	78(1)	-17(1)	-23(1)	-56(1)
S(8)	78(1)	157(2)	78(1)	-33(2)	-15(1)	-61(2)
C(3)	33(3)	63(5)	45(4)	-20(3)	-3(3)	-20(3)
N(1)	38(3)	51(4)	39(3)	-4(3)	6(2)	-9(3)
C(2)	49(4)	61(5)	54(4)	-11(3)	-4(3)	-30(3)
C(1)	43(3)	50(4)	35(3)	-6(3)	-5(3)	-17(3)
C(14)	40(3)	54(4)	41(4)	-12(3)	-3(3)	-15(3)
C(12)	35(3)	61(5)	44(4)	-7(3)	1(3)	-19(3)
C(13)	47(4)	92(6)	51(4)	-25(4)	-1(3)	-27(4)
C(4)	55(4)	53(5)	66(4)	1(3)	-16(3)	-28(4)
C(10)	51(4)	38(4)	54(4)	1(3)	-3(3)	-20(3)
C(5)	53(4)	30(4)	56(4)	-9(3)	-4(3)	-10(3)
C(15)	40(4)	61(5)	52(4)	-12(3)	5(3)	-13(4)
C(11)	60(4)	52(5)	60(4)	9(3)	-18(4)	-31(4)
C(19)	55(4)	50(5)	47(4)	-9(4)	6(3)	-8(4)
N(2)	41(3)	46(3)	43(3)	-7(3)	5(3)	-16(3)
C(16)	49(4)	88(6)	51(4)	-26(4)	8(3)	-18(4)
C(24)	43(4)	54(5)	48(4)	-13(3)	6(3)	-21(3)
C(9)	75(5)	63(5)	71(5)	-11(4)	-17(4)	-38(4)
C(6)	56(4)	48(5)	86(5)	-22(4)	-7(4)	-13(4)
C(20)	74(5)	70(5)	75(5)	-35(4)	23(4)	-37(4)
C(8)	104(7)	69(6)	73(6)	-19(4)	-8(5)	-35(5)
C(18)	75(5)	53(5)	53(4)	-5(4)	-9(4)	-12(4)
C(17)	53(4)	81(6)	59(5)	-21(5)	-5(4)	3(4)
C(7)	78(6)	61(5)	80(5)	-33(4)	20(5)	-18(4)
C(23)	61(4)	58(5)	53(4)	-9(4)	13(4)	-23(4)
C(22)	92(6)	73(6)	90(6)	-26(5)	30(5)	-51(5)
C(21)	131(8)	77(6)	107(7)	-56(5)	47(6)	-67(6)

Table 5. Hydrogen coordinates (x 10^4) and isotropic displacement parameters (A^2 x 10^3) for C24H18N2NiS10.

	x	y	z	U(iso)
H(4A)	4801	4898	957	68
H(4B)	3082	5536	1245	68
H(15)	9350	1398	839	64
H(11A)	8031	5163	1631	68
H(11B)	6736	5151	973	68
H(19)	8503	-600	3230	66
H(16)	11552	-98	628	76
H(24)	4390	1472	3700	57
H(9)	7514	5581	3197	79
H(6)	2641	5709	2998	76
H(20)	6166	-245	1639	81
H(8)	5801	6209	4385	96
H(18)	10646	-2180	3020	77
H(17)	12278	-1902	1757	86
H(7)	3379	6230	4313	88
H(23)	3201	168	4348	70
H(22)	3487	-1360	3583	94
H(21)	5029	-1594	2246	111

8.2.3 1:1 adduct of [4,5(2'-cyanoethylthio)-1,3-dithione]:[IBr], compound [81]

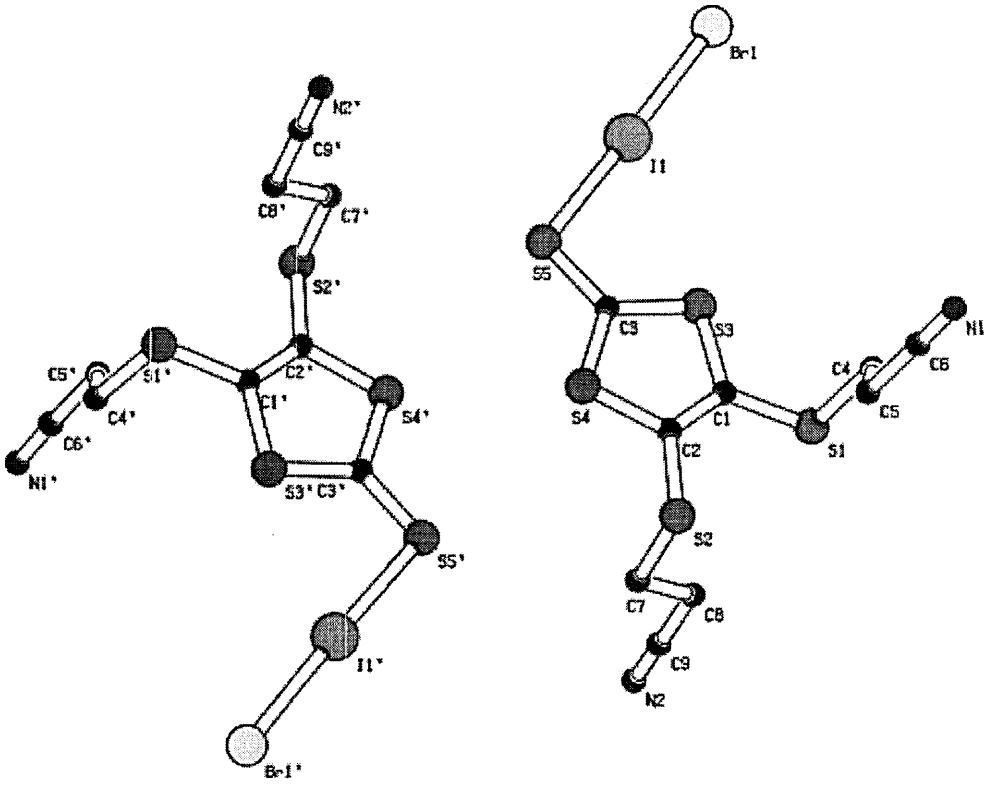

Table 1. Crystal data and structure refinement for rory3.

Identification code	s92
Empirical formula	C9 H8 Br I N2 S5
Formula weight	511.28
Temperature	150(2) K
Wavelength	0.71073 A
Crystal system, space group	Orthorhombic, P2(1)2(1)2(1)
Unit cell dimensions	a = 8.50950(10) A alpha = 90 deg. b = 13.5128(2) A beta = 90 deg. c = 27.7591(5) A gamma = 90 deg.
Volume	3191.94(8) A^3
Z, Calculated density	8, 2.128 Mg/m^3
Absorption coefficient	5.147 mm^-1
F(000)	1952
Crystal size	0.25 x 0.05 x 0.05 mm
Theta range for data collection	2.50 to 26.00 deg.
Limiting indices	-10<=h<=10, -13<=k<=16, -32<=l<=34
Reflections collected / unique	25989 / 6259 [R(int) = 0.1072]
Completeness to theta = 26.00	99.7 %
Max. and min. transmission	0.7829 and 0.3594

Refinement method	Full-matrix least-squares on F^2
Data / restraints / parameters	6259 / 0 / 335
Goodness-of-fit on F^2	0.888
Final R indices [I>2sigma(I)]	R1 = 0.0469, wR2 = 0.0687
R indices (all data)	R1 = 0.1207, wR2 = 0.0778
Absolute structure parameter	-0.004(13)
Largest diff. peak and hole	0.932 and -0.718 e.A^-3

Table 2. Atomic coordinates (x 10^4) and equivalent isotropic displacement parameters (A^2 x 10^3) for rory3.
U(eq) is defined as one third of the trace of the orthogonalized Uij tensor.

	x	y	z	U(eq)
I(1)	3574(1)	15120(1)	2086(1)	28(1)
Br(1)	4241(1)	16985(1)	1799(1)	37(1)
S(1)	5177(3)	11981(2)	517(1)	32(1)
S(3)	4338(3)	13090(2)	1402(1)	30(1)
S(5)	2996(3)	13334(2)	2398(1)	34(1)
S(2)	4932(3)	9909(2)	1268(1)	34(1)
S(4)	3819(3)	11378(2)	1990(1)	31(1)
N(1)	11197(9)	12375(6)	694(3)	40(2)
C(1)	4756(9)	11955(6)	1130(3)	25(2)
C(2)	4505(9)	11152(6)	1410(3)	23(2)
C(3)	3713(10)	12639(6)	1944(3)	26(2)
C(4)	7177(10)	12458(7)	514(4)	33(3)
C(5)	8335(10)	11691(6)	688(4)	34(2)
C(6)	9965(12)	12084(7)	687(3)	33(3)
C(7)	2967(9)	9470(6)	1115(3)	31(2)
C(8)	2464(11)	9849(7)	618(4)	36(3)
N(2)	-416(10)	9333(6)	414(3)	46(2)
N(2')	10212(10)	2013(6)	5389(3)	46(2)
I(1')	6445(1)	7909(1)	7087(1)	28(1)
Br(1')	5771(1)	9756(1)	6768(1)	38(1)
S(1')	4913(3)	4675(2)	5561(1)	34(1)
S(2')	5097(3)	2658(2)	6356(1)	34(1)
S(3')	5713(3)	5846(2)	6434(1)	29(1)
S(4')	6211(3)	4180(2)	7048(1)	31(1)
S(5')	7010(3)	6159(2)	7429(1)	35(1)
C(6')	136(13)	4762(8)	5708(3)	44(3)
C(9')	8994(12)	2274(7)	5519(3)	30(3)
C(1')	5313(9)	4687(7)	6191(3)	26(2)
C(2')	5521(9)	3906(6)	6471(3)	21(2)
C(3')	6335(9)	5446(5)	6988(3)	23(2)
C(4')	2902(10)	5109(8)	5536(4)	33(3)
C(5')	1760(10)	4356(7)	5688(3)	34(3)
N(1')	-1082(10)	5085(6)	5736(3)	46(3)
C(7')	7003(9)	2228(6)	6159(3)	24(2)
C(8')	7484(10)	2650(7)	5674(3)	34(3)
C(9)	841(12)	9541(7)	508(3)	29(3)

Table 3. Selected bond lengths [A] and angles [deg] for rory3.

Symmetry transformations used to generate equivalent atoms:

Table 4. Bond lengths [A] and angles [deg] for rory3.

I(1)-S(5)	2.611(2)
I(1)-Br(1)	2.7044(11)
S(1)-C(1)	1.740(9)
S(1)-C(4)	1.821(9)
S(3)-C(3)	1.708(8)
S(3)-C(1)	1.746(8)
S(5)-C(3)	1.685(8)
S(2)-C(2)	1.763(8)
S(2)-C(7)	1.825(8)
S(4)-C(3)	1.711(8)
S(4)-C(2)	1.740(9)
N(1)-C(6)	1.119(11)
C(1)-C(2)	1.351(10)
C(4)-C(5)	1.510(11)
C(5)-C(6)	1.486(13)
C(7)-C(8)	1.532(12)
C(8)-C(9)	1.474(13)
N(2)-C(9)	1.136(10)
N(2')-C(9')	1.153(11)
I(1')-S(5')	2.594(2)
I(1')-Br(1')	2.7100(11)
S(1')-C(1')	1.781(8)
S(1')-C(4')	1.810(9)
S(2')-C(2')	1.754(8)
S(2')-C(7')	1.808(8)
S(3')-C(3')	1.716(8)
S(3')-C(1')	1.739(9)
S(4')-C(3')	1.722(7)
S(4')-C(2')	1.746(8)
S(5')-C(3')	1.661(8)
C(6')-N(1')	1.128(12)
C(6')-C(5')	1.487(14)
C(9')-C(8')	1.447(13)
C(1')-C(2')	1.322(10)
C(4')-C(5')	1.469(11)
C(7')-C(8')	1.517(11)

S(5)-I(1)-Br(1)	177.56(6)
C(1)-S(1)-C(4)	101.8(4)
C(3)-S(3)-C(1)	97.6(4)
C(3)-S(5)-I(1)	101.5(3)
C(2)-S(2)-C(7)	99.9(4)
C(3)-S(4)-C(2)	97.1(4)
C(2)-C(1)-S(1)	127.6(7)
C(2)-C(1)-S(3)	115.1(6)
S(1)-C(1)-S(3)	116.6(5)
C(1)-C(2)-S(4)	116.4(6)
C(1)-C(2)-S(2)	127.2(7)
S(4)-C(2)-S(2)	116.3(5)
S(5)-C(3)-S(3)	124.9(5)
S(5)-C(3)-S(4)	121.2(5)
S(3)-C(3)-S(4)	113.8(5)
C(5)-C(4)-S(1)	111.4(6)
C(6)-C(5)-C(4)	111.3(8)
N(1)-C(6)-C(5)	178.8(12)
C(8)-C(7)-S(2)	111.0(6)
C(9)-C(8)-C(7)	110.8(8)
S(5')-I(1')-Br(1')	177.23(6)
C(1')-S(1')-C(4')	102.4(4)
C(2')-S(2')-C(7')	100.3(4)
C(3')-S(3')-C(1')	97.1(4)
C(3')-S(4')-C(2')	98.2(4)
C(3')-S(5')-I(1')	101.2(3)
N(1')-C(6')-C(5')	177.8(12)
N(2')-C(9')-C(8')	177.2(11)
C(2')-C(1')-S(3')	117.7(6)
C(2')-C(1')-S(1')	126.5(7)
S(3')-C(1')-S(1')	115.3(5)
C(1')-C(2')-S(4')	114.6(6)
C(1')-C(2')-S(2')	129.3(7)
S(4')-C(2')-S(2')	116.0(5)
S(5')-C(3')-S(3')	125.9(5)
S(5')-C(3')-S(4')	121.7(5)
S(3')-C(3')-S(4')	112.4(4)
C(5')-C(4')-S(1')	112.9(7)

C(4')-C(5')-C(6')	111.7(8)
C(8')-C(7')-S(2')	113.0(6)
C(9')-C(8')-C(7')	111.8(8)
N(2)-C(9)-C(8)	177.6(11)

Symmetry transformations used to generate equivalent atoms:

Table 5. Anisotropic displacement parameters (A^2 x 10^3) for rory3.
The anisotropic displacement factor exponent takes the form:
-2 pi^2 [h^2 a*^2 U11 + ... + 2 h k a* b* U12]

	U11	U22	U33	U23	U13	U12
I(1)	27(1)	27(1)	30(1)	-2(1)	1(1)	1(1)
Br(1)	42(1)	31(1)	38(1)	2(1)	4(1)	-5(1)
S(1)	24(1)	49(2)	24(1)	-1(1)	-2(1)	-6(1)
S(3)	32(1)	28(2)	28(1)	5(1)	1(1)	-2(1)
S(5)	42(2)	26(1)	33(2)	-1(1)	9(1)	2(1)
S(2)	23(1)	33(2)	47(2)	-4(1)	0(1)	-1(1)
S(4)	30(1)	31(1)	33(1)	3(1)	2(1)	0(1)
N(1)	23(5)	52(6)	45(5)	-5(5)	-2(5)	0(5)
C(1)	21(5)	27(5)	26(5)	-11(5)	-3(4)	-5(4)
C(2)	15(5)	24(5)	30(5)	1(5)	-9(4)	-1(4)
C(3)	14(5)	32(5)	31(5)	8(5)	-14(5)	-1(5)
C(4)	32(6)	30(7)	37(7)	15(6)	10(5)	-4(5)
C(5)	27(6)	38(6)	36(6)	-8(6)	-19(5)	3(5)
C(6)	29(6)	40(6)	31(6)	-13(5)	-14(5)	-1(5)
C(7)	22(5)	30(6)	40(6)	-18(5)	2(5)	-7(4)
C(8)	33(6)	24(6)	50(7)	9(5)	8(5)	7(5)
N(2)	44(6)	50(6)	43(5)	-3(5)	-2(5)	-14(5)
N(2')	46(6)	46(6)	46(6)	-7(5)	8(5)	16(5)
I(1')	28(1)	26(1)	31(1)	-1(1)	0(1)	-1(1)
Br(1')	45(1)	30(1)	39(1)	5(1)	-5(1)	4(1)
S(1')	24(1)	54(2)	24(1)	-6(1)	0(1)	10(1)
S(2')	24(1)	34(2)	43(2)	-5(1)	0(1)	-8(1)
S(3')	30(1)	31(2)	27(1)	2(1)	-2(1)	1(1)
S(4')	36(1)	23(1)	34(1)	0(1)	-2(1)	-1(1)
S(5')	48(2)	26(1)	33(2)	-1(1)	-6(1)	-4(1)
C(6')	46(8)	64(8)	23(6)	-5(6)	0(6)	-16(7)
C(9')	42(7)	22(6)	26(6)	1(5)	6(5)	5(5)
C(1')	13(5)	39(6)	26(5)	2(5)	-4(4)	7(4)
C(2')	13(5)	29(5)	21(5)	-5(5)	5(4)	-5(4)
C(3')	18(4)	22(5)	28(5)	-12(4)	-4(5)	3(4)
C(4')	16(6)	48(7)	35(6)	-3(6)	-1(5)	-4(5)
C(5')	33(7)	37(6)	31(6)	-6(6)	-18(5)	14(5)
N(1')	27(6)	40(5)	71(6)	-27(5)	-6(5)	2(4)
C(7')	20(5)	24(5)	28(6)	-1(5)	-1(4)	4(4)
C(8')	32(6)	37(7)	33(6)	-5(5)	3(5)	17(5)
C(9)	33(7)	26(6)	28(6)	-4(5)	5(5)	10(5)

8.2.4 1:1 adduct of ethane bridge ligand with diiodine, compound [82]

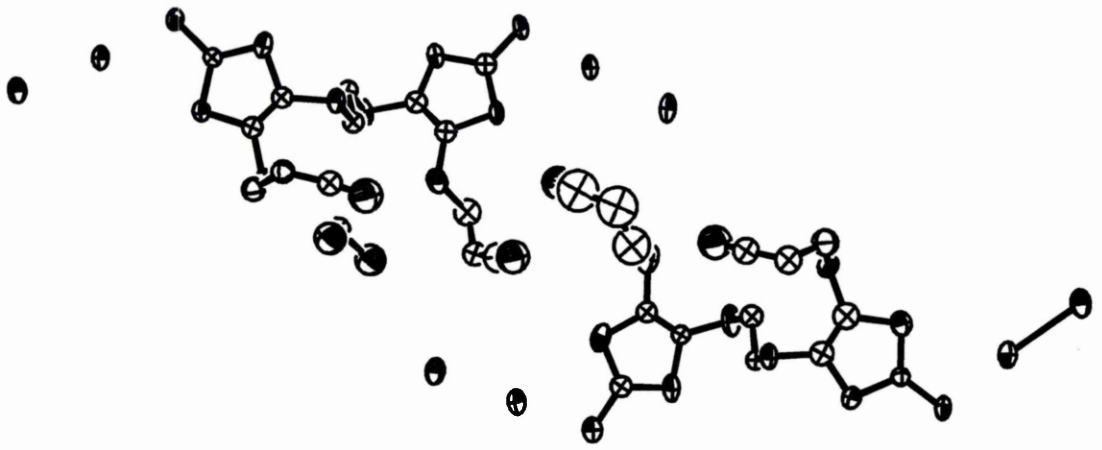

Table 1. Crystal data and structure refinement for roryi2.

Identification code	s92	
Empirical formula	C29 H26 Cl2 I8 N4 S20	
Formula weight	2157.84	
Temperature	150(2) K	
Wavelength	0.71073 Å	
Crystal system	Monoclinic	
Space group	P2(1)/c	
Unit cell dimensions	a = 29.9725(11) Å	a= 90°.
	b = 14.7887(5) Å	b=
95.0010(12)°.		
	c = 13.6400(4) Å	g = 90°.
Volume	6023.0(3) $Å^3$	
Z	4	
Density (calculated)	2.380 Mg/m^3	
Absorption coefficient	4.932 mm^{-1}	
F(000)	4024	
Crystal size	0.10 x 0.10 x 0.02 mm^3	
Theta range for data collection	2.98 to 23.26°.	
Index ranges	-33<=h<=33, -16<=k<=16, -15<=l<=15	
Reflections collected	40567	
Independent reflections	8382 [R(int) = 0.0789]	
Completeness to theta = 23.26°	96.8 %	
Absorption correction	Multiscan	
Max. and min. transmission	0.9078 and 0.6383	
Refinement method	Full-matrix least-squares on F^2	
Data / restraints / parameters	8382 / 285 / 545	
Goodness-of-fit on F^2	2.292	
Final R indices [I>2sigma(I)]	R1 = 0.1168, wR2 = 0.3427	
R indices (all data)	R1 = 0.1450, wR2 = 0.3489	
Extinction coefficient	0.0021(2)	
Largest diff. peak and hole	3.339 and -2.247 $e.Å^{-3}$	

Table 2. Atomic coordinates (x 10^4) and equivalent isotropic displacement parameters ($Å^2$x 10^3) for roryi2. U(eq) is defined as one third of the trace of the orthogonalized U^{ij} tensor.

	x	y	z	U(eq)
I(1)	3883(1)	3767(1)	20277(2)	55(1)
I(2)	4355(1)	3720(1)	18556(1)	47(1)
I(3)	4437(1)	6226(1)	6972(2)	47(1)
I(4)	4024(1)	6261(1)	4997(2)	52(1)
C(1)	4480(7)	3624(16)	16027(15)	34(6)
C(2)	4161(8)	3721(17)	14194(17)	55(8)
C(3)	3787(8)	3802(19)	14764(19)	68(10)
C(4)	4188(7)	4890(12)	12681(17)	36(6)
C(5)	3720(8)	5343(14)	12612(19)	50(8)
C(6)	2980(9)	2951(17)	14210(20)	69(9)
C(7)	3126(10)	2470(18)	13323(19)	73(9)
C(8)	2992(10)	2890(20)	12350(20)	67(9)
C(9)	2198(17)	5450(30)	8440(40)	180(20)
C(10)	2408(14)	4980(30)	9380(30)	170(20)
C(11)	2840(12)	5210(20)	9730(30)	142(18)
C(12)	3582(7)	6303(16)	10124(16)	44(7)
C(13)	3865(7)	6348(15)	10953(15)	35(6)
C(14)	4369(7)	6308(17)	9508(16)	47(8)
N(1)	2877(11)	3220(20)	11640(20)	109(6)
N(2)	2092(13)	6160(20)	7970(30)	109(6)
S(1)	4850(2)	3527(5)	17021(5)	47(2)
S(2)	4656(2)	3565(5)	14878(5)	46(2)
S(3)	3919(2)	3783(4)	16055(6)	48(2)
S(4)	4141(3)	3677(4)	12935(5)	43(2)
S(5)	3235(2)	4067(5)	14360(6)	51(2)
S(6)	3760(3)	6488(5)	12171(6)	62(2)
S(7)	2995(3)	6356(6)	10152(7)	72(3)
S(8)	4436(3)	6378(5)	10728(5)	54(2)
S(9)	3816(3)	6231(4)	9007(6)	54(2)
S(10)	4815(3)	6269(5)	8816(5)	52(2)
I(5)	1387(1)	6137(1)	10619(1)	56(1)
I(6)	869(1)	6239(1)	8747(1)	39(1)
I(7)	342(1)	3823(1)	-2823(1)	39(1)
I(8)	608(1)	3870(1)	-4792(1)	44(1)
C(15)	733(7)	6392(18)	6213(16)	46(7)
C(16)	1074(8)	6286(16)	4534(17)	47(8)
C(17)	1426(8)	6054(16)	5257(18)	46(7)
C(18)	897(7)	5244(12)	2930(17)	38(6)
C(19)	1256(7)	4483(13)	3093(18)	42(7)
C(20)	2324(8)	6435(18)	5770(20)	75(10)
C(21)	2781(8)	6031(17)	5950(20)	58(9)
C(22)	2841(12)	5200(20)	6540(30)	91(12)
C(23)	1898(9)	1872(19)	2670(20)	55(8)
C(24)	1738(9)	1640(18)	1597(19)	50(7)
C(25)	1889(9)	2226(16)	882(19)	53(8)
C(26)	1227(7)	3504(17)	763(16)	41(7)
C(27)	937(7)	3522(17)	1464(15)	41(7)
C(28)	447(7)	3732(15)	-177(15)	33(6)
N(3)	2845(11)	4500(20)	6890(20)	109(6)
N(4)	2062(11)	2070(20)	3490(20)	109(6)
S(11)	364(2)	6541(5)	7064(5)	42(2)
S(12)	587(2)	6579(5)	4997(5)	40(2)
S(13)	1274(2)	6048(5)	6479(5)	43(2)
S(14)	1128(3)	6361(4)	3292(5)	44(2)
S(15)	1956(2)	5655(5)	5055(5)	55(2)
S(16)	1027(2)	3393(4)	2741(5)	39(2)
S(17)	1809(2)	3454(5)	1029(5)	46(2)
S(18)	368(2)	3638(5)	1018(5)	47(2)
S(19)	1004(2)	3619(5)	-439(5)	40(2)
S(20)	10(2)	3798(5)	-1064(5)	48(2)
Cl(1)	2470(4)	5278(7)	2497(8)	100(2)
Cl(2)	2745(4)	6969(7)	3401(8)	100(2)
C(29)	2381(11)	6308(19)	2640(30)	62(9)

Table 3. Selected bond lengths [Å] and angles [°] for roryi2.

Symmetry transformations used to generate equivalent atoms:

Table 4. Bond lengths [Å] and angles [°] for roryi2.

I(1)-I(2)	2.845(3)
I(2)-S(1)	2.685(7)
I(3)-S(10)	2.667(8)
I(3)-I(4)	2.865(3)
C(1)-S(1)	1.68(2)
C(1)-S(2)	1.70(2)
C(1)-S(3)	1.70(2)
C(2)-C(3)	1.42(3)
C(2)-S(2)	1.70(2)
C(2)-S(4)	1.71(2)
C(3)-S(5)	1.74(2)
C(3)-S(3)	1.77(3)
C(4)-C(5)	1.55(3)
C(4)-S(4)	1.835(18)
C(5)-S(6)	1.80(2)
C(6)-C(7)	1.50(3)
C(6)-S(5)	1.82(2)
C(7)-C(8)	1.48(3)
C(8)-N(1)	1.12(3)
C(9)-N(2)	1.26(4)
C(9)-C(10)	1.53(4)
C(10)-C(11)	1.38(3)
C(11)-S(7)	1.83(3)
C(12)-C(13)	1.36(3)
C(12)-S(9)	1.74(2)
C(12)-S(7)	1.76(2)
C(13)-S(6)	1.73(2)
C(13)-S(8)	1.76(2)
C(14)-S(8)	1.66(2)
C(14)-S(10)	1.71(2)
C(14)-S(9)	1.74(2)
I(5)-I(6)	2.875(3)
I(6)-S(11)	2.674(7)
I(7)-S(20)	2.676(7)
I(7)-I(8)	2.868(3)
C(15)-S(11)	1.69(2)
C(15)-S(12)	1.70(2)
C(15)-S(13)	1.71(2)
C(16)-C(17)	1.42(3)
C(16)-S(12)	1.70(2)
C(16)-S(14)	1.72(2)
C(17)-S(15)	1.74(2)
C(17)-S(13)	1.76(2)
C(18)-C(19)	1.56(3)
C(18)-S(14)	1.842(18)
C(19)-S(16)	1.80(2)
C(20)-C(21)	1.49(3)
C(20)-S(15)	1.82(2)
C(21)-C(22)	1.47(3)
C(22)-N(3)	1.13(3)
C(23)-N(4)	1.22(3)
C(23)-C(24)	1.53(3)
C(24)-C(25)	1.41(3)
C(25)-S(17)	1.84(2)
C(26)-C(27)	1.35(3)
C(26)-S(19)	1.72(2)
C(26)-S(17)	1.75(2)
C(27)-S(16)	1.75(2)
C(27)-S(18)	1.77(2)
C(28)-S(18)	1.67(2)
C(28)-S(20)	1.71(2)
C(28)-S(19)	1.75(2)
Cl(1)-C(29)	1.56(3)
Cl(2)-C(29)	1.74(3)
S(1)-I(2)-I(1)	173.90(18)
S(10)-I(3)-I(4)	177.55(16)
S(1)-C(1)-S(2)	120.3(12)

S(1)-C(1)-S(3)	125.3(13)
S(2)-C(1)-S(3)	114.5(12)
C(3)-C(2)-S(2)	113.7(18)
C(3)-C(2)-S(4)	126.2(19)
S(2)-C(2)-S(4)	119.8(14)
C(2)-C(3)-S(5)	128(2)
C(2)-C(3)-S(3)	115.1(18)
S(5)-C(3)-S(3)	116.2(14)
C(5)-C(4)-S(4)	110.4(14)
C(4)-C(5)-S(6)	109.8(14)
C(7)-C(6)-S(5)	111.6(18)
C(8)-C(7)-C(6)	117(2)
N(1)-C(8)-C(7)	177(4)
N(2)-C(9)-C(10)	150(5)
C(11)-C(10)-C(9)	119(3)
C(10)-C(11)-S(7)	123(3)
C(13)-C(12)-S(9)	117.6(16)
C(13)-C(12)-S(7)	122.3(17)
S(9)-C(12)-S(7)	120.1(13)
C(12)-C(13)-S(6)	130.8(17)
C(12)-C(13)-S(8)	113.8(16)
S(6)-C(13)-S(8)	115.1(12)
S(8)-C(14)-S(10)	121.6(13)
S(8)-C(14)-S(9)	115.3(12)
S(10)-C(14)-S(9)	123.1(13)
C(1)-S(1)-I(2)	104.5(8)
C(2)-S(2)-C(1)	100.0(11)
C(1)-S(3)-C(3)	96.6(11)
C(2)-S(4)-C(4)	99.0(11)
C(3)-S(5)-C(6)	102.1(13)
C(13)-S(6)-C(5)	103.3(11)
C(12)-S(7)-C(11)	100.3(13)
C(14)-S(8)-C(13)	97.8(10)
C(12)-S(9)-C(14)	95.4(10)
C(14)-S(10)-I(3)	103.5(8)
S(11)-I(6)-I(5)	173.07(17)
S(20)-I(7)-I(8)	174.30(17)
S(11)-C(15)-S(12)	121.4(13)
S(11)-C(15)-S(13)	124.1(13)
S(12)-C(15)-S(13)	114.5(12)
C(17)-C(16)-S(12)	114.5(18)
C(17)-C(16)-S(14)	124.9(18)
S(12)-C(16)-S(14)	120.5(14)
C(16)-C(17)-S(15)	127.2(19)
C(16)-C(17)-S(13)	114.8(17)
S(15)-C(17)-S(13)	117.5(14)
C(19)-C(18)-S(14)	111.8(14)
C(18)-C(19)-S(16)	111.5(14)
C(21)-C(20)-S(15)	109.8(18)
C(22)-C(21)-C(20)	119(2)
N(3)-C(22)-C(21)	171(4)
N(4)-C(23)-C(24)	175(3)
C(25)-C(24)-C(23)	115(2)
C(24)-C(25)-S(17)	118.6(18)
C(27)-C(26)-S(19)	116.9(16)
C(27)-C(26)-S(17)	123.1(17)
S(19)-C(26)-S(17)	119.8(12)
C(26)-C(27)-S(16)	130.6(17)
C(26)-C(27)-S(18)	114.9(16)
S(16)-C(27)-S(18)	114.4(11)
S(18)-C(28)-S(20)	122.1(12)
S(18)-C(28)-S(19)	114.2(12)
S(20)-C(28)-S(19)	123.3(12)
C(15)-S(11)-I(6)	102.3(8)
C(16)-S(12)-C(15)	99.4(11)
C(15)-S(13)-C(17)	96.7(11)
C(16)-S(14)-C(18)	98.1(11)
C(17)-S(15)-C(20)	102.6(12)
C(27)-S(16)-C(19)	100.9(11)
C(26)-S(17)-C(25)	98.9(11)
C(28)-S(18)-C(27)	97.4(10)
C(26)-S(19)-C(28)	96.5(10)
C(28)-S(20)-I(7)	108.3(8)

Cl(1)-C(29)-Cl(2)	121(2)

Symmetry transformations used to generate equivalent atoms:

Table 5. Anisotropic displacement parameters ($Å^2 x\ 10^3$)for roryi2. The anisotropic displacement factor exponent takes the form: $-2p^2[\ h^2a^{*2}U^{11} + ... + 2\ h\ k\ a^*\ b^*\ U^{12}\ ]$

	U^{11}	U^{22}	U^{33}	U^{23}	U^{13}	U^{12}
I(1)	83(2)	43(1)	39(1)	-4(1)	10(1)	2(1)
I(2)	70(1)	38(1)	34(1)	-1(1)	2(1)	-1(1)
I(3)	70(1)	38(1)	34(1)	1(1)	9(1)	-1(1)
I(4)	76(2)	39(1)	40(1)	-1(1)	-2(1)	-1(1)
C(1)	34(6)	33(6)	33(6)	0(2)	3(2)	-1(2)
C(2)	56(9)	55(9)	55(9)	0(2)	4(2)	0(2)
C(3)	68(10)	68(10)	68(10)	0(2)	5(2)	0(2)
C(4)	36(6)	36(7)	35(7)	0(2)	3(2)	0(2)
C(5)	50(8)	50(8)	50(8)	0(2)	4(2)	0(2)
C(6)	69(9)	69(9)	69(9)	1(2)	6(2)	0(2)
C(7)	73(10)	73(10)	73(10)	0(2)	7(2)	0(2)
C(8)	67(9)	67(9)	67(9)	0(2)	6(2)	0(2)
C(9)	180(20)	180(20)	180(20)	0(2)	16(3)	0(2)
C(10)	170(20)	170(20)	170(20)	0(2)	15(3)	0(2)
C(11)	142(18)	142(18)	142(18)	0(2)	12(3)	0(2)
C(12)	44(7)	44(7)	44(7)	0(2)	4(2)	0(2)
C(13)	35(7)	35(7)	35(7)	0(2)	3(2)	0(2)
C(14)	47(8)	47(8)	47(8)	0(2)	4(2)	0(2)
N(1)	109(6)	109(6)	109(6)	0(1)	9(1)	0(1)
N(2)	109(6)	109(6)	109(6)	0(1)	9(1)	0(1)
S(1)	59(5)	57(5)	24(4)	5(4)	-1(3)	0(4)
S(2)	47(4)	54(5)	37(5)	5(4)	-1(3)	2(4)
S(3)	61(5)	38(4)	45(5)	5(3)	8(4)	0(3)
S(4)	64(5)	38(4)	27(4)	-2(3)	3(3)	6(3)
S(5)	53(5)	56(5)	43(5)	2(4)	-3(4)	6(4)
S(6)	104(7)	48(5)	36(5)	7(4)	11(4)	6(5)
S(7)	96(7)	65(6)	51(6)	-9(4)	-8(5)	-1(5)
S(8)	83(6)	50(5)	28(4)	-1(4)	4(4)	8(4)
S(9)	79(6)	39(5)	41(5)	11(4)	-10(4)	-7(4)
S(10)	65(5)	52(5)	39(5)	-1(4)	5(4)	0(4)
I(5)	87(2)	50(1)	28(1)	3(1)	-3(1)	3(1)
I(6)	61(1)	33(1)	24(1)	0(1)	5(1)	4(1)
I(7)	56(1)	33(1)	26(1)	1(1)	1(1)	2(1)
I(8)	64(1)	39(1)	31(1)	5(1)	5(1)	2(1)
C(15)	47(8)	46(8)	46(8)	0(2)	4(2)	0(2)
C(16)	47(8)	47(8)	47(8)	0(2)	4(2)	0(2)
C(17)	46(8)	46(8)	46(8)	0(2)	4(2)	0(2)
C(18)	39(7)	38(7)	38(7)	0(2)	3(2)	0(2)
C(19)	42(7)	41(7)	42(7)	0(2)	3(2)	0(2)
C(20)	75(10)	75(10)	75(10)	0(2)	6(2)	0(2)
C(21)	58(9)	58(9)	58(9)	0(2)	5(2)	0(2)
C(22)	91(12)	92(12)	92(12)	0(2)	8(2)	0(2)
C(23)	55(8)	55(8)	55(8)	0(2)	5(2)	0(2)
C(24)	50(8)	50(8)	50(8)	0(2)	4(2)	-1(2)
C(25)	53(8)	53(8)	53(8)	-1(2)	5(2)	0(2)
C(26)	42(7)	41(7)	41(7)	0(2)	3(2)	0(2)
C(27)	41(7)	41(7)	41(7)	0(2)	4(2)	0(2)
C(28)	33(7)	33(7)	33(7)	0(2)	4(2)	0(2)
N(3)	109(6)	109(6)	109(6)	0(1)	9(1)	0(1)
N(4)	109(6)	109(6)	109(6)	0(1)	9(1)	0(1)
S(11)	62(5)	43(4)	23(4)	5(3)	12(3)	6(4)
S(12)	60(5)	32(4)	28(4)	0(3)	9(3)	1(3)
S(13)	56(5)	55(5)	19(4)	1(3)	4(3)	3(4)
S(14)	77(5)	32(4)	25(4)	4(3)	16(4)	0(4)
S(15)	62(5)	60(5)	45(5)	-21(4)	13(4)	3(4)
S(16)	57(5)	29(4)	29(4)	0(3)	1(3)	3(3)
S(17)	62(5)	45(4)	29(4)	-5(4)	-1(3)	0(4)
S(18)	60(5)	46(5)	32(4)	-3(3)	-6(4)	3(4)
S(19)	44(4)	47(4)	27(4)	1(3)	3(3)	-1(3)
S(20)	47(4)	70(6)	27(4)	7(4)	-1(3)	8(4)
Cl(1)	101(3)	101(3)	100(3)	-1(1)	12(1)	-2(1)
Cl(2)	101(3)	101(3)	100(3)	-1(1)	12(1)	-2(1)
C(29)	62(9)	62(9)	62(9)	0(2)	6(2)	0(2)

8.2.5 Diiodine adduct of 1,3-dithiole-2-thione-4,5-dicarboxylate, compound [83]

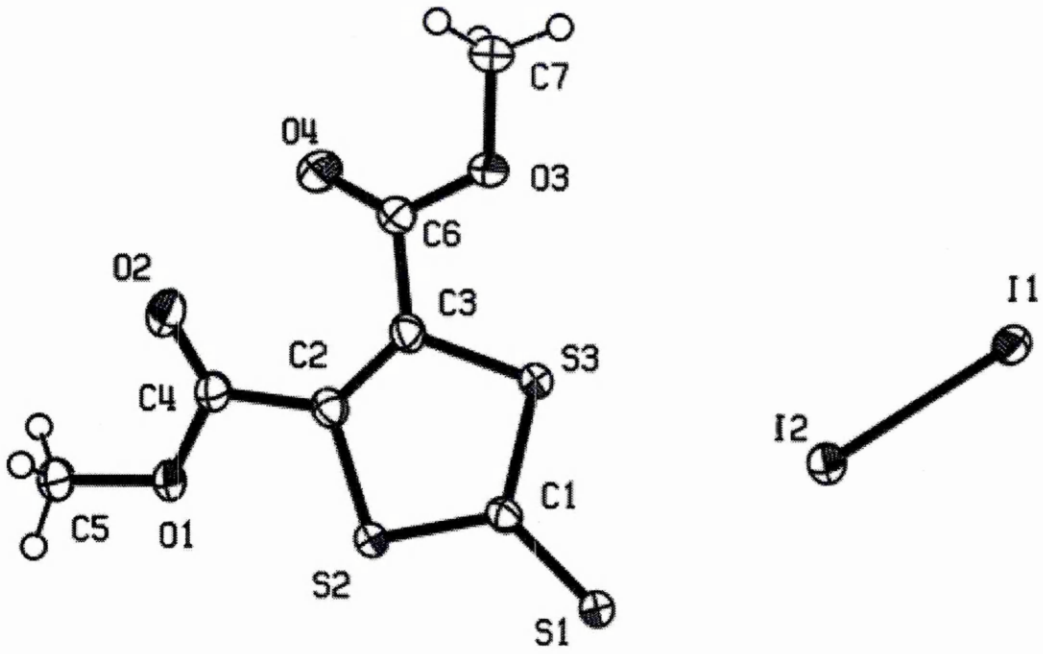

Table 1. Crystal data and structure refinement for sl1.

Identification code	s92	
Empirical formula	C7 H6 I2 O4 S3	
Formula weight	504.10	
Temperature	150(2) K	
Wavelength	0.71073 Å	
Crystal system	Monoclinic	
Space group	P2(1)/n	
Unit cell dimensions	a = 9.807(2) Å	a= 90°.
	b = 10.614(2) Å	b= 100.91(3)°.
	c = 13.293(3) Å	g = 90°.
Volume	1358.8(5) $Å^3$	
Z	4	
Density (calculated)	2.464 Mg/m^3	
Absorption coefficient	5.084 mm^{-1}	
F(000)	936	
Crystal size	0.2 x 0.075 x 0.075 mm^3	
Theta range for data collection	3.06 to 27.50°.	
Index ranges	-12<=h<=12, -13<=k<=13, -15<=l<=17	
Reflections collected	11773	
Independent reflections	3093 [R(int) = 0.0573]	
Completeness to theta = 27.50°	99.2 %	
Absorption correction	Semi-empirical from equivalents	
Max. and min. transmission	0.763 and 0.473	
Refinement method	Full-matrix least-squares on F^2	
Data / restraints / parameters	3093 / 0 / 147	
Goodness-of-fit on F^2	0.755	
Final R indices [I>2sigma(I)]	R1 = 0.0353, wR2 = 0.0913	
R indices (all data)	R1 = 0.0490, wR2 = 0.1055	
Largest diff. peak and hole	1.239 and -1.895 $e.Å^{-3}$	

Table 2. Atomic coordinates (x 10^4) and equivalent isotropic displacement parameters ($Å^2$x 10^3) for sl1. U(eq) is defined as one third of the trace of the orthogonalized U^{ij} tensor.

	x	y	z	U(eq)
I(1)	4159(1)	2176(1)	8327(1)	25(1)
I(2)	5830(1)	2725(1)	6902(1)	27(1)
S(1)	7503(1)	3432(1)	4863(1)	29(1)
S(2)	8410(1)	5902(1)	4133(1)	24(1)
S(3)	6633(1)	5869(1)	5628(1)	24(1)
O(1)	9557(3)	8121(3)	3658(3)	32(1)
O(2)	8000(4)	9511(3)	3983(3)	54(1)
O(3)	5552(3)	8057(3)	6220(3)	30(1)
O(4)	6937(4)	9515(3)	5740(3)	49(1)
C(1)	7524(3)	5001(4)	4862(3)	22(1)
C(2)	7938(4)	7370(4)	4543(3)	23(1)
C(3)	7098(5)	7352(4)	5249(3)	23(1)
C(4)	8503(4)	8484(4)	4066(3)	26(1)
C(5)	10199(5)	9088(4)	3130(4)	38(1)
C(6)	6532(4)	8458(4)	5745(3)	25(1)
C(7)	4900(5)	9013(5)	6756(4)	38(1)

Table 3. Selected bond lengths [Å] and angles [°] for sl1.

Symmetry transformations used to generate equivalent atoms:

Table 4. Bond lengths [Å] and angles [°] for sl1.

I(1)-I(2)	2.7899(8)
S(1)-C(1)	1.666(5)
S(2)-C(1)	1.712(4)
S(2)-C(2)	1.742(4)
S(3)-C(1)	1.728(4)
S(3)-C(3)	1.741(4)
O(1)-C(4)	1.313(5)
O(1)-C(5)	1.453(5)
O(2)-C(4)	1.193(5)
O(3)-C(6)	1.316(5)
O(3)-C(7)	1.455(5)
O(4)-C(6)	1.191(5)
C(2)-C(3)	1.361(7)
C(2)-C(4)	1.496(6)
C(3)-C(6)	1.503(6)
C(1)-S(2)-C(2)	97.5(2)
C(1)-S(3)-C(3)	97.0(2)
C(4)-O(1)-C(5)	116.0(4)
C(6)-O(3)-C(7)	116.0(4)
S(1)-C(1)-S(2)	124.5(2)
S(1)-C(1)-S(3)	121.7(2)
S(2)-C(1)-S(3)	113.8(3)
C(3)-C(2)-C(4)	128.6(4)
C(3)-C(2)-S(2)	115.7(3)
C(4)-C(2)-S(2)	115.7(3)
C(2)-C(3)-C(6)	127.9(3)
C(2)-C(3)-S(3)	116.0(3)
C(6)-C(3)-S(3)	116.1(3)
O(2)-C(4)-O(1)	125.0(4)
O(2)-C(4)-C(2)	125.6(4)
O(1)-C(4)-C(2)	109.0(4)
O(4)-C(6)-O(3)	125.6(4)
O(4)-C(6)-C(3)	125.6(4)
O(3)-C(6)-C(3)	108.8(4)

Symmetry transformations used to generate equivalent atoms:

Table 5. Anisotropic displacement parameters ($Å^2 x\ 10^3$)for sl1. The anisotropic displacement factor exponent takes the form: $-2p^2[\ h^2a^{*2}U^{11} + ... + 2\ h\ k\ a^*\ b^*\ U^{12}\ ]$

	U^{11}	U^{22}	U^{33}	U^{23}	U^{13}	U^{12}
I(1)	27(1)	21(1)	27(1)	1(1)	5(1)	0(1)
I(2)	26(1)	26(1)	29(1)	2(1)	8(1)	-1(1)
S(1)	39(1)	20(1)	35(1)	0(1)	22(1)	-2(1)
S(2)	28(1)	20(1)	26(1)	0(1)	14(1)	-1(1)
S(3)	28(1)	20(1)	26(1)	0(1)	13(1)	-1(1)
O(1)	37(2)	23(2)	43(2)	6(1)	24(2)	-1(1)
O(2)	63(2)	28(2)	83(3)	19(2)	47(2)	12(2)
O(3)	34(2)	22(2)	40(2)	-3(1)	20(2)	1(1)
O(4)	63(2)	23(2)	69(3)	-10(2)	39(2)	-7(2)
C(1)	26(2)	23(2)	18(2)	-2(2)	7(2)	-2(1)
C(2)	20(2)	26(2)	23(2)	2(2)	5(2)	1(2)
C(3)	20(2)	24(2)	25(2)	1(2)	6(2)	-2(2)
C(4)	25(2)	22(2)	34(2)	3(2)	12(2)	-1(2)
C(5)	40(3)	25(2)	58(3)	2(2)	31(2)	-5(2)
C(6)	23(2)	24(2)	27(2)	0(2)	7(2)	0(2)
C(7)	44(3)	27(2)	49(3)	0(2)	26(2)	7(2)

8.2.6 IBr adduct of Dimethyl 1,3-dithiole-2-thione-4,5-dicarboxylate, compound [84]

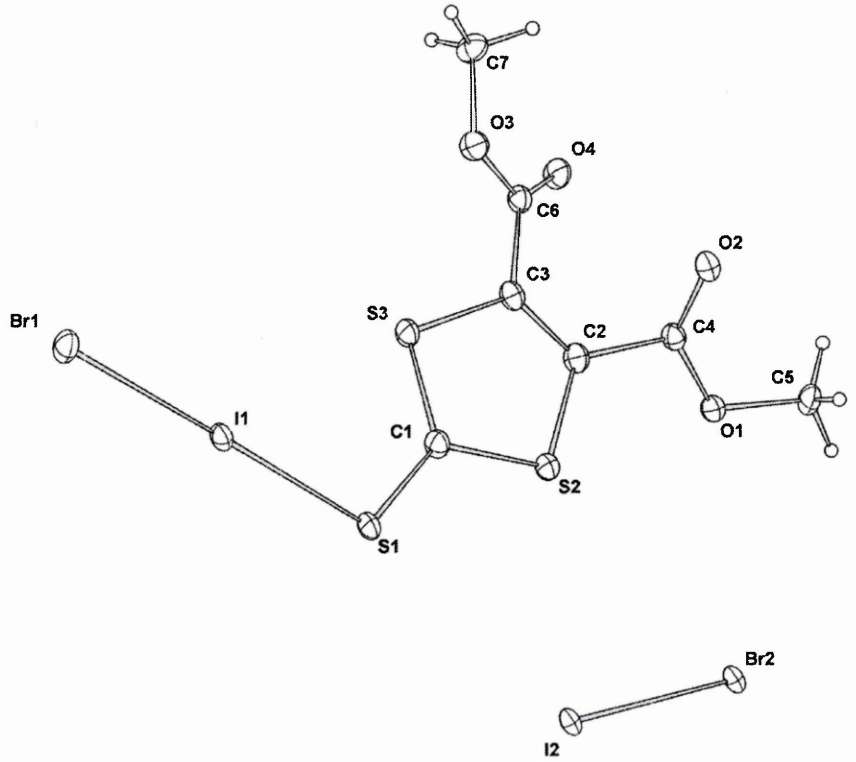

Table 1. Crystal data and structure refinement for sl2.

Identification code	s92	
Empirical formula	C7 H6 Br1.50 I1.50 O4 S3	
Formula weight	560.51	
Temperature	150(2) K	
Wavelength	0.71073 Å	
Crystal system	Triclinic	
Space group	$P^{-}1$(no.2)	
Unit cell dimensions	a = 5.8163(3) Å	a= 77.310(2)°.
	b = 8.7676(4) Å	b= 83.073(2)°.
	c = 14.8481(9) Å	g = 84.686(2)°.
Volume	731.58(7) $Å^3$	
Z	2	
Density (calculated)	2.545 Mg/m^3	
Absorption coefficient	7.765 mm^{-1}	
F(000)	520	
Crystal size	0.20 x 0.20 x 0.20 mm^3	
Theta range for data collection	3.02 to 25.03°.	
Index ranges	-6<=h<=6, -10<=k<=10, -16<=l<=17	
Reflections collected	5844	
Independent reflections	2518 [R(int) = 0.0645]	
Completeness to theta = 25.03°	97.8 %	
Absorption correction	Multiscan, SORTAV	
Max. and min. transmission	0.3057 and 0.3057	
Refinement method	Full-matrix least-squares on F^2	
Data / restraints / parameters	2518 / 0 / 158	
Goodness-of-fit on F^2	1.074	
Final R indices [I>2sigma(I)]	R1 = 0.0535, wR2 = 0.1539	
R indices (all data)	R1 = 0.0567, wR2 = 0.1574	
Extinction coefficient	0.0073(13)	
Largest diff. peak and hole	3.535 and -1.847 e.$Å^{-3}$	

Table 2. Atomic coordinates (x 10^4) and equivalent isotropic displacement parameters ($Å^2$x 10^3) for sl2. U(eq) is defined as one third of the trace of the orthogonalized U^{ij} tensor.

	x	y	z	U(eq)
I(1)	529(1)	9478(1)	6344(1)	25(1)
I(2)	-1706(1)	5761(1)	5477(1)	21(1)
Br(2)	-1706(1)	5761(1)	5477(1)	21(1)
Br(1)	4187(2)	7429(1)	6819(1)	35(1)
S(1)	-3073(4)	11366(3)	5893(2)	28(1)
S(2)	-6453(4)	13126(3)	6998(2)	27(1)
S(3)	-2792(4)	11157(3)	7924(2)	27(1)
C(1)	-4047(17)	11840(11)	6909(7)	26(2)
O(1)	-10001(11)	14513(8)	8166(5)	26(2)
O(2)	-7613(12)	14835(8)	9187(5)	32(2)
O(3)	-2212(12)	11806(8)	9745(5)	30(2)
C(4)	-8069(17)	14247(11)	8586(7)	24(2)
C(3)	-4727(17)	12201(11)	8592(7)	25(2)
C(2)	-6372(16)	13131(11)	8146(7)	26(2)
C(6)	-4476(16)	11889(11)	9608(7)	25(2)
O(4)	-6055(12)	11670(9)	10210(5)	31(2)
C(7)	-1746(17)	11398(13)	10738(8)	32(2)
C(5)	-11667(17)	15701(12)	8458(8)	30(2)

Table 3. Selected bond lengths [Å] and angles [°] for sl2.

I(1)-S(1)	2.605(2)
I(1)-Br(1)	2.7107(11)
I(2)-Br(2)#1	2.7173(13)
I(2)-I(2)#1	2.7173(13)
S(1)-C(1)	1.673(10)
S(2)-C(2)	1.712(10)
S(2)-C(1)	1.725(10)
S(3)-C(1)	1.718(10)
S(3)-C(3)	1.740(10)
O(1)-C(4)	1.327(12)
O(1)-C(5)	1.457(11)
O(2)-C(4)	1.190(12)
O(3)-C(6)	1.350(12)
O(3)-C(7)	1.491(13)
C(4)-C(2)	1.518(13)
C(3)-C(2)	1.337(14)
C(3)-C(6)	1.496(14)
C(6)-O(4)	1.200(12)
S(1)-I(1)-Br(1)	178.01(7)
Br(2)#1-I(2)-I(2)#1	0.00(3)
C(1)-S(1)-I(1)	101.2(4)
C(2)-S(2)-C(1)	95.9(5)
C(1)-S(3)-C(3)	95.8(5)
S(1)-C(1)-S(3)	124.8(6)
S(1)-C(1)-S(2)	120.6(6)
S(3)-C(1)-S(2)	114.6(5)
C(4)-O(1)-C(5)	115.3(8)
C(6)-O(3)-C(7)	114.7(7)
O(2)-C(4)-O(1)	126.8(9)
O(2)-C(4)-C(2)	122.9(9)
O(1)-C(4)-C(2)	110.1(8)
C(2)-C(3)-C(6)	126.9(9)
C(2)-C(3)-S(3)	116.0(8)
C(6)-C(3)-S(3)	116.9(7)
C(3)-C(2)-C(4)	123.7(9)
C(3)-C(2)-S(2)	117.6(8)
C(4)-C(2)-S(2)	118.5(7)
O(4)-C(6)-O(3)	125.2(9)
O(4)-C(6)-C(3)	124.7(9)
O(3)-C(6)-C(3)	110.1(8)

Symmetry transformations used to generate equivalent atoms:

Symmetry transformations used to generate equivalent atoms:
#1 -x,-y+1,-z+1

Table 5. Anisotropic displacement parameters ($Å^2 x\ 10^3$)for sl2. The anisotropic displacement factor exponent takes the form: $-2p^2[\ h^2a^{*2}U^{11} + ... + 2\ h\ k\ a^*\ b^*\ U^{12}\ ]$

	U^{11}	U^{22}	U^{33}	U^{23}	U^{13}	U^{12}
I(1)	26(1)	25(1)	22(1)	-9(1)	3(1)	1(1)
I(2)	25(1)	19(1)	19(1)	-8(1)	5(1)	-2(1)
Br(2)	25(1)	19(1)	19(1)	-8(1)	5(1)	-2(1)
Br(1)	29(1)	36(1)	34(1)	-5(1)	2(1)	9(1)
S(1)	31(1)	31(1)	22(1)	-11(1)	1(1)	8(1)
S(2)	29(1)	29(1)	23(1)	-8(1)	-2(1)	6(1)
S(3)	27(1)	30(1)	22(1)	-7(1)	3(1)	6(1)
C(1)	26(5)	27(5)	23(5)	-5(4)	2(4)	1(4)
O(1)	24(3)	29(4)	24(4)	-9(3)	-1(3)	2(3)
O(2)	31(4)	34(4)	32(4)	-14(3)	-2(3)	5(3)
O(3)	25(4)	36(4)	27(4)	-6(3)	2(3)	-1(3)
C(4)	28(5)	22(5)	21(5)	-4(4)	2(4)	0(4)
C(3)	24(5)	26(5)	26(5)	-9(4)	5(4)	-2(4)
C(2)	22(5)	27(5)	28(5)	-7(4)	3(4)	-2(4)
C(6)	21(5)	26(5)	28(5)	-9(4)	-1(4)	1(4)
O(4)	22(4)	41(4)	27(4)	-6(3)	4(3)	5(3)
C(7)	21(5)	42(6)	30(6)	-4(5)	-3(4)	-1(4)
C(5)	22(5)	30(5)	38(6)	-11(4)	-5(4)	8(4)

8.2.7 1,3-dithiole-2-thione-4-ferrocene adduct with diiodine, compound [85]

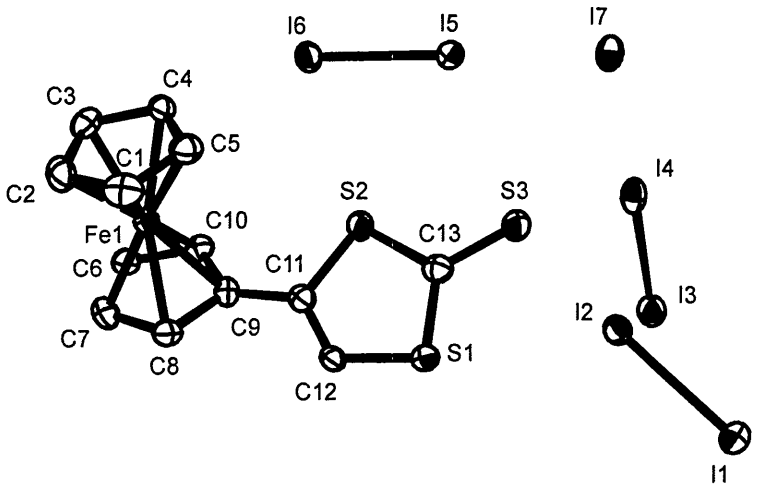

Table 1. Crystal data and structure refinement for fci5.

Identification code	s92	
Empirical formula	C13 H10 Fe I7 S3	
Formula weight	1206.54	
Temperature	150(2) K	
Wavelength	0.71073 Å	
Crystal system	Triclinic	
Space group	P-1	
Unit cell dimensions	a = 9.6074(19) Å	a= 94.50(3)°.
	b = 9.838(2) Å	b= 100.14(3)°.
	c = 14.600(3) Å	g = 112.38(3)°.
Volume	1239.9(4) $Å^3$	
Z	2	
Density (calculated)	3.232 Mg/m^3	
Absorption coefficient	9.574 mm^{-1}	
F(000)	1066	
Crystal size	0.17 x 0.13 x 0.02 mm^3	
Theta range for data collection	2.99 to 27.45°.	
Index ranges	-12<=h<=12, -12<=k<=12, -18<=l<=18	
Reflections collected	18434	
Independent reflections	5610 [R(int) = 0.0681]	
Completeness to theta = 27.45°	99.2 %	
Absorption correction	Semi-empirical from equivalents	
Max. and min. transmission	0.8316 and 0.2851	
Refinement method	Full-matrix least-squares on F^2	
Data / restraints / parameters	5610 / 0 / 217	
Goodness-of-fit on F^2	1.001	
Final R indices [I>2sigma(I)]	R1 = 0.0448, wR2 = 0.0982	
R indices (all data)	R1 = 0.0682, wR2 = 0.1085	
Largest diff. peak and hole	1.612 and -1.972 $e.Å^{-3}$	

Table 2. Atomic coordinates (x 10^4) and equivalent isotropic displacement parameters ($Å^2$x 10^3) for fci5. U(eq) is defined as one third of the trace of the orthogonalized U^{ij} tensor.

	x	y	z	U(eq)
I(1)	9337(1)	425(1)	-3949(1)	39(1)
I(2)	8888(1)	2110(1)	-2429(1)	27(1)
I(3)	4052(1)	2512(1)	-4405(1)	38(1)
I(4)	6438(1)	4934(1)	-3187(1)	33(1)
I(5)	7695(1)	7172(1)	-58(1)	25(1)
I(6)	6263(1)	6658(1)	1482(1)	31(1)
I(7)	9026(1)	7741(1)	-1810(1)	31(1)
Fe(1)	6965(1)	2656(1)	3282(1)	20(1)
S(1)	7657(2)	894(2)	-379(1)	26(1)
S(2)	7193(2)	3287(2)	622(1)	30(1)
S(3)	8482(3)	3844(2)	-1058(1)	36(1)
C(1)	9215(9)	3197(9)	4047(6)	36(2)
C(2)	8258(9)	3303(9)	4660(5)	35(2)
C(3)	7689(8)	4389(8)	4405(5)	29(2)
C(4)	8300(8)	4938(8)	3629(5)	24(2)
C(5)	9226(9)	4205(8)	3407(5)	31(2)
C(6)	4562(8)	1690(8)	2977(5)	24(2)
C(7)	5165(9)	608(8)	3207(5)	30(2)
C(8)	6043(9)	466(8)	2552(5)	29(2)
C(9)	5980(8)	1466(8)	1896(5)	23(2)
C(10)	5076(8)	2234(8)	2174(5)	24(2)
C(11)	6665(8)	1610(8)	1075(5)	23(2)
C(12)	6889(8)	538(7)	601(5)	21(2)
C(13)	7789(9)	2693(8)	-321(5)	27(2)

Table 3. Selected bond lengths [Å] and angles [°] for fci5.

Symmetry transformations used to generate equivalent atoms:

Table 4. Bond lengths [Å] and angles [°] for fci5.

I(1)-I(2)	2.8566(11)
I(2)-S(3)	2.705(2)
I(3)-I(4)	2.7988(17)
I(5)-I(6)	2.8183(10)
I(5)-I(7)	3.0541(10)
Fe(1)-C(7)	2.075(7)
Fe(1)-C(2)	2.077(7)
Fe(1)-C(6)	2.081(7)
Fe(1)-C(3)	2.082(7)
Fe(1)-C(4)	2.084(7)
Fe(1)-C(10)	2.090(7)
Fe(1)-C(5)	2.091(8)
Fe(1)-C(1)	2.094(7)
Fe(1)-C(8)	2.101(7)
Fe(1)-C(9)	2.115(7)
S(1)-C(13)	1.719(7)
S(1)-C(12)	1.722(7)
S(2)-C(13)	1.725(8)
S(2)-C(11)	1.751(7)
S(3)-C(13)	1.658(8)
C(1)-C(5)	1.413(11)
C(1)-C(2)	1.416(13)
C(2)-C(3)	1.419(11)
C(3)-C(4)	1.417(10)
C(4)-C(5)	1.404(11)
C(6)-C(10)	1.417(10)
C(6)-C(7)	1.428(10)
C(7)-C(8)	1.413(11)
C(8)-C(9)	1.436(10)
C(9)-C(10)	1.437(11)
C(9)-C(11)	1.457(10)
C(11)-C(12)	1.323(10)
S(3)-I(2)-I(1)	176.33(4)
I(6)-I(5)-I(7)	175.65(2)

C(7)-Fe(1)-C(2)	107.8(3)
C(7)-Fe(1)-C(6)	40.2(3)
C(2)-Fe(1)-C(6)	121.7(3)
C(7)-Fe(1)-C(3)	123.3(3)
C(2)-Fe(1)-C(3)	39.9(3)
C(6)-Fe(1)-C(3)	107.5(3)
C(7)-Fe(1)-C(4)	159.7(3)
C(2)-Fe(1)-C(4)	66.5(3)
C(6)-Fe(1)-C(4)	124.5(3)
C(3)-Fe(1)-C(4)	39.8(3)
C(7)-Fe(1)-C(10)	66.9(3)
C(2)-Fe(1)-C(10)	156.9(3)
C(6)-Fe(1)-C(10)	39.7(3)
C(3)-Fe(1)-C(10)	122.6(3)
C(4)-Fe(1)-C(10)	110.1(3)
C(7)-Fe(1)-C(5)	158.5(3)
C(2)-Fe(1)-C(5)	66.5(3)
C(6)-Fe(1)-C(5)	160.7(3)
C(3)-Fe(1)-C(5)	66.6(3)
C(4)-Fe(1)-C(5)	39.3(3)
C(10)-Fe(1)-C(5)	126.5(3)
C(7)-Fe(1)-C(1)	122.9(3)
C(2)-Fe(1)-C(1)	39.7(3)
C(6)-Fe(1)-C(1)	157.2(3)
C(3)-Fe(1)-C(1)	66.8(3)
C(4)-Fe(1)-C(1)	66.2(3)
C(10)-Fe(1)-C(1)	162.1(3)
C(5)-Fe(1)-C(1)	39.5(3)
C(7)-Fe(1)-C(8)	39.6(3)
C(2)-Fe(1)-C(8)	124.0(3)
C(6)-Fe(1)-C(8)	67.2(3)
C(3)-Fe(1)-C(8)	159.0(3)
C(4)-Fe(1)-C(8)	159.9(3)
C(10)-Fe(1)-C(8)	67.3(3)
C(5)-Fe(1)-C(8)	124.9(3)
C(1)-Fe(1)-C(8)	109.7(3)
C(7)-Fe(1)-C(9)	66.4(3)
C(2)-Fe(1)-C(9)	160.7(3)
C(6)-Fe(1)-C(9)	66.8(3)
C(3)-Fe(1)-C(9)	158.8(3)
C(4)-Fe(1)-C(9)	125.2(3)
C(10)-Fe(1)-C(9)	40.0(3)
C(5)-Fe(1)-C(9)	111.6(3)
C(1)-Fe(1)-C(9)	126.4(3)
C(8)-Fe(1)-C(9)	39.8(3)
C(13)-S(1)-C(12)	95.8(4)
C(13)-S(2)-C(11)	96.2(4)
C(13)-S(3)-I(2)	104.0(3)
C(5)-C(1)-C(2)	107.8(7)
C(5)-C(1)-Fe(1)	70.1(4)
C(2)-C(1)-Fe(1)	69.5(4)
C(1)-C(2)-C(3)	108.3(7)
C(1)-C(2)-Fe(1)	70.8(4)
C(3)-C(2)-Fe(1)	70.2(4)
C(4)-C(3)-C(2)	107.1(7)
C(4)-C(3)-Fe(1)	70.2(4)
C(2)-C(3)-Fe(1)	69.8(4)
C(5)-C(4)-C(3)	108.7(7)
C(5)-C(4)-Fe(1)	70.6(4)
C(3)-C(4)-Fe(1)	70.0(4)
C(4)-C(5)-C(1)	108.1(7)
C(4)-C(5)-Fe(1)	70.1(4)
C(1)-C(5)-Fe(1)	70.4(4)
C(10)-C(6)-C(7)	107.7(7)
C(10)-C(6)-Fe(1)	70.5(4)
C(7)-C(6)-Fe(1)	69.7(4)
C(8)-C(7)-C(6)	109.1(6)
C(8)-C(7)-Fe(1)	71.2(4)
C(6)-C(7)-Fe(1)	70.1(4)
C(7)-C(8)-C(9)	107.3(7)
C(7)-C(8)-Fe(1)	69.2(4)
C(9)-C(8)-Fe(1)	70.6(4)
C(8)-C(9)-C(10)	107.8(6)

C(8)-C(9)-C(11)	125.2(7)
C(10)-C(9)-C(11)	126.9(6)
C(8)-C(9)-Fe(1)	69.6(4)
C(10)-C(9)-Fe(1)	69.1(4)
C(11)-C(9)-Fe(1)	128.8(5)
C(6)-C(10)-C(9)	108.0(6)
C(6)-C(10)-Fe(1)	69.8(4)
C(9)-C(10)-Fe(1)	70.9(4)
C(12)-C(11)-C(9)	125.1(6)
C(12)-C(11)-S(2)	115.1(6)
C(9)-C(11)-S(2)	119.7(6)
C(11)-C(12)-S(1)	118.6(5)
S(3)-C(13)-S(1)	125.4(5)
S(3)-C(13)-S(2)	120.3(5)
S(1)-C(13)-S(2)	114.2(4)

Symmetry transformations used to generate equivalent atoms:

Table 5. Anisotropic displacement parameters ($Å^2 x\ 10^3$)for fci5. The anisotropic displacement factor exponent takes the form: $-2p^2[\ h^2a^{*2}U^{11} + ... + 2\ h\ k\ a^*\ b^*\ U^{12}\ ]$

	U^{11}	U^{22}	U^{33}	U^{23}	U^{13}	U^{12}
I(1)	55(1)	33(1)	32(1)	5(1)	18(1)	19(1)
I(2)	27(1)	26(1)	26(1)	6(1)	7(1)	8(1)
I(3)	46(1)	38(1)	36(1)	12(1)	14(1)	22(1)
I(4)	39(1)	47(1)	28(1)	15(1)	14(1)	28(1)
I(5)	26(1)	27(1)	24(1)	5(1)	4(1)	14(1)
I(6)	38(1)	31(1)	30(1)	10(1)	14(1)	18(1)
I(7)	27(1)	45(1)	25(1)	8(1)	7(1)	17(1)
Fe(1)	19(1)	23(1)	20(1)	5(1)	3(1)	9(1)
S(1)	29(1)	22(1)	27(1)	2(1)	9(1)	9(1)
S(2)	45(1)	29(1)	27(1)	10(1)	15(1)	22(1)
S(3)	56(1)	32(1)	31(1)	10(1)	18(1)	23(1)
C(1)	21(4)	36(5)	44(5)	2(4)	-5(4)	10(4)
C(2)	35(5)	38(4)	24(4)	9(3)	0(3)	9(4)
C(3)	25(4)	33(4)	24(4)	-3(3)	3(3)	10(4)
C(4)	25(4)	21(3)	21(4)	4(3)	3(3)	5(3)
C(5)	28(4)	27(4)	34(4)	2(3)	8(3)	9(3)
C(6)	21(4)	26(4)	30(4)	3(3)	9(3)	13(3)
C(7)	27(4)	31(4)	31(4)	11(3)	10(3)	8(4)
C(8)	33(4)	22(4)	28(4)	2(3)	5(3)	9(3)
C(9)	17(4)	28(4)	21(4)	5(3)	4(3)	8(3)
C(10)	22(4)	25(4)	23(4)	1(3)	-1(3)	10(3)
C(11)	22(4)	24(4)	20(4)	4(3)	0(3)	7(3)
C(12)	21(4)	18(3)	23(4)	5(3)	5(3)	5(3)
C(13)	27(4)	26(4)	27(4)	3(3)	2(3)	10(3)

9 REFERENCE SECTION

(1) Cassoux, P. *Coordination Chemistry Reviews* **1999**, *185-186*, 213-232.

(2) Interrante, L. V.; Hampden-Smith, M. J. *Chemistry of Advanced Materials*; Wiley-VCH: New York, 1998.

(3) Huheey, J. E.; Keiter, E. A.; Keiter, R. L. *Inorganic Chemistry, Principles of structure and reactivity*; 4 ed.; HarperCollins College Publishers: New York, 1993.

(4) Bruce, D. W.; O'Hare, D. *Inorganic Materials*; 2 ed.; John Wiley and Sons: Chichester, 1997.

(5) Gunn, M.; Porter, J. *New Scientist* **1988**, *118*, 58-63.

(6) Cox, T. *New Scientist* **1988**, *118*, 64-66.

(7) Jerome, D. *Science* **1991**, *252*, 1509-1514.

(8) Mori, H. *International Journal of Modern Physics B* **1994**, *8*, 1-45.

(9) Levy, L. P. *Magnetism and Superconductivity*; 1 st ed.; Springer: New York, 2000.

(10) Cotton, F. A.; Wilkinson, G. *Advanced Inorganic Chemistry*; 5 ed.; John Wiley and Sons: New York, 1988.

(11) Rao, C. N. R. *Journal of Materials Chemistry* **1999**, *9*, 1-14.

(12) Melby, L. R.; Harder, R. J.; Hertler, W. R.; Mahler, W.; Benson, R. E.; Mochel, W. E. *Journal of the American Chemical Society* **1962**, *84*, 3374-3387.

(13) Scott, B. A.; LaPlaca, S. J.; Torrancet, J. B.; Silverman, B. D.; Welber, B. *Annals of the New York Academy of Sciences* **1978**, *313*, 369-376.

(14) Bryce, M. R. *Chemical Society Reviews* **1991**, *20*, 355-390.

(15) Wudl, F.; Smith, G. M.; Hufnagel, E. J. *Chemical Communications* **1970**, 1453-1454.

(16) Miller, J. S. *Annals of the New York Academy of Sciences* **1978**, *313*, 25-59.

(17) Ferraris, J.; Cowan, D. O.; Walatka, V.; Perlstein, J. H. *Journal of the American Chemical Society* **1973**, *95*, 948-949.

(18) Kistenmacher, T. J.; Phillips, T. E.; Cowan, D. *Acta crystallographica B* **1974**, *30*, 763-768.

(19) Graja, A. *Condensed Matter news* **1994**, *3*, 14-26.

(20) Roncali, J. *Journal of Materials Chemistry* **1997**, *7*, 2307-2321.

(21) Meline, R. L.; Elsenbaumer, R. L. *Journal of the Chemical Society - Perkin Transactions 1* **1997**, *24*, 3575-3576.

(22) Bras, Y. L.; Salle, M.; Leriche, P.; Mingotaud, C.; Richomme, P.; Moller, J. *Journal of Materials Chemistry* **1997**, *7*, 2393-2396.

(23) Fourmigue, M.; Uzelmeier, C. E.; Boubekeur, K.; Bartley, S. L.; Dunbar, K. R. *Journal of Oraganometallic Chemistry* **1997**, *529*, 343-350.

(24) Fox, M. A.; Pan, H. L. *Journal of Organic Chemistry* **1994**, *59*, 6519-6527.

(25) Brisset, H.; Moustarder, S. L.; Blanchard, P.; Illien, B.; Riou, A.; Orduna, J.; Garin, J.; Roncali, J. *Journal of Materials Chemistry* **1997**, *7*, 2027-2032.

(26) Li, H. Q.; Tan, G. Z.; Song, Y. X.; Yu, X. D.; Yao, Z. Q. *Synthetic Metals* **1997**, *87*, 151-156.

(27) Underhill, A. E.; Hawkins, I.; Edge, S.; Wilkes, S. B.; Varma, K. S.; Kobayashi, A.; Kobayashi, H. *Synthetic Metals* **1993**, *56*, 1914-1919.

(28) Ramos, J.; Yartsev, V. M.; Golhen, S.; Ouahab, L.; Delhaes, P. *Journal of Materials Chemistry* **1997**, *7*, 1313-1319.

(29) Miguel, P. D.; Bryce, M. R.; Goldenberg, L. M.; Beeby, A.; Khodorkovsky, V.; Shapiro, L.; Niemz, A.; Cuello, A. O.; Rotello, V. *Journal of Materials Chemistry* **1998**, *8*, 71-76.

(30) McCullough, R. D.; Belot, J. A. *Chemistry of Materials* **1994**, *6*, 1396-1403.

(31) Simonsen, K. B.; Svenstrup, N.; Lau, J.; Simonsen, O.; Mork, P.; Kristensen, G. J.; Becher, J. *Synthesis* **1996**, 407-418.

(32) Martin, N.; Sanchez, L.; Seoane, C. *Journal of Organic Chemistry* **1998**, *63*, 1268-1279.

(33) Zhilyaeva, E. I.; Lyubovskaya, R. N.; Konovalikhin, S. V.; Dyachenko, O. N.; Lyubovski, R. B. *Synthetic Metals* **1998**, *94*, 35-40.

(34) Devonport, W.; Bryce, M. R.; Marshallsay, G. J.; Moore, A. J.; Goldenberg, L. M. *Journal of Materials Chemistry* **1998**, *8*, 1361-1372.

(35) Kini, A. M.; Parakka, J. P.; Geiser, U.; Wang, H.; Rivas, F.; DiNino, E.; Thomas, S.; Dudek, J. D.; Williams, J. M. *Journal of Materials Chemistry* **1999**, *9*, 883-892.

(36) Rezzonico, B.; Dubois, M. G. *Journal of Chemical Research* **1994**, 142-143.

(37) Meline, R. L.; Elsenbaumer, R. L. *Perkin Transactions 1* **1998**, 2467-2469.

(38) Moore, A. J.; Bryce, M. R. *Synthesis* **1997**, 407-409.

(39) Krief, A. *Tetrahedron* **1986**, *42*, 1209-1252.

(40) Bryce, M.; Skabara, P. J.; Moore, A.; Batsanov, A.; Howard, J.; Hoy, V. *Tetrahedron* **1997**, *53*, 17781-17794.

(41) McCullough, R.; Petruska, M.; Belot, J. *Tetrahedron* **1999**, *55*, 9979-9998.

(42) Kobayashi, H.; Sato, A.; Tanaka, H.; Kobayashi, A.; Cassoux, P. *Coordination Chemistry Reviews* **1999**, *190-192*, 921-932.

(43) Bryce, M. R. *Journal of Materials Chemistry* **1995**, *5*, 1481-1496.

(44) Bryce, M. R. *Journal of Materials Chemistry* **2000**, *10*, 589-598.

(45) Bryce, M. R. *Advanced Materials* **1999**, *11*, 11-23.

(46) Williams, J. M.; Schultz, A. J.; Geiser, U.; Carlson, K. D.; Kini, A. M.; Wang, H. H.; Kwok, W. K.; Whangbo, M. H.; Schirber, J. E. *Science* **1991**, *252*, 1501-1508.

(47) Murray, S. G.; Hartley, F. R. *Chemical Reviews* **1981**, *81*, 365-414.

(48) Torre, G. d.; Vazquez, P.; Agullo-Lopez, F.; Torres, T. *Journal of Materials Chemistry* **1998**, *8*, 1671-1683.

(49) Polat, M.; Gul, A. *Journal of Chemical Research* **1999**, 130-131.

(50) McKeown, N. B. *Journal of Materials Chemistry* **2000**, *10*, 1979-1997.

(51) Robertson, N.; Bergemann, C.; Becker, H.; Agarwal, P.; Julian, S. R.; Friend, R. H.; Hatton, N. J.; Underhill, A. E.; Kobayashi, A. *Journal of Materials Chemistry* **1999**, *9*, 1713-1717.

(52) Pullen, A. E.; Pokhodnya, K. I.; Faulmann, C.; Tokumoto, M.; Cassoux, P. *Synthetic Metals* **1999**, *103*, 2310-2311.

(53) Pullen, A. E.; Faulmann, C.; Pokhodnya, K. I.; Cassoux, P.; Tokumoto, M. *Inorganic Chemistry* **1998**, *37*, 6714-6720.

(54) Bai, J.; Zuo, J.; Tan, W.; Ji, W.; Shen, Z.; Fun, H.; Chinnakali, K.; Razak, I.; You, X.; Che, C. *Journal of Materials Chemistry* **1999**, *9*, 2419-2423.

(55) Underhill, A. E.; Hill, C. A. S.; Winter, C. S.; Oliver, S. N.; Rush, J. D. *Molecular Crystals Liquid Crystals* **1992**, *217*, 7-12.

(56) Winter, C. S.; Manning, R. J.; Oliver, S. N.; Hill, C. A. S. *Optics Communications* **1992**, *90*, 139-143.

(57) Winter, C. S.; Oliver, S. N.; Manning, R. J.; Rush, J. D.; Hill, C. A. S.; Underhill, A. E. *Journal of Materials Chemistry* **1992**, *2*, 443-447.

(58) Veldhuizen, Y. S. J.; Veldman, N.; Spek, A. L.; Cassoux, P.; Carlier, R.; Mulder, M. J. J.; Haasnoot, J. G.; Reedijk, J. *Journal of the Chemical Society, Dalton Transctions* **1998**, 2989-2993.

(59) Huyett, J. E.; Choudhury, S. B.; Eichhorn, D. M.; Bryngelson, P. A.; Maroney, M. J.; Hoffman, B. M. *Inorganic Chemistry* **1998**, *37*, 1361-1367.

(60) Takahashi, M.; Robertson, N.; Kobayashi, A.; Becker, H.; Friend, R. H.; Underhill, A. E. *Journal of Materials Chemistry* **1998**, *8*, 319-324.

(61) Saito, G.; Izukashi, H.; Shibata, M.; Yoshida, K.; Kushch, L.; Kondo, T.; Yamochi, H.; Drozdova, O.; Matsumoto, K.; Kusunoki, M.;

Sakaguchi, K.; Kojima, N.; Yagubskii, E. *Journal of Materials Chemistry* **2000**, *10*, 893-910.

(62) Singh, N.; Gupta, S. *Synthetic Metals* **2000**, *110*, 207-212.

(63) Robertson, N.; Roehrs, S.; Akutawa, T.; Nakamura, T.; Underhill, A. E. *Journal of Chemical Research* **1999**, 54-55.

(64) Uruichi, M.; Yakushi, K.; Yamashita, Y.; Qin, J. *Journal of Materials Chemistry* **1998**, *8*, 141-146.

(65) Sellmann, D.; Sutter, J. *Accounts of Chemical Research* **1997**, *30*, 460-469.

(66) Hay, R. W. *Bio-Inorganic Chemistry*; 3rd ed.; Ellis Horwood Limited: Chichester, 1993.

(67) Sellmann, D.; Utz, J.; Heinemann, F. W. *Inorganic Chemistry* **1999**, *38*, 459-466.

(68) Sellmann, D.; Utz, J.; Heinemann, F. W. *European Journal of Inorganic Chemistry* **1999**, 341-348.

(69) Sellmann, D.; Utz, J.; Heinmann, F. W. *Inorganic Chemistry* **1999**, *38*, 459-466.

(70) Svenstrup, N.; Becher, J. *Synthesis - Stuttgart* **1995**, 215-294.

(71) Wang, C.; Batsanov, A. S.; Bryce, M. R.; Howard, J. A. K. *Synthesis* **1998**, 1615-1618.

(72) Svenstrup, N.; Rasmussen, K. M.; Hanson, T. K.; Becher, J. *Synthesis* **1994**, *8*, 809-812.

(73) Faulmann, C.; Errami, A.; Donnadieu, B.; Malfant, I.; Legros, J. P.; Cassoux, P.; Rovira, C.; Canadell, E. *Inorganic Chemistry* **1996**, *35*, 3856-3873.

(74) Cerrada, E.; Garcia, J. F.; Laguna, M.; Terraba, R.; Villacampa, M. D. *Journal of the Chemical Society - Dalton Transactions* **1998**, 3511-3516.

(75) Olk, R. M.; Olk, B.; Dietzsch, W.; Kirmse, R.; Hoyer, E. *Coordination Chemistry Reviews* **1992**, *117*, 99-131.

(76) Zhao, W.; Shen, Y.; Li, Y.; Yang, J. *Synthetic Metals* **1997**, *89*, 91-93.

(77) Kumar, E. V. K. S.; Singh, J. D.; Singh, H. B.; Das, K.; Yakhmi, J. V.; Butcher, R. J. *Journal of the Chemical Society, Perkin Transactions 1* **1998**, 1769-1777.

(78) Perez-Benftez, A.; Tarres, J.; Ribera, E.; Veciana, J.; Rovira, C. *Synthesis* **1999**, 577-579.

(79) Jeppesen, J. O.; Takimiya, K.; Thorup, N.; Becher, J. *Synthesis* **1999**, 803-810.

(80) Cassoux, P.; Valade, L.; Kobayashi, H.; Kobayashi, A.; Clark, R. A.; Underhill, A. E. *Coordination Chemistry Reviews* **1991**, *110*, 115-160.

(81) Andreu, R.; Garin, J.; Orduna, J.; Royo, J. M. *Tetrahedron Letters* **2000**, *41*, 5207-5210.

(82) Rosa, A.; Ricciardi, G.; Baerends, E. J. *Inorganic Chemistry* **1998**, *37*, 1368-1379.

(83) Tommasino, J. B.; Pomarede, B.; Medus, D.; deMontauzon, D.; Cassoux, P. *Molecular Crystals Liquid Cystals* **1993**, *237*, 445-456.

(84) Faulmann, C.; Legros, J. P.; Cassoux, P.; Cornelissen, J. C.; Haasnoot, J. G.; Reedijk, J. *Synthetic Metals* **1993**, *55-57*, 2063-2068.

(85) Noh, D. Y.; Mizuno, M.; Choy, J. H. *Synthetic Metals* **1993**, *55-57*, 1705-1710.

(86) Valade, L.; Legros, J. P.; Tejel, C.; Pomarede, B.; Garreau, B.; Bruniquel, M. F.; Cassoux, P.; Ulmet, J. P.; Audouard, A.; Brossard, L. *Synthetic Metals* **1991**, *41-43*, 2268-2274.

(87) Cerrada, E.; Jones, P. G.; Laguna, A.; Laguna, M. *Inorganica Chimica Acta* **1996**, *249*, 163-168.

(88) Cerrada, E.; Laguna, M.; Sorolla, P. A. *Polyhedron* **1998**, *17*, 295-298.

(89) Cerrada, E.; Laguna, M. *Canadian Journal of Chemistry* **1998**, *76*, 1033-1037.

(90) Cerrada, E.; Laguna, M.; Villacampa, M. D. *Acta Crystallographica section C* **1998**, *54*, 201-203.

(91) Pomarede, B.; Garreau, B.; Malfant, I.; Valade, L.; P.Cassoux; Legros, J. P.; Audouard, A.; Brossard, L.; Ulmet, J. P.; Doublet, M. L.; Canadell, E. *Inorganic Chemistry* **1994**, *33*, 3401-3414.

(92) Valade, L.; Legros, J. P.; Bousseau, M.; Cassoux, P.; Garbauskas, M.; Interrante, L. V. *Journal of the Chemical Society Dalton Transactions* **1985**, 783-794.

(93) Errami, A.; Bowlas, C. J.; Menou, F.; Faulmann, C.; Gangneron, F.; Valade, L.; Cassoux, P.; Lahlil, K.; Moradpour, A. *Synthetic Metals* **1995**, *71*, 1895-1896.

(94) Faulmann, C.; Veldhuizen, Y. S. J.; Haasnoot, J. G.; Reedijk, J.; Cassoux, P. *Acta Crystallographica Section C* **1998**, *C54*, 1827-1830.

(95) Garreau, B.; Pomarede, B.; Cassoux, P.; Legros, J. P. *Journal of Materials Chemistry* **1993**, *3*, 315-316.

(96) Kahn, O. *Accounts of Chemical Research* **2000**, *33*, 647-657.

(97) Barclay, T. M.; Cordes, A. W.; George, N. A.; Hadden, R. C.; Oakley, R. T.; Palstra, T. T. M.; Patenaude, G. W.; Reed, R. W.; Richardson, J. F.; Zhang, H. *Chemical Comunications* **1997**, *9*, 873-874.

(98) Barclay, T. M.; A.W.Cordes; deLaat, R. H.; Goddard, J. D.; Haddon, R. C.; Jeter, D. Y.; Mawhinney, R. C.; Oakley, R. T.; Palstra, T. T. M.; Patenaude, G. W.; Reed, R. W.; Westwood, N. P. C. *Jounal of the American Chemical Society* **1997**, *119*, 2633-2641.

(99) Banister, A. J.; Batsanov, A. S.; Dawe, O. G.; Herbertson, P. L.; Howard, J. A. K.; Lynn, S.; May, I.; Smith, J. N. B.; Rawson, J. M.; Rogers, T. E.; Tanner, B. K.; Antorrena, G.; Palacio, F. *Journal of the Chemistry Society - Dalton Transactions* **1997**, 2539-2541.

(100) Chandrasekhar, V.; Chivers, T.; Parvez, M.; Vargas-Baca, I.; Ziegler, T. *Inorganic Chemistry* **1997**, *36*, 4772-4777.

(101) Barclay, T. M.; Cordes, A. W.; George, N. A.; Haddon, R. C.; Itkis, M. E.; Mashuta, M. S.; Oakley, R. T.; Patenaude, G. W.; Reed, R. W.; Richardson, J. F.; Zhang, H. *Journal of the American Chemical Society* **1998**, *120*, 352-360.

(102) Carlin, R. L. *Magnetochemistry*; 1 ed.; Springer-Verlag Berlin Heidelberg: Berlin, 1986.

(103) Kahn, O. *Magnetism: A Supramolecular Function*; 1 st ed.; Kluwer Academic Publishers: London, 1996.

(104) Miller, J. S.; Epstein, A. J. *Chemical Communications* **1998**, 1319-1325.

(105) Bricklebank, N.; Skabara, P. J.; Hibbs, D.; Hursthouse, M.; AbdulMalik, K. M. *Dalton Transations* **1999**, 3007-3014.

(106) Blake, A. J.; Devillanova, F. A.; Garau, A.; Isaia, F.; Lippolis, V.; Parsons, S.; Schroder, M. *Dalton Transactions* **1999**, 525-531.

(107) Bigoli, F.; Deplano, P.; Ienco, A.; Mealli, C.; Mercuri, M. L.; Pellinghelli, M. A.; Pintus, G.; Saba, G.; Trogu, E. F. *Inorganic Chemistry* **1999**, *38*, 4626-4636.

(108) Arangoni, M. C.; Arca, M.; Devillanova, F. A.; Garau, A.; Isaia, F.; Lippolis, V.; Verani, G. *Coordination Chemistry Reviews* **1999**, *184*, 271-290.

(109) Bailey, R. D.; Hook, L. L.; Pennington, W. T. *Chemical Communications* **1998**, 1181-1182.

(110) Konarev, D. V.; Valeev, E. F.; Slovokhotov, Y. L.; Shul'ga, Y. M.; Roschupkina, O. S.; Lyubovskaya, R. N. *Synthetic Metals* **1997**, *88*, 85-87.

(111) Olejniczak, I.; Pukacki, W.; Graja, A.; Liu, Y. Q.; Liu, S. G.; Zhu, D. B. *Synthetic Metals* **1998**, *94*, 51-55.

(112) Perepichka, I. F.; Kuz`mina, L. G.; Perepichka, D. F.; Bryce, M. R.; Goldenberg, L. M.; Popov, A. F.; Howard, J. A. K. *Journal of Organic Chemistry* **1998**, *63*, 6484-6493.

(113) Sun, S.; Wu, P.; Zhang, Q.; Zhu, D. *Synthetic Metals* **1998**, *94*, 161-166.

(114) Yamada, M.; Saruyama, H.; Aida, K. *Spectrochimica Acta* **1972**, *28A*, 439-446.

(115) Yu, H.; Zhang, B.; Zhu, D. *Journal of Materials Chemistry* **1998**, *8*, 77-80.

(116) Askew, H. F.; Gates, P. N.; Muir, A. S. *Journal of Raman Spectroscopy* **1991**, *22*, 265-274.

(117) Bricklebank, N.; Godfrey, S.; McAuliffe, C.; Deplano, P.; Mercuri, M.; Sheffield, J. *Dalton Transactions* **1998**, 2379-2382.

(118) Skabara, P. J.; Bricklebank, N.; Berridge, R.; Long, S.; Light, M. E.; Coles, S. J.; Hursthouse, M. B. *Dalton Transactions* **2000**, 3235-3236.

(119) Tasaki, K.; Basaki, S.; Matsuzaki, S.; Yartsev, V. M. *Synthetic Metals* **1998**, *94*, 65-68.

(120) Deplano, P.; Ferraro, J. R.; Mercuri, M. L.; Trogu, E. F. *Coordination Chemistry Reviews* **1999**, *188*, 71-95.

(121) Bigoli, F.; Deplano, P.; Mercuri, M. L.; Pellinghelli, M. A.; Trogu, E. F. *Phosphorus, Sulfur and Silicon* **1992**, *72*, 65-72.

(122) Boyle, P. D.; Christie, J.; Dyer, T.; Godfrey, S. M.; Howson, I. R.; McArthur, C.; Omar, B.; Pritchard, R. G.; Williams, G. R. *Journal of the Chemical Society, Dalton Transactions* **2000**, 3106-3112.

(123) Esseffar, M.; Bouab, W.; Lamsabhi, A.; Abboud, J. L. M.; Notario, R.; Yanez, M. *Journal of the American Chemical Society* **2000**, *122*, 2300-2308.

(124) LTD, S. S. *Magnetic susceptibility Balence Instruction Manual*; Sherwood Scientific LTD, 1 The Paddocks, Cherry Hinton Road, Cambridge, UK, 2000.

(125) Silverstein, R. M.; Bassler, G. C.; Morrill, T. C. *Spectroscopic Identification of Organic Compounds*; John Wiley & Sons: Chichester, 1991.

(126) Gordon, A. J.; Ford, R. A. *The Chemists companion - A Handbook of Pratical Data, Techniques, and References*; John Wiley & Sons: Chichester, 1972.

(127) Skoog, D. A.; Leary, J. J. *Principles of Instrumental Analysis*; 4th ed.; Saunders College Publishing: London, 1992.

(128) Morrison, R. T.; Boyd, R. N. *Organic Chemistry*; 6th ed.; Prentice-Hall International: London, 1992.

(129) Streitwieser, A.; Heathcock, C. H.; Kosower, E. M. *Introduction to Organic Chemistry*; 4th ed.; Macmillan Publishing Company: New York, 1992.

(130) Furniss, B. S.; Hannaford, A. J.; Smith, P. W. G.; Tatchell, A. R. *Vogel's Textbook of Pratical Organoc Chemistry*; 5th ed.; John Wiley & Sons: New York, 1989.

(131) Bellamy, L. J. *Advances in Infrared Group Frequencies*; 1 ed.; Chapman and Hall: London, 1975.

(132) Colthup, N. B.; Daly, L. H.; Wiberley, S. E. *Introduction to Infrared and Raman Spectroscopy*; 2nd ed.; Academic Press: London, 1975.

(133) Gottlieb, H. E.; Kotlyar, V.; Nudelman, A. *Journal of Organic Chemistry* **1997**, *62*, 7512-7515.

(134) Reichardt, C. *Solvents and solvent effects in organic chemistry*; 2nd ed.; Wiley: Weinhein Germany, 1988.

(135) Blair, S.; Goolsby, B.; Brodbelt, J. *International Journal of Mass Spectrometry* **1999**, *187*, 49-59.

(136) Noel, M.; Vasu, K. I. *Cyclic Voltammetry and the frontiers of Electrochemistry*; Aspect Publications Ltd.

(137) Rieger, P. H. *Electrochemistry*; 2 nd ed.; Chapman and Hall: London, 1994.

(138) Sawyer, D. T.; Sobkowiak, A.; Roberts, J. L. *Electrochemistry for Chemists*; 2 ed.; John Wiley & Sons: New York, 1995.

(139) Kumasaki, M.; Tanaka, H.; Kobayashi, A. *Journal of Materials Chemistry* **1998**, *8*, 301-307.

(140) Ueda, K.; Goto, M.; Iwamatsu, M.; Sugimoto, T.; Endo, S.; Toyota, N.; Yamamoto, K.; Fujita, H. *Journal of Materials Chemistry* **1998**, *8*, 2195-2198.

(141) Selwood, P. W. *Magnetochemistry*; 2 nd ed.; Interscience Publishers LTD: London, 1956.

(142) Lai, C. H.; Reibenspies, J. H.; Darensbourg, M. Y. *Chemical Communications* **1999**, 2473-2474.

(143) Huston, P.; Espenson, J. H.; Bakac, A. *Journal of the American Chemical Society* **1992**, *114*, 9510-9516.

(144) Yang, X. G.; Rauchfuss, T. B.; Wilson, S. *Journal of the Chemical Society, Chemical Communications* **1990**, 34-36.

(145) O'Connor, B. R.; Jones, F. N. *Journal of Organic Chemistry* **1970**, *35*, 2002-2005.

(146) Ueno, Y.; Sano, H.; Okawara, M. *Chemical Communications* **1980**, 28-30.

(147) Bochmann, M. *Organometallics 2*; The Bath Press: Bath, 1996.

(148) Long, G. J. *Mossbauer Spectroscopy Applied to Inorganic Chemistry*; 1st ed.; Plenum Press: London, 1984; Vol. 1.

(149) Goldanskii, V. I.; Herber, R. H. *Chemical Applications of Mossbauer Spectroscopy*; 1st ed.; Academic Press: London, 1968.

(150) Palacio, F. *Molecular Crystals, Liquid Crystals* **1997**, 385-99.

(151) Swink, L. N.; Carpenter, G. B. *Acta Crystallographica section B* **1968**, *24*, 429-433.

(152) Atzei, D.; Deplano, P.; Trogu, E. F.; Bigoli, F.; Pellinghelli, M. A.; Sabatini, A.; Vacca, A. *Canadian Journal of Chemistry* **1989**, *67*, 1416-1420.

(153) Cristiani, F.; Demartin, F.; Devillanova, F. A.; Isaia, F.; Saba, G.; Verani, G. *Journal of the Chemical Society, Dalton Transactions* **1992**, 3553-3560.

(154) Herbstein, F. H.; Schwotzer, W. *Journal of the American Chemical Society* **1984**, *106*, 2367-2373.

(155) Svensson, P. H.; Kloo, L. *Dalton Transactions* **2000**, 2449-2454.

(156) Narvor, N. L.; Robertson, N.; Wallace, E.; Killburn, J. D.; Underhill, A. E.; Bartlett, P. N.; Webster, M. *Journal of the Chemical Society - Dalton Transactions* **1996**, 823-828.

(157) Nakazono, T.; Nakano, M.; Tamura, H.; Matsubayashi, G. *Journal of Materials Chemistry* **1999**, *9*, 2413-2417.

(158) Narvor, N. L.; Robertson, N.; Weyland, T.; Kilburn, J. D.; Underhill, A. E.; Webster, M.; Svenstrup, N.; Becher, J. *Chemical Communications* **1996**, 1363-1364.

(159) Durfey, D. A.; Kirss, R. U.; Frommen, C.; Feighery, W. *Inorganic Chemistry* **2000**, *39*, 3506-3514.

ELSEVIER

Synthetic Metals 120 (2001) 1023–1024

SYNTHETIC METALS

www.elsevier.com/locate/synmet

Novel transition metal complexes based on covalently linked DMIT systems

R. Berridge,[a] N. Bricklebank,[a] D. W. Allen,[a] P. J. Skabara,[a†*] K. M. A. Malik,[b] S. J. Coles,[c] M. B. Hursthouse[c]

[a]*Materials Research Institute, Sheffield Hallam University, Pond Street, Sheffield, UK S1 1WB*
[b]*Department of Chemistry, Cardiff University, P.O. Box 912, Cardiff, U.K. CF10 3TB*
[c]*Department of Chemistry, University of Southampton, Highfield, Southampton, UK SO17 1BJ*
[†]*New address: Department of Chemistry, University of Manchester, Oxford Road, Manchester, UK M13 9PL*

Abstract The synthesis of a novel series of transition metal ligands and complexes is reported; the materials are related to the well-studied DMIT systems, allowing greater versatility in terms of structural design and processability.
Keywords:Heterocycle synthesis, organic conductors based on radical cation and/or anion salts.

Due to their highly interesting electroactive properties, transition metal complexes (**1**) based on the sulfur heterocycle DMIT have been studied extensively for several decades. The literature is abundant with materials exhibiting semiconducting and metallic properties and to date there are nine examples of DMIT based superconductors [1].

In the case of the DMIT complexes **1**, previous work has been constrained to the variation of the transition metal and/or the counter-anion. The work herein concerns the synthesis of a novel series of electroactive ligands, similar to the well-known DMIT species. In contrast to the DMIT ligand, our target derivatives incorporate two thioether and two dithiolate environments as the overall chelating entity. The thioether functionalities are linked via suitable spacer groups and this feature should present a major advantage over traditional DMIT complexes, by adding solubility and synthetic versatility to the overall nature of the complex.

Our strategy involves the preparation of bis(5-

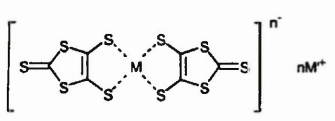

1

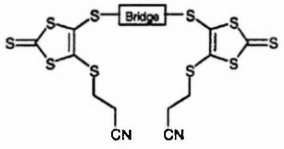

2

cyanoethylthio-1,3-dithiole-2-thione) derivatives **2**, which are linked at the 4(4')-positions of the sulfur heterocycles via a spacer group. These compounds can be prepared from the reaction of compound **3** [2] with one equivalent of base, followed by the addition of a suitable difunctional bridging unit, such as 1,2-dibromoethane or 1,2-bis(bromomethyl)benzene (Scheme 1). Using this methodology, we are presented with a vast range of possible derivatives due to the abundance of available difunctional systems which are capable of undergoing

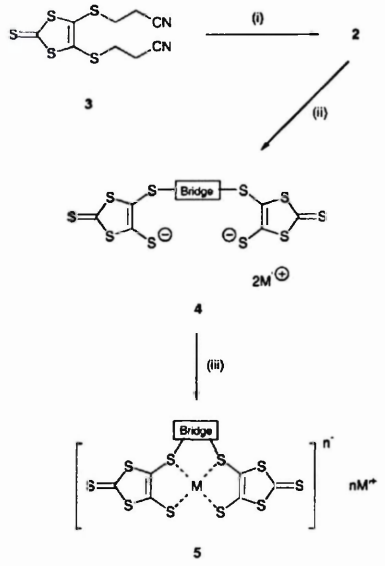

Scheme 1 *Reagents and conditions* (i) base, THF, then Br-spacer-Br; (ii) base, THF; (iii) MX_n, THF.

nucleophilic substitution reactions with a thiolate functionality. Furthermore, the spacer group can be designed to incorporate other features into the ligand, such

* Corresponding author. Tel: +44-161-275-4781; fax: +44-161-275-4598; E-mail: peter.skabara@man.ac.uk

PII: S0379-6779(00)01076-6

as chirality, rigidity, additional chelating atoms and even other redox-active groups. Examples of the bridging ligands used include the ethylene and *o*-xylyl derivatives **6** and **7**, which have been isolated from **3** in 75% and 60% yield, respectively. Under mildly basic conditions, derivatives of **2** can be easily deprotected to the corresponding dithiolate salts **4** (Scheme 1), affording strong ligands for complexation to transition metal species. For example, compound **7** was treated with tetramethyl ammonium hydroxide to afford salt **8** in 90% yield. This intermediate was filtered under nitrogen using Schlenk apparatus and recrystallised from methanol as an orange crystalline solid.

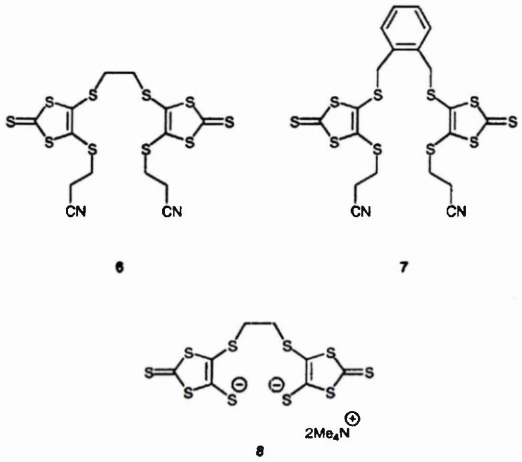

6 **7** **8**

The X-ray crystal structure of **8** [3] (Fig 1), shows that the ligand adopts a non-planar conformation. The asymmetric unit comprises a half molecule with an inversion centre between the C4-C4' bond. The crystal packing diagram (Fig 2) shows stacks of molecules in the 010 direction, with an interatomic distance of 8.716 Å between adjacent equivalent atoms within the stacks. There are no close S···S intermolecular contacts in the structure.

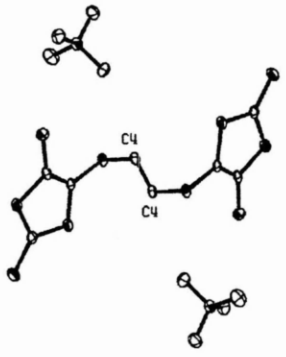

Figure 1 X-ray crystal structure of dithiolate salt **8**.

Depending on the oxidation state of the chosen metal, the target complexes can be isolated as discrete molecular species with an overall charge of zero, thus the electroactive material will be independent of any counteranions. The synthesis of such materials is well-

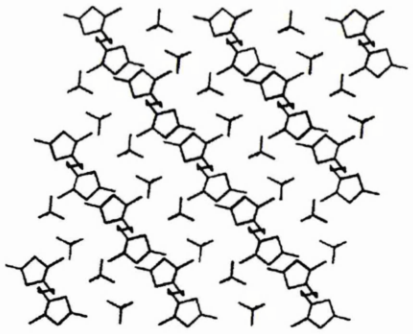

Figure 2 X-ray crystal packing diagram of **8** viewed in the 010 direction.

founded, since there are numerous analogues in the literature which contain benzene units rather than the dithiole-thione fragment. [4]

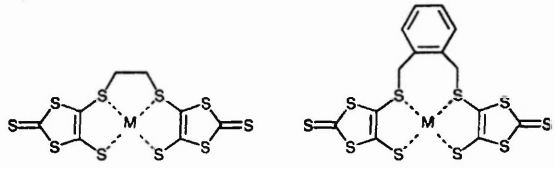

9 **10**

Using the synthetic strategy outlined in Scheme 1, two series of complexes (**9** and **10**) have been prepared in 65-90% yield, where M = Zn, Cu, Ni, PdCOD and NiDPPP. Cyclic voltammetric studies [5] show an irreversible oxidation process for all complexes at *ca.* 1.4 – 1.6 V, corresponding to the removal of an electron from the sulfur heterocycle. The reduction processes for the complexes are dependent upon the metal. The zinc derivatives do not show any reductive electroactivity, whereas the Cu materials each show a single irreversible process ($Cu^{2+} \rightarrow Cu^{+}$, at *ca.* –1.0 V) and the Ni and Pd complexes exhibit two sequential irreversible reductions ($M^{2+} \rightarrow M^{+} \rightarrow M^{0}$, at *ca.* –0.7 and –1.1 V). A more detailed electrochemical study will be reported elsewhere.

In summary, we have presented an efficient strategy for the synthesis of some new transition-metal complexes which incorporate the traditional chelating DMIT framework as a single molecular species. Electrocrystallisation experiments are currently being made and we are also preparing further ligands by varying the nature of the bridging unit.

[1] P. Cassoux, Coord. Chem. Rev. 185-186 (1999) 213.
[2] N. Svenstrup, K. M. Rasmussen, T. K. Hansen, J. Becher, Synthesis (1994) 809.
[3] *Crystal Data:* $C_8H_{14}NS_5$, M = 284.5, monoclinic, space group $P2_1/n$, a = 12.213(2), b = 8.716(2), c = 12.548(3)Å, β = 101.861(14)°, U = 1307.2(5)Å^3, T = 150(2)K, Z = 4, μ(Mo-Kα) = 0.851mm^{-1}, $F(000)$ = 596, 5416 reflections collected, 2012 unique (R_{int} = 0.1064), wR_2 = 0.1176 and R_1 = 0.0430 [I>2σI] and 0.1251 and 0.0534 respectively for all data. Deposition number; CCDC 147053.
[4] D. Sellmann, J. Sutter, Acc. Chem. Res. 30 (1997) 460.
[5] Au disk working electrode, Pt counter electrode, Ag/AgCl reference electrode, substrate *ca.* 10^{-3} M, *n*-Bu_4PF_6 supporting electrolyte (0.1 M) in DMF.

Crystal engineering towards highly ordered polymeric structures of 1,3-dithiole-2-thione–dihalogen adducts †

DALTON COMMUNICATION

Peter J. Skabara,*[a] Neil Bricklebank,*[b] Rory Berridge,[b] Stephen Long,[b] Mark E. Light,[c] Simon J. Coles[c] and Michael B. Hursthouse[c]

[a] *Department of Chemistry, University of Manchester, Manchester, UK M13 9PL. E-mail: peter.skabara@man.ac.uk*
[b] *Division of Chemistry and Materials Research Institute, Sheffield Hallam University, Sheffield, UK S1 1WB. E-mail: N.Bricklebank@shu.ac.uk*
[c] *Department of Chemistry, University of Southampton, Southampton, UK S017 1BJ*

Received 11th July 2000, Accepted 25th August 2000
First published as an Advance Article on the web 11th September 2000

The crystal structure of an iodine monobromide adduct of dimethyl 1,3-dithiole-2-thione-4,5-dicarboxylate reveals a layered polymeric network of donor and acceptor molecules linked primarily through S···I–Br charge-transfer and hydrogen bonded interactions.

The reaction of heteroatom donor molecules with dihalogens (I_2, Br_2, Cl_2) or interhalogens (IBr, ICl) can follow a variety of pathways, the most prevalent being the formation of donor–acceptor or charge-transfer adducts containing a linear D···X–Y moiety (X = I; Y = I, Br, Cl) or insertion products containing an X–D–Y fragment (X = Y = Br, Cl).[1] Recently we have been investigating dihalogen adducts of thiocarbonyl donors based on the 1,3-dithiole-2-thione unit.[1] We are keen to explore the role that charge-transfer interactions might play in the formation of functional supramolecular assemblies. It has been postulated that these types of adduct can be used as components in molecular electronics,[2] but in order to realise this function, the materials have to conform to certain structural and electronic requirements. Consequently, the adduct has to offer some form of advantageous electroactivity, such as the ability to form stable radicals for conducting and magnetic properties, or exhibit assymetric charge-transfer for nonlinear optical applications. In the former example, the material needs to exhibit long range order in the bulk solid to achieve a magnetic state, and also an extensive network of intermolecular π-interactions for conductivity.

In view of the above, thiocarbonyl compounds containing 1,3-dithiole fragments are suitable candidates for dihalogen complexes featuring interesting electronic properties. Previous studies have shown that charge-transfer interactions can be used to link multidentate/macrocyclic donors, such as thioether crowns[3] or diazines,[4] and polymeric coordination complexes,[5] though little work has been carried out on the formation of ordered supramolecular assemblies containing relatively simple monodentate donors. We are particularly interested in the self-assembly of substituted 1,3-dithiole-2-thione species as dihalogen adducts. In this work, we have prepared the IBr adduct of dimethyl 1,3-dithiole-2-thione-4,5-dicarboxylate **1**;[6] the X-ray crystal structure of the adduct **2** reveals an array of S···I, I···Br and hydrogen bonding interactions, many of which are unprecedented for thiocarbonyl–dihalogen adducts.

Treatment of **1** with an equimolar quantity of IBr in refluxing acetonitrile resulted in the formation of a brown coloured solution. On cooling at −5 °C overnight, orange crystals of the adduct $[(\mathbf{1}\cdot IBr)_2IBr]$ (**2**) were deposited (no elemental analysis data are available as **2** slowly loses IBr).

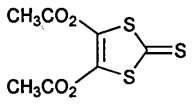

1

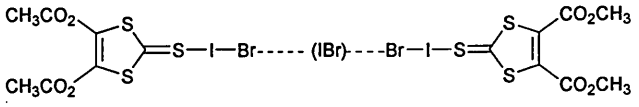

2

The X-ray crystal structure of **2** is shown in Fig. 1.‡ The close contact between atoms S(1) and I(1) arises from a 'charge-transfer' process from the thiocarbonyl-sulfur to the interhalogen. Thus, electron density from a lone pair of the sulfur is donated to the σ* antibonding orbital of the I–Br bond. This situation results in the formation of a weak bond [2.605(2) Å] which is significantly shorter than the sum of the van der Waals radii of the corresponding atoms (3.75 Å),[7] and a lengthened I(1)–Br(1) bond of 2.7107(11) Å [bond length of uncoordinated IBr is 2.521(4) Å].[8] The bond angle S(1)···I(1)–Br(1) between

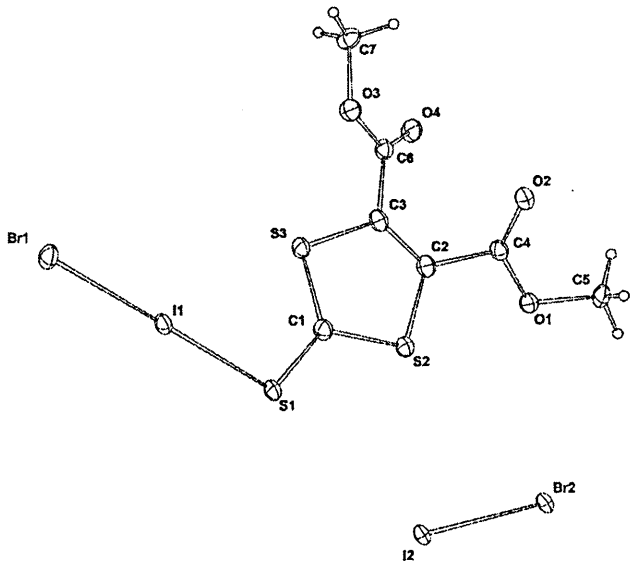

Fig. 1 Solid state structure of **2** with atom numbering scheme. Thermal ellipsoids are drawn at the 50% probability level. The molecule I(2)–Br(2) is shown fully, however, the molecule is disordered and the asymmetric unit contains 0.5 I(2)–Br(2).

† Electronic supplementary information (ESI) available: colour versions of the packing diagram of **2** viewed along the *b* axis with and without H-bonds. See http://www.rsc.org/suppdata/dt/b0/b005570k/

DOI: 10.1039/b005570k

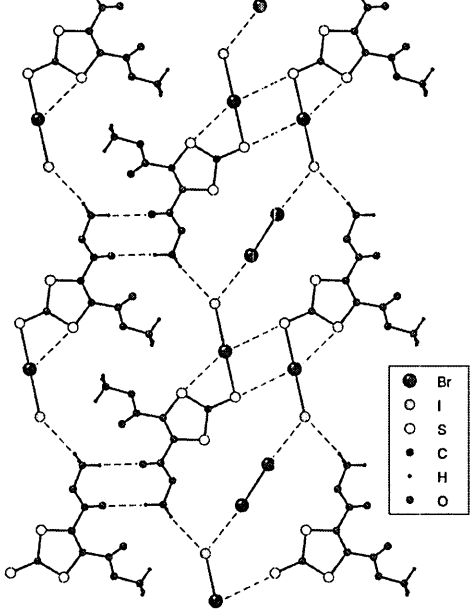

Fig. 2 Packing diagram of **2** viewed along the *b* axis showing intermolecular S I, halogen–halogen close contacts and H-bonds.

the two components is 178.01(7)° giving a linear conformation. A further significant intramolecular interaction is seen between the heterocyclic sulfur S(3) and I(1) [3.361(3) Å]; thus, the donor effectively chelates the iodine monobromide, resulting in a four-membered ring involving the S(1) I(1) S(3)–C(1) atoms.

A further half molecule of IBr is included in the asymmetric unit, with a 50% probability of iodine or bromine [Fig. 1 shows the complete I(2)–Br(2) molecule]. This molecule is independent of any interactions from the heterocycle and effectively acts as a bridge between two adjacent **1**·IBr units; the I–Br bond in the bridging iodine monobromide molecule is elongated [$d_{I(2)-Br(2)}$ = 2.7173(13) Å]. The distances between the terminal bromine atoms of the **1**·IBr moieties of **2** and the bridging IBr molecule, Br(1) I(2)/Br(2), are 3.3614(13) Å. The bond angles I(2)–Br(2) Br(1) and I(1)–Br(1) Br(2) are 175.21 and 130.14°, respectively.

The supramolecular structure of **2** is illustrated in Fig. 2.§ The structure contains perfectly eclipsed stacks of the donor and interhalogen acceptor and the interatomic distance between identical atoms in each layer is 5.816 Å. The S(1)–I(1) unit of the complex forms dimers through weak intermolecular bonds (3.669 Å) between S(1)–I(1′) and S(1′)–I(1), forming a four-membered ring between the adducts. In conjunction with the interactions between the dihalogen molecules, this feature gives rise to polymer chains within each sheet of the structure, which can be seen in Fig. 2.

The role of the diester functionality in the solid is also identified in Fig. 2, which includes further interactions through hydrogen bonding. A second set of dimers is formed between the methyl protons of one ester group and the adjacent molecule [H(5a) O(2) = 2.427 Å]. Through a similar interaction, the second ester functionality serves to link adjacent molecules within the same stack, giving rise to a second polymer chain rather than forming dimers [H(7b) O(4) = 2.430 Å, not shown in Fig. 2]. Finally, a third hydrogen bond between H(5b) and Br(1) (2.8183 Å) provides an additional interstack interaction. Overall, the hydrogen bonding network serves as a cross-linker to the linear polymer chain, resulting in a very rigid three-dimensional self-assembled superstructure.

The low frequency Raman spectrum of **2** contains two bands, a strong, broad, band at 186 cm^{-1}, together with a slightly weaker one at 147 cm^{-1}. These two bands can be attributed to the antisymmetric and symmetric stretching vibrations of the S–I–Br components of **2** respectively. Given the similarity in the bond lengths between the chelated and the bridging IBr molecules in **2**, it seems likely that the band at 186 cm^{-1} also has a contribution from the bridging IBr molecules.

In summary, we have presented the X-ray crystal structure of a new 1,3-dithiole-2-thione–IBr adduct (**2**) and identified two key points: (i) the precedence for occluding a free molecule of IBr, which could interact with suitable strong donors analogous to **1**, thereby providing open shell species *via* a formal charge-transfer process; (ii) a highly ordered array of supramolecular interactions which is desirable for magnetic and/or conducting properties in the bulk solid. In the pursuit of electroactive thiocarbonyl-dihalogen adducts for molecular electronics applications, the major challenge now is to design stronger thiocarbonyl electron donors than **1**, whilst retaining a highly ordered structure through suitable supramolecular functionalities.

Notes and references

‡ Crystal data for **2**. $C_7H_6BrIO_4S_3$·0.5IBr, M = 560.51, triclinic, a = 5.8163(3), b = 8.7676(4), c = 14.8481(9) Å, α = 77.310(2), β = 83.073(2), γ = 84.686(2)°, V = 731.58(7) Å^3, T = 150(2) K, space group $P\bar{1}$, Z = 2, μ = 7.765 mm^{-1}, 5844 reflections measured, 2518 unique (R_{int} = 0.0645) which were used in all calculations. CCDC reference number 186/2163. See http://www.rsc.org/suppdata/dt/b0/b005570k/ for crystallographic files in .cif format.

§ The molecule I(2)–Br(2) is disordered around the inversion centre such that opposing orientations are statistically distributed throughout the crystal.

1 For example, see: N. Bricklebank, P. J. Skabara, D. E. Hibbs, M. B. Hursthouse and K. M. A. Malik, *J. Chem. Soc., Dalton Trans.*, 1999, 3007.
2 J. R. Ferraro and J. M. Williams, *Introduction to Synthetic Electric Conductors*, Academic Press, New York, 1987.
3 A. J. Blake, F. A. Devillanova, A. Garau, F. Isia, V. Lippolis, S. Parsons and M. Schröder, *J. Chem. Soc., Dalton Trans.*, 1999, 525.
4 R. D. Bailey, M. L. Buchanan and W. T. Pennington, *Acta Crystallogr., Sect. B*, 1992, **48**, 2259.
5 R. D. Bailey, L. L. Hook and W. T. Pennington, *Chem. Commun.*, 1998, 1181.
6 B. R. O'Connor and F. N. Jones, *J. Org. Chem.*, 1970, **35**, 219.
7 J. E. Huheey, *Inorganic Chemistry: Principles of Structure and Reactivity*, 3rd edn., Harper and Row, New York, 1983.
8 L. N. Swink and G. B. Carpenter, *Acta Crystallogr., Sect. B*, 1968, **24**, 429.